

DESIGN, SYNTHESSES AND STRUCTURE-PROPERTY RELATIONSHIPS OF
BENZAZOLE AND ISOINDIGO COMPRISING CONDUCTING POLYMERS

A THESIS SUBMITTED TO
THE GRADUATE SCHOOL OF NATURAL AND APPLIED SCIENCES
OF
MIDDLE EAST TECHNICAL UNIVERSITY



BY
SEZA GÖKER

IN PARTIAL FULFILLMENT OF THE REQUIREMENTS
FOR
THE DEGREE OF DOCTOR OF PHILOSOPHY
IN
CHEMISTRY

SEPTEMBER 2019

Approval of the thesis:

**DESIGN, SYNTHESSES AND STRUCTURE-PROPERTY RELATIONSHIPS
OF BENZAZOLE AND ISOINDIGO COMPRISING CONDUCTING
POLYMERS**

submitted by **SEZA GÖKER** in partial fulfillment of the requirements for the degree
of **Doctor of Philosophy in Chemistry Department, Middle East Technical
University** by,

Prof. Dr. Halil Kalıpçılar
Dean, Graduate School of **Natural and Applied Sciences**

Prof. Dr. Cihangir Tanyeli
Head of Department, **Chemistry**

Prof. Dr. Levent Toppare
Supervisor, **Chemistry, METU**

Assoc. Prof. Dr. Görkem Günbaş
Co-Supervisor, **Chemistry, METU**

Examining Committee Members:

Prof. Dr. Ali Çırpan
Chemistry, METU

Prof. Dr. Levent Toppare
Chemistry, METU

Prof. Dr. Yasemin Arslan Udum
Technical Sciences Vocational School, Gazi University

Assoc. Prof. Dr. Akın Akdağ
Chemistry, METU

Prof. Dr. Ertuğrul Şahmetlioğlu
Chemistry, Erciyes University

Date: 03.09.2019



I hereby declare that all information in this document has been obtained and presented in accordance with academic rules and ethical conduct. I also declare that, as required by these rules and conduct, I have fully cited and referenced all material and results that are not original to this work.

Name, Surname: Seza Göker

Signature:

ABSTRACT

DESIGN, SYNTHESIS AND STRUCTURE-PROPERTY RELATIONSHIPS OF BENZAZOLE AND ISOINDIGO COMPRISING CONDUCTING POLYMERS

Göker, Seza

Doctor of Philosophy, Chemistry

Supervisor: Prof. Dr. Levent Toppare

Co-Supervisor: Assoc. Prof. Dr. Gökem Günbaş

September 2019, 232 pages

Donor–acceptor (D–A) conjugated polymers have been widely used for potential applications such as organic light emitting diodes, solar cells, electrochromic devices and organic field effect transistors. Benzazole comprising conducting polymers are popular for the last few decades since they can be used as low-band-gap donor materials because of their strong intramolecular charge transfer characteristics and excellent photovoltaic performances. Strong electron-donating and withdrawing building blocks are necessary to lower the band gaps and HOMO energy levels of D–A polymers. Alkoxy substitution to the acceptor groups provides polymers better solubility and higher molecular weight whereas fluorine substitution increases the strength of the acceptors via lowering electron density. In this thesis, 2,1,3-benzazole moieties were substituted with alkoxy and fluorine groups. Benzazole and isoindigo were coupled with several donor groups via both Stille and Suzuki polycondensation reactions to investigate structure-property relationships. On the other hand, Direct Heteroarylation Polymerization (DHAP) was also performed to obtain new polymers via an eco-friendly method. Molecular weights of polymers were investigated with GPC analysis. Oxidation and reduction behavior of the polymers were conducted using cyclic voltammetry. Polymers were used as active layers in optoelectronic

applications. The effect of thermal and solvent annealing on morphology were determined. After optimizing thickness and morphologies of polymer:PCBM, device production and current/voltage property measurements were performed in a nitrogen-filled glove box system. The analysis of the photovoltaic devices (ITO/ PEDOT:PSS/ Polymer: PCBM/ Metal) were achieved by means of the energy conversion efficiency measured under standard AM 1.5G illumination.

Keywords: Donor-Acceptor Approach, Benzazole, Isoindigo, Conducting Polymers, Photovoltaic



ÖZ

BENZAZOLE VE İZOİNDİGO İÇEREN İLETKEN POLİMERLERİN DİZAYNI, SENTEZİ VE YAPI-ÖZELLİK İLİŞKİLERİ

Göker, Seza

Doktora, Kimya

Tez Danışmanı: Prof. Dr. Levent Toppare

Ortak Tez Danışmanı: Doç. Dr. Görkem Günbaş

Eylül 2019, 232 sayfa

Donor–akseptör (D–A) tipi konjüge polimerler organik ışık yayan diyotlar, güneş pilleri, elektrokromik cihazlar ve organik transistörler gibi çeşitli uygulamalarda kullanılmaktadır. Benzazole içeren iletken polimerler kuvvetli intramoleküler yük transfer özelliği ve yüksek fotovoltaiik performansından dolayı düşük bant aralıklı donör malzemeler olarak kullanabildiği için son yıllarda popüler olmuşlardır. Kuvvetli elektron alıcı ve verici özelliğe sahip üniteler, D-A tipi polimerlerin bant aralığı ve HOMO enerji seviyesini düşürmek için gereklidirler. Akseptör ünitelerine alkoksi grupların ikame edilmesi polimerlerin daha iyi çözünürlüğe ve daha yüksek moleküler ağırlığa sahip olmalarını sağlarken flor atomunun ikame edilmesi elektron yoğunluğunu azaltarak akseptör ünitelerinin daha kuvvetli hale gelmesini sağlar. Bu tezde, 2,1,3-benzazol ünitelerine hem flor hem de alkoksi grupları ikame edilmiştir. Benzazole ve izoindigo yapı-özellik ilişkisini incelemek amacıyla Stille ve Suzuki kenetlenme reaksiyonları kullanılarak donör üniteleri ile eşleştirilmiştir. Diğer yandan, çevre dostu bir metot olan Doğrudan Heteroarilasyon Polimerleştirme (DHAP) yöntemi ile yeni polimerler elde edilmiştir. Değişik donör ve akseptör üniteleri eşleştirilerek polimerlerin yapı-özellik ilişkileri incelenecek ve polimerler optoelektronik uygulamalarda kullanılacaktır. Polimerlerin molekül ağırlığı GPC

analizi ile incelenmiştir. İndirgenme ve yükseltgenme davranışları dönüşümlü voltametri ile çalışılmıştır. Polimerler optoelektronik uygulamalarda aktif tabaka olarak kullanılmıştır. Termal ve çözelti tavlama yöntemlerinin morfolojiye etkisine bakılmıştır. Kalınlık ve morfoloji optimizasyonundan sonra, pilin üretimi ve akım/gerilim özellikleri azot dolu eldivenli kabin sisteminde gerçekleştirilmiştir. Güneş pillerinin (ITO/PEDOT: PSS/polimer:PCBM/ metal) analizleri güç çevirim verimi AM 1,5G aydınlatma ile hesaplanmıştır.

Anahtar Kelimeler: Donör-Akseptör Yaklaşımı, Benzazol, İzindigo, İletken Polimerler, Fotovoltaik



To Sezgi

ACKNOWLEDGMENTS

I would like to express my deepest gratitude to Prof. Dr. Levent Toppare. He never gave up believing in me. He encouraged me all time during this adventure.

I would like to thank Assoc. Prof. Dr. Görkem Günbaş for giving motivation, showing the light inside me. I cannot explain how much fun I've had while discussing organic synthesis.

I would like to thank Prof. Iain McCulloch. I gained lots of experiences about the synthesis of NFAs.

Dreams came true with the chance that Prof. Mario Leclerc gave me. I learned a lot in his laboratory.

I would like to thank Prof. Dr. Yasemin Arslan Udum for electrochemical characterizations.

Thanks for Dr. Gönül Hızalan Özsoy and Mert Can for construction of solar cells.

Thanks go to Ecem and Mustafa for their great friendship and helps. D-156 was amazing with them.

Big thanks to Ceren, Nehir and Esra for friendship, sharing incredible moments.

Thanks for each members of Toppare and Günbaş Research Groups for friendship during late night/weekend experiments.

This thesis is partially supported by Katip Çelebi Newton Fund-TÜBİTAK (Project No: 216Z129).

Many thanks my beloved friend Melis. She knows how to put a smile on my face. The only thing I regret is to meet her so late.

Special thanks go to my bestie Ebru. She shows up whenever I need. Memories and our laughter are inutterable. Our friendship will never grow old! I know she'll always be there, listen to me relentlessly.

I owe my special thanks to Sezgi. I cannot express how deeply I am bounded to her. No words can describe my gratitude for her endless patience and understanding. She is my mentor, the reason of my smile, my harbor.

The last but not the least I would like to thank my parents for their everlasting love and understanding.



TABLE OF CONTENTS

ABSTRACT	v
ÖZ	vii
ACKNOWLEDGMENTS	x
TABLE OF CONTENTS	xii
LIST OF TABLES	xx
LIST OF FIGURES	xxi
LIST OF ABBREVIATIONS.....	xxviii
CHAPTERS	
1. INTRODUCTION.....	1
1.1. Conducting Organic Polymers: From past to present	1
1.2. Types of Polymers	3
1.2.1. Homopolymers	4
1.2.2. Copolymers: Alternating and Random Copolymers	4
1.3. Electropolymerization.....	4
1.4. Classical polymerization types.....	7
1.4.1. Migita–Stille Coupling	8
1.4.2. Miyaura–Suzuki Coupling	10
1.5. Direct Heteroarylation Polymerization (DHAP).....	11
1.6. Applications of Polymers.....	12
1.6.1. Organic Photovoltaics	12
1.7. Non-Fullerene Acceptors	15
1.8. Aim of This Study.....	17

2. EXPERIMENTAL.....	19
2.1. Materials	19
2.2. Methods and Equipment.....	19
2.3. Syntheses of Monomers	20
2.3.1. Synthesis of 6-bromo-1-undecylindoline-2,3-dione	20
2.3.2. Synthesis of 6-bromo-1-undecylindolin-2-one	21
2.3.3. Synthesis of (E)-6,6'-dibromo-1,1'-diundecyl-[3,3'-biindolinylidene]-2,2'-dione (IID)	22
2.3.4. Synthesis of 1,2-bis(octyloxy) benzene	22
2.3.5. Synthesis of 1,2-dinitro-4,5-bis(octyloxy)benzene.....	23
2.3.6. Synthesis of 1,2-dibromo-4,5-bis(octyloxy)benzene.....	24
2.3.7. Synthesis of 4,5-bis(octyloxy)benzene-1,2-diaminium chloride.....	25
2.3.8. Synthesis of 5,6-bis(octyloxy)benzo[c][1,2,5]oxadiazole	25
2.3.9. Synthesis of 4,7-dibromo-5,6-bis(octyloxy)benzo[c][1,2,5]oxadiazole ...	26
2.3.10. Synthesis of 5,6-bis(octyloxy)benzo[c][1,2,5]selenadiazole	27
2.3.11. Synthesis of 4,7-dibromo-5,6-bis(octyloxy)benzo[c][1,2,5]selenadiazole	28
2.3.12. Synthesis of tributyl(thieno[3,2-b]thiophen-2-yl)stannane	28
2.3.13. Synthesis of 5,6-bis(octyloxy)-4,7-bis(thieno[3,2-b]thiophen-2-yl)benzo[c][1,2,5]selenadiazole	29
2.3.14. Synthesis of 5,6-bis(octyloxy)-4,7-di(selenophen-2-yl)benzo[c][1,2,5]selenadiazole	30
2.3.15. Synthesis of 4,7-di(furan-2-yl)-5,6-bis(octyloxy)benzo[c][1,2,5]selenadiazole	31
2.3.16. Synthesis of tributyl(selenophen-2-yl)stannane	32

2.3.17. Synthesis of 5,6-bis(octyloxy)-4,7-di(thieno[3,2- <i>b</i>]thiophen-2-yl)benzo[<i>c</i>][1,2,5]oxadiazole.....	32
2.3.18. Synthesis of 3,3'-(4,5-bis(octyloxy)-1,2-phenylene)dithiophene (NDT-Pre)	33
2.3.19. Synthesis of 5,6-bis(octyloxy)naphtho[2,1- <i>b</i> :3,4- <i>b'</i>]dithiophene (NDT)	34
2.3.20. Synthesis of 4,7-dibromobenzo[<i>c</i>][1,2,5]oxadiazole	35
2.3.21. Synthesis of 5,6-bis(octyloxy)-4,7-di(selenophen-2-yl)benzo[<i>c</i>][1,2,5]oxadiazole.....	36
2.3.22. Synthesis of 4,7-bis(5-bromothieno[3,2- <i>b</i>]thiophen-2-yl)-5,6-bis(octyloxy)benzo[<i>c</i>][1,2,5]oxadiazole.....	37
2.3.23. Synthesis of 4,7-bis(5-bromoselenophen-2-yl)-5,6-bis(octyloxy)benzo[<i>c</i>][1,2,5]oxadiazole.....	37
2.3.24. Synthesis of 5,6-bis(octyloxy)-4,7-di(furan-2-yl)benzo[<i>c</i>][1,2,5]oxadiazole.....	38
2.3.25. Synthesis of 4,7-bis(5-bromofuran-2-yl)-5,6-bis(octyloxy)benzo[<i>c</i>][1,2,5]oxadiazole.....	39
2.3.26. Synthesis of (E)-6,6'-bis(thieno[3,2- <i>b</i>]thiophen-2-yl)-1,1'-diundecyl-[3,3'-biindolinylidene]-2,2'-dione.....	40
2.3.27. Synthesis of 5-(2-ethylhexyl)-1,3-bis(thieno[3,2- <i>b</i>]thiophen-2-yl)-4H-thieno[3,4- <i>c</i>]pyrrole-4,6(5H)-dione.....	40
2.3.28. Synthesis of 4-methylbenzo[<i>c</i>][1,2,5]thiadiazole.....	41
2.3.29. Synthesis of 4-bromo-7-methylbenzo[<i>c</i>][1,2,5]thiadiazole.....	42
2.3.30. Synthesis of 4-bromo-7-dibromomethyl-2,1,3-benzothiadiazole	43
2.3.31. Synthesis 7-bromobenzo[<i>c</i>][1,2,5]thiadiazole-4-carbaldehyde.....	43
2.3.32. Synthesis of 2,5-dibromoterephthalic acid	44

2.3.33. Synthesis of diethyl 2,5-dibromoterephthalate	44
2.3.34. Synthesis of diethyl 2,5-di(thiophen-2-yl)terephthalate	45
2.3.35. Synthesis of 2,5-di(thiophen-2-yl)terephthalic acid	46
2.3.36. Synthesis of 5,6-difluorobenzo[<i>c</i>][1,2,5]oxadiazole 1-oxide	47
2.3.37. Synthesis of 5,6-difluorobenzo[<i>c</i>][1,2,5]oxadiazole.....	47
2.3.38. Synthesis of 2-bromo-3,4-difluoro-6-nitroaniline	48
2.3.39. Synthesis of 4-bromo-5,6-difluorobenzo[<i>c</i>][1,2,5]oxadiazole 1-oxide ..	49
2.3.40. Synthesis of 4-bromo-5,6-difluorobenzo[<i>c</i>][1,2,5]oxadiazole	49
2.3.41. Synthesis of 4-methylbenzo[<i>c</i>][1,2,5]oxadiazole 1-oxide	50
2.3.42. Synthesis of 2,5-dibromopyridine-3,4-diamine	51
2.3.43. Synthesis of 1,2-bis(3,4-bis(octyloxy)phenyl)ethane-1,2-dione.....	51
2.3.44. Synthesis of 2,3-bis(3,4-bis(octyloxy)phenyl)-5,8-dibromopyrido[3,4- <i>b</i>]pyrazine	52
2.3.45. Synthesis of 5,8-dibromo-2,3-di(thiophen-2-yl)pyrido[3,4- <i>b</i>]pyrazine .	53
2.3.46. Synthesis of 4,7-dibromo-[1,2,5]selenadiazolo[3,4- <i>c</i>]pyridine	53
2.3.47. Synthesis of 5,8-dibromo-2,3-di(pyridin-2-yl)pyrido[3,4- <i>b</i>]pyrazine	54
2.3.48. Synthesis of 7,7'-(5,6-bis(octyloxy)naphtho[2,1- <i>b</i> :3,4- <i>b'</i>]dithiophene-2,9-diyl)bis(benzo[<i>c</i>][1,2,5]thiadiazole-4-carbaldehyde)	54
2.3.49. Synthesis of 7,7'-(5,11-bis(2-hexyldecyl)-5,11-dihydroindolo[3,2- <i>b</i>]carbazole-3,9-diyl)bis(benzo[<i>c</i>][1,2,5]thiadiazole-4-carbaldehyde)	55
3. HOMOPOLYMERS via ELECTROPOLYMERIZATION.....	57
3.1. The effect of electron rich moieties for homopolymers	57
3.1.1. Electrochemistry	57
3.1.2. Spectroelectrochemistry.....	61
3.1.3. Kinetic Studies	63

3.2. The effect of electron poor moieties for homopolymers.....	65
3.2.1. Electropolymerization	65
3.2.2. Spectroelectrochemistry	67
4. ALTERNATING COPOLYMERS via STILLE and SUZUKI COUPLINGS..	71
4.1. Stille Coupling for Polymerizations of Alternating Copolymers.....	71
4.1.1. Syntheses	71
4.1.1.1. Synthesis of PIIDDTP	71
4.1.1.2. Synthesis of SG-2-ST	72
4.1.1.3. Synthesis of SG-3-ST	73
4.1.1.4. Synthesis of SG-4-ST	74
4.1.1.5. Synthesis of SG-6-ST	75
4.1.1.6. Synthesis of SG-6-ST2	75
4.1.1.7. Synthesis of SG-6-ST3	76
4.1.1.8. Synthesis of SG-7-ST	77
4.1.1.9. Synthesis of SG-8-ST	77
4.1.1.10. Synthesis of SG-9-ST	78
4.1.2. Results and Discussion for PIIDDTP	79
4.2. Suzuki Coupling for Polymerizations of Alternating Copolymers.....	82
4.2.1. Syntheses	82
4.2.1.1. Synthesis of PIIDINDC	82
4.2.1.2. Synthesis of PSBSC.....	83
4.2.1.3. Synthesis of PFBFC.....	84
4.2.1.4. Synthesis of PSBSFL.....	85
4.2.1.5. Synthesis of PFBFFL.....	86

4.2.2. Results and Discussion	87
4.2.2.1. Electrochemical Studies	87
4.2.2.2. Spectroelectrochemical Studies	90
4.2.2.3. Photovoltaic Studies	93
5. RANDOM COPOLYMERS via TERPOLYMER APPROACH	97
5.1. Terpolymer Approach	97
5.2. Syntheses	98
5.2.1. The Impact of Donor Moieties on the Polymer Backbone	98
5.2.1.1. Synthesis of P1	98
5.2.1.2. Synthesis of P2	99
5.2.1.3. Synthesis of P3	100
5.3. Results and Discussion	101
5.3.1. Electrochemical Studies	101
5.3.2. Optical Studies	105
5.3.3. Kinetic Studies	107
5.3.4. Photovoltaic Studies	109
5.4. The Impact of Acceptor Moieties on the Polymer Backbone	112
5.4.1. Syntheses	112
5.4.1.1. Synthesis of RP1	112
5.4.1.2. Synthesis of RP2	114
5.4.1.3. Synthesis of RP3	115
5.4.2. Results and Discussion	117
5.4.2.1. Electrochemistry Studies	117
5.4.2.2. Spectroelectrochemistry Studies	118

5.4.2.3. Preliminary Photovoltaic Studies	120
6. DIRECT HETEROARYLATION POLYMERIZATION (DHAP).....	125
6.1. General Information.....	125
6.2. Syntheses of Polymers	126
6.2.1. Synthesis of SG-1	126
6.2.2. Synthesis of SG-2.....	127
6.2.3. Synthesis of SG-3.....	128
6.2.4. Synthesis of SG-4.....	129
6.2.5. Synthesis of SG-5.....	130
6.2.6. Synthesis SG-6	130
6.2.7. Synthesis of SG-6-2.....	131
6.2.8. Synthesis of SG-6-3.....	132
6.2.9. Synthesis of SG-7.....	132
6.2.10. Synthesis of SG-8.....	133
6.2.11. Synthesis of SG-9.....	133
6.2.12. Synthesis of SG-10.....	134
6.3. Results and Discussion.....	135
6.3.1. Electrochemistry and Spectroelectrochemistry of SG-2-ST and SG-9-ST	135
6.3.2. Optical Properties of Some Polymers Synthesized via DHAP and Stille Coupling	138
6.3.3. Photovoltaic Studies/Preliminary Results for SG-4	140
7. CONCLUSIONS	145
REFERENCES	153

APPENDICES	157
A. NMR Spectra of Materials	157
B. The Results for Thermal Analyses and Elemental Analyses of Polymers	206
C. FTIR Analyses of Polymers.....	221
CURRICULUM VITAE	229



LIST OF TABLES

TABLES

Table 3.1. The optoelectronic properties of benzoxadiazole based D-A-D type polymers: Previously Synthesized Polymers* and PTTBO, PSBO, PFBO	58
Table 4.1. Summary of electronic properties of polymer	81
Table 4.2. Summary of optical properties of polymer	82
Table 4.3. The comparison of optoelectronic properties of all polymers	90
Table 4.4 Summary of colorimetry studies according to CIE	93
Table 4.5. Summary of the Photovoltaic Parameters	95
Table 5.1 Comparison of optical and electronic properties of random copolymers	107
Table 5.2 Summary of colorimetry studies according to CIE	107
Table 5.3 Summary of results of kinetic studies for P2 and P3.....	108
Table 5.4 Summary of the photovoltaic parameters for P2	111
Table 5.5. The comparison of optoelectronic properties of random copolymers....	120
Table 5.6 Summary of the preliminary photovoltaic studies for RP1	122
Table 5.7 Summary of the preliminary photovoltaic studies for RP3	123
Table 6.1. Summary of electronic properties for some polymers.....	136
Table 6.2. Summary of optical properties of polymers	138
Table 6.3. Summary of photovoltaic parameters for optimization studies of SG-4	142
Table 6.4. Comparison of maximum absorption and molecular weights of polymers synthesized via DHAP and Stille reaction.....	143
Table 6.5. Comparison of maximum absorption and molecular weights of polymers synthesized via Stille reaction	143

LIST OF FIGURES

FIGURES

Figure 1.1. Common conjugated polymers and their structures	3
Figure 1.2. Representation of chemical composition of polymers	3
Figure 1.3. Electropolymerization of selenophene	7
Figure 1.4. Aryltin material synthesis reported by Eaborn	8
Figure 1.5. Coupling between organotins and halides	8
Figure 1.6. The detailed mechanism of Stille coupling	9
Figure 1.7. The catalytic cycle for Suzuki coupling	10
Figure 1.8. The proposed mechanisms for DHAP	12
Figure 1.9. Schematic representation of a solar cell construction.....	14
Figure 2.1. Synthetic route for alkylation of 6-bromoisatin.....	21
Figure 2.2. Synthetic route for oxindole	21
Figure 2.3. Synthetic route for isoindigo	22
Figure 2.4. Synthesis of 1,2-bis(octyloxy) benzene.....	23
Figure 2.5. Synthetic route of 1,2-dinitro-4,5-bis(octyloxy)benzene.....	24
Figure 2.6. Synthesis of 1,2-dibromo-4,5-bis(octyloxy)benzene.....	25
Figure 2.7. Synthesis of 4,5-bis(octyloxy)benzene-1,2-diaminium chloride.....	25
Figure 2.8. Synthetic route of 5,6-bis(octyloxy)benzo[c][1,2,5]oxadiazole	26
Figure 2.9. Synthetic route of 4,7-dibromo-5,6-bis(octyloxy)benzo[c][1,2,5]oxadiazole	27
Figure 2.10. Synthetic route of 5,6-bis(octyloxy)benzo[c][1,2,5]selenadiazole.....	27
Figure 2.11. Synthetic route of 4,7-dibromo-5,6-bis(octyloxy)benzo[c][1,2,5]selenadiazole	28
Figure 2.12. Synthetic route of tributyl(thieno[3,2-b]thiophen-2-yl)stannane	29
Figure 2.13. Synthetic route of 5,6-bis(octyloxy)-4,7-bis(thieno[3,2-b]thiophen-2-yl)benzo[c][1,2,5]selenadiazole	30

Figure 2.14. Synthetic route of 5,6-bis(octyloxy)-4,7-di(selenophen-2-yl)benzo[c][1,2,5]selenadiazole.....	31
Figure 2.15. Synthetic route of 4,7-di(furan-2-yl)-5,6-bis(octyloxy)benzo[c][1,2,5]selenadiazole.....	31
Figure 2.16. Synthetic route of tributyl(selenophen-2-yl)stannane	32
Figure 2.17. Synthetic route of 5,6-bis(octyloxy)-4,7-di(thieno[3,2-b]thiophen-2-yl)benzo[c][1,2,5]oxadiazole.....	33
Figure 2.18. Synthetic route of 3,3'-(4,5-bis(octyloxy)-1,2-phenylene)dithiophene (NDT-Pre).....	34
Figure 2.19. Synthetic route of 5,6-bis(octyloxy)naphtho[2,1-b:3,4-b']dithiophene (NDT)	35
Figure 2.20. Synthetic route of 4,7-dibromobenzo[c][1,2,5]oxadiazole	35
Figure 2.21. Synthetic route of 5,6-bis(octyloxy)-4,7-di(selenophen-2-yl)benzo[c][1,2,5]oxadiazole.....	36
Figure 2.22. Synthetic route of 4,7-bis(5-bromothieno[3,2-b]thiophen-2-yl)-5,6-bis(octyloxy)benzo[c][1,2,5]oxadiazole	37
Figure 2.23. Synthetic route of 4,7-bis(5-bromoselenophen-2-yl)-5,6-bis(octyloxy)benzo[c][1,2,5]oxadiazole	38
Figure 2.24. Synthetic route of 5,6-bis(octyloxy)-4,7-di(furan-2-yl)benzo[c][1,2,5]oxadiazole.....	39
Figure 2.25. Synthetic route of 4,7-bis(5-bromofuran-2-yl)-5,6-bis(octyloxy)benzo[c][1,2,5]oxadiazole	39
Figure 2.26. Synthetic route of (E)-6,6'-bis(thieno[3,2-b]thiophen-2-yl)-1,1'-diundecyl-[3,3'-biindolinylidene]-2,2'-dione	40
Figure 2.27. Synthetic route of 5-(2-ethylhexyl)-1,3-bis(thieno[3,2-b]thiophen-2-yl)-4H-thieno[3,4-c]pyrrole-4,6(5H)-dione.....	41
Figure 2.28. Synthetic route of 4-methylbenzo[c][1,2,5]thiadiazole.....	42
Figure 2.29. Synthetic route of 4-bromo-7-methylbenzo[c][1,2,5]thiadiazole	42
Figure 2.30. Synthetic route of 4-bromo-7-dibromomethyl-2,1,3-benzothiadiazole	43
Figure 2.31. Synthetic route of 7-bromobenzo[c][1,2,5]thiadiazole-4-carbaldehyde	44

Figure 2.32. Synthetic route of 2,5-dibromoterephthalic acid	44
Figure 2.33. Synthetic route of diethyl 2,5-dibromoterephthalate	45
Figure 2.34. Synthetic route of diethyl 2,5-di(thiophen-2-yl)terephthalate	46
Figure 2.35. Synthetic route of 2,5-di(thiophen-2-yl)terephthalic acid	46
Figure 2.36. Synthetic route of 5,6-difluorobenzo[c][1,2,5]oxadiazole 1-oxide	47
Figure 2.37. Synthetic route of 5,6-difluorobenzo[c][1,2,5]oxadiazole	48
Figure 2.38. Synthetic route of 2-bromo-3,4-difluoro-6-nitroaniline	48
Figure 2.39. Synthetic route of 4-bromo-5,6-difluorobenzo[c][1,2,5]oxadiazole 1-oxide	49
Figure 2.40. Synthetic route of 4-bromo-5,6-difluorobenzo[c][1,2,5]oxadiazole	50
Figure 2.41. Synthetic route of 4-methylbenzo[c][1,2,5]oxadiazole 1-oxide	50
Figure 2.42. Synthetic route of 2,5-dibromopyridine-3,4-diamine	51
Figure 2.43. Synthetic route of 1,2-bis(3,4-bis(octyloxy)phenyl)ethane-1,2-dione ..	52
Figure 2.44. Synthetic route of 2,3-bis(3,4-bis(octyloxy)phenyl)-5,8-dibromopyrido[3,4-b]pyrazine	52
Figure 2.45. Synthetic route of 5,8-dibromo-2,3-di(thiophen-2-yl)pyrido[3,4-b]pyrazine	53
Figure 2.46. Synthetic route of 4,7-dibromo-[1,2,5]selenadiazolo[3,4-c]pyridine	53
Figure 2.47. Synthetic route of 5,8-dibromo-2,3-di(pyridin-2-yl)pyrido[3,4-b]pyrazine	54
Figure 2.48. Synthesis of 7,7'-(5,6-bis(octyloxy)naphtho[2,1-b:3,4-b'])dithiophene-2,9-diyl)bis(benzo[c][1,2,5]thiadiazole-4-carbaldehyde) (NFA-1 precursor)	55
Figure 2.49. Synthesis of 7,7'-(5,11-bis(2-hexyldecyl)-5,11-dihydroindolo[3,2-b]carbazole-3,9-diyl)bis(benzo[c][1,2,5]thiadiazole-4-carbaldehyde) (NFA-2 precursor)	56
Figure 3.1. Electrochemical deposition of a) PTTBO, b) PSBO and c) PFBO on ITO in 0.1M NaClO ₄ -LiClO ₄ /DCM/ACN electrolyte/solvent couple at a scan rate of 100 mV/s	59
Figure 3.2. Single scan cyclic voltammograms of (a) PTTBO, (b) PSBO and c) PFBO in a monomer free 0.1 M LiClO ₄ -NaClO ₄ /ACN solution	59

Figure 3.3. Chemical structures with monomer colors and abbreviations of homopolymers	60
Figure 3.4. Scan rate dependence of polymers a) PTTBO b) PSBO c) PFBO.....	60
Figure 3.5. Linear relationship between the current density and the scan rate.....	61
Figure 3.6. Absorption spectra of a) PTTBO, b) PSBO, and c) PFBO recorded in a monomer free 0.1 M ACN/NaClO ₄ / LiClO ₄ solution	62
Figure 3.7. Electrochromic switching and percent transmittance changes observed at the absorption maxima of a) PTTBO and b) PFBO when switched between in system NaClO ₄ -LiClO ₄ /ACN	64
Figure 3.8. Multi-scan cyclic voltammograms of a)PTPDThTh and b) PIIDThTh in 0.1 M TBAPF ₆ /ACN supporting electrolyte/solvent couple (scan rate: 100 mV/s)..	67
Figure 3.9. Single scan cyclic voltammograms of polymers in a monomer free solution (0.1 M TBAPF ₆ /ACN supporting electrolyte/solvent couple) a)PTPDThTh and b) PIIDThTh.....	67
Figure 3.10. Electronic absorption spectra of polymers a) PTPDThTh and b) PIIDThTh.....	69
Figure 4.1. Synthesis of PIIDDTP.....	72
Figure 4.2. Synthetic route for SG-2-ST	73
Figure 4.3. Synthetic route for SG-3-ST	74
Figure 4.4. Synthetic route for SG-4-ST	74
Figure 4.5. Synthetic route for SG-6-ST	75
Figure 4.6. Synthetic route for SG-6-ST2	76
Figure 4.7. Synthetic route for SG-6-ST3	76
Figure 4.8. Synthetic route for SG-7-ST	77
Figure 4.9. Synthetic route for SG-8-ST	78
Figure 4.10. Synthetic route for SG-9-ST	78
Figure 4.11. Single scan cyclic voltammogram of PIIDDTP in 0.1 M TBAPF ₆ /ACN solution at a scan rate of 100 mV/s.....	80
Figure 4.12. Electronic absorption spectra of the polymer upon applied gradual potential	80

Figure 4.13. Percent transmittance change for polymer at absorption maxima.....	81
Figure 4.14. Synthesis of PIIDINDC	83
Figure 4.15. Synthetic route for PSBSC	84
Figure 4.16. Synthetic route for PFBFC	85
Figure 4.17. Synthetic route for PSBSFL	86
Figure 4.18. Synthetic route for PFBFFL	87
Figure 4.19. Single scan cyclic voltammograms of polymers a) PSBSC b) PSBSFL c) PFBFC d) PFBFFL on ITO in 0.1 M TBAPF ₆ / ACN electrolyte/solvent couple at a scan rate of 100 mV/s.....	90
Figure 4.20. Change in the electronic absorption spectra of polymers in 0.1 M TBAPF ₆ /ACN solution between 0.0 V and 1.2 V for PSBSC (a), 0.0 V and 1.2 V for PSBSFL (b), 0.0 V and 1.1 V for PFBFC (c), and 0.0 V and 1.1 V for PFBFFL (d).....	92
Figure 4.21. Colors of polymers. (a) PSBSC, (b) PSBSFL, (c) PFBFC, and (d) PFBFFL on ITO coated glass electrode	92
Figure 4.22. I–V curves for the photovoltaic devices	94
Figure 4.23. AFM images of the polymer PCBM blends (scale bar is 400 nm).....	94
Figure 4.24. IPCE curves of the photovoltaic devices based on PSBSC:PC ₇₁ BM, PSBSFL:PC ₇₁ BM PFBFC: PC ₇₁ BM, and PFBFFL: PC ₇₁ BM blends.....	95
Figure 5.1. General structure of conjugated D–A random terpolymers.....	98
Figure 5.2. Synthetic route for P1	99
Figure 5.3. Synthetic route for P2	100
Figure 5.4. Synthetic route for P3	101
Figure 5.5. Single scan cyclic voltammograms of polymers a)P1 b)P2 c)P3	104
Figure 5.6. Scan rate studies polymers a) P1 b) P2.....	104
Figure 5.7. Electronic absorption spectra of polymers in 0.1 M NaClO ₄ -LiClO ₄ /ACN solution a) P1 b) P2 c) P3.....	106
Figure 5.8. Colors of polymers upon applied potential a) P1 b) P2 c) P3	107
Figure 5.9. Percent transmittance change and electrochromic switching times of a) P2 and b) P3 when switched between neutral and oxidized states in 0.1 M NaClO ₄ -LiClO ₄ /ACN.....	108

Figure 5.10. Current density - voltage curves of the optimized P2:PC ₇₁ BM (1:1) devices with and without 1.0 vol % DIO.....	110
Figure 5.11. AFM images of P2:PC ₇₁ BM (1:1) films spin coated (a) from dichlorobenzene without additive (b) from dichlorobenzene with 1.0 % DIO. (Scale bar is 400 nm) TEM images of P2:PC ₇₁ BM (1:1) films spin coated (c) from dichlorobenzene without additive (d) from dichlorobenzene with 1.0 % DIO	110
Figure 5.12. IPCE curve of the photovoltaic device based on P2:PC ₇₁ BM (1:1) spin coated from dichlorobenzene with 1.0 % DIO	111
Figure 5.13. Synthetic route for RP1	114
Figure 5.14. Synthetic route for RP2	115
Figure 5.15. Synthetic route for RP3	116
Figure 5.16. Single scan cyclic voltammograms of a) RP1-os b)RP1-ss c) RP2 and d) RP3	118
Figure 5.17. Electronic absorption spectra of a) RP1-os b)RP1-ss c) RP2 and d) RP3	119
Figure 5.18. The colors of the RP3 a) Hexane phase b) Chloroform phase	119
Figure 5.19. Current density - voltage curves for RP1 using different chlorinated solvents	121
Figure 5.20. Current density - voltage curves of the optimized RP1:PC ₇₁ BM devices with different polymer:PCBM ratios	122
Figure 5.21. Current density - voltage curves of the optimized RP3:PC ₇₁ BM devices with different polymer:PCBM ratios	123
Figure 6.1. Synthetic route for SG-1	126
Figure 6.2. Synthetic route for SG-2	127
Figure 6.3. Synthetic route for SG-3	128
Figure 6.4. Synthetic route for SG-4	129
Figure 6.5. Synthetic route for SG-5	130
Figure 6.6. Synthetic route for SG-6	131
Figure 6.7. Synthetic route for SG-6-2	131
Figure 6.8. Synthetic route for SG-6-3	132

Figure 6.9. Synthetic route for SG-7	133
Figure 6.10. Synthetic route for SG-8.....	133
Figure 6.11. Synthetic route for SG-9.....	134
Figure 6.12. Synthetic route for SG-10.....	135
Figure 6.13. Cyclic voltammograms of some polymers a) SG-2-ST b) SG-9-ST ...	136
Figure 6.14. Electronic absorption spectra of a) SG-2-ST b) SG-9-ST	137
Figure 6.15. Change in percent transmittances a) SG-2-ST and b) SG-9-ST	137
Figure 6.16. Comparison of UV-Vis absorption of polymers synthesized via Stille reaction and DHAP (in solution)	139
Figure 6.17. Normalized UV-Vis absorption of polymers synthesized via Stille reaction (in solution)	140
Figure 6.18. Current density - voltage curves of the optimized SG-4:PC ₇₁ BM (1:1) devices with and without 3.0 vol % DPE.....	141
Figure 6.19. Current density - voltage curves of the optimized SG-4-ST:PC ₇₁ BM (1:1) devices with different blend ratios	142

LIST OF ABBREVIATIONS

ABBREVIATIONS

ACN	Acetonitrile
Ag	Silver
Al	Aluminum
AM 1.5G	Air Mass 1.5 Global
BHJ	Bulk Heterojunction Solar Cell
CE	Counter Electrode
CIE	La Commission Internationale de l'Eclairage
CP	Conducting Polymer
CV	Cyclic Voltammetry
DCM	Dichloromethane/ Methylene Chloride
DHAP	Direct Hetero-Arylation Polymerization
DIO	1,8-Diiodooctane
DMF	Dimethylformamide
DPE	Diphenyl ether
EDOT	3,4-Ethylenedioxythiophene
E _g	Band gap
EtOH	Ethanol
FMO	Frontier Molecular Orbital
GPC	Gel Permeation Chromatography
HRMS	High Resolution Mass Spectrometer

HOAc	Acetic Acid
HOMO	Highest Occupied Molecular Orbital
IID	Isoindigo
IPCE	Incident Photon to Current Efficiency
<i>J</i> _{sc}	Short Circuit Current
ITO	Indium Tin Oxide
J-V	Current Density-Voltage
L, a, b	Luminance, hue, saturation
LiClO ₄	Lithium perchlorate
MeOH	Methanol
NaClO ₄	Sodium perchlorate
NIR	Near Infrared
NFA	Non Fullerene Acceptor
NMR	Nuclear Magnetic Resonance Spectrometer
OLED	Organic Light Emitting Diode
o-DCB	Orto-Dichlorobenzene
OSC	Organic Solar Cell
PCE	Power Conversion Efficiency
PhMe	Toluene
PLED	Polymer Light Emitting Diode
Pt	Platinum
UV	Ultra-Violet

Vis	Visible
V_{oc}	Open circuit voltage
3-TBA	3-Thiopheneboronic acid
TBAB	Tetrabutylammonium bromide
TBAPF ₆	Tetrabutylammonium hexafluorophosphate
TEA	Triethylamine
THF	Tetrahydrofuran
TLC	Thin Layer Chromatography
PA	Polyacetylene
PAn	Polyaniline
PivOH	Pivalic acid
PPy	Polypyrrole

CHAPTER 1

INTRODUCTION

1.1. Conducting Organic Polymers: From past to present

The modern era of conducting polymers (CPs) began with Heeger and MacDiarmid's synthesis of polyacetylene, $(CH)_n$, obtained by Shirakawa's method at the end of the 1970s. There was a 12 order of magnitude increase of conductivity upon charge-transfer oxidative doping.

The history of electrically conductive conjugated polymers date back to the early 1960s, particularly with the work of René Buvet and Marcel Jozefowicz on polyaniline (PAn) and Donald Weiss on polypyrrole (PPy). Those compounds are semiconductors in their neutral state and exhibit enhanced conductivity in their doped states (oxidized or reduced forms).

The oldest known polymeric organic substances which are electrically conductive are the carbon blacks made up of carbonizing of oil, wood, vegetables and other organic matter. Those materials were important due to high electrical conductivity (up to $50 \Omega^{-1} \text{ cm}^{-1}$), and high thermal stability. The modern carbon black definition is a quasigraphitic carbon material. Earlier studies revealed that carbon blacks are three-dimensional, crosslinked organic polymers with different structures and elemental constitutions based on their specific origin. The structures of "carbonaceous polymers" were too complex and not clearly understood. Hence, at the beginning of the 1950s scientist focused on polymers with more defined and controllable compositions. Examples are the production of poly(vinyl chloride) and poly(vinyl alcohol), polyacetylenes via the Ziegler-Natta catalyzed reactions and polyphenylenes via coupling of several dihalobenzenes.

In 1959, polypyrroles were prepared via heating tetraiodopyrrole under nitrogen atmosphere to transfer iodine vapor away from the reaction by Weiss and coworkers. The products were insoluble, black powders.

By 1966, Jozefowicz and coworkers had developed new methods to produce emeraldine (a form of polyaniline) via the oxidative polymerization of aniline with persulfate. [1]

In 1967, polymerization rate was accelerated via very high catalyst concentration (by accident). Acetylene gas contacted the catalyst solution. [2] Eventually, polyacetylene was obtained as a thin film on the surface. Shirakawa could reproducibly obtain silvery films of polyacetylene via optimizing the accidental conditions. After MacDiarmid and Heeger worked on poly(sulfur nitride), they discovered that the addition of Br_2 to poly(sulfur nitride) resulted in drastic increase in conductivity. Halogen treatment to the material might result in unusual electronic properties which was derived from IR transmission without any visible change in the appearance of the films. Previously, Heeger and MacDiarmid had found that the addition of halogen vapor to a polymer could result in significant increase in conductivity. The scientists repeated the similar scenario for polyacetylene based on the collective results. In 1977, it was shown that polyacetylene could be transformed to a semiconductor depending on chemical doping (removal of electrons through oxidation or introducing electrons through reduction). [3] In 2000, Alan J. Heeger, Alan G. MacDiarmid and Hideki Shirakawa were awarded with the Nobel Prize in Chemistry "for the discovery and development of conductive polymers". [4]

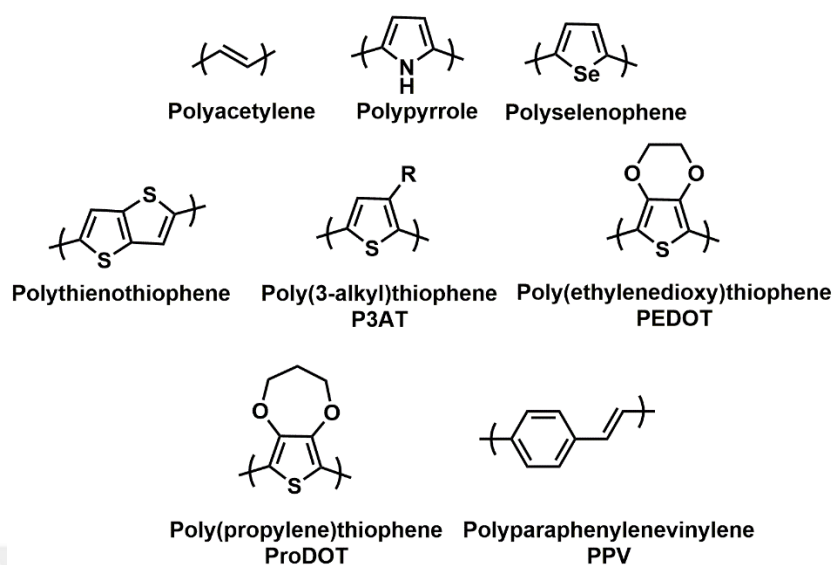


Figure 1.1. Common conjugated polymers and their structures

1.2. Types of Polymers

Polymers can be mainly divided into two based on their chemical composition; homopolymers and copolymers. One type of chemical repeat unit or monomer is repeated many times for homopolymers to produce a macromolecule of high molecular weight. [5a] As opposed to a homopolymer in which only one type of monomer is used at least two different types of monomers are linked throughout the same polymer chain for a copolymer. [5b]

Homopolymer



Alternating copolymer



Random copolymer



Figure 1.2. Representation of chemical composition of polymers

1.2.1. Homopolymers

Homopolymer refers repeating of one type of monomer along a linear polymer backbone. Homopolymers can be obtained via electropolymerization or oxidative chemical polymerization using anhydrous Lewis acid catalysts like MoCl_5 and FeCl_3 . The optical and electronic properties of chemically synthesized polymers could be very similar to electrochemically synthesized ones by adjusting the reaction time hence molecular weight of the corresponding polymers. [5]

1.2.2. Copolymers: Alternating and Random Copolymers

The term copolymerization involves the simultaneous polymerization of two or more types of monomer. For alternating copolymers, two different monomer units, are distributed in an alternating manner throughout the linear polymer backbone. For random copolymers, at least three different monomer units are randomly distributed along the polymer chain. Besides, terpolymerization and multicomponent polymerization imply polymerization of three types of monomer and three or more types of monomer, respectively. [6]

1.3. Electropolymerization

Electropolymerization also called electro-initiated polymerization is the application of anodic/cathodic potential to a monomer dissolved in an appropriate solvent comprising anionic doping salt. A radical cation of the monomer is formed after initial oxidation and it reacts with other monomers in solution to obtain first oligomers and eventually the polymer. The synthesis and doping of the polymer are performed simultaneously. The anion is incorporated into the polymer to ensure the electrical neutrality of the film and, at the end of the reaction, a polymeric film of controllable thickness is formed at the anode. [7] Any electrode surface stable up to oxidation of monomer can be used for electro-polymerization. Pt, glassy carbon, indium tin oxide (ITO), or SnO_2 coated glass, Au (for monomers with relatively low oxidation potentials), stainless steel are some examples of electrodes. Generally, a slower deposition rate provides a more uniform film formation. Electropolymerization allows

scientists to avoid extra chemical agents such as the oxidant, or catalyst and gives the polymer in the form of a film at the electrode surface with no need for further purification. One of the important parameter should be taken into account in the electropolymerization is the applied potential. The potential must be high enough to oxidize the monomer and polymerize it, however it also must be low enough to allow the electrode to undergo an electrochemical reaction and induce corrosion. The essential advantage of electropolymerization is the straightforward deposition of a redox and an electroconducting film with an electro-controllable thickness, tunable interfacial properties for numerous electrochemical applications. Temperature, the solvent, pH and monomer substitution are the parameters that have an impact on electropolymerization.

The value of potential for deposition alters very much for different polymers, mostly parallel to the oxidation potential of the corresponding monomer (some being relatively low, e.g., for EDOT, much higher for benzene). Chemical modification of the monomer, in particular, by substitution in positions not used for polymerization (for instance 3rd or 4th position of thiophene) changes potential drastically. Electron donating groups ease the oxidation of monomer i.e. shifting deposition potential to lower values whereas electron accepting moieties result in an opposite effect. [8]

Electropolymerization can be mainly classified into three; galvanostatic, potentiodynamic and potentiostatic. Potentiodynamic electropolymerization is characterized by a cyclic sweep of potential between the limits of the monomer oxidation and the reduction of conducting polymer. The growing polymer film continuously changes from its neutral state to its doped (or conducting) state as the potential is swept back and forth. This process is accompanied by the continuous absorption and desorption of the electrolyte. The solvent should be chosen to stabilize the growing film. Applying a constant current with a constant rate to a monomer results in a conducting polymer in the galvanostatic electropolymerization. At the very beginning, the potential may rise for a short period and then decrease after a while. It may be proposed that the sudden increase in potential is brought about by the

formation of the redox-active charged oligomers on the electrode. The subsequent decrease in the potential is brought about by the catalytic effect of the charged oligomers to oxidize the monomers. Potentiostatic electropolymerization involves the application of constant potential with a three-electrode system. A potentiostat is used to maintain the potential between the working and reference electrodes. The rate of polymerization could be controlled based on the applied potential. This method is similar to the galvanostatic electropolymerization and is different to potentiodynamic electropolymerization because no material is discharged from the deposited film during the coating procedure. [9]

The electrochemically obtained polymers with the same chemical structure may differ according to the used method. Polypyrrole films via potentiostatic electropolymerization (and also via galvanostatic electropolymerization) were of dendritic type with a low adhesion strength on the substrate. On the other hand, when pyrrole was polymerized potentiodynamically, a shiny black polymer film was obtained with a strong adhesion on the substrate, a smooth and homogenous surface morphology. This could be attributed to the formation of a large number of equivalent nucleation sites during the growth process. Besides, poly(3-methylthiophene) films revealed better electrical properties like conductivity, charge mobility, number of free carriers, and band gap when via potentiostatic polymerization than polymerized potentiodynamic polymerization. [10-13]

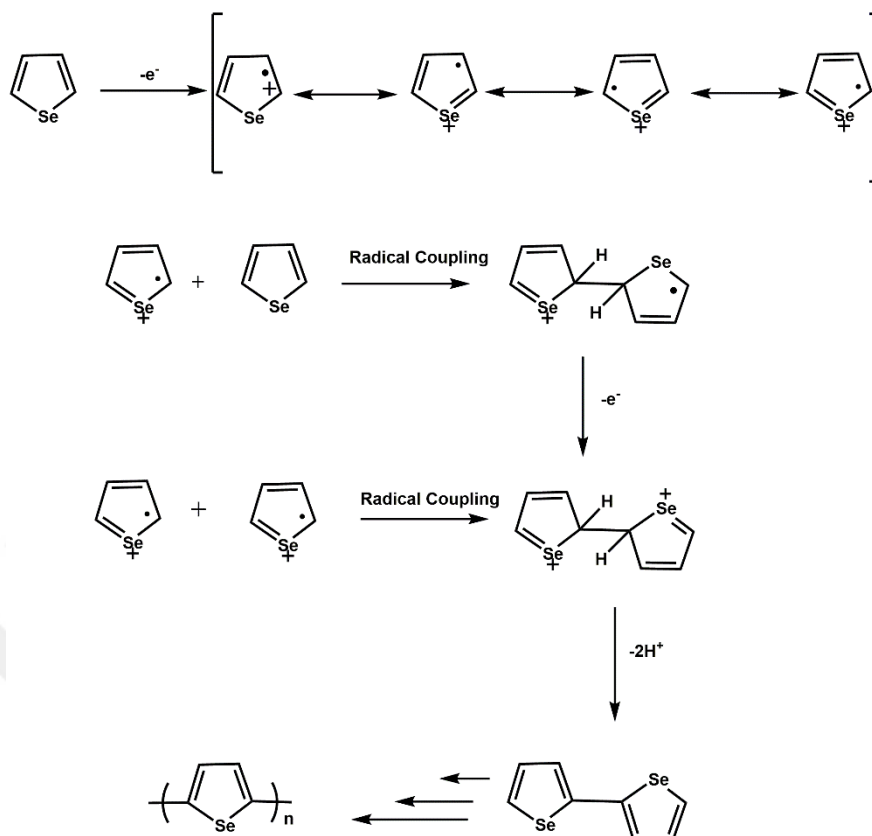


Figure 1.3. Electropolymerization of selenophene

1.4. Classical polymerization types

In literature, there several synthetic strategies for the development of conjugated materials such as Ziegler Natta polymerization, Kumada reaction, Heck reaction, Negishi reaction, Migita–Stille Coupling and Miyaura–Suzuki Coupling. [14-15] For polycondensations based on transition metal catalyzed C-C bond formation, Migita–Stille and Miyaura–Suzuki are the mostly used reactions among the other classical polymerization types. Stille reaction is one of the most popular synthetic methods to obtain organic functional compounds due to its excellent compatibility with several functional groups and high reaction yield. Suzuki reaction also results in high reaction yield under mild conditions using readily available starting materials.

1.4.1. Migita–Stille Coupling

The cross-coupling reaction between an organotin (also called organostannane) and an organic electrophile to generate a new C-C bond using a palladium catalyst is traditionally known as Stille reaction. In 1976, the preparation of aryltin materials using bis(tributyltin) also called hexabutyldistannane was reported by Eaborn in 1976. [16]

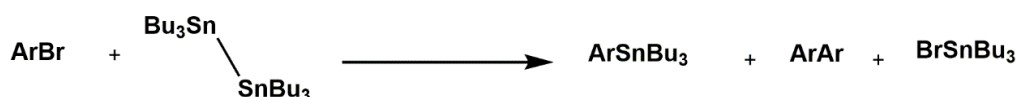


Figure 1.4. Aryltin material synthesis reported by Eaborn

In 1977, Kosugi-Migita preceded the first report on the topic by Milstein and Stille using a similar method to form C-C bond between acyl chlorides/ aryl halides and organotins which was considered as the first example of cross-coupling reactions for electrophilic compounds and organostannanes.

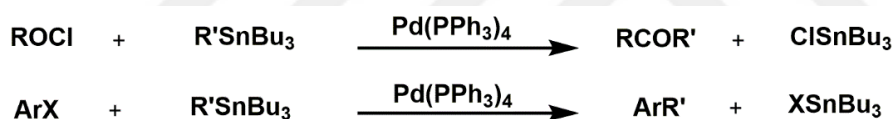


Figure 1.5. Coupling between organotins and halides

In 1978, John K. Stille and his coworkers reported the synthesis of ketones from acyl chlorides and organostannanes. Stille reaction is considered as one of the most useful synthetic methods to form functional materials especially extended conjugated systems comprising $\text{sp}^2\text{-sp}^2$ C-C bonds.

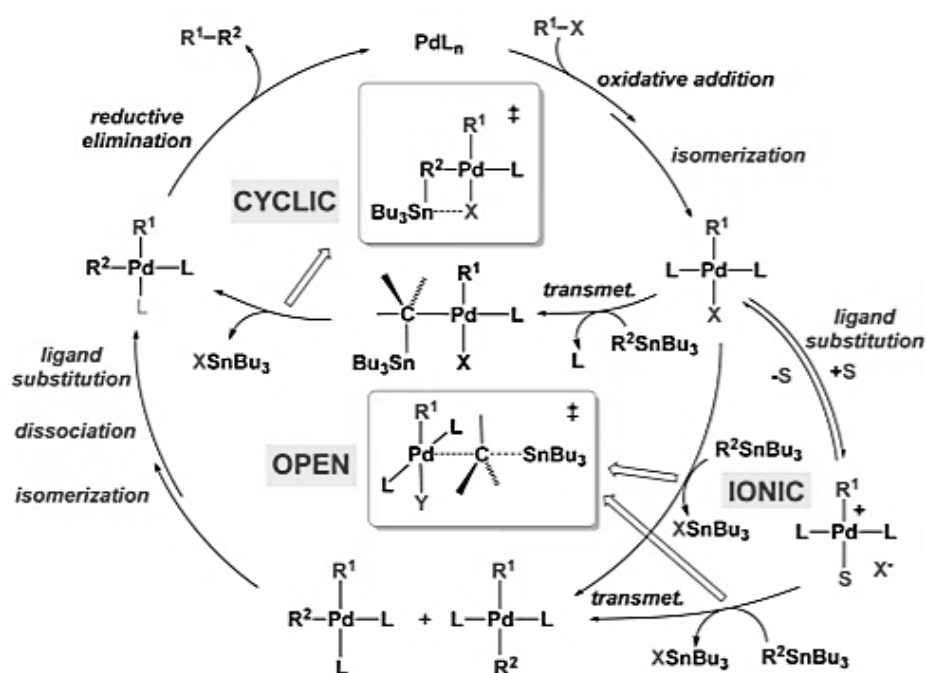


Figure 1.6. The detailed mechanism of Stille coupling

The main difference between Stille cross-coupling and Pd-catalyzed direct arylation reaction is in the transmetalation step. The organotin materials interact with the Pd center, Sn-C bond is broken and Pd-C bond is formed subsequently.

Stille reaction is more advantageous in terms of its stereospecificity, regioselectivity, and excellent reaction yields. Organotin and organohalide materials can be readily prepared, without protecting functionalities in the monomers, and these are far less oxygen- and moisture-sensitive than the other organometallic counterparts like Grignard reagents and organolithium reagents.

The biggest challenge of Stille coupling is the toxicity of organotin compounds. In the presence of organolithium reagent like lithium diisopropylamine or *n*-butyllithium, tri-*n*-butyltin or trimethyltin chloride is used to synthesize ditin monomers. The volatility and toxicity are lower for tri-*n*-butyltin compounds; however, purification of these compounds is more difficult via recrystallization. The impurity of such compounds prevents the obtaining of high molecular weight polymers. [17-18]

1.4.2. Miyaura–Suzuki Coupling

The reaction between organoboronates and organohalides to produce C-C bond using a palladium catalyst is known as Suzuki coupling. Organoborons are highly electrophilic, however organic groups on boron are weakly nucleophilic which limits the use of organoboron reagents for the ionic reactions. To increase the nucleophilicity of boron atom, the coordination of a negatively charged base to the boron atom was aimed to be an efficient method to transfer the organic group on boron to the adjacent positive center. Fortunately, organoborons (organoboronic acids or esters) reveal enough reactivity for the transmetalation to other metals. These boron compounds are generally stable to thermal treatment. Organoboronates show higher stability in air and are handled easily for isolation (by flash chromatography on silica gel).

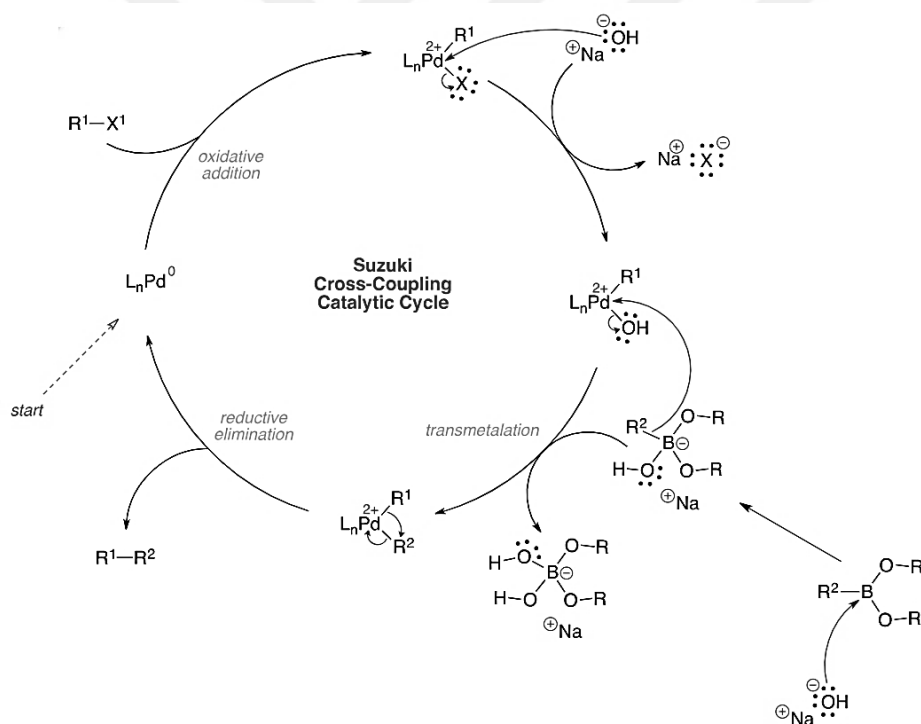


Figure 1.7. The catalytic cycle for Suzuki coupling

The catalytic cycle for Suzuki coupling is the same as other cross-coupling processes having organometallic reagents. Oxidative addition of organic halide to $Pd(0)$ complex is the first step. Then, transmetalation occurs between the intermediate and

the boronate compound with the help of base which accelerates this step. The final step is reductive elimination of the product and the catalyst recovery. The neat organoboron materials do not react with the complex L_nXPdR^1 however boronate complexes like $R_3BOR'Na$ directly give cross coupling products. Pd(0) is the mainly used catalyst for Suzuki cross-coupling. $Pd(PPh_3)_4$, $Pd[P(o-tolyl)_3]$ are some examples for commonly used catalytic systems. The purity is more problematic for boronic acids since they are hydroscopic. Hence, pinacol ester of boronic acid compounds are highly preferred since they do not tend to absorb water and also not easily dehydrate. Also, pinacol esters are advantageous in terms of stability, solubility and easy purification. The disadvantage of using pinacol ester derivatives is need to use stronger bases in the reaction medium due to their lower reactivity. [18-19]

1.5. Direct Heteroarylation Polymerization (DHAP)

Versatile synthetic methodologies to produce well-defined polymers and carbon-based materials were and are Ziegler-Natta, Stille, Kumada, Heck, Suzuki, Negishi reactions which involve several synthetic steps and expensive organometallic compounds resulting in metallic by-products. Direct hetero-arylation has attracted great attention to obtain organic semiconductors in a greener and cheaper manner. Fewer synthetic steps, lower production cost, easier purification and most importantly the generation of only benign byproducts are some undeniable benefits of metal catalyzed direct arylation to form carbon-carbon bonds between hetero-arenes and hetero-aryl halides having no organometallic intermediates. Proposed mechanisms in this type of reaction include electrophilic aromatic substitution (S_EAr), Heck-type coupling and concerted metalation-deprotonation (CMD) but the mechanism is still a subject of investigation. [18]

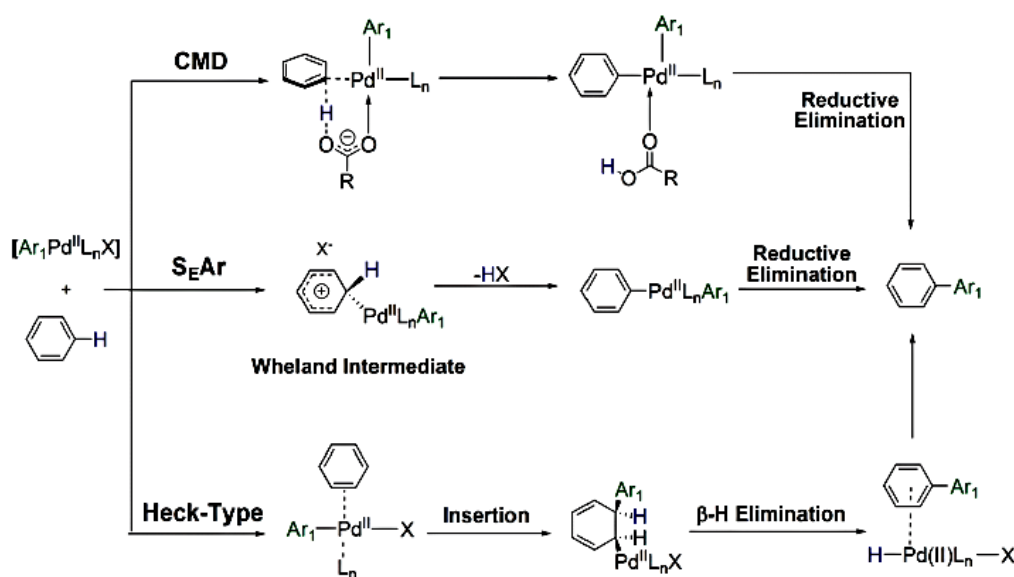


Figure 1.8. The proposed mechanisms for DHAP

Transition states for the carboxylate-assisted concerted metalation-deprotonation (CMD), aromatic electrophilic substitution (S_EAr) and Heck-type reaction mechanisms using benzene as a model (Figure 1.8). To become a useful approach, DHAP must be able to obtain compounds which offer at least comparable or even superior performance to those produced using the classical polymerization methods.

1.6. Applications of Polymers

π -Conjugated polymers having tunable properties through synthesis are the vast majority of organic electronic and photonic materials. Chemical and biochemical sensors, organic light emitting diodes (OLEDs), organic photovoltaics (OPV), dye sensitized solar cells (DSSC), organic field effect transistors (OFETs), thermoelectric components can be classified as the low-cost printed electronics using conjugated conducting polymers. [20]

1.6.1. Organic Photovoltaics

Since the sun is the only fully renewable and clean source, photovoltaics have an important role to meet the world's large and growing energy demand via converting sunlight into electricity. The first generation of solar cells is wafer-size single junction

devices using crystalline silicon. However, the high cost of manufacture of those devices lead scientists to find out new materials to reduce the cost for the produced electricity. The second generation of solar technologies are thin-film solar cells based on inorganic materials such as amorphous silicon semiconductors. Dye sensitized solar cells, hybrid solar cells (quantum dots doped organic materials) and organic solar cells are the examples of third generation for solar technology.

Organic solar cells have various advantages compared to their inorganic counterparts in addition to their product on cost. The solution processability, ease of tuning properties, low temperature processing and capability of printing on top of plastics substrate (providing portable electronics) are some advantages of organic materials. Small molecules and polymers are organic materials used in solar cell applications.

For many inorganic materials, exciton binding energy (E_b) is small (for instance ~ 15 meV for silicon) which is easily overcome by thermal energy (~ 25.85 meV at 300 K). However, most of organic materials exhibit large exciton binding energy values (for example, 0.7 eV for poly(3-hexylthiophene)) resulting in very inefficient charge separation. To provide successful charge separation, organic photovoltaics are generally constructed with an active layer composed of an electron-rich material and an electron-poor material. These materials should be chosen so that there would be a driving force for charge separation. [21]

Active layer possessing the following intrinsic features could give a highly efficient solar cell : (a) a broad absorption in the solar spectrum with a high extinction coefficient resulting in more solar photons; (b) a bicontinuous network with nanoscale phase separation for exciton diffusion and charge separation; (c) an appropriate molecular energy level alignment between the highest occupied molecular orbital (HOMO) and the lowest unoccupied molecular orbital (LUMO) energy levels for a sufficient driving force for efficient charge separation with minimum energy loss; and (d) a high charge mobility. [22]

There are four main steps to convert sun light into electricity by OSCs after capturing of photons by the photoactive layer; i) exciton (Coulombically bound holes and electrons) generation, ii) exciton diffusion, iii) exciton dissociation, iv) charge transport to the corresponding electrodes. To obtain high efficiency each step is crucial. Excitons could form charge-transfer states at the donor–acceptor interface which can then dissociate into free holes and electrons. Generally, exciton diffusion lengths are typically around 5-20 nm in organic semiconductors. Then, holes and electrons are transported through the donor-rich and acceptor-rich phases, respectively. The charges are collected to the relevant electrodes before decay or recombine.

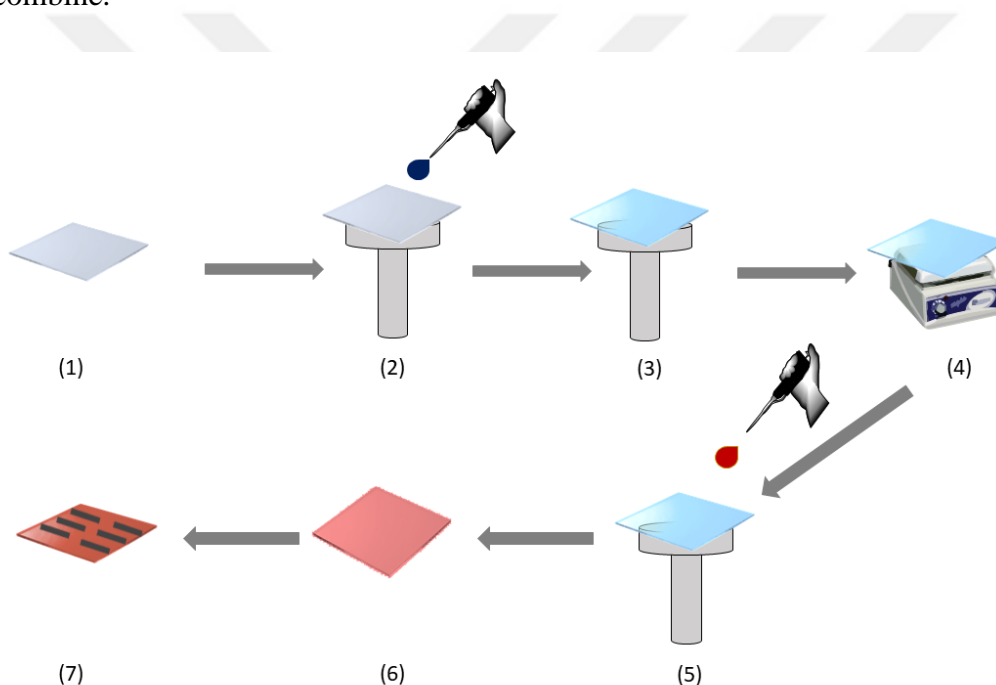


Figure 1.9. Schematic representation of a solar cell construction

Construction of a solar cell include several steps (Figure 1.8). Firstly, ITO coated glass electrodes are cleaned with toluene, de-ionized water and isopropanol, respectively (2). PEDOT: PSS, the hole-transporting layer, is spin casted onto cleaned ITO surfaces (3) using suitable rpm value to adjust the desired thickness. PEDOT: PSS coated are heated for 15 min to remove water residue (4). Polymer: PCBM blend is coated on

ITO substrate (5). Finally metals are thermally evaporated which are the cathode layers (6).

Organic photovoltaics are characterized under 1000 mW/cm² light having a spectrum match that of sun light on earth's surface at an angle of 48.2 ° called AM 1.5 G spectrum. The power conversion efficiency (PCE) which is one of the most important parameters of organic solar cells (OSCs) is given by:

$$PCE = \frac{V_{oc} * J_{sc} * FF}{P_{in}}$$

where P_{in} incident light power density, J_{sc} is the short-circuit current, V_{oc} is the open-circuit voltage and FF is the fill factor. J_{sc} is affected by the rate at which the donor and acceptor materials absorb photons and the efficiency of exciton dissociation.

Fill factor is influenced by efficiencies with which the resultant charges are transported to and collected at the electrodes. Since charge carrier mobility is sensitive to the morphology of thin films, fill factor is limited by the film morphology. V_{oc} is generally correlated to the differences between HOMO of donor and LUMO of acceptor energy level which drives the movement of charge carriers. [23] V_{oc} can be increased by lowering the HOMO of the donor. Improving both V_{oc} and J_{sc} simultaneously is often a challenge. Narrowing the band gap of a material which provide higher J_{sc} due to enhanced absorption may decrease V_{oc} of the device. [24]

1.7. Non-Fullerene Acceptors

In the field of organic photovoltaics (OPV), phenyl-C₆₁-butyric acid methyl ester (PC₆₁BM) and phenyl- C₇₁-butyric acid methyl ester (PC₇₁BM) derived from the parent C₆₀ and C₇₀ fullerenes with improved solubility and processability are used as the acceptor materials. The dominance of fullerene-based acceptors in the OPV research area stems from advantages including (i) the ability to accept and transport electrons in three dimensions thanks to delocalized LUMO over the whole surface of a molecule, (ii) high electron mobilities, (iii) multiple electrochemical reductions, and (iv) forming mixed domains of the appropriate length scale for charge separation. On

the other hand, there are important limitations of fullerene-based acceptors including (i) limited photocurrent harvesting due to weak absorption in the abundant region of the incident solar spectrum arising from its cage structure, (ii) high costs, especially for the high performing C₇₀ derivative, and (iii) morphological instability due to fullerene diffusion and aggregation in the thin film over time due to poor solubility. It is not so easy to tune the fullerene's absorption and energy levels via chemical modification.

Non-fullerene acceptors can be classified as the alternative materials to fullerenes to cope with the poor optical properties and long term morphological instability with an excellent synthetic flexibility. These the state-of-the-art materials could have strong absorption in the visible and near IR region of the solar spectrum via donor-acceptor hybridization which are similar to donor polymers. [25] A common feature of non-fullerene acceptors is introducing alkyl chains for better solubility in most common organic solvents to control over their aggregation properties and ease of processability. When both the donor and the acceptor moieties can absorb photons in different regions of the spectrum, the total number of excitons is increased resulting in maximized photocurrent. Non-fullerene acceptors via chemical modification lead to control over the frontier molecular orbitals (FMOs) providing the use of a wider range of possible donor polymers. Hence, a much higher V_{OC} in devices could be achieved.

Ideal properties of NFAs should exhibit are strong absorptions in regions of the visible and NIR spectrum that are complementary to those in which donor materials absorb, suitable energy levels to achieve charge separation with donors, the ability to produce exudation pathways for charge transport supporting high μ_e (carrier mobility) in the morphologies and good molecular and morphological thermal stability and photo stability [26] The molecular design for NFAs is crucial to obtain high-efficiency OSCs. Based on the equation below where N is the mobile carrier concentration, μ is the carrier mobility, and E is the internal electric field;

$$J = Nq\mu E$$

the carrier mobility is one of parameters determining the electrical current. The electron mobility in fullerenes (PCBM) is usually on the order of $10^{-4} - 10^{-2} \text{ cm}^2 / (\text{V} \cdot \text{s})$

To date, the electron mobilities for most organic acceptors reported are low, generally below $10^{-3} \text{ cm}^2 / (\text{V} \cdot \text{s})$, hindering high-efficiency non-fullerene OSCs. However, chemically modification of acceptors could increase the probability of a solution-processable acceptor with an electron mobility of greater than $10^{-2} \text{ cm}^2 / (\text{V} \cdot \text{s})$.

To synthesize efficient non-fullerene acceptors, aromatic rigid fused structures like rylene diimides (perylene diimide or naphthalene diimide) or strong dye-based chromophores (diketopyrrolopyrrole or isoindigo) are mostly used molecules for enhanced device performance due to higher charge carrier mobilities. Besides, flanking NFAs with cyano and rhodanine affects the optical and electrochemical properties and can be a common strategy to synthesize novel acceptor materials. [27]

1.8. Aim of This Study

In this study, different strategies were used to obtain conjugated polymers with several types such as homopolymers, copolymers and small molecules for synthesis of active layer materials for solar cells.

Electropolymerization, classical polymerization reactions like Stille and Suzuki couplings, direct arylation polymerization were performed to obtain benzazole and iso-indigo based conjugated polymers to investigate structure-property relationships. Electropolymerization was performed to obtain homopolymers to be used in several applications like biosensors. The effect of donor units and acceptors units on the polymer backbone were discussed. Optoelectronic properties were determined via spectroelectrochemical and electrochemical characterizations. Copolymers which are composed of various donor and acceptor materials distributed alternately throughout the polymer backbone were synthesized for solar cell applications via classical polymerization methods like Stille and Suzuki couplings. Optical and electronic properties were determined to see the impact of electron poor and rich materials. Solar cells were constructed using these polymers. Apart from alternating copolymers,

donor–acceptor terpolymers were synthesized to broaden the optical absorption and therefore improve the light-harvesting properties. Those copolymers were also used as the active layers in photovoltaic devices to illustrate the benefits of terpolymer approach in relation to OPV device performance. Direct heteroarylation polymerization (DHAP) was successfully performed to obtain several polymers. DHAP is a very simple, new and eco-friendly synthetic method to produce organic electronic materials. Polymers were both synthesized via Stille coupling and DHAP to compare synthetic methods in terms of molecular weights and optical properties. Apart from these, solar cells are constructed.

Non-fullerene acceptors have better stability, red shift in absorption with higher intensity when compared to PCBM. For the last chapter of this study, new materials were synthesized to obtain non-fullerene acceptors for solar cells. To the best of our knowledge, direct heteroarylation reaction was not used to non-fullerene acceptor up to date. One of the materials for non-fullerene acceptors was synthesized via direct heteroarylation for the first time in literature. After characterization of the materials, solar cells are aimed to be constructed.

CHAPTER 2

EXPERIMENTAL

2.1. Materials

Most of chemicals were purchased from Aldrich, Merck, Luminescence Technology Corp. (Lumtec). All reactions were carried out under argon atmosphere unless otherwise stated. THF and toluene were freshly distilled and degassed before use. ITO coated glass electrodes with a resistance of 8 ohm/square were purchased from Delta Technologies which were used for electrochemistry studies. For spectroelectrochemistry studies, glass electrodes were purchased from Aldrich.

For photovoltaic studies, ITO coated glass substrates from Visiontek were used. Anhydrous solvents to be used in active layer preparation were purchased from Aldrich. PC₆₁BM and PC₇₁BM were the products of Solenne. PTFE syringe filters were purchased from Ossila having a pore size of 0.22µm or 0.45µm. High purity metals from Kurt J. Lesker Company and tungsten boats from R.D. Mathis Company were used during evaporation of cathode layer. Coating of metals thicknesses were measured with QCM sensors.

2.2. Methods and Equipment

A three-electrode cell was used to achieve electro-polymerization of monomers in which a platinum wire was the counter electrode, Ag wire was the reference electrode and Indium Tin Oxide (ITO) doped coated glass was the working electrode under ambient conditions. To keep a constant voltage between the working and reference electrodes and to compensate the decrease in voltage, a potentiostat was used during the electrolysis. Electrochemical studies for homopolymers were performed to provide constant potential in the electrochemical polymerization. To record cyclic voltammetry studies of alternating and random copolymers, GAMRY Reference 600

potentiostat was used. All measurements were carried out at room temperature and were recorded under nitrogen atmosphere for the n-doped states. The reference electrode was calibrated with respect to Fc/Fc^+ . The spectroelectrochemical properties of the polymers were examined using Varian Cary 5000 UV–Vis spectrophotometer. HOMO-LUMO values were calculated considering the value of NHE as -4.75 eV vs vacuum. CDCl_3 and d-DMSO were used as the solvents to run ^1H and ^{13}C NMR spectra on Bruker Spectrospin Avance DPX-400 Spectrometer and tetramethylsilane was the internal reference. High resolution mass spectroscopy was performed to determine exact mass of the monomers using Waters Synapt MS System.

2.3. Syntheses of Monomers

2.3.1. Synthesis of 6-bromo-1-undecylindoline-2,3-dione

6-Bromoindoline-2,3-dione (5.00 g, 22.1 mmol), K_2CO_3 (9.20 g, 66.0 mmol) and $\text{C}_{11}\text{H}_{23}\text{Br}$ (18.7 g, 66.0 mmol) were mixed in anhydrous DMF (40 mL) and stirred at 65 °C for 2 hours under argon atmosphere. The mixture was cooled to room temperature and poured into distilled water. The dark red product was extracted with ethyl acetate several times. The organic phases were combined and dried over Na_2SO_4 . The evaporation of solvent under reduced pressure affords a crude product which was purified via column chromatography on silica gel using dichloromethane. Then recrystallization from cold methanol was performed to obtain orange crystalline solid. Yield: 46 %

^1H NMR (400 MHz, CDCl_3): δ 7.46 (d, J = 7.9 Hz, 1H), 7.28 (m, 1H), 7.07 (d, J = 1.4 Hz, 1H), 3.70 (t, J = 6.8 Hz, 2H), 1.85-1.53 (m, 2H), 1.44-1.16 (m, 15H), 0.88 (t, J = 6.8 Hz, 3H)

^{13}C NMR (100 MHz, CDCl_3): δ 182.4, 157.9, 151.9, 133.5, 126.8, 126.3, 113.8, 40.46, 31.87, 29.55, 29.52, 29.45, 27.17, 26.82, 14.11

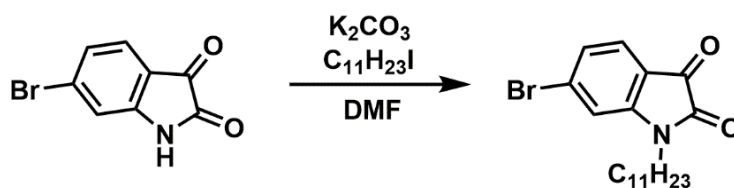


Figure 2.1. Synthetic route for alkylation of 6-bromoindolin-2-one

2.3.2. Synthesis of 6-bromo-1-undecylindolin-2-one

6-Bromo-1-undecylindolin-2,3-dione (3.00 g, 7.89 mmol) was stirred in distilled water (34 mL). 64-65 % hydrazine monohydrate (24 mL) was added to the suspension. The mixture was heated to reflux for 72 hours. The organic layer was then extracted in ethyl acetate and dried over Na_2SO_4 . Evaporation of the solvent afforded the corresponding 2-oxindole as an orange liquid. Yield: 96 %

^1H NMR (400 MHz, CDCl_3): δ 7.17-7.08 (m, 2H), 6.95 (d, $J = 1.6$ Hz, 1H), 3.46 (t, $J = 6.8$ Hz, 2H), 3.46 (s, 2H), 1.65 (m, 18H), 0.88 (t, $J = 6.8$ Hz, 3H)

^{13}C NMR (100 MHz, CDCl_3): δ 174.7, 146.1, 125.6, 124.8, 123.5, 121.3, 111.7, 40.19, 35.37, 31.90, 29.57, 29.51, 29.32, 29.27, 27.33, 26.93, 22.69, 14.13

One carbon around 29.0 ppm may overlap.

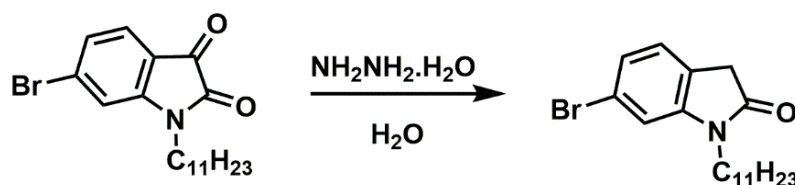


Figure 2.2. Synthetic route for oxindole

2.3.3. Synthesis of (E)-6,6'-dibromo-1,1'-diundecyl-[3,3'-biindolinylidene]-2,2'-dione (IID)

6-Bromo-1-undecylindoline-2,3-dione (2.80 g, 7.64 mmol) and 6-bromo-1-undecylindoline-2,3-dione (2.91 g, 7.64 mmol) were dissolved and stirred in a mixture of HCl (20 mL) and HOAc (20 mL) under argon atmosphere for 24 hours at 110 °C. Later, the solution was cooled to room temperature. The precipitate was filtered and washed with water, ethanol and ethyl acetate, respectively. The product was dried under vacuum and obtained as dark red crystals. Yield: 80 %

^1H NMR (400 MHz, CDCl_3): δ 9.07 (d, $J = 8.6$ Hz, 2H), 7.17 (dd, $J_1 = 1.8$ Hz, $J_2 = 8.6$ Hz, 2H), 6.93 (d, $J = 1.8$ Hz, 2H), 3.73 (t, $J = 7.4$ Hz, 4H), 1.93-1.62 (m, 18H), 1.35-1.25 (m, 18H), 0.87 (t, $J = 6.8$ Hz, 6H)

^{13}C NMR (100 MHz, CDCl_3): δ 167.7, 145.8, 132.7, 126.7, 125.1, 120.4, 111.3, 40.28, 31.90, 29.57, 29.56, 29.50, 29.31, 29.27, 27.38, 26.98, 22.68, 14.12

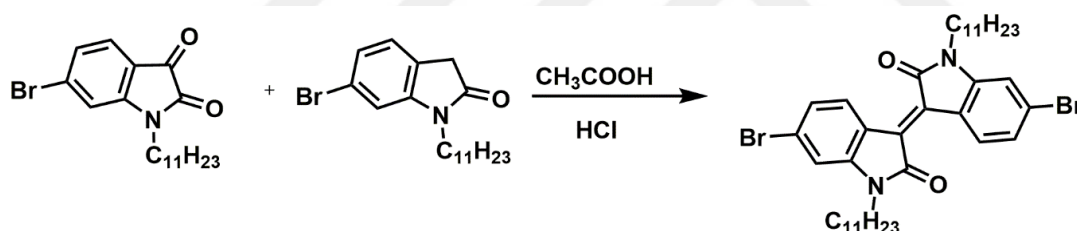


Figure 2.3. Synthetic route for isoindigo

2.3.4. Synthesis of 1,2-bis(octyloxy) benzene

Pyrocatechol (3.96 g, 36.0 mmol), K_2CO_3 (13.0 g, 94.0 mmol) and $\text{C}_8\text{H}_{17}\text{Br}$ (14.1 g, 75.0 mmol) were mixed in DMF (40 mL) and stirred at 115 °C for 40 hours under inert atmosphere. The mixture was cooled to room temperature and poured into distilled water. The milky-brown product was extracted with methylene chloride several times. The organic phases were combined and dried over MgSO_4 . The

evaporation of solvent under reduced pressure affords a crude product which was recrystallized from methanol to obtain white solid. Yield: 86 %

^1H NMR (400 MHz, CDCl_3): δ 6.82 (s, 4H), 3.92 (t, J = 6.7 Hz, 4H), 1.74 (q, J = 6.8 Hz, 4H), 1.41-1.21 (m, 20H), 0.81 (t, J = 6.7 Hz, 6H)

^{13}C NMR (100 MHz, CDCl_3): δ 147.9, 119.7, 112.9, 68.01, 30.54, 28.11, 28.06, 27.99, 24.76, 21.38, 12.80

HR-MS (ESI) for $\text{C}_{22}\text{H}_{38}\text{O}_2$ calculated 334.2872, found 334.2888

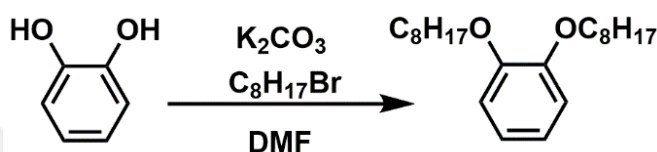


Figure 2.4. Synthesis of 1,2-bis(octyloxy) benzene

2.3.5. Synthesis of 1,2-dinitro-4,5-bis(octyloxy)benzene

In a two-neck round bottom flask, 1,2-bis(octyloxy)benzene (0.85 g, 2.50 mmol), glacial acetic acid (12 mL) and dichloromethane (12 mL) were mixed and the mixture was cooled to 10 °C. After dropwise addition of 65 % HNO_3 (2 mL) was completed, the mixture was warmed to room temperature and stirred for 1.5 hours. The reaction medium was again cooled to 10 °C and 100 % HNO_3 (6 mL) was added dropwise. The mixture was cooled to room temperature and stirred for 40 hours. The orange mixture was poured into ice-water and extracted with dichloromethane. The organic layer was then washed with NaHCO_3 , water and brine. The organic phase was dried over MgSO_4 , the evaporation of solvent under reduced pressure afford a crude solid. The product was obtained as a yellow solid after recrystallization from cold ethanol. Yield: 93 %

^1H NMR (400 MHz, CDCl_3): δ 7.23 (s, 2H), 4.03 (t, J = 6.5 Hz, 4H), 1.84-1.76 (m, 4H), 1.45-1.36 (m, 10H), 1.31-1.20 (m, 10H), 0.82 (t, J = 6.8 Hz, 6H)

^{13}C NMR (100 MHz, CDCl_3): δ 151.8, 134.5, 107.9, 70.20, 31.76, 29.19, 28.70, 25.81, 22.65, 14.09

HR-MS (ESI) for $\text{C}_{22}\text{H}_{36}\text{N}_2\text{O}_6$, calculated 425.2573 $[\text{M}+\text{H}]^+$, found 425.2652

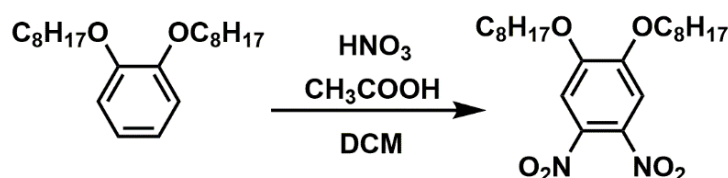


Figure 2.5. Synthetic route of 1,2-dinitro-4,5-bis(octyloxy)benzene

2.3.6. Synthesis of 1,2-dibromo-4,5-bis(octyloxy)benzene

1,2-Bis(octyloxy)benzene (4.65 g, 13.9 mmol) was dissolved in degassed DCM (120 mL) in a two neck round bottom flask and the solution was cooled to 0°C under argon atmosphere. Bromine (0.23 mL, 29.2 mmol) in DCM (32 mL) was then added to the reaction medium dropwise. When bromine addition completed, the solution was warmed to room temperature and stirred under dark for 19 hours. Saturated NaHSO_3 was added to quench excess bromine. Organic layer was washed with brine and distilled water, respectively. MgSO_4 was added to the organic layer. The solution was filtered and solvent was evaporated using rotary evaporator. The product recrystallized from cold ethanol and used without further purification. Yield: 87 %

^1H NMR (400 MHz, CDCl_3): δ 6.99 (s, 2H), 3.87 (t, $J= 6.6$ Hz, 4H), 0.81 (t, $J= 6.9$ Hz, 6H)

^{13}C NMR (100 MHz, CDCl_3): δ 149.1, 118.1, 114.7, 69.63, 31.81, 29.30, 29.23, 29.05, 22.67, 14.10

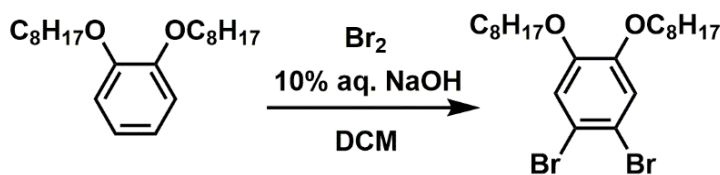


Figure 2.6. Synthesis of 1,2-dibromo-4,5-bis(octyloxy)benzene

2.3.7. Synthesis of 4,5-bis(octyloxy)benzene-1,2-diaminium chloride

To a mixture of 1,2-dinitro-4,5-bis(octyloxy)benzene (2.00 g, 4.71 mmol) in ethanol (50 mL) and conc. HCl (28 mL), $\text{SnCl}_2 \cdot 2\text{H}_2\text{O}$ (8.48 g, 37.6 mmol) was added under inert atmosphere. The mixture was heated to 85 °C overnight. Then, the solution was cooled to room temperature, the product was filtered and washed with methanol. The product was obtained as an off-white solid after drying at room temperature under argon purge and used without further purification. Yield: 80 %

NMR spectra of the compound cannot be recorded due to instability of the product.

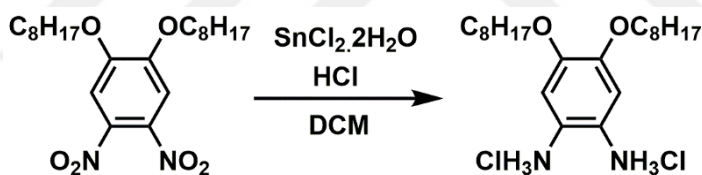


Figure 2.7. Synthesis of 4,5-bis(octyloxy)benzene-1,2-diaminium chloride

2.3.8. Synthesis of 5,6-bis(octyloxy)benzo[c][1,2,5]oxadiazole

A mixture of 1,2-dinitro-4,5-bis(octyloxy)benzene (5.50 g, 15.0 mmol), NaN_3 (4.02 g, 62.0 mmol) and tetra-*n*-butylammonium bromide (0.71 g, 2.20 mmol) was refluxed in 50 mL toluene under argon atmosphere for 20 hours at 125 °C. Then, triphenylphosphine (3.90 g, 15.2 mmol) was added and the mixture was refluxed for an additional 20 hours. The reaction mixture was cooled to room temperature and the solvent was evaporated under reduced pressure. The crude product was purified by

column chromatography on silica gel using 3:1 Hexane: DCM. Evaporation of solvent and recrystallization from ethanol afforded a yellow solid. Yield: 34 %

^1H NMR (400 MHz, CDCl_3): δ 6.74 (s, 2H), 4.01 (t, J = 6.5 Hz, 4H), 1.82 (q, J = 6.6 Hz, 4H), 1.25-1.48 (m, 20H), 0.82 (t, J = 6.6 Hz, 3H)

^{13}C NMR (100 MHz, CDCl_3): δ 153.3, 145.1, 89.01, 67.68, 30.08, 27.56, 27.53, 26.90, 24.27, 20.95, 12.37

HR-MS (ESI) for $\text{C}_{22}\text{H}_{36}\text{N}_2\text{O}_3$ calculated 377.2804, found 377.2816

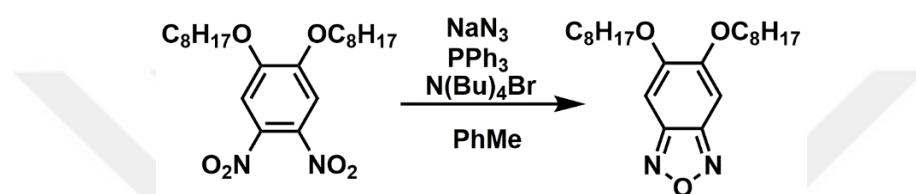


Figure 2.8. Synthetic route of 5,6-bis(octyloxy)benzo[c][1,2,5]oxadiazole

2.3.9. Synthesis of 4,7-dibromo-5,6-bis(octyloxy)benzo[c][1,2,5]oxadiazole

5,6-Bis(octyloxy)benzo[c][1,2,5]oxadiazole (2.40 g, 6.40 mmol) was dissolved in dichloromethane (50 mL) and glacial acetic acid (16 mL) was added to the solution. The reaction mixture was stirred at room temperature and bromine (3.57 g, 45.0 mmol) was added. The mixture was stirred at room temperature for 72 hours. The excess acid was quenched by aqueous NaOH solution. The organic layer was collected, washed with brine and dried over MgSO_4 . The evaporation of solvent under reduced pressure afforded a solid product which was then purified by column chromatography on silica gel using 3:1 Hexane: DCM. The product was a white solid. Yield: 58 %

^1H NMR (400 MHz, CDCl_3): δ 4.08 (t, J = 6.6 Hz, 4H), 1.72 (q, J = 6.8 Hz, 4H), 1.23-1.44 (m, 20H), 0.83 (t, J = 6.6 Hz, 6H)

^{13}C NMR (100 MHz, CDCl_3): δ 153.9, 145.6, 97.76, 75.19, 73.59, 29.98, 28.38, 27.51, 24.07, 20.73, 12.26

HR-MS (ESI) for $C_{22}H_{34}N_2O_3Br_2$, calculated 533.0936 $[M+H]^+$, found 533.1014

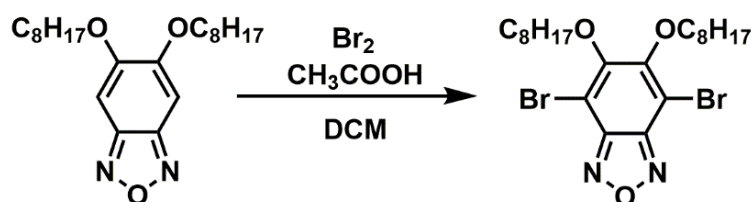


Figure 2.9. Synthetic route of 4,7-dibromo-5,6-bis(octyloxy)benzo[c][1,2,5]oxadiazole

2.3.10. Synthesis of 5,6-bis(octyloxy)benzo[c][1,2,5]selenadiazole

4,5-Bis (octyloxy)benzene-1,2-diaminium chloride (1.25 g, 2.85 mmol) was added in a two neck flask under inert atmosphere. After addition of freshly distilled DCM (44 mL) the solution was heated to reflux. Triethyl amine (6.00 mL, 43.2 mmol) was added slowly to the solution. After 1 hour stirring, SeO_2 (2.13 g, 19.1 mmol) was added. The mixture was refluxed overnight. Through removal of solvent by rotary evaporation, the crude product was obtained. Then, distilled water was poured and the solution was stirred for 1 hour. After filtration, a peach like orange color solid was collected. The product was purified by column chromatography on silica gel using methylene chloride. The product was an off-white solid. Yield: 46 %

1H NMR (400 MHz, $CDCl_3$): δ 6.86 (s, 2H), 3.99 (t, J = 6.6 Hz, 4H), 1.83 (q, J = 6.7 Hz, 4H), 1.44 (m, 4H), 1.33-1.23 (m, 16H), 0.82 (t, J = 6.6 Hz, 6H)

^{13}C NMR (100 MHz, $CDCl_3$): δ 157.5, 154.6, 99.37, 69.07, 31.79, 29.30, 29.25, 28.69, 26.01, 22.66, 14.09

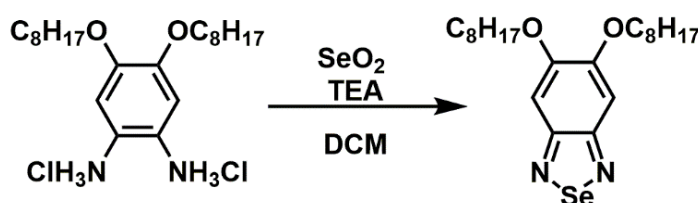


Figure 2.10. Synthetic route of 5,6-bis(octyloxy)benzo[c][1,2,5]selenadiazole

2.3.11. Synthesis of 4,7-dibromo-5,6-bis(octyloxy)benzo[c][1,2,5]selenadiazole

5,6-Bis(octyloxy)benzo[c][1,2,5]selenadiazole (540 mg, 1.23 mmol) was dissolved in a mixture of acetic acid (27 mL) and dichloromethane (66 mL) at room temperature in a 200 mL round bottom flask. After addition of bromine (0.52 mL, 10.1 mmol), the solution was stirred for 36 hours. Distilled water was added to the solution and the organic layer was extracted with dichloromethane. The organic layers were washed with NaHCO₃ and Na₂CO₃, respectively and dried over MgSO₄. The solvent was evaporated using rotary evaporator, the product was purified via column chromatography (eluent: DCM). Yield: 80 %

¹H NMR (400 MHz, CDCl₃): δ 4.09 (t, *J*= 6.6 Hz, 4H), 1.91-1.73(m, 4H), 1.63-1.36 (m, 4H), 1.36-1.06 (m, 16H), 0.82 (t, *J*= 6.8 Hz, 6H)

¹³C NMR (100 MHz, CDCl₃): δ 154.9, 154.5, 107.9, 75.06, 31.83, 30.28, 29.39, 25.99, 22.66, 14.10

One carbon around 30.0 ppm may overlap.

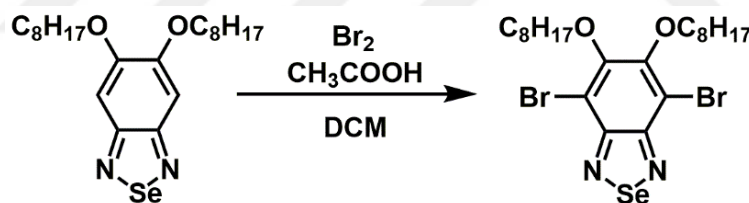


Figure 2.11. Synthetic route of 4,7-dibromo-5,6-bis(octyloxy)benzo[c][1,2,5]selenadiazole

2.3.12. Synthesis of tributyl(thieno[3,2-b]thiophen-2-yl)stannane

Thienothiophene (2.00 g, 14.3 mmol) and freshly distilled THF (20 mL) were added in a three-necked flask under argon atmosphere. After the system reaches to -78 °C, n- butyl lithium (5.72 mL, 2.5 M in hexane, 14.3 mmol) was added dropwise and the solution was stirred for 1 hour while the temperature was maintained at - 78 °C. Tributyltin chloride (4.64 mL, 15.1 mmol) was added drop wise. The mixture was

maintained at -78°C for 4 hours then allowed to reach room temperature. The mixture was stirred for another 24 hours. After evaporation of solvent under reduced pressure, distilled water was poured into the crude product and the product was extracted with diethyl ether. The organic layer was dried over anhydrous MgSO_4 . Through removal of solvent by rotary evaporation, a purple liquid was obtained. Yield: 61 %

^1H NMR (400 MHz, CDCl_3): δ 7.27 (d, $J = 5.2$ Hz, 1H), 7.19 (s, 1H), 7.16 (d, $J = 5.1$ Hz, 1H), 1.52 (q, $J = 7.2$ Hz, 6H), 1.27 (m, 6H), 1.07 (t, $J = 8.3$ Hz, 9H)

^{13}C NMR (100 MHz, CDCl_3): δ 134.4, 126.9, 126.6, 119.0, 28.96, 22.27, 13.66, 10.93

Two carbons in the aromatic region may overlap.

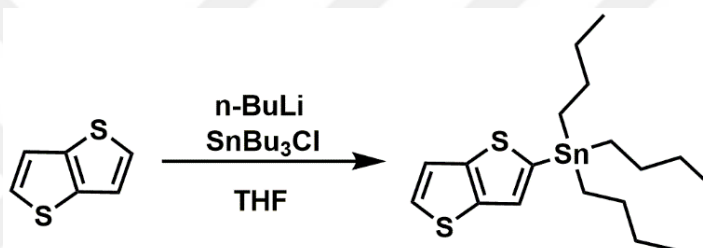


Figure 2.12. Synthetic route of tributyl(thieno[3,2-*b*]thiophen-2-yl)stannane

2.3.13. Synthesis of 5,6-bis(octyloxy)-4,7-bis(thieno[3,2-*b*]thiophen-2-yl)benzo[*c*][1,2,5]selenadiazole

4,7-Dibromo-5,6-bis(octyloxy)benzo[*c*][1,2,5]selenadiazole (0.40 g, 0.67 mmol), tributyl(thieno[3,2-*b*]thiophen-2-yl)stannane (1.15 g, 2.68 mmol) and $\text{PdCl}_2(\text{PPh}_3)_2$ (2.35 mg, 0.03 mmol) were dissolved in a 15 mL of anhydrous THF. The reaction mixture was heated to reflux and stirred under argon atmosphere until starting material ran out. The solution was concentrated on rotary evaporator and the compound was purified by column chromatography using 1:1 Hexane: DCM to afford the product as a dark red solid. Yield: 65 %

^1H NMR (400 MHz, CDCl_3): δ 8.60 (d, J = 4.0 Hz, 2H), 8.12 (d, J = 5.8 Hz, 2H), 7.41 (s, 2H), 4.02 (t, J = 7.1 Hz, 2H), 2.00-1.75 (m, 4H), 1.29 (dd, J_1 = 8.5 Hz, J_2 = 5.6 Hz, 22H), 0.81 (t, J = 6.8 Hz, 6H)

^{13}C NMR (100 MHz, CDCl_3): δ 155.3, 151.1, 137.7, 132.4, 131.9, 128.4, 119.0, 72.23, 30.79, 29.45, 28.48, 28.24, 24.92, 21.64, 13.09

Quaternary carbon peaks around 93.0 ppm are missing.

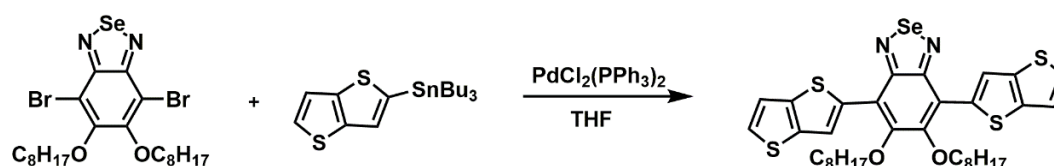


Figure 2.13. Synthetic route of 5,6-bis(octyloxy)-4,7-bis(thieno[3,2-*b*]thiophen-2-yl)benzo[*c*][1,2,5]selenadiazole

2.3.14. Synthesis of 5,6-bis(octyloxy)-4,7-di(selenophen-2-yl)benzo[*c*][1,2,5]selenadiazole

4,7-Dibromo-5,6-bis(octyloxy)benzo[*c*][1,2,5]selenadiazole (0.40 g, 0.67 mmol), tributyl(selenophen-2-yl)stannane (1.15 g, 2.68 mmol) and $\text{PdCl}_2(\text{PPh}_3)_2$ (2.35 mg, 0.03 mmol) were dissolved in a 15 mL of anhydrous THF. The reaction mixture was heated to reflux and stirred under argon atmosphere until starting material ran out. The solution was concentrated on rotary evaporator and the compound was purified by column chromatography using 4:1 Hexane: DCM to afford the product as a dark red solid. Yield: 70 %

^1H NMR (400 MHz, CDCl_3): δ 8.61 (d, J = 4.0 Hz, 2H), 8.14 (d, J = 5.8 Hz, 2H), 7.39 (dd, J_1 = 5.7 Hz, J_2 = 4.0 Hz, 2H), 4.03 (t, J = 7.1 Hz, 4H), 1.97-1.74 (m, 4H), 1.51-1.00 (m, 20H), 0.82 (t, J = 6.8 Hz, 6H)

^{13}C NMR (100 MHz, CDCl_3): δ 156.4, 152.2, 138.8, 133.4, 132.9, 129.5, 120.0, 74.29, 31.84, 30.56, 29.52, 29.28, 25.97, 22.69, 14.13

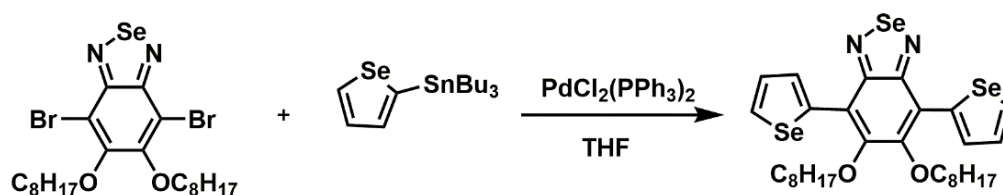


Figure 2.14. Synthetic route of 5,6-bis(octyloxy)-4,7-di(selenophen-2-yl)benzo[c][1,2,5]selenadiazole

2.3.15. Synthesis of 4,7-di(furan-2-yl)-5,6-bis(octyloxy)benzo[c][1,2,5]selenadiazole

4,7-Dibromo-5,6-bis(octyloxy)benzo[c][1,2,5]selenadiazole (0.40 g, 0.67 mmol), tributyl(furan-2-yl)stannane (1.15 g, 2.68 mmol) and $\text{PdCl}_2(\text{PPh}_3)_2$ (2.35 mg, 0.03 mmol) were dissolved in a 15 mL of anhydrous THF. The reaction mixture was heated to reflux and stirred under argon atmosphere until starting material ran out. The solution was concentrated on rotary evaporator and the compound was purified by column chromatography using 4:1 Hexane: DCM to afford the product as a green solid. Yield: 50 %

^1H NMR (400 MHz, CDCl_3): δ 8.62 (dd, $J_1 = 4.0$ Hz, $J_2 = 0.9$ Hz, 2H), 8.15 (dd, $J_1 = 5.8$ Hz, $J_2 = 0.9$ Hz, 2H), 7.39 (dd, $J_1 = 5.8$ Hz, $J_2 = 4.1$ Hz, 2H), 4.03 (t, $J = 7.1$ Hz, 4H), 1.89-1.80 (m, 4H) 1.40-1.33 (m, 10H), 1.29-1.18 (m, 10H), 0.82 (t, $J = 6.9$ Hz, 6H)

^{13}C NMR (100 MHz, CDCl_3): δ 156.4, 152.1, 138.8, 133.5, 132.9, 129.5, 120.0, 74.29, 31.84, 30.56, 29.52, 29.28, 25.96, 22.69, 14.13

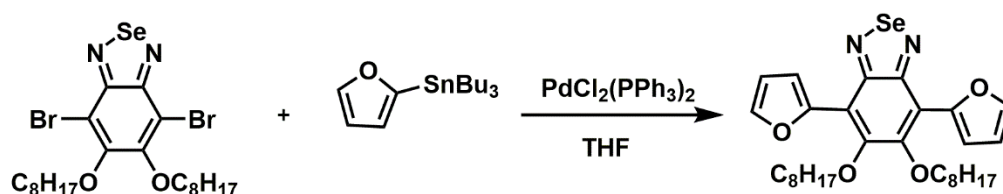


Figure 2.15. Synthetic route of 4,7-di(furan-2-yl)-5,6-bis(octyloxy)benzo[c][1,2,5]selenadiazole

2.3.16. Synthesis of tributyl(selenophen-2-yl)stannane

Selenophene (2.50 g, 19.1 mmol) and freshly distilled THF (50 mL) were mixed in a three-necked flask under argon atmosphere. The system was cooled to -78 °C then, *n*-butyl lithium (15.3 mL, 2.5 M in hexane, 38.3 mmol) was added dropwise. Tributyltin chloride (12.4 mL, 45.8 mmol) was added drop wise while the system was maintained at -78 °C for 1 hour. After the addition of tributyltin chloride completed, the mixture was stirred at -78 °C for 4 hours. The mixture was stirred for overnight at room temperature. Through removal of solvent under reduced pressure, dichloromethane was poured into the crude product and organic layer was washed with NaHCO₃, water and brine. The organic layers were combined and dried over anhydrous MgSO₄. After removal of solvent, a yellow liquid was obtained and used without further purification. Yield: 63 %

¹H NMR (400 MHz, CDCl₃): δ 8.28 (d, *J* = 4.7 Hz, 1H), 7.44 (t, *J* = 3.5 Hz, 1H), 7.42 (d, *J* = 4.4 Hz, 1H), 1.50 (q, *J* = 6.9 Hz, 6H), 1.28 (m, 6H), 1.03 (t, *J* = 8.3 Hz, 9H)

¹³C NMR (100 MHz, CDCl₃): δ 143.6, 137.9, 135.3, 130.6, 28.99, 27.29, 13.67, 11.13

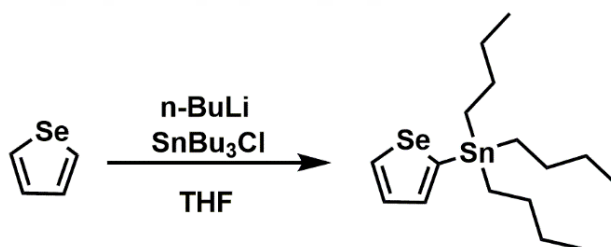


Figure 2.16. Synthetic route of tributyl(selenophen-2-yl)stannane

2.3.17. Synthesis of 5,6-bis(octyloxy)-4,7-di(thieno[3,2-*b*]thiophen-2-yl)benzo[*c*][1,2,5]oxadiazole

4,7-Dibromo-5,6-bis(octyloxy)benzo[*c*][1,2,5]oxadiazole (0.75 g, 1.40 mmol), tributyl(thieno[3,2-*b*]thiophen-2-yl)stannane (1.83 g, 4.20 mmol) and PdCl₂(PPh₃)₂ (49 mg, 0.07 mmol) were dissolved in a 40 mL of anhydrous THF. The reaction

mixture was heated to reflux and stirred under argon atmosphere for 48 hours. The product was concentrated on rotary evaporator and purified by column chromatography using 5:1 Hexane: DCM to afford the product as a red solid. Yield: 66 %

^1H NMR (400 MHz, CDCl_3): δ 8.65 (s, 2H), 7.42 (d, $J=5.2$ Hz, 2H), 7.26 (d, $J=5.2$ Hz, 2H), 4.12 (t, $J=7.3$ Hz, 4H), 1.98 (q, $J=7.5$ Hz, 4H), 1.44-1.23 (m, 20H), 0.83 (t, $J=6.6$ Hz, 6H)

^{13}C NMR (100 MHz, CDCl_3): δ 142.0, 139.6, 135.0, 129.1, 123.1, 119.4, 113.6, 74.91, 31.83, 30.30, 29.54, 29.31, 25.89, 22.69, 14.12

Two carbons which belong to thienothiophene unit may overlap.

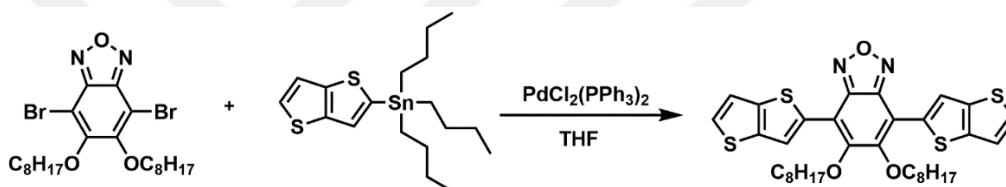


Figure 2.17. Synthetic route of 5,6-bis(octyloxy)-4,7-di(thieno[3,2-*b*]thiophen-2-yl)benzo[*c*][1,2,5]oxadiazole

2.3.18. Synthesis of 3,3'-(4,5-bis(octyloxy)-1,2-phenylene)dithiophene (NDT-Pre)

1,2-Dibromo-4,5-bis(octyloxy)benzene (2.52 g, 5.12 mmol), 3-thienylboronic acid (1.96 g, 15.4 mmol) were added in a two neck round bottom flask kept under inert atmosphere for 1 hour. $\text{Pd}(\text{PPh}_3)_4$ (354 mg, 0.31 mmol), Aliquat 336 (2-3 drops) and K_2CO_3 (2M, 30.8 mL) were added and dissolved in freshly distilled toluene (50 mL) under inert atmosphere. The mixture was heated to 85 °C. After 48 hours, solvent was evaporated under reduced pressure. Ethyl acetate was added to the crude product. Organic layer was washed with water and brine several times to remove alkali residue. Organic phase was dried over MgSO_4 . After removal of the solvent, the product was purified by column chromatography on silica gel (3:1 Hexane: DCM) to obtain white solid. Yield: 70 %

^1H NMR (400 MHz, CDCl_3): δ 8.65 (s, 2H), 7.42 (d, $J = 5.2$ Hz, 2H), 7.26 (d, $J = 5.2$ Hz, 2H), 4.12 (t, $J = 7.3$ Hz, 4H), 1.98 (q, $J = 7.5$ Hz, 4H), 1.44-1.23 (m, 20H), 0.83 (t, $J = 6.6$ Hz, 6H)

^{13}C NMR (100 MHz, CDCl_3): δ 142.0, 139.6, 135.0, 129.1, 123.1, 119.4, 113.6, 74.91, 31.83, 30.30, 29.54, 29.31, 25.89, 22.69, 14.12

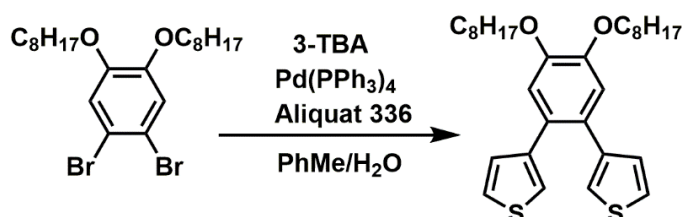


Figure 2.18. Synthetic route of 3,3'-(4,5-bis(octyloxy)-1,2-phenylene)dithiophene (NDT-Pre)

2.3.19. Synthesis of 5,6-bis(octyloxy)naphtho[2,1-*b*:3,4-*b'*]dithiophene (NDT)

3,3'-(4,5-Bis(octyloxy)-1,2-phenylene) dithiophene (500 mg, 1.00 mmol) was dissolved in anhydrous DCM (30 mL) in a three neck round bottom flask. In another flask kept under argon atmosphere, anhydrous iron (III) chloride (406 mg, 2.50 mmol) was dissolved in anhydrous acetonitrile (7.5 mL). The prepared acidic solution was added dropwise and the mixture was stirred for 1 hour at room temperature. Later, methanol (7.5 mL) was added to the mixture and further stirred for 30 min. After evaporation of solvent, the crude product was dissolved in DCM. Organic layer was washed with aqueous NH_4Cl several times and dried over MgSO_4 . Column chromatography on silica gel was (2:1 Hexane: Chloroform) used to obtain the product as a white solid. Yield: 60 %

^1H NMR (400 MHz, CDCl_3): δ 7.08 (dd, $J_1 = 3.0$ Hz, $J_2 = 4.9$ Hz, 2H), 6.93 (dd, $J_1 = 1.2$ Hz, $J_2 = 3.0$ Hz, 2H), 6.69 (dd, $J_1 = 1.2$ Hz, $J_2 = 3.0$ Hz, 2H), 3.96 (t, $J = 6.6$ Hz, 4H), 1.76 (q, $J = 6.9$ Hz, 4H), 1.44-1.18 (m, 20H), 0.81 (t, $J = 6.8$ Hz, 6H)

^{13}C NMR (100 MHz, CDCl_3): δ 148.4, 142.1, 129.1, 128.0, 124.5, 122.3, 115.8, 69.51, 31.86, 29.40, 29.35, 29.32, 26.07, 22.70, 14.13

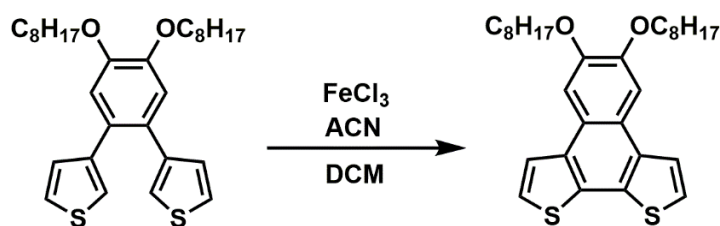


Figure 2.19. Synthetic route of 5,6-bis(octyloxy)naphtho[2,1-*b*:3,4-*b'*]dithiophene (NDT)

2.3.20. Synthesis of 4,7-dibromobenzo[*c*][1,2,5]oxadiazole

Benzo[*c*][1,2,5]oxadiazole (2.50 g, 20.8 mmol) and iron dust (233 mg, 4.16 mmol) were mixed at 90 °C in a two neck flask. After melting, bromine (3.38 mL, 66.0 mmol) was added dropwise to the heterogeneous solution. The solution was stirred for 2 hours. Then, distilled water and NaHCO₃ solution were added to the mixture. After additional stirring for 1 hour, the precipitate was filtered. Column chromatography (3:1 Chloroform: Hexane) was used to obtain pure compound as a pale yellow solid. Yield: 55 %

¹H NMR (400 MHz, CDCl₃): δ 7.45 (s, 2H)

¹³C NMR (100 MHz, CDCl₃): δ 134.2, 108.7

Quaternary carbon around 140 ppm could not be observed.

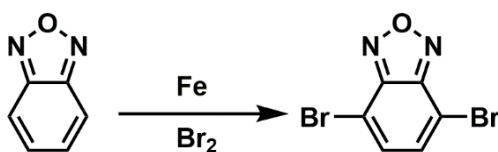


Figure 2.20. Synthetic route of 4,7-dibromobenzo[*c*][1,2,5]oxadiazole

2.3.21. Synthesis of 5,6-bis(octyloxy)-4,7-di(selenophen-2-yl)benzo[c][1,2,5]oxadiazole

4,7-Dibromo-5,6-bis(octyloxy)benzo[c][1,2,5]oxadiazole (0.75 g, 1.40 mmol) and tributyl(selenophen-2-yl)stannane (1.78 g, 4.20 mmol) were dissolved in anhydrous THF (35 mL). The reaction mixture was heated to reflux under argon atmosphere for 1 hour and then $\text{PdCl}_2(\text{PPh}_3)_2$ (49.0 mg, 0.07 mmol) was added. The mixture was stirred under inert atmosphere at 125 °C for 48 hours. The solvent was removed on rotary evaporator and the crude product was purified by column chromatography (4 Hexane: 1 Chloroform) to afford orange crystalline solid. Yield: 81 %

^1H NMR (400 MHz, CDCl_3): δ 8.71 (d, $J = 4.6$ Hz, 2H), 8.16 (d, $J = 5.7$ Hz, 2H), 7.41 (dd, $J_1 = 4.9$ Hz, $J_2 =$ Hz, 2H), 4.10 (t, $J = 7.5$ Hz, 4H), 1.95 (q, $J = 7.4$ Hz, 4H), 1.41-1.27 (m, 20H) 0.83 (t, $J = 6.6$ Hz, 6H)

^{13}C NMR (100 MHz, CDCl_3): δ 135.5, 132.7, 132.2, 128.9, 73.75, 30.78, 29.52, 28.49, 28.23, 24.81, 21.63, 13.07

HR-MS (ESI) for $\text{C}_{30}\text{H}_{40}\text{N}_2\text{O}_3\text{Se}_2$ calculated 636.1369 found 636.1354

Three carbons around 126.0 and 103.0 ppm are difficult to see therefore they could not be observed.

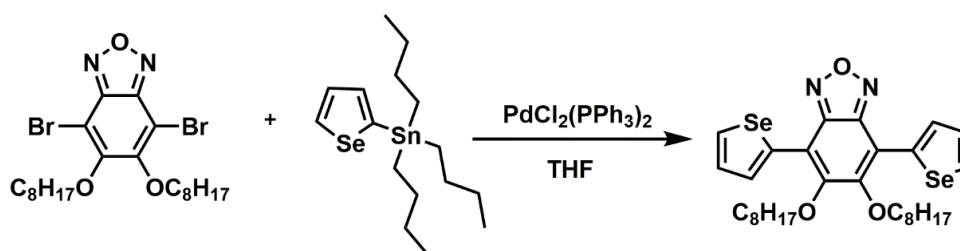


Figure 2.21. Synthetic route of 5,6-bis(octyloxy)-4,7-di(selenophen-2-yl)benzo[c][1,2,5]oxadiazole

2.3.22. Synthesis of 4,7-bis(5-bromothieno[3,2-*b*]thiophen-2-yl)-5,6-bis(octyloxy)benzo[*c*][1,2,5]oxadiazole

5,6-Bis(octyloxy)-4,7-di(thieno[3,2-*b*]thiophen-2-yl)benzo[*c*][1,2,5]oxadiazole (200 mg, 0.31 mmol), N- bromosuccimide (NBS) (137 mg, 0.77 mmol), glacial acetic acid (10 mL), and chloroform (10 mL) were stirred at room temperature for 24 hours in the dark. After solvent removal under reduced pressure, chloroform was poured into the product and the mixture was washed with NaHCO₃ and water. After evaporation of solvent, the product was recrystallized from cold ethanol to afford orange-red crystal. Yield: 85 %

¹H NMR (400 MHz, CDCl₃): δ 8.56 (s, 2H), 7.29 (s, 2H), 4.17 (t, *J* = 7.3 Hz, 4H), 2.17-1.93 (m, 4H), 1.54-1.15 (m, 20H), 0.90 (t, *J* = 6.9 Hz, 6H)

¹³C NMR (100 MHz, CDCl₃): δ 151.6, 146.3, 140.6, 139.7, 134.2, 122.5, 122.1, 115.6, 113.3, 74.91, 31.82, 30.29, 29.53, 25.86, 22.68, 14.11

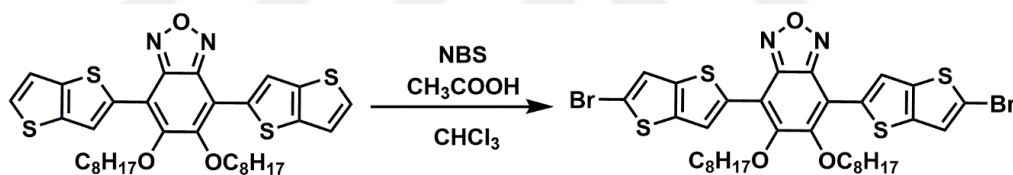


Figure 2.22. Synthetic route of 4,7-bis(5-bromothieno[3,2-*b*]thiophen-2-yl)-5,6-bis(octyloxy)benzo[*c*][1,2,5]oxadiazole

2.3.23. Synthesis of 4,7-bis(5-bromoselenophen-2-yl)-5,6-bis(octyloxy)benzo[*c*][1,2,5]oxadiazole

5,6-Bis(octyloxy)-4,7-di(selenophen-2-yl)benzo[*c*][1,2,5]oxadiazole (200 mg, 0.32 mmol), N- bromosuccimide (NBS) (112 mg, 0.63 mmol), glacial acetic acid (8 mL), and chloroform (8 mL) were stirred at room temperature for 24 hours in the dark. The solvent was removed using rotary evaporator under reduced pressure. The product was afforded as a red crystalline solid after recrystallization from cold methanol. Yield: 70 %

^1H NMR (400 MHz, CDCl_3): δ 8.41 (d, J = 4.4 Hz, 2H), 7.33 (d, J = 4.4 Hz, 2H), 4.09 (t, J = 7.5 Hz, 4H), 1.94 (q, J = 8.0 Hz, 4H), 1.40-1.19 (m, 20H) 0.83 (t, J = 6.6 Hz, 6H)

^{13}C NMR (100 MHz, CDCl_3): δ 149.6, 144.8, 136.9, 132.3, 132.0, 119.5, 113.5, 74.05, 30.78, 29.87, 28.45, 28.24, 24.73, 21.66, 13.09

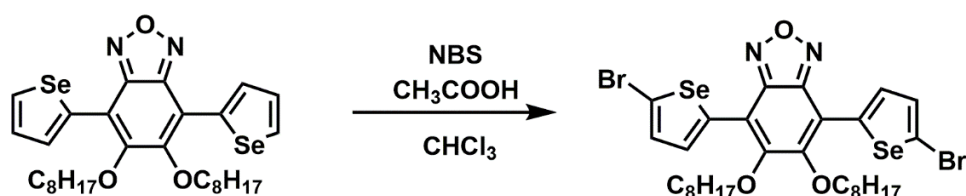


Figure 2.23. Synthetic route of 4,7-bis(5-bromoselenophen-2-yl)-5,6-bis(octyloxy)benzo[c][1,2,5]oxadiazole

2.3.24. Synthesis of 5,6-bis(octyloxy)-4,7-di(furan-2-yl)benzo[c][1,2,5]oxadiazole

4,7-Dibromo-5,6-bis(octyloxy)benzo[c][1,2,5]oxadiazole (0.83 g, 1.57 mmol) and tributyl(furan-2-yl)stannane (1.65 g, 4.71 mmol) were dissolved in anhydrous THF (25 mL). The reaction mixture was heated to reflux under argon atmosphere for 1h and then $\text{PdCl}_2(\text{PPh}_3)_2$ (90.0 mg, 0.13 mmol) was added. The mixture was stirred under inert atmosphere at 125 °C for 50 hours. The product was concentrated on rotary evaporator and the crude product was purified by column chromatography using 3 DCM:1 Hexane to afford dark green solid. Yield: 94 %

^1H NMR (400 MHz, CDCl_3): δ 7.62 (d, J =1.7 Hz, 2H), 7.33 (d, J = 3.4 Hz, 2H), 6.57 (dd, J_1 =3.4 Hz, J_2 =1.8 Hz, 2H), 4.04 (t, J = 6.9 Hz, 4H), 1.83 (q, J = 7.0 Hz, 4H), 1.41(m, 4H), 1.30-1.22 (m, 16H), 0.82 (t, J =6.8 Hz, 6H)

^{13}C NMR (100 MHz, CDCl_3): δ 152.3, 146.7, 145.7, 143.5, 114.0, 111.9, 109.4, 74.78, 31.81, 30.36, 29.46, 29.27, 26.00, 22.65, 14.08

HR-MS (ESI) for $\text{C}_{30}\text{H}_{40}\text{N}_2\text{O}_5$, calculated 508.2937, found 508.2920

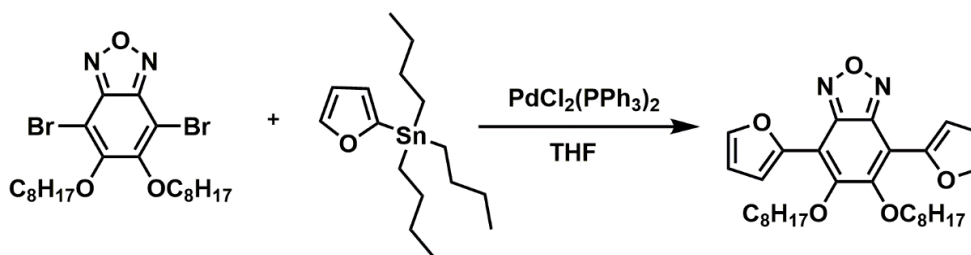


Figure 2.24. Synthetic route of 5,6-bis(octyloxy)-4,7-di(furan-2-yl)benzo[c][1,2,5]oxadiazole

2.3.25. Synthesis of 4,7-bis(5-bromofuran-2-yl)-5,6-bis(octyloxy)benzo[c][1,2,5]oxadiazole

4,7-Di(furan-2-yl)-5,6-bis(octyloxy)benzo[c][1,2,5]oxadiazole (200 mg, 0.39 mmol), N-bromosuccinimide (NBS) (175 mg, 0.98 mmol), glacial acetic acid (14 mL), and chloroform (14 mL) were stirred at room temperature overnight in the dark. The solvent was removed using rotary evaporator under reduced pressure. The product was purified via recrystallization from cold ethanol and afforded as a yellow solid. Yield: 80 %

^1H NMR (400 MHz, CDCl_3): δ 7.32 (d, J = 3.5 Hz, 2H), 6.49 (d, J = 3.5 Hz, 2H), 4.05 (t, J = 6.8 Hz, 6H), 1.87 (m, 4H), 1.44-1.24 (m, 20H), 0.83 (t, J = 6.6 Hz, 6H)

^{13}C NMR (100 MHz, CDCl_3): δ 152.5, 148.5, 145.2, 116.6, 113.9, 108.6, 75.26, 31.84, 30.29, 29.56, 29.27, 26.07, 22.67, 14.09

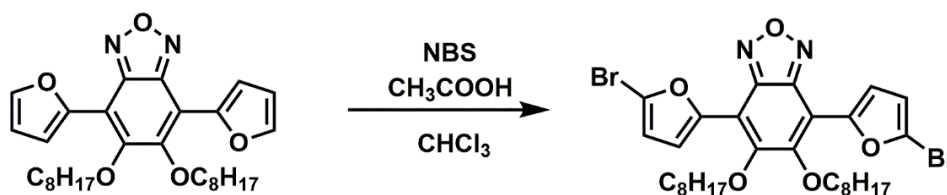


Figure 2.25. Synthetic route of 4,7-bis(5-bromofuran-2-yl)-5,6-bis(octyloxy)benzo[c][1,2,5]oxadiazole

2.3.26. Synthesis of (E)-6,6'-bis(thieno[3,2-*b*]thiophen-2-yl)-1,1'-diundecyl-[3,3'-biindolinylidene]-2,2'-dione

In a 50 mL flask, (E)-6,6'-dibromo-1,1'-diundecyl-[3,3'-biindolinylidene]-2,2'-dione (1.61 g, 2.21 mmol) and tributyl(thieno[3,2-*b*]thiophen-2-yl)stannane (3.80 g, 8.85 mmol) were dissolved in anhydrous THF (30 mL) and then PdCl₂(PPh₃)₂ (93 mg, 0.13 mmol) was added to the solution under argon atmosphere. The mixture was stirred under inert atmosphere at 85 °C for 30 hours. The solvent was evaporated using rotary evaporator and the crude product was purified by column chromatography to afford dark purple solid. Yield: 38 %

¹H NMR (400 MHz, CDCl₃): δ 9.12 (d, *J* = 8.4 Hz, 2H), 7.55 (s, 2H), 7.35 (d, *J* = 5.2 Hz, 2H), 6.91 (s, 2H), 3.76 (t, *J* = 7.3 Hz, 4H), 1.94-1.56 (m, 4H), 1.28 (d, *J* = Hz, 32H), 0.79 (t, *J* = Hz, 6H)

¹³C NMR (100 MHz, CDCl₃): δ 165.8, 143.5, 142.9, 137.9, 137.0, 135.8, 129.5, 128.1, 125.7, 119.0, 117.3, 116.8, 114.1, 102.1, 37.74, 29.56, 27.27, 27.20, 27.00, 25.93, 25.23, 24.73, 24.43, 20.34, 14.95

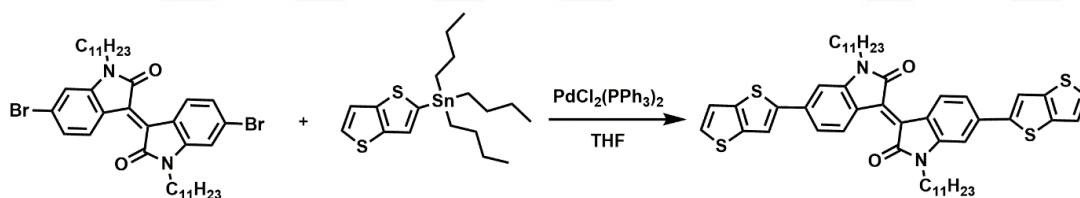


Figure 2.26. Synthetic route of (E)-6,6'-bis(thieno[3,2-*b*]thiophen-2-yl)-1,1'-diundecyl-[3,3'-biindolinylidene]-2,2'-dione

2.3.27. Synthesis of 5-(2-ethylhexyl)-1,3-bis(thieno[3,2-*b*]thiophen-2-yl)-4H-thieno[3,4-*c*]pyrrole-4,6(5H)-dione

In a 30 mL flask, 1,3-dibromo-5-(2-ethylhexyl)-4H-thieno[3,4-*c*]pyrrole-4,6(5H)-dione (200 mg, 0.47 mmol) and tributyl(thieno[3,2-*b*]thiophen-2-yl)stannane (812 mg, 1.89 mmol) were dissolved in anhydrous toluene (10 mL) and then Pd(PPh₃)₄ (27.3 mg, 0.03 mmol) was added to the solution under argon atmosphere. The mixture was stirred under inert atmosphere at 90 °C for 18 hours. The solvent was evaporated using

rotary evaporator and the crude product was purified by column chromatography to afford orange solid. Yield:

^1H NMR (400 MHz, CDCl_3): δ 8.30 (s, 2H), 7.41 (d, $J = 5.2$ Hz, 2H), 7.15 (d, $J = 5.2$ Hz, 2H), 3.48 (d, $J = 7.3$ Hz, 2H), 2.03-1.59 (m, 5H), 1.56-0.68 (m, 8H), 0.87 (t, $J = 6.6$ Hz, 3H), 0.83 (t, $J = 6.8$ Hz, 3H)

^{13}C NMR (100 MHz, CDCl_3): δ 162.9, 141.0, 140.3, 136.9, 133.8, 130.3, 128.7, 122.3, 119.4, 42.56, 38.39, 28.68, 23.07, 14.12, 10.49

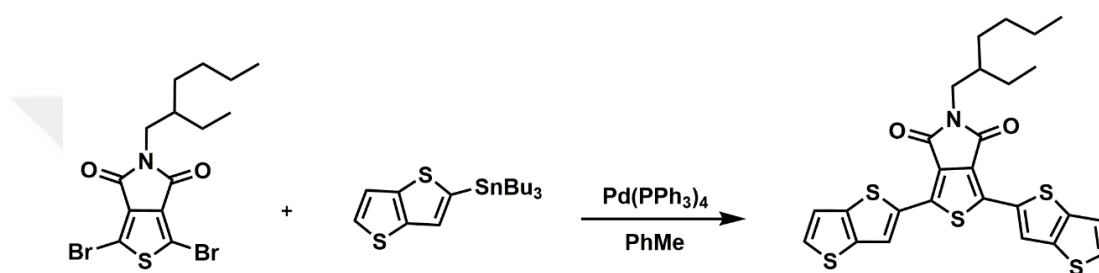


Figure 2.27. Synthetic route of 5-(2-ethylhexyl)-1,3-bis(thieno[3,2-*b*]thiophen-2-yl)-4H-thieno[3,4-*c*]pyrrole-4,6(5H)-dione

2.3.28. Synthesis of 4-methylbenzo[*c*][1,2,5]thiadiazole

2,3-Diaminotoluene (500 mg, 4.09 mmol) was dissolved in anhydrous DCM (20.5 mL). The solution was cooled to 0 °C for 15 min. Triethylamine (2.30 mL, 16.4 mmol) was slowly added to the solution. Thionyl chloride (0.60 mL, 8.20 mmol) was firstly dissolved in anhydrous DCM (6.75 mL) and then added dropwise to the solution at 0 °C. The reaction mixture was stirred for 1 hour at 0 °C under argon atmosphere. Then, the solution was heated to 40 °C for 15 hours. After cooling to room temperature 2N HCl (7 mL) was added to the solution. Organic phase was extracted using DCM and washed with brine, distilled water and dried over MgSO_4 . After filtration, the product was concentrated on rotary evaporator and the crude product was purified by column chromatography to afford colorless liquid. Yield: 66 %

^1H NMR (400 MHz, CDCl_3): δ 7.66 (d, J = 8.8 Hz, 1H), 7.45-7.25 (m, 1H), 7.15 (s, 1H)

^{13}C NMR (100 MHz, CDCl_3): δ 155.4, 154.9, 131.6, 129.4, 127.8, 118.9, 17.84

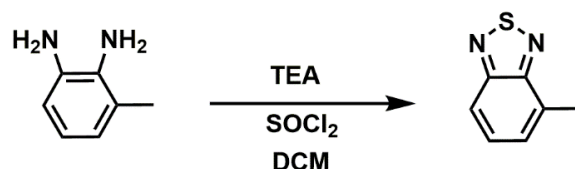


Figure 2.28. Synthetic route of 4-methylbenzo[c][1,2,5]thiadiazole

2.3.29. Synthesis of 4-bromo-7-methylbenzo[c][1,2,5]thiadiazole

4-Methylbenzo[c][1,2,5]thiadiazole (500 mg, 3.32 mmol) and 48 % HBr (12.5 mL) were stirred at room temperature in a two neck flask. Bromine (0.20 mL, 3.43 mmol) in 48 % HBr (12.5 mL) was added dropwise to the reaction medium. Then, the solution was heated to reflux for 16 hours. After cooling to room temperature, the mixture was poured into saturated sodium bisulfite solution to remove excess bromine. The mixture was stirred for 30 min and then extracted with dichloromethane. The combined organic layer was dried over anhydrous Na_2SO_4 , filtered, and then the solvent was evaporated under reduced pressure. The crude product was purified by column chromatography to afford compound as a white solid. Yield: 92 %

^1H NMR (400 MHz, CDCl_3): δ 7.63 (d, J = 7.3 Hz, 1H), 7.15 (d, J = 7.3 Hz, 1H), 2.61 (s, 3H)

^{13}C NMR (100 MHz, CDCl_3): δ 155.4, 154.9, 132.0, 131.2, 128.6, 111.2, 17.69

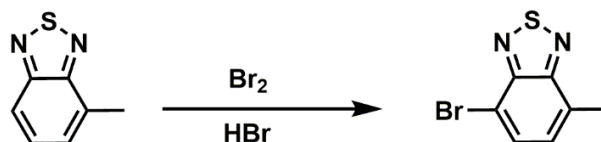


Figure 2.29. Synthetic route of 4-bromo-7-methylbenzo[c][1,2,5]thiadiazole

2.3.30. Synthesis of 4-bromo-7-dibromomethyl-2,1,3-benzothiadiazole

A mixture of 4-bromo-7-methylbenzo[c][1,2,5]thiadiazole (300 mg, 1.30 mmol), N-bromosuccinimide (477 mg, 2.68 mmol) and benzoyl peroxide (0.12 g, 0.48 mmol) were dissolved in chlorobenzene (5 mL) and stirred overnight at 80 °C. After cooling to room temperature, the succinimide precipitate was removed by filtration and water was added to the filtrate which was then extracted with dichloromethane and dried over MgSO₄. Column chromatography on silica gel (eluent: 1 Hexane: 1 DCM) followed by recrystallization from ethanol afforded the product as a white crystalline solid. Yield: 57 %

¹H NMR (400 MHz, CDCl₃) δ: 7.90 (d, *J*= 5.8 Hz, 1H), 7.85 (d, *J*= 5.0 Hz, 1H), 7.34 (s, 1H)

¹³C NMR (100 MHz, CDCl₃) δ: 155.4, 153.2, 132.0, 131.3, 129.6, 111.2, 33.86

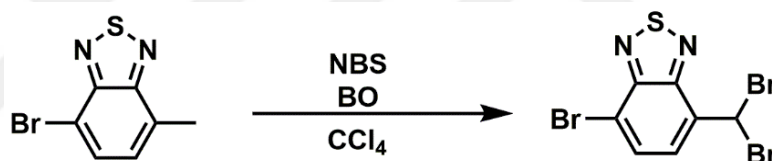


Figure 2.30. Synthetic route of 4-bromo-7-dibromomethyl-2,1,3-benzothiadiazole

2.3.31. Synthesis 7-bromobenzo[c][1,2,5]thiadiazole-4-carbaldehyde

4-Bromo-7-dibromomethyl-2,1,3-benzothiadiazole (300 mg, 0.78 mmol) was dissolved in 95 % formic acid (3 mL) and the solution refluxed at 110 °C. After 2 hours, the solution was cooled to room temperature and poured into water. The resulting precipitate was filtered and washed with water until the filtrate was of neutral pH, then the product was obtained as an off-white crystalline solid. Yield: 92 %

¹H NMR (400 MHz, CDCl₃) δ: 10.7 (s, 1H), 8.03 (d, *J*=5.7 Hz, 1H), 7.99 (d, *J*=5.7 Hz, 1H)

¹³C NMR (100 MHz, CDCl₃) δ: 188.4, 154.0, 152.4, 132.2, 131.7, 126.8, 121.9

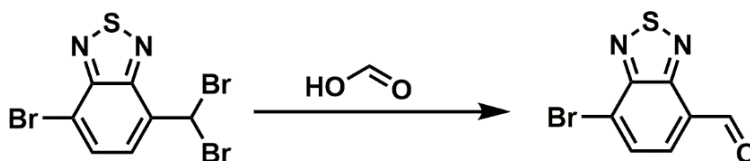


Figure 2.31. Synthetic route of 7-bromobenzo[c][1,2,5]thiadiazole-4-carbaldehyde

2.3.32. Synthesis of 2,5-dibromoterephthalic acid

In a three-neck flask, 2,5-dibromo-p-xylene (5.00 g, 0.019 mol), celite (7.50 g) and a mixture of water/ tert-butanol (50/50 mL) were added. KMnO_4 (15.0 g, 0.10 mol) was added to the suspension in portions within 30 min. The mixture was stirred at 100 °C for 36 hours. After cooling to 70 °C, ethanol (20 mL) was added slowly to remove unreacted KMnO_4 . The mixture was filtered off and the filtrate was concentrated to 20 mL under reduced pressure. Concentrated HCl (5 mL) was added to the residue and the precipitate was collected by filtration and washed with cold ethanol to obtain the product as a white solid. Yield: 80 %. The product was directly used in the next step without further purification.

^1H NMR (400 MHz, d-DMSO) δ : 13.96 (s, 2H), 8.02 (s, 2H)

^{13}C NMR (100 MHz, d-DMSO) δ : 165.6, 137.0, 134.9, 118.8

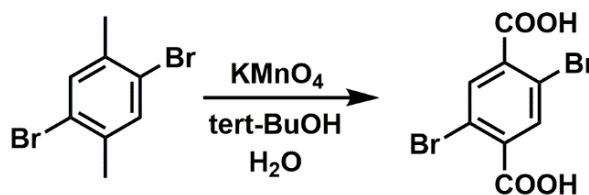


Figure 2.32. Synthetic route of 2,5-dibromoterephthalic acid

2.3.33. Synthesis of diethyl 2,5-dibromoterephthalate

To a solution of 2,5-dibromoterephthalic acid (2.50 g, 0.01 mol) in absolute ethanol (13 mL) was added concentrated H_2SO_4 (4 mL). The mixture was refluxed overnight

before being cooled to room temperature. The precipitate was collected by filtration and further purified by recrystallization from cold ethanol to obtain the product as a white solid. Yield: 91 %

^1H NMR (400 MHz, d-DMSO) δ : 8.01 (s, 2H), 4.35 (q, J = 7.1 Hz, 4H), 1.33 (t, J = 7.0 Hz, 6H)

^{13}C NMR (100 MHz, d-DMSO) δ : 163.9, 136.2, 135.1, 119.0, 62.17, 13.86

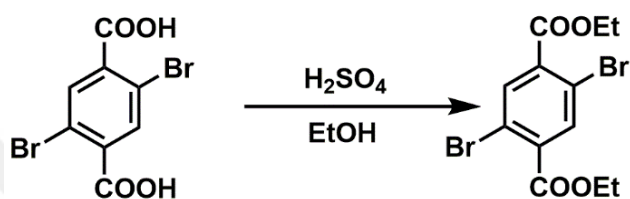


Figure 2.33. Synthetic route of diethyl 2,5-dibromoterephthalate

2.3.34. Synthesis of diethyl 2,5-di(thiophen-2-yl)terephthalate

2-(Tributylstannyl)thiophene (5.08 g, 13.6 mmol) was added to a solution of diethyl 2,5-dibromoterephthalate (1.50 g, 4.53 mmol) and $\text{PdCl}_2(\text{PPh}_3)_2$ (160 mg, 0.23 mmol) in anhydrous toluene (45 mL) under argon atmosphere. The reaction mixture was stirred at 85 °C for 40 h before being cooled to room temperature. The mixture was treated with potassium fluoride aqueous solution (10 wt. %, 20 mL) for 2 h. The product was extracted with dichloromethane three times and the combined organic phases were washed with water three times and then dried over MgSO_4 . After filtration, the solvent was removed under reduced pressure. The residue was purified by silica gel chromatography (eluent: hexane/chloroform) to afford the product as a white solid. Yield: 30 %

^1H NMR (400 MHz, CDCl_3) δ : 7.75 (s, 2H), 7.32 (dd, J_1 = 4.7 Hz, J_2 = 1.5 Hz, 2H), 7.08-6.94 (m, 4H), 4.15 (q, J = 7.1 Hz, 4H), 1.08 (t, J = 7.1 Hz, 6H)

^{13}C NMR (100 MHz, CDCl_3) δ : 167.7, 140.5, 134.1, 131.9, 127.4, 127.0, 126.5, 61.67, 13.82

One carbon around 128.0 ppm may overlap.

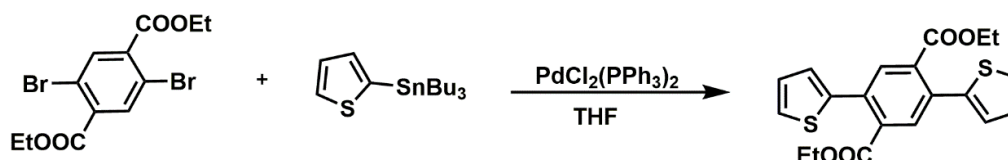


Figure 2.34. Synthetic route of diethyl 2,5-di(thiophen-2-yl)terephthalate

2.3.35. Synthesis of 2,5-di(thiophen-2-yl)terephthalic acid

Diethyl 2,5-di(thiophen-2-yl)terephthalate (200 mg, 0.52 mmol) was dissolved in 5 mL of ethanol. Potassium hydroxide (200 mg, 3.56 mmol) was dissolved in 8 mL of distilled water. The reaction mixture was stirred at 85 °C for 15 hours before being cooled to room temperature. The solvent was removed under vacuum. The residue was dissolved in hydrochloric acid and dried to afford the product as an off-white solid. Yield: 96 %

^1H NMR (400 MHz, $d\text{-DMSO}$) δ : 7.76 (s, 2H), 7.73 (d, J = 4.2 Hz, 2H), 7.32 (d, J = 3.5 Hz, 2H), 7.25-7.15 (m, 2H)

^{13}C NMR (100 MHz, $d\text{-DMSO}$) δ : 168.8, 139.6, 134.5, 131.4, 130.1, 127.9, 127.5, 127.1

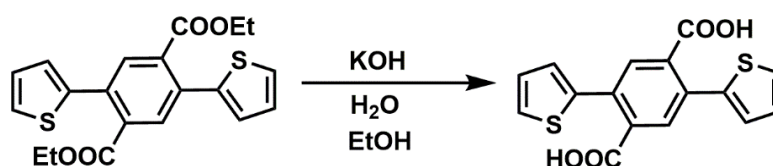


Figure 2.35. Synthetic route of 2,5-di(thiophen-2-yl)terephthalic acid

2.3.36. Synthesis of 5,6-difluorobenzo[c][1,2,5]oxadiazole 1-oxide

5,6-difluoro-2-nitroaniline (500 mg, 2.87 mmol) and potassium hydroxide (168 mg, 3.00 mmol) were dissolved in 2 mL ethanol which was kept in an ice bath. Then, dropwise addition of sodium hypochlorite solution (11-14 % available chlorine, 1.7 mL) was performed. The mixture was stirred for additional 10-20 minutes at room temperature. The orange precipitate was filtered and washed with distilled water. The solid was left to dry overnight and purified via column chromatography (eluent: DCM). The bright yellow solid compound was used without further purification. Yield: 63 %

^1H NMR (400 MHz, CDCl_3) δ : 8.04 (dd, $J_1 = 11.2$ Hz, $J_2 = 8.6$ Hz, 1H), 6.98 (dd, $J_1 = 12.7$ Hz, $J_2 = 7.3$ Hz, 1H)

^{13}C NMR (100 MHz, d-DMSO) δ : 144.6, 113.6, 105.5, 105.3

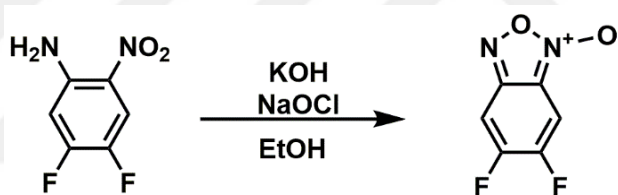


Figure 2.36. Synthetic route of 5,6-difluorobenzo[c][1,2,5]oxadiazole 1-oxide

2.3.37. Synthesis of 5,6-difluorobenzo[c][1,2,5]oxadiazole

5,6-difluorobenzo[c][1,2,5]oxadiazole 1-oxide (271 mg, 1.58 mmol) and triethylphosphite (0.34 mL, 1.63 mmol) were dissolved in 4.1 mL of anhydrous THF under inert atmosphere. The red solution was stirred overnight at 75 °C. After cooling to room temperature, the solvent was evaporated under vacuum. The dark red color residue was purified using column chromatography (eluent: DCM). The pure compound was obtained as a pale yellow solid. Yield: 55 %

^1H NMR (400 MHz, CDCl_3) δ : 7.32 (d, $J = 9.1$ Hz, 1H), 6.89 (d, $J = 7.4$ Hz, 1H)

^{13}C NMR (100 MHz, CDCl_3) δ : 99.01, 92.46

Removal of triethyl phosphate from the material could not be achieved successfully. Peaks of the material were observed in the NMR spectra.

One carbon around 147.0 ppm was missing.

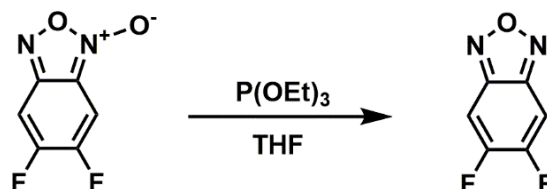


Figure 2.37. Synthetic route of 5,6-difluorobenzo[c][1,2,5]oxadiazole

2.3.38. Synthesis of 2-bromo-3,4-difluoro-6-nitroaniline

4,5-Difluoro-2-nitroaniline (1.00 g, 5.75 mmol) was dissolved in acetic acid (6 mL) at room temperature. Then, bromine (1.28 g, 8.00 mmol) was added drop wise at 50- 56 ° C, and the solution was stirred for 72 hours. The reaction mixture was poured into ice water. The resulting precipitate was collected by filtration and washed with water, NaHCO_3 and NaHSO_3 to quench bromine and residual acid. The yellow solid was dried under vacuum and used without further purification. Yield: 82 %

^1H NMR (400 MHz, CDCl_3) δ : 8.01 (dd, $J_1 = 10.3$ Hz, $J_2 = 8.2$ Hz, 1H), 6.62 (br, 2H)

^{13}C NMR (100 MHz, CDCl_3) δ : 152.0, 140.8, 113.7, 113.6, 113.4, 99.96, 99.75

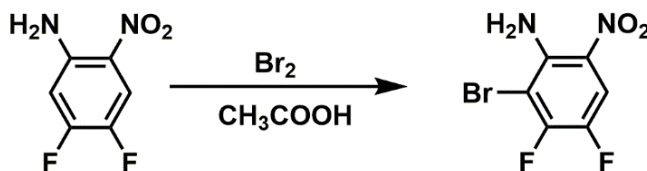


Figure 2.38. Synthetic route of 2-bromo-3,4-difluoro-6-nitroaniline

2.3.39. Synthesis of 4-bromo-5,6-difluorobenzo[c][1,2,5]oxadiazole 1-oxide

2-bromo-3,4-difluoro-6-nitroaniline (900 mg, 3.54 mmol) was dissolved in ethanol (5 mL) at 0 °C. Sodium hypochlorite solution (10-15 % chlorine available, 3.55 mL) was added dropwise to the reaction medium. Precipitation was observed after 0.5 stirring. The red solid was filtered. Washing with excess distilled water was performed to remove residual base. The compound was dried under vacuum and used without purification. Yield: 60 %

^1H NMR and ^{13}C NMR could not be recorded due to instability of the material.

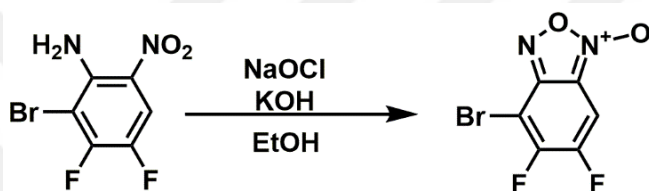


Figure 2.39. Synthetic route of 4-bromo-5,6-difluorobenzo[c][1,2,5]oxadiazole 1-oxide

2.3.40. Synthesis of 4-bromo-5,6-difluorobenzo[c][1,2,5]oxadiazole

4-bromo-5,6-difluorobenzo[c][1,2,5]oxadiazole 1-oxide (270 mg, 1.06 mmol) and triethyl phosphite (0.22 mL, 1.27 mmol) were dissolved in 2.9 mL anhydrous THF under argon atmosphere. After heating to reflux overnight, the solution was cooled to room temperature. Evaporation of solvent under vacuum gave a dark red color solid. The residue was purified using column chromatography (eluent: DCM). The pure compound was obtained as an orange solid. Yield: 45 %

^1H NMR (400 MHz, CDCl_3) δ : 7.45 (dd, $J_1 = 8.3$ Hz, $J_2 = 6.7$ Hz, 1H)

^{13}C NMR (100 MHz, CDCl_3) δ : 158.5, 155.9, 152.7, 147.2, 98.94, 92.42

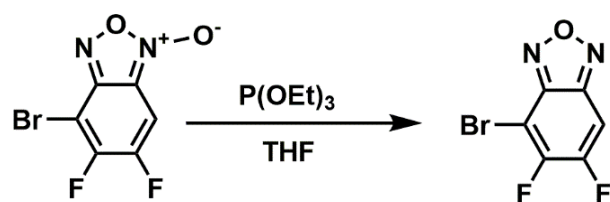


Figure 2.40. Synthetic route of -4-bromo-5,6-difluorobenzo[c][1,2,5]oxadiazole

2.3.41. Synthesis of 4-methylbenzo[c][1,2,5]oxadiazole 1-oxide

2-methyl-6-nitroaniline (300 mg, 1.97 mmol), and potassium hydroxide pellets (117 mg, 2.09 mmol) were dissolved in 1.6 mL ethanol and the solution was cooled to 0 °C in a two neck flask. Sodium hypochlorite solution (11-14 % chlorine available, 2.5 mL) was added drop wise to the reaction medium. A dark red solid compound precipitated after additional 2 hours stirring. The compound was filtered and washed with distilled water several times. After drying the compound overnight, a sticky reddish oil was obtained. However, NMR spectra of the crude product could not prove the successful synthesis.

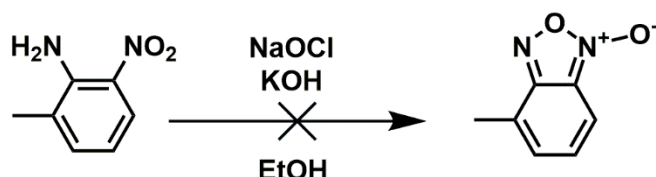


Figure 2.41. Synthetic route of 4-methylbenzo[c][1,2,5]oxadiazole 1-oxide

The synthesis was repeated using THF as the solvent under argon atmosphere to obtain the compound. Different reaction times were also tried. None of the syntheses worked for NFA starting material.

2.3.42. Synthesis of 2,5-dibromopyridine-3,4-diamine

3,4-Diaminopyridine (1.00 g, 9.16 mmol) was dissolved in 48 % HBr solution (7.5 mL) in a two neck flask. Br₂ (1.5 mL) was added drop wise. Then, the solution was heated to reflux for 16 hours. After cooling to room temperature, the solid precipitate was filtered and washed with Na₂SO₄, NaHCO₃ and water, respectively. The product was used directly without further purification. Yield: 55 %

¹H NMR (400 MHz, d-DMSO) δ: 7.52 (s, 1H), 5.99 (s, 1H), 5.05 (br, 2H)

¹³C NMR (100 MHz, d-DMSO) δ: 139.2, 138.4, 128.8, 125.9, 104.5

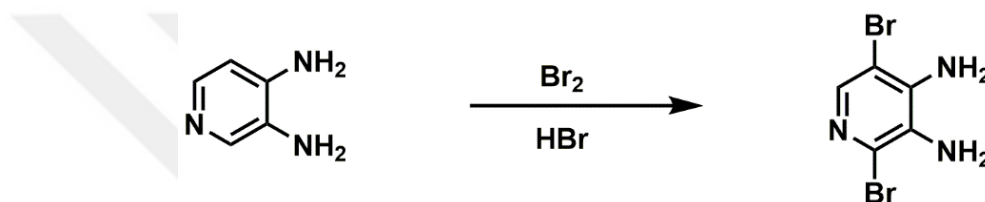


Figure 2.42. Synthetic route of 2,5-dibromopyridine-3,4-diamine

2.3.43. Synthesis of 1,2-bis(3,4-bis(octyloxy)phenyl)ethane-1,2-dione

1,2-Bis(octyloxy)benzene (2.00 g, 5.97 mmol), AlCl₃ (1.20 g, 8.97 mmol) and urea (351 mg, 5.85 mmol) were dissolved in anhydrous DCM (4 mL) under inert atmosphere at 0°C. Oxalyl chloride (380 mg, 3.00 mmol) was added dropwise to the solution. The solution was kept at 0 °C for additional 4 hours. Then, the solution was warmed to room temperature and stirred overnight. Distilled water was added to the solution and organic phase was extracted with DCM. The organic layer was washed with NaHCO₃ and dried over Na₂SO₄. After evaporation of solvent under reduced pressure, the product was obtained via recrystallization from cold methanol as a white solid. Yield: 85 %

^1H NMR (400 MHz, CDCl_3) δ : 7.50 (d, $J=2.0$ Hz, 2H), 7.36 (dd, $J_1=3.0$ Hz, $J_2=8.4$ Hz, 4H), 3.99 (dt, $J_1=6.6$ Hz, $J_2=1.6$ Hz, 8H), 2.05-1.63 (m, 48H), 0.81 (t, $J=6.8$ Hz, 12H)

^{13}C NMR (100 MHz, CDCl_3) δ : 193.8, 155.0, 149.3, 112.3, 111.6, 69.26, 69.13, 31.82, 29.34, 29.29, 29.26, 29.23, 29.08, 28.93, 25.99, 25.92, 22.67, 14.10

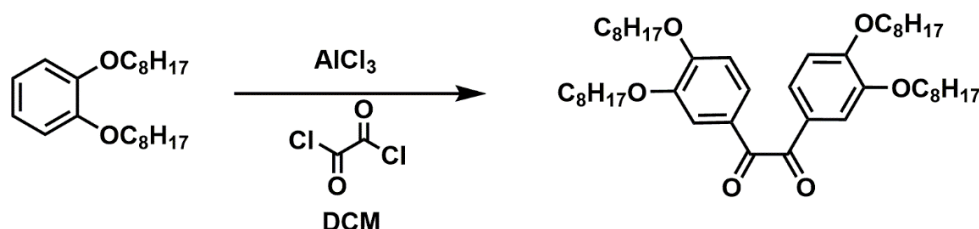


Figure 2.43. Synthetic route of 1,2-bis(3,4-bis(octyloxy)phenyl)ethane-1,2-dione

2.3.44. Synthesis of 2,3-bis(3,4-bis(octyloxy)phenyl)-5,8-dibromopyrido[3,4-*b*]pyrazine

1,2-Bis(3,4-bis(octyloxy)phenyl)ethane-1,2-dione (1.36 g, 1.88 mmol) and 2,5-dibromopyridine-3,4-diamine (500 mg, 1.88 mmol) were dissolved in glacial acetic acid (19 mL) under argon atmosphere. The solution was heated to reflux for 12 hours. After cooling to room temperature, yellow solid was filtered. Column chromatography (eluent: 2 petroleum ether: 1 DCM) was performed to obtain the compound. The synthesis did not work with various reaction conditions like solvent screening (i.e. ethanol) and catalytic amount of acid which was *p*-Toluenesulfonic acid. The compound could not be obtained.

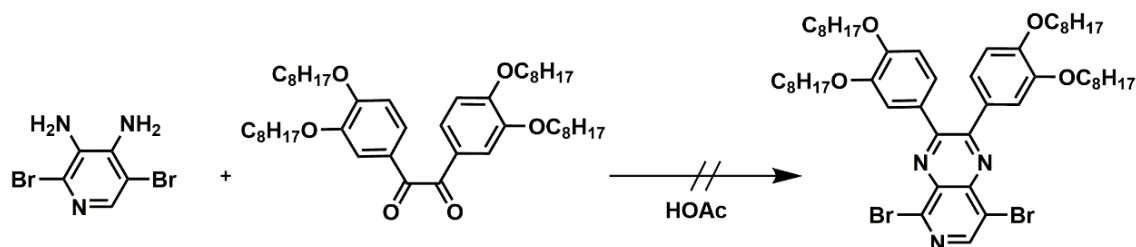


Figure 2.44. Synthetic route of 2,3-bis(3,4-bis(octyloxy)phenyl)-5,8-dibromopyrido[3,4-*b*]pyrazine

2.3.45. Synthesis of 5,8-dibromo-2,3-di(thiophen-2-yl)pyrido[3,4-*b*]pyrazine

1,2-Di(thiophen-2-yl)ethane-1,2-dione (393 mg, 1.77 mmol) and 2,5-dibromopyridine-3,4-diamine (472 mg, 1.77 mmol) were dissolved in glacial acetic acid (18 mL) under argon atmosphere. The solution was heated to reflux for 12 hours. After cooling to room temperature, yellow solid was filtered. Column chromatography (eluent: 2 petroleum ether: 1 DCM) was performed to obtain the compound. The compound could not be achieved with similar reaction conditions as in the case of alkoxybenzene derivative as diketone.

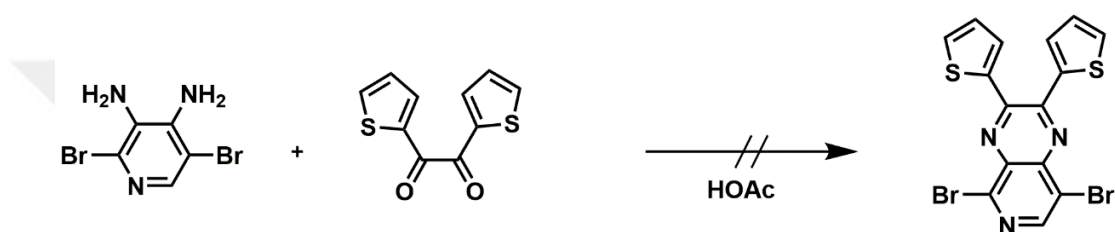


Figure 2.45. Synthetic route of 5,8-dibromo-2,3-di(thiophen-2-yl)pyrido[3,4-*b*]pyrazine

2.3.46. Synthesis of 4,7-dibromo-[1,2,5]selenadiazolo[3,4-*c*]pyridine

Selenium dioxide (196 mg, 1.77 mmol) and 2,5-dibromopyridine-3,4-diamine (472 mg, 1.77 mmol) were dissolved in glacial acetic acid (20 mL) under argon atmosphere. The solution was heated to reflux overnight. After cooling to room temperature, greenish yellow precipitate solid was filtered. The crude product was washed with ethanol. The synthesis could be successfully done. The reaction was repeated using ethanol as the solvent, it did not work as well.

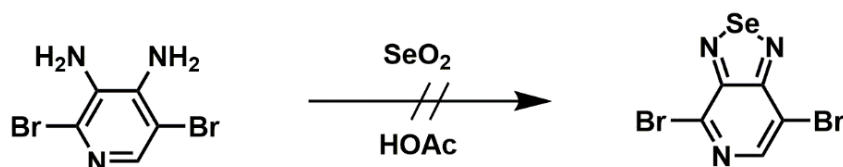


Figure 2.46. Synthetic route of 4,7-dibromo-[1,2,5]selenadiazolo[3,4-*c*]pyridine

2.3.47. Synthesis of 5,8-dibromo-2,3-di(pyridin-2-yl)pyrido[3,4-*b*]pyrazine

Similar procedures were used. None of the reactions did work.

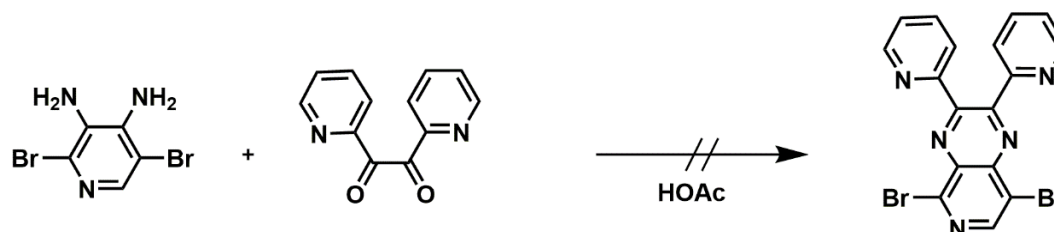


Figure 2.47. Synthetic route of 5,8-dibromo-2,3-di(pyridin-2-yl)pyrido[3,4-*b*]pyrazine

(*E*)-6,6'-dibromo-1,1'-bis(2-hexyldecyl)-[3,3'-biindolinylidene]-2,2'-dione was synthesized in the lab of Prof. Mario Leclerc's research group.

2.3.48. Synthesis of 7,7'-(5,6-bis(octyloxy)naphtho[2,1-*b*:3,4-*b'*]dithiophene-2,9-diyl)bis(benzo[*c*][1,2,5]thiadiazole-4-carbaldehyde)

A solution of 7-bromobenzo[*c*][1,2,5]thiadiazole-4-carbaldehyde (117 mg, 0.48 mmol), 5,6-bis(octyloxy)naphtho[2,1-*b*:3,4-*b'*]dithiophene (104 mg, 0.21 mmol) pivalic acid (21.4 mg, 0.21 mmol) and Cs₂CO₃ (205 mg, 0.63 mmol) were dissolved in freshly distilled toluene (2 mL) under argon atmosphere. The solution was degassed before addition of tris(4-methoxyphenyl)phosphine (16.7 mg, 0.03 mmol) and Herrmann Beller catalyst (9.80 mg, 0.01 mmol). Then, the mixture was placed pre-heated oil bath at 90 °C and stirred under argon for 4 hours. After cooling to room temperature, the reaction was quenched with acidic water and organic layer was extracted with ethyl acetate. Flash column chromatography on silica gel with CH₂Cl₂ as the eluent, followed by recrystallization from CH₂Cl₂/hexane, afforded the product as a solid. Yield: 35 %

¹H NMR (400 MHz, CDCl₃) δ: 10.64 (s, 2H), 8.14 (d, *J*=5.7 Hz, 2H), 7.80 (d, *J*= 5.7 Hz, 2H), 7.12 (s, 2H), 6.93 (s, 2H), 4.00 (t, *J*= 7.2 Hz, 4H), 1.82 (q, *J*= Hz, 4H), 1.78-1.22 (m, 20H), 0.81 (t, *J*= 7.4 Hz, 6H)

^{13}C NMR could not be recorded insufficient amount of the material.

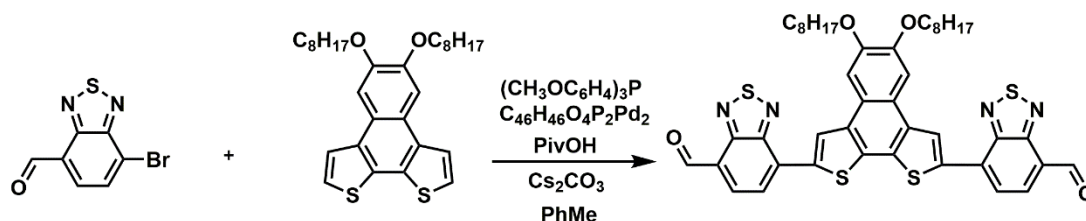


Figure 2.48. Synthesis of 7,7'-(5,6-bis(octyloxy)naphtho[2,1-b:3,4-b']dithiophene-2,9-diyl)bis(benzo[c][1,2,5]thiadiazole-4-carbaldehyde) (NFA-1 precursor)

2.3.49. Synthesis of 7,7'-(5,11-bis(2-hexyldecyl)-5,11-dihydroindolo[3,2-*b*]carbazole-3,9-diyl)bis(benzo[c][1,2,5]thiadiazole-4-carbaldehyde)

A solution of 7-bromobenzo[c][1,2,5]thiadiazole-4-carbaldehyde (100 mg, 0.41 mmol) and 5,11-bis(2-hexyldecyl)-3,9-bis(4,4,5,5-tetramethyl-1,3,2-dioxaborolan-2-yl)-5,11-dihydroindolo[3,2-*b*]carbazole (179 mg, 0.19 mmol) in freshly distilled toluene (2 mL) was degassed before addition of $\text{Pd}(\text{PPh}_3)_4$ (10.8 mg, 0.05 eq) and subsequent degassing for 0.5 hr. Aliquat 336 (1-2 drops), K_2CO_3 solution (2M, 0.30 mL) were then added and the reaction was placed pre-heated oil bath which is at 85 °C. The solution was stirred under argon overnight. After cooling to room temperature, the reaction was quenched with water and extracted with CH_2Cl_2 . Flash column chromatography on silica gel with CH_2Cl_2 as the eluent, followed by recrystallization from CH_2Cl_2 /hexane, afforded the product as a solid. Yield: 30 %

The monomer could not be fully purified. ^{13}C NMR will be recorded after successful purification.

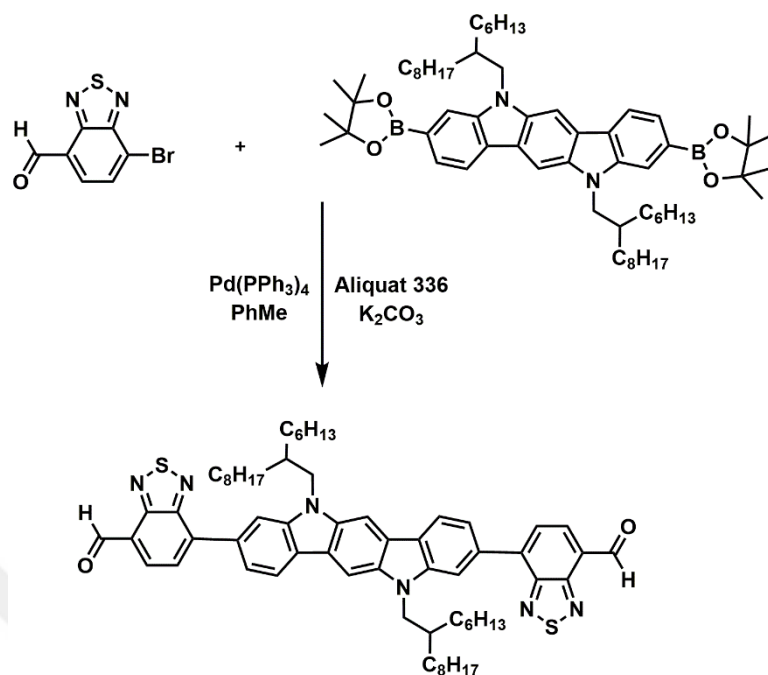


Figure 2.49. Synthesis of 7,7'-(5,11-bis(2-hexyldecyl)-5,11-dihydroindolo[3,2-*b*]carbazole-3,9-diyl)bis(benzo[*c*][1,2,5]thiadiazole-4-carbaldehyde) (NFA-2 precursor)

CHAPTER 3

HOMOPOLYMERS via ELECTROPOLYMERIZATION

3.1. The effect of electron rich moieties for homopolymers

3.1.1. Electrochemistry

All electrochemical polymerization reactions were carried out in a 0.1 M solution comprising perchlorate/lithium perchlorate (NaClO_4 / LiClO_4) as the supporting electrolyte, dichloromethane (DCM)/ acetonitrile (ACN) (5/95, v/v) as solvents with 0.01 M monomer at a scan rate of 100 mV/s (Figure 3.1). In order to increase the solubility of monomers, a mixture of DCM and ACN (5/95, v/v) was chosen as the solvent to provide good polymer film formation on ITO coated glass slides. The first cycle of voltammograms shows irreversible monomer oxidation peaks arising at 1.21 V, 1.30 V, 1.32 V for TTBO, SBO and FBO, respectively (Figure 3.1). The deposition of polymer film on ITO coated glass slides was demonstrated with an increase in the anodic and cathodic current densities. The redox behaviors of the resulting polymers PTTBO, PSBO and PFBO were examined by cyclic voltammetry studies. Cyclic voltammetry indicates the reversibility of the electron transfer for the polymers. The p-type and n-type doping properties of potentiodynamically synthesized polymers were investigated in a monomer free solution (Figure 3.2). The polymers are p-dopable with reversible redox couples at 1.13 V/ 0.95 V for PTTBO and at 1.16 V/ 0.94 V for PSBO and 1.28 V/ 0.61 V for PFBO vs. Ag wire pseudo-reference electrode (0.35 V vs Fc/Fc^+). The potential difference between the monomer oxidation peaks is related with the different electron densities on thienothiophene, selenophene and furan. PTTBO has higher electron density with extended conjugation due to thienothiophene group therefore the monomer has lower oxidation potential than that of different donor substituted benzooxadiazole based monomers. The higher

resonance stabilization energy of the fused rings have higher resonance stabilization energies resulting in lower HOMO energy level and harder electron abstraction from the system. On account of that reason, PTTBO monomer oxidation peak arose at a slightly higher potential than EDOT based polymer even if it is expected to have the lowest oxidation peak among all polymers [29]. Selenophene has lower oxidation potential than that of thiophene [30] however, monomers comprising selenophene and thiophene units have oxidation peaks at similar potentials revealing the interaction between donor and acceptor units. The polymers have multicolors upon applied potentials (Figure 3.3). The linear relation between current density versus scan rate graphs revealed that during doping-dedoping process in the cyclic voltammetry studies of electroactive polymer, the mass transfer is non-diffusion controlled (Figure 3.4). The onset potentials were determined from the intersection of two tangents drawn at the base line and the increasing current line in the cyclic voltammogram. The HOMO and LUMO energy levels were estimated relative to ferrocene energy level. HOMO levels are calculated as -5.71 eV for PTTBO, -5.88 eV for PSBO and -5.76 eV for PFBO, respectively. LUMO energy levels were estimated from optical the band gap values as -4.26 eV for PTTBO, -4.48 eV for PSBO and -4.20 eV for PFBO. Due to the electron-rich EDOT units in the PBODHT chains, the polymer film exhibited lower redox potentials compared to other polymers as expected.

Table 3.1. *The optoelectronic properties of benzoxadiazole based D-A-D type polymers: Previously Synthesized Polymers* and PTTBO, PSBO, PFBO*

Polymer	$E_{ox,mon}$ (V)	$E_{p,doping}$ (V)	$E_{p}^{de-doping}$ (V)	λ_{max} (nm)	E_g^{op} (eV)	HOMO (eV)
PBODT*	1.27	1.25	0.93	551	1.25	-5.73
PBOHT*	1.25	1.23	0.88	577	1.27	-5.54
PBODHT*	0.99	0.95	-0.49	590	1.50	-4.73
PTTBO	1.21	1.13	0.95	566	1.45	-5.71
PSBO	1.30	1.16	0.94	519	1.40	-5.88
PFBO	1.32	1.28	0.61	589	1.56	-5.76

*Previously synthesized monomers for MSc Thesis

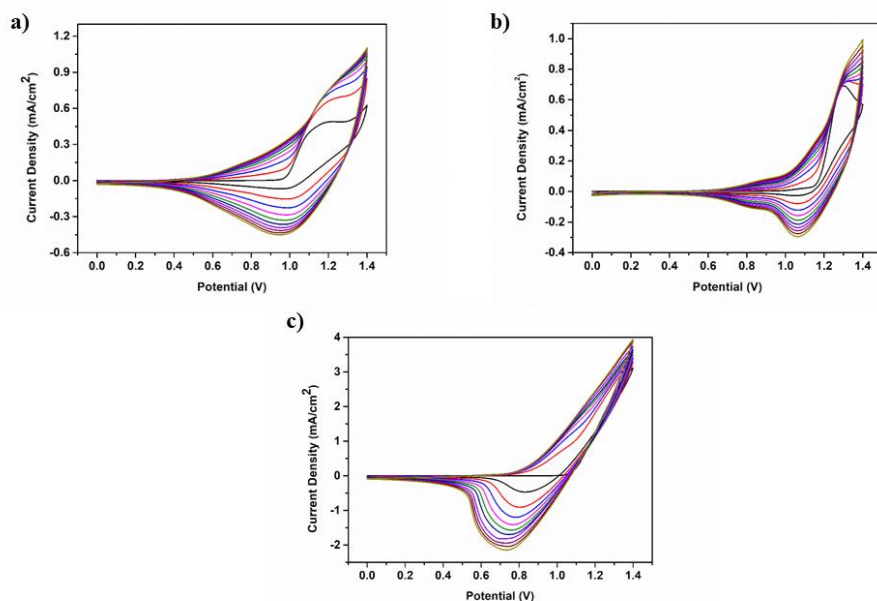


Figure 3.1. Electrochemical deposition of a) PTTBO, b) PSBO and c) PFBO on ITO in 0.1M NaClO₄-LiClO₄ /DCM/ACN electrolyte/solvent couple at a scan rate of 100 mV/s

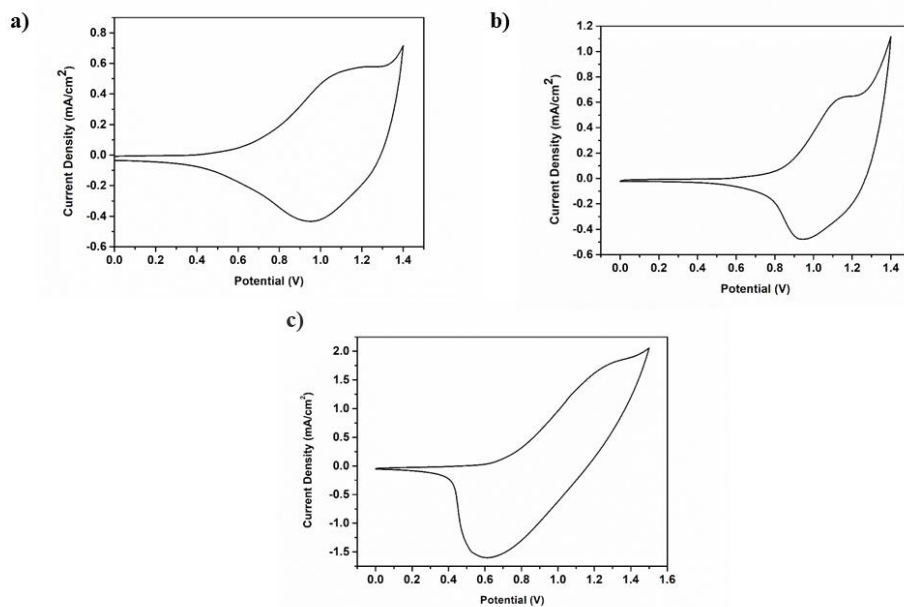


Figure 3.2. Single scan cyclic voltammograms of (a) PTTBO, (b) PSBO and c) PFBO in a monomer free 0.1 M LiClO₄-NaClO₄/ACN solution

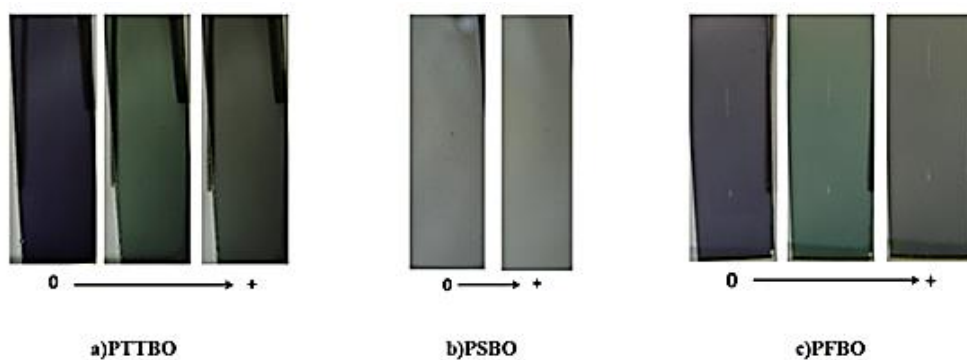


Figure 3.3. Chemical structures with monomer colors and abbreviations of homopolymers

Scan rate dependence of the polymers (Figure 3.4.) showed that electroactive polymers were stable at different scan rates in the cyclic voltammetry studies. Linear relationship between the current density and the scan rate (Figure 3.5) proves the nondiffusion controlled mass transfer during doping-dedoping process in the cyclic voltammetry studies of electroactive polymers.

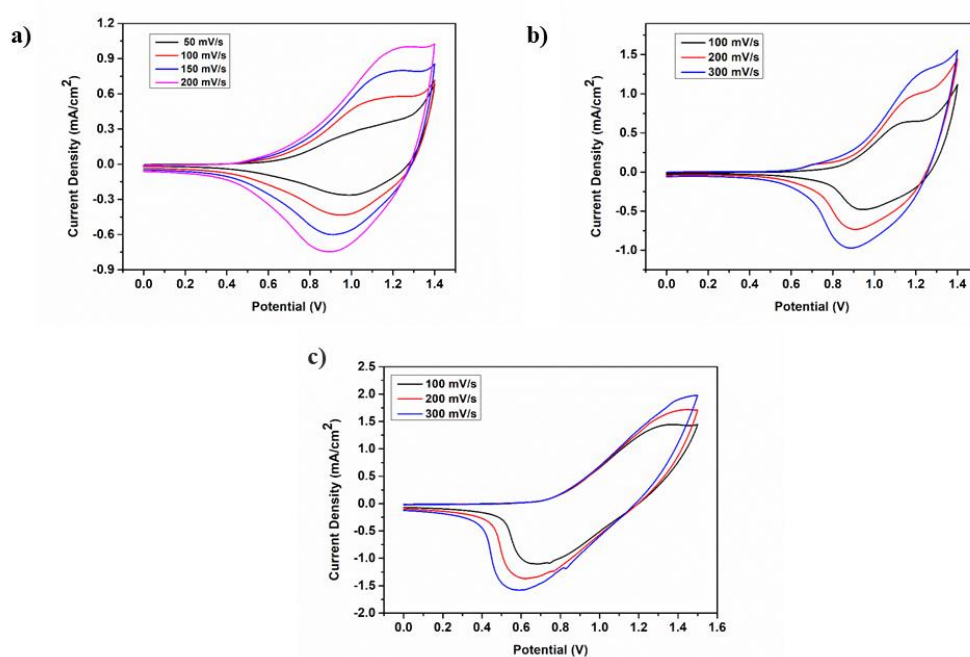


Figure 3.4. Scan rate dependence of polymers a) PTTBO b) PSBO c) PFBO

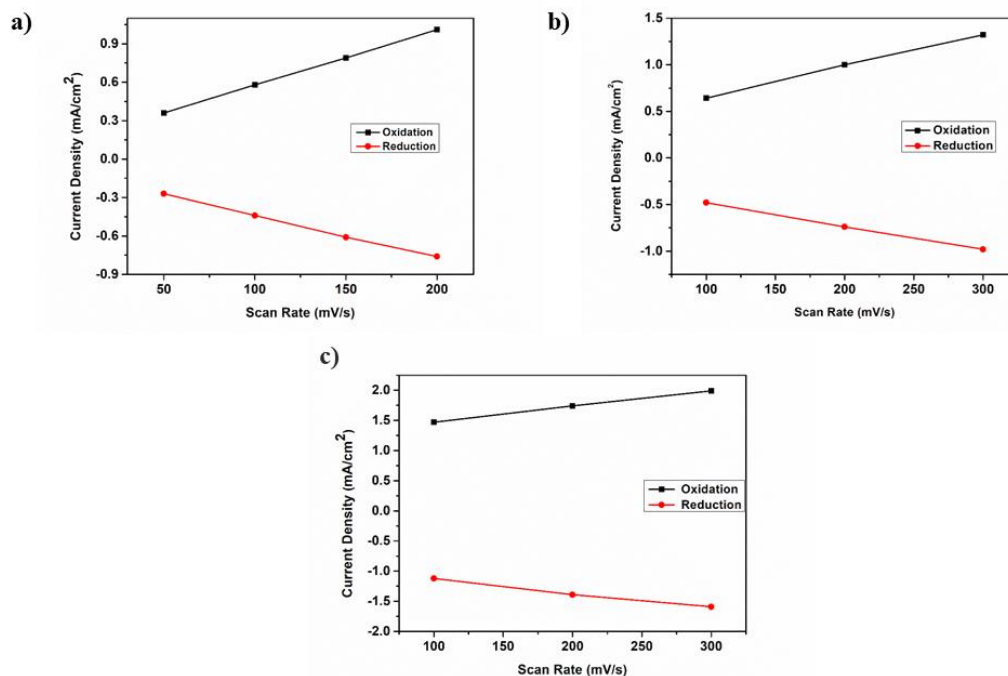


Figure 3.5. Linear relationship between the current density and the scan rate

3.1.2. Spectroelectrochemistry

The normalized optical UV-Vis-NIR absorption spectra of the polymers were recorded at room temperature to investigate optical and electronic changes upon doping. Figure 3.6 displays the absorption spectra of PTTBO, PSBO, and PFBO recorded in a monomer free 0.1 M ACN/NaClO₄/ LiClO₄ solution. The optical data including band gap (E_g), the absorption peak wavelengths (λ_{max}), the intergap states that appear upon doping and polaronic and bipolaronic band formations were obtained from spectroelectrochemistry studies. Polymer films were washed with acetonitrile before spectroelectrochemistry experiments to discard unreacted monomers present on ITO glass slides. In a monomer free 0.1 M ACN/NaClO₄/ LiClO₄ solution, potential was swept between 0.0 V and 1.4 V for PTTBO, 0.0 V and 1.30 V for PSBO and 0.0 V to 1.40 V for PFBO. Increase in absorbance of the polymers proves

the formation of lower energy charge carriers (polaron and bipolaron) in the electronic absorption spectra. From 420 to 700 nm, broader absorption corresponds to intramolecular charge transfer between the acceptor (BO-benzoxadiazole) and donor units. The absorption maximum revealed at 566 nm for PTTBO, at 519 nm for PSBO and at 589 nm for PFBO assign to localized π - π^* transitions. The optical band gaps of the polymers were calculated from those transitions as 1.45, 1.40 and 1.56 eV for PTTBO, PSBO and PFBO respectively. Polaronic and bipolaronic bands appeared at 860 nm and 1510 nm for PTTBO. Bipolaronic bands appear at 1200 nm for PSBO and 1610 nm for PFBO. Optical and electrochemical data showed that EDOT units in the conjugated system exert stronger influence on polymer electronic properties (Table 3.2). Due to its electron rich property a red shift in absorption and a decrease in oxidation potential were observed compared to other homopolymers.

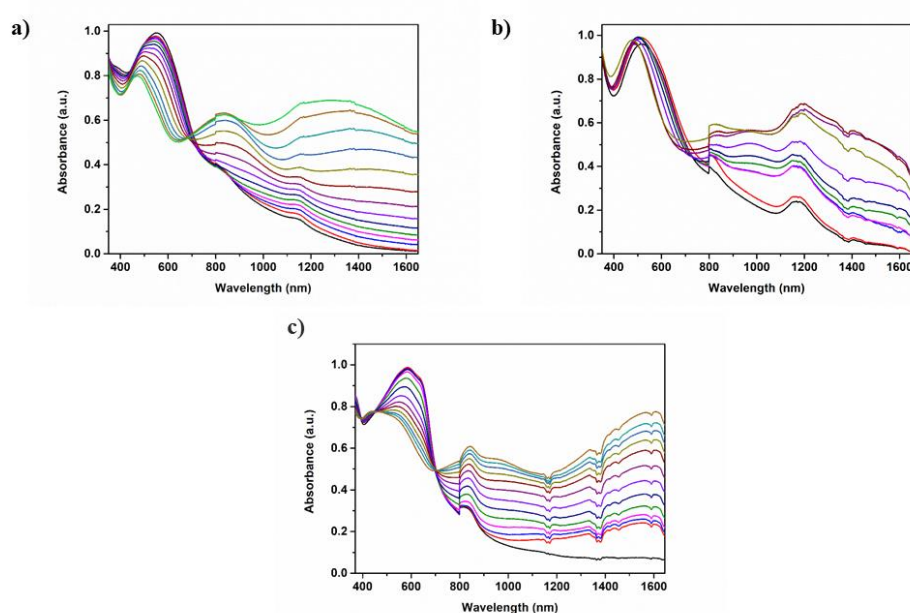


Figure 3.6. Absorption spectra of a) PTTBO, b) PSBO, and c) PFBO recorded in a monomer free 0.1 M ACN/NaClO₄/ LiClO₄ solution

CIE (Commission Internationale de l'Eclairage) coordinates were carried out to express the colors in a more scientific way. In the colorimetric measurements, L

represents the brightness of the color (L= 0 yields black and L= 100 indicates diffuse white), a represents the color between red/magenta and green, b represents the color between yellow and blue. The electrochemically synthesized polymer films show multichromic character upon p-doping/dedoping. L,a,b results were reported in Table 3.2.

Table 3.2. *Colorimetric measurements of the polymers*

Polymer	Applied Potential	L	a	b
PTTBO	0.0 V	42	-0.9	1
	1.2 V	44	-11	8
	1.5 V	55	-7	11
PSBO	0.0 V	66	-5	2
	1.5 V	80	-6	6
PFBO	0.0 V	31	-2	-4
	1.2 V	53	-13	7
	1.5 V	38	-2	0.2

3.1.3. Kinetic Studies

Percent transmittance changes were recorded while the potential was stepped continuously between fully neutral and oxidized states within a time interval of 5 s. Switching time is described as the time required for the coloring/bleaching process of the electrochromic material at a 95 % contrast value which the human eye is sensitive. Electrolyte conductivity, ion diffusion to the electroactive film, magnitude of the applied potential, thickness of electroactive film, and thin film morphology can be classified as some parameters affecting the switching time. Switching times and optical contrasts were calculated from kinetic studies in a monomer free 0.1 M NaClO₄-LiClO₄/ACN solution. The transmittance changes at dominant wavelengths are pointed out in Table 3.3. The optical contrasts were determined as 18 % at 570 nm, 29 % at 860 nm and 51 % at 1510nm for PTTBO (Figure 3.7). PFBO has

switching times of 3.9 s in the visible region (600 nm) and 3.5 s in the NIR region (1610 nm) whereas PTTBO revealed switching times of 0.6 s at 570 nm, 0.5 s at 860 nm and 1.8 s at 1510 nm. PFBO is expected to have lower optical contrast in the visible region than PTTBO due to its extended absorption at around 600 nm. However, their optical contrasts are similar to each other. Selenophene based polymer showed very poor stability hence its optical contrast could not be calculated via chronoamperometry studies. PBODHT exhibited the shortest switching time as well as the highest optical contrast among all polymers due to the strongest electron rich character as shown in Table 3.3.

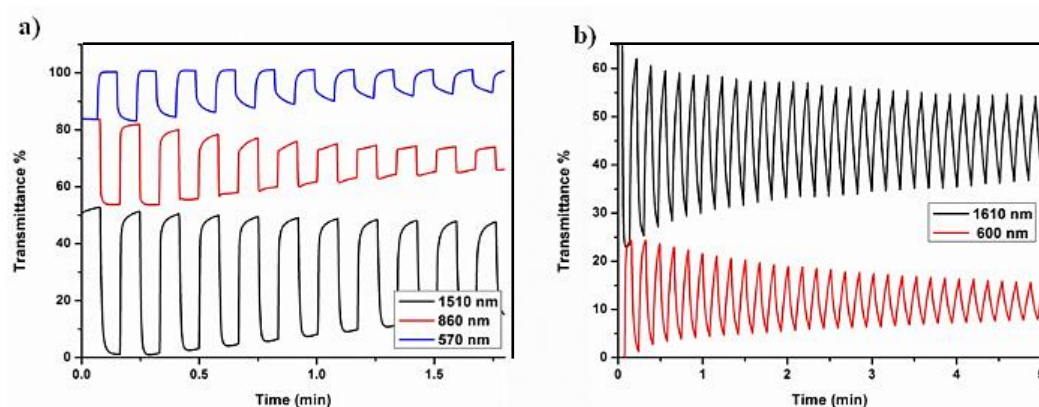


Figure 3.7. Electrochromic switching and percent transmittance changes observed at the absorption maxima of a) PTTBO and b) PFBO when switched between in system $\text{NaClO}_4\text{-LiClO}_4/\text{ACN}$

Table 3.3. Summary and comparison of optical properties of benzooxadiazole comprising homopolymers

Polymer	<i>Optical Contrasts (%T)</i>			<i>Switching Times (s)</i>		
PTTBO	18 % (570 nm)	29 % (860 nm)	51 % (1510 nm)	0.6 (570 nm)	0.5 (860 nm)	1.8 (1510 nm)
PFBO	24 % (600 nm)	39 % (1610 nm)		3.9 (600 nm)	3.5 (1610 nm)	
PBODHT*	75 % (590 nm)	88 % (1500 nm)		0.9 (590 nm)	1.1 (1500 nm)	
PBOHT*	17 % (580 nm)	33 % (1290 nm)		2.5 (580 nm)	1.5 (1290 nm)	
PBODT*	18 % (555 nm)	37 % (1300 nm)		1.1 (555 nm)	0.5 (1300 nm)	

*Previously synthesized polymers in MSc Thesis.

3.2. The effect of electron poor moieties for homopolymers

3.2.1. Electropolymerization

Electrochemical polymerization reactions were carried out in a 0.1M dichloromethane (DCM)/ acetonitrile (ACN) (5/95, v/v) solvent couple for PIIDThTh and (DCM)/ acetonitrile (ACN) (50/50, v/v) solvent couple for PTPDThTh. The solutions contain tetrabutylammonium hexafluorophosphate (TBAPF₆) as the supporting electrolyte with 0.1 M monomer at a scan rate of 100 mV/s (Figure 3.8). The reason to increase the solubility of monomers, a mixture of DCM and ACN was chosen as. Since thienopyrrolodione (TPD) based monomer has lower solubility than isoindigo (IID) based monomer due to shorter carbon chain as a pendant group, the ratio of solvent mixture is different for each monomer (higher amount of polar solvent for TPD based monomer). The redox behaviors of the resulting polymers PIIDThTh and PTPDThTh were examined via cyclic voltammetry studies.

The first cycle of voltammograms reveal irreversible monomer oxidation peaks at 1.37 V for TPDThTh and at 1.03 V and 1.24 V for IIDThTh (Figure 3.9). PIIDThTh has higher electron density with extended conjugation due to fused benzene groups even the monomer has lower oxidation potential than that of thienopyrrolodione substituted

thienothiophene based monomers. For potentiodynamically synthesized polymers, ambipolar characteristics were investigated in a monomer free solution (Figure 3.9). The polymers are p-dopable with reversible redox couples at 1.24 V/0.93 V for PTPDThTh and 1.37 V / 0.92 V for PIIDThTh. Besides, the polymers are n-dopable with reversible redox couples at -1.15 V/-1.08 V for PTPDThTh and two reduction couples appeared for PIIDThTh which were -1.15 V / -0.83 V and -1.53 V / -1.25 V for PIIDThTh. The potential difference between the monomer oxidation peaks is related with the different electron densities on isoindigo and thienopyrrolo-dione. The onset values for oxidation and reduction peaks were found as 0.84 V and -0.91 V for PTPDThTh. For PIIDThTh, the onset values for oxidation and reduction peaks were found as 0.84 V and -0.91 V for are obtained as 0.85 V for oxidation and -0.73 V for reduction. The HOMO and LUMO energy levels were estimated relative to ferrocene energy level. HOMO levels are calculated as -5.59 eV for PIIDThTh, -5.60 eV for PTPDThTh, respectively. LUMO energy levels are calculated as -3.84 eV for PIIDThTh, -4.02 eV for PTPDThTh. The electronic band gaps are 1.58 eV for PIIDThTh and 1.75 eV for PTPDThTh (Table 3.4).

The lower band gap of PIIDThTh may arise from higher solubility of monomer leading to a longer chain in the polymer backbone. Hence it is possible to obtain a higher molecular weight polymer. However, since the adhesion of such homopolymers is very strong, they cannot be removed from the surface. GPC results generally could not be recorded for homopolymer to prove this hypothesis.

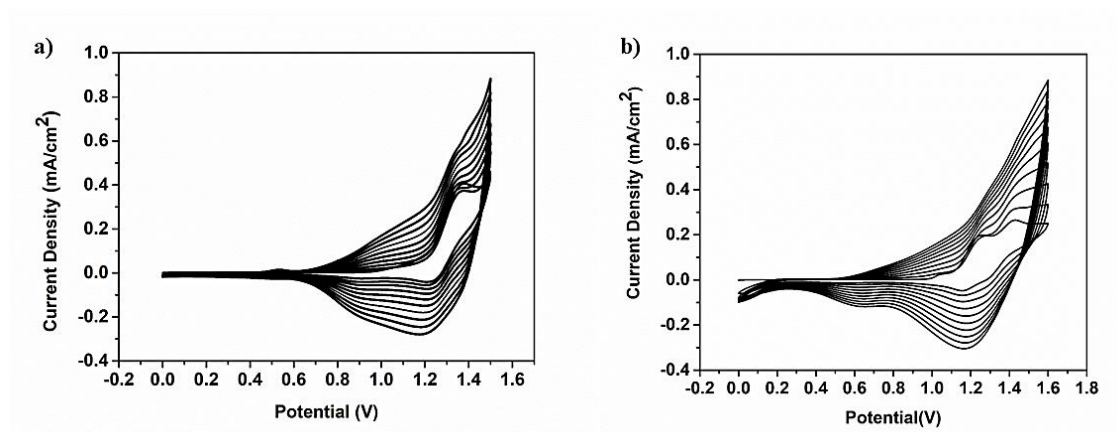


Figure 3.8. Multi-scan cyclic voltammograms of a)PTPDThTh and b) PIIDThTh in 0.1 M TBAPF₆/ACN supporting electrolyte/solvent couple (scan rate: 100 mV/s)

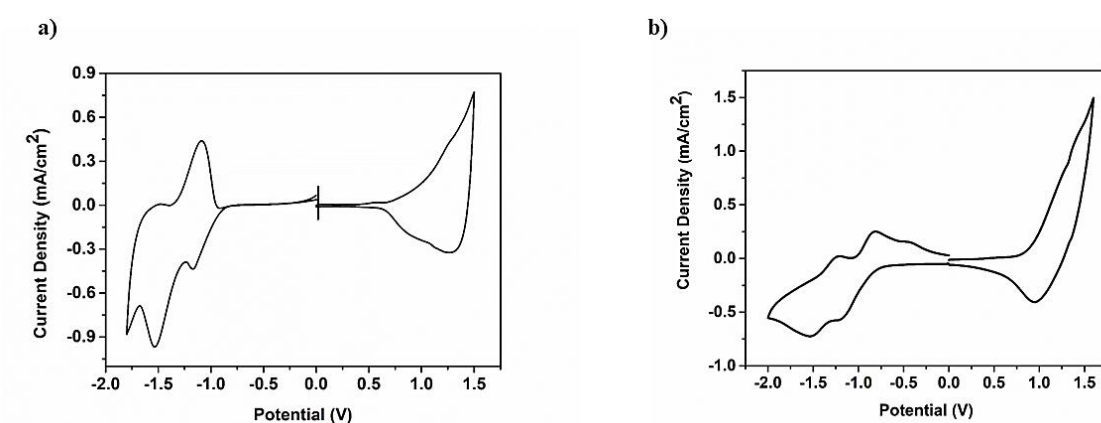


Figure 3.9. Single scan cyclic voltammograms of polymers in a monomer free solution (0.1 M TBAPF₆/ACN supporting electrolyte/solvent couple) a)PTPDThTh and b) PIIDThTh

3.2.2. Spectroelectrochemistry

Table 3.5 summarizes the optical properties of homopolymers. The electronic absorption spectra were performed at room temperature. Figure 3.10 reveals the absorption spectra of PTPDThTh and PIIDThTh which were recorded in a monomer free 0.1 M ACN/TBAPF₆ solution to determine the optical and electronic changes upon applied potential. The optical data including band gap (E_g), the absorption peak wavelengths (λ_{max}), the intergap states that appear upon doping and polaronic and

bipolaronic band formations were obtained from spectroelectrochemistry studies. Washing of polymer films with acetonitrile before performing spectroelectrochemistry experiments was achieved to remove unreacted monomers from ITO surfaces. In a monomer free solution, potential was swept between 0.0 V and 1.50 V for PTPDThTh and 0.0 V to 1.75 V for PIIDThTh. Increase in absorbance of the polymers proves the formation of lower energy charge carriers (polaron and bipolaron) in the electronic absorption spectra. From 420 to 700 nm, broader absorption corresponds to intramolecular charge transfer between the acceptor (BO) and donor units. The absorption maximum revealed at 519 nm for PTPDThTh and at 625 nm for PIIDThTh. The optical band gaps of the polymers were calculated from localized π - π^* transitions as 1.70 and 1.16 eV for PTPDThTh and PIIDThTh respectively. The much lower optical band gap could be attributed to enhanced absorption of isoindigo based polymer. Isoindigo based monomer has also a very deep purple color in the solid state which has a broad absorption whereas thienopyrrolodione based monomer has an orange color in the solid state. For the homopolymers, the same trend which is red shift in the absorption for isoindigo was also observed most probably due to richer electron density. A very low band gap polymer was potentiodynamically produced. For future studies, chemically synthesized homopolymer may be a good candidate for solar cells due to enhanced absorption, low band gap which increases photon harvesting.

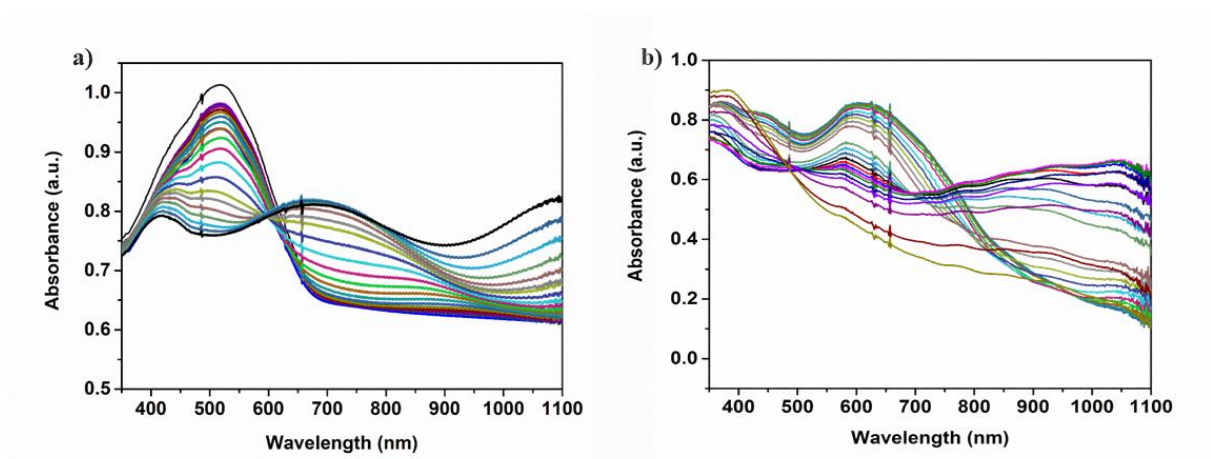


Figure 3.10. Electronic absorption spectra of polymers a) PTPDThTh and b) PIIDThTh

Table 3.4. Summary of electronic properties of homopolymers

Polymer	$E_{ox,mon}$ (V)	$E_{p,doping}$ (V)	$E_{n,doping}$ (V)	$E_{p^{de-doping}}$ (V)	$E_{n^{de-doping}}$ (V)	HOMO (eV)	LUMO (eV)	E_g^{el} (eV)
PTPDThTh	1.37	1.24	-1.15	0.93	-1.08	-5.59	-3.84	1.75
PIIDThTh	1.03/1.24	1.37	-1.15/ -1.53	0.92	-0.83/ -1.25	-5.60	-4.02	1.58

Table 3.5. Summary of optical properties of homopolymers

Polymer	λ_{max} (nm)	$\lambda_{max,onset}$ (nm)	E_g^{op} (eV)
PTPDThTh	519	730	1.70
PIIDThTh	625	1073	1.16

CHAPTER 4

ALTERNATING COPOLYMERS via STILLE and SUZUKI COUPLINGS

4.1. Stille Coupling for Polymerizations of Alternating Copolymers

4.1.1. Syntheses

4.1.1.1. Synthesis of PIIDDTP

(E)-6,6'-dibromo-1,1'-diundecyl-[3,3'-biindolinylidene]-2,2'-dione (IID) (176 mg, 0.24 mmol), 4-(2-ethylhexyl)-2,6-bis(trimethylstannyl)-4H-dithieno[3,2-*b*:2',3'-*d*]pyrrole (149 mg, 0.24 mmol), Pd₂(dba)₃ (8.86 mg, 0.01 mmol), tri(*o*-tolyl)phosphine (8.84 mg, 0.03 mmol) were added in a 30 mL schlenk tube kept under inert atmosphere. Then, freshly distilled toluene (15 mL) was added to the reaction mixture. TLC controlled reaction was stirred for 24 hours. After removal of toluene, the polymer was precipitated in cold methanol and filtered through Soxhlet thimble. Washing with acetone and hexane was achieved to remove short chain fractions. Chloroform was used to extract the polymer. Evaporation of solvent using rotary evaporator gave the corresponding polymer as a deep green solid. Yield: 40 %

ν_{\max} (KBr, cm⁻¹): 3840-3770 (O-H), 2922 (N-H), 2852 (N-H), 2634 (S-H), 2349 (O=C=O), 1688-1650 (CO, δ -lactam), 1620 (α,β -unsaturated ketone, C=C). 1605 (C=C, conjugated alkene), 1508 (N-O), 1458 (C-H, alkane), 1387(C-H, alkane), 1265(C-N, aromatic amine), 1107 (C-O), 867 (C-H, substituted benzene), 796-729 (C-H, benzene derivative), 520 (C-Br).

Mw: 11370 Da Mn: 7800 Da PDI: 1.46

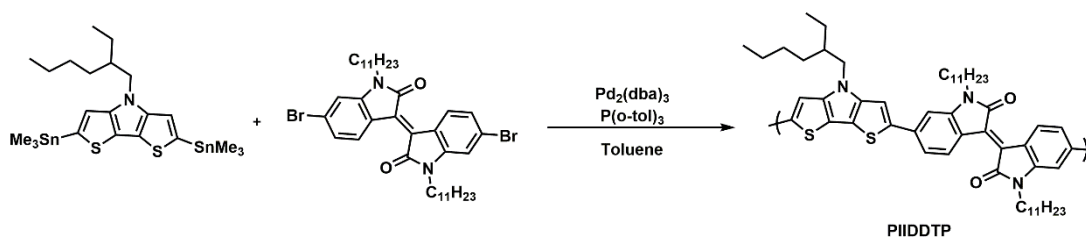


Figure 4.1. Synthesis of PIIDDTP

4.1.1.2. Synthesis of SG-2-ST

4,7-Dibromo-5,6-bis(octyloxy)benzo[*c*][1,2,5]oxadiazole (89.7 mg, 0.17 mmol), (4,8-didodecylbenzo[1,2-*b*:4,5-*b'*]dithiophene-2,6-diyl)bis(trimethylstannane) (143 mg, 0.17 mmol), Pd₂(dba)₃ (3.08 mg, 0.03 mmol), triphenylarsine (4.12 mg, 0.13 mmol) were added in a 10 mL schlenk tube under inert atmosphere. Then, freshly distilled toluene (1.7 mL) was added to the reaction mixture. The solution was stirred for 2 hours. 5 mL *o*-Dichlorobenzene was added to the solution which was stirred for additional 20 min. The solution was cooled to room temperature and added drop wise to cold methanol for precipitation of the polymer. Later, the polymer was filtered through Soxhlet thimble and washed with acetone and hexane to remove oligomers. Chloroform was used to extract the polymer. Evaporation of solvent using rotary evaporator gave the corresponding polymer. Yield: 35 %

ν_{\max} (KBr, cm⁻¹): 2955-2921 (C-H, alkane), 2851 (C-H), 1589-1527 (C=C stretching, conjugated alkene), 1455 (O-H), 1298 (S-O), 1200 (C-O), 1057 (C-O, alkoxy group), 997 (C=C, alkene), 721 (C-H, benzene derivative), 655-577 (C-Br), 481 (C-Br)

Mw: 8737 Da Mn: 6508 Da PDI: 1.34

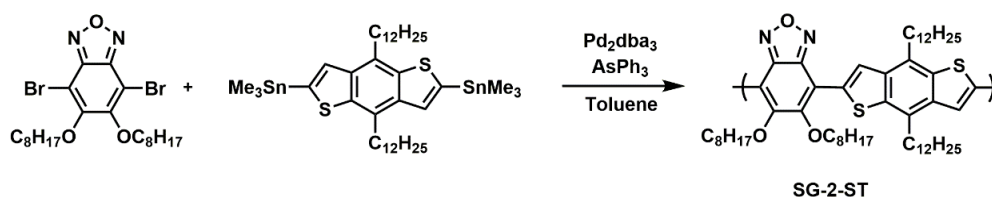


Figure 4.2. Synthetic route for SG-2-ST

4.1.1.3. Synthesis of SG-3-ST

(4,8-Didodecylbenzo[1,2-*b*:4,5-*b'*]dithiophene-2,6-diyl)bis(trimethylstannane) (159 mg, 0.19 mmol), (E)-6,6'-dibromo-1,1'-diundecyl-[3,3'-biindolinylidene]-2,2'-dione (136 mg, 0.19 mmol), triphenylarsine (4.55 mg, 0.02 mmol), Pd₂(dba)₃ (3.40 mg, 0.004 mmol) were added to a schlenk tube which is held under inert atmosphere. After addition of anhydrous and degassed toluene to a sealed schlenk tube, the solution was placed into pre-heated oil bath which was 110 °C. After 1 hour stirring, gelation occurred. 5 mL of o-dichlorobenzene was added to the reaction medium and stirred for 30 min. Polymer was filtered through Soxhlet thimble after precipitation using cold methanol. Washing of polymer with acetone and hexane removed low molecular weight fractions. To recover the polymer chloroform was used and later evaporated under reduced pressure. Yield: 20 %

ν_{\max} (KBr, cm⁻¹): 3839-3740 (O-H), 3649 (O-H), 2922 (C-H, alkane), 2850 (C-H), 2646 (S-H), 2286 (S-H), 2050 (C-H, aromatic), 1689 (C=N), 1607 (C=C, conjugated alkene), 1459 (C-H, alkane), 1357 (S-O), 1171 (C-O), 1109 (C-O), 1085 (), 815 (C-H, substituted benzene), 721 (C-H, benzene derivative), 522-460 (C-Br).

Mw: 28388 Da Mn: 19926 Da PDI: 1.42

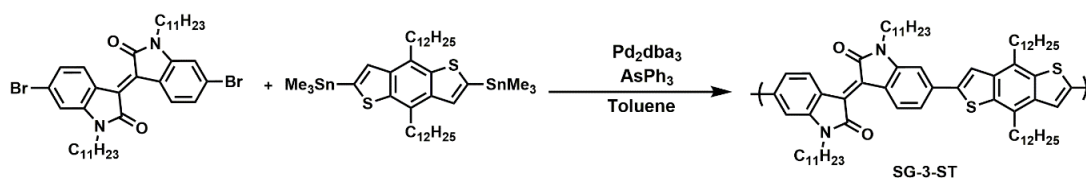


Figure 4.3. Synthetic route for SG-3-ST

4.1.1.4. Synthesis of SG-4-ST

Using the similar procedure mentioned above, 4,7-bis(5-bromoselenophen-2-yl)-5,6-bis(octyloxy)benzo[c][1,2,5]oxadiazole (150 mg, 0.19 mmol), (4,8-didodecylbenzo[1,2-*b*:4,5-*b'*]dithiophene-2,6-diyl)bis(trimethylstannane) (162 mg, 0.19 mmol), triphenylarsine (4.65 mg, 0.02 mmol), Pd₂(dba)₃ (3.47 mg, 0.004 mmol) were polymerized in anhydrous toluene (1.9 mL) under inert atmosphere to give the corresponding polymer. Yield: 55 %

ν_{\max} (KBr, cm⁻¹): 3840-3740 (O-H), 2920 (C-H, alkane), 2851 (C-H), 2347 (O=C=O), 2050 (C=C), 1459 (C-H, alkane), 1375 (S-O), 1298 (S-O), 1296-1235 (S-O), 1167 (S-O), 988 (C=C, alkene), 898 (C-H, substituted benzene), 784-721 (C-H, benzene derivative), 563 (C-Br), 437 (C-Br)

Mw: 14577 Da Mn: 8812 Da PDI: 1.65

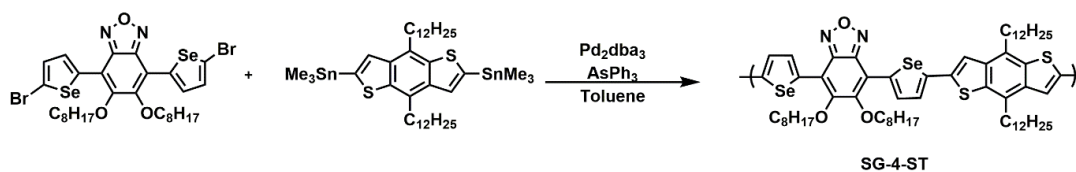


Figure 4.4. Synthetic route for SG-4-ST

4.1.1.5. Synthesis of SG-6-ST

In a 10 mL schlenk tube, (E)-6,6'-dibromo-1,1'-bis(2-hexyldecyl)-[3,3'-biindolinylidene]-2,2'-dione (159 mg, 0.18 mmol), (4,8-didodecylbenzo[1,2-*b*:4,5-*b'*]dithiophene-2,6-diyl)bis(trimethylstannane) (155 mg, 0.18 mmol), Pd₂(dba)₃ (3.33 mg, 0.004 mmol), triphenylarsine (4.46 mg, 0.02 mmol), freshly distilled toluene (1.8 mL) were added under inert atmosphere and stirred until gelation (4 hours). After 20 min. stirring with the addition of o-dichlorobenzene to the reaction medium, the solution was cooled to room temperature. The polymer was precipitated using cold methanol. Soxhlet apparatus was used to remove oligomers via washing with acetone and hexane. The chloroform fraction was reduced to 5-10 mL and then poured into cold methanol. The precipitate was filtered and air-dry to give of the desired polymer. Yield: 92 %

Mw: 27657 Da Mn: 16414 Da PDI: 1.69

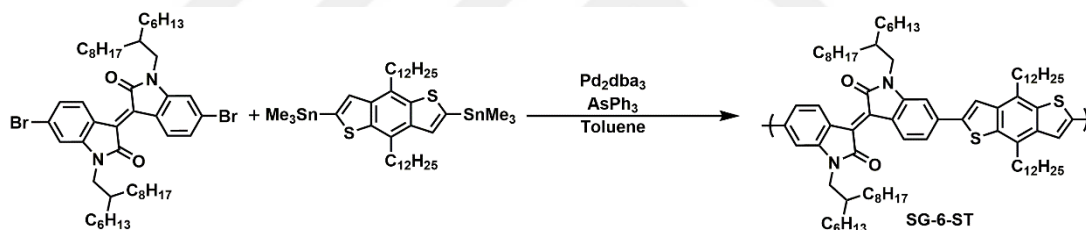


Figure 4.5. Synthetic route for SG-6-ST

4.1.1.6. Synthesis of SG-6-ST2

Using the similar procedure for SG-6-ST, (E)-6,6'-dibromo-1,1'-bis(2-hexyldecyl)-[3,3'-biindolinylidene]-2,2'-dione (209 mg, 0.24 mmol), (4,8-didodecylbenzo[1,2-*b*:4,5-*b'*]dithiophene-2,6-diyl)bis(trimethylstannane) (205 mg, 0.24 mmol), Pd₂(dba)₃ (4.40 mg, 0.005 mmol), triphenylarsine (5.88 mg, 0.02 mmol), freshly distilled toluene (1.8 mL) were added under inert atmosphere and polymerized after 24 hours mixing to give SG-6-ST2. Yield: 77 %

Mw: 19902 Da Mn: 11699 Da PDI: 1.70

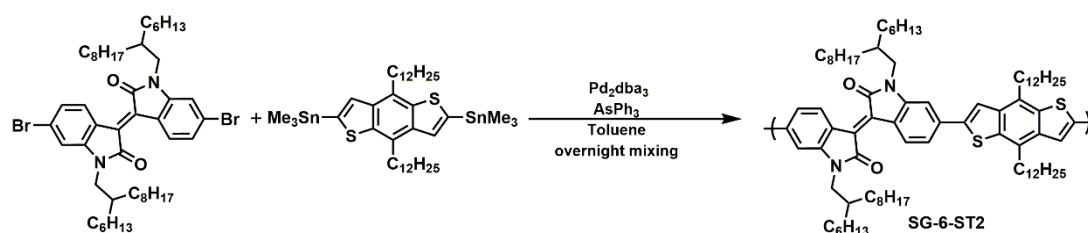


Figure 4.6. Synthetic route for SG-6-ST2

4.1.1.7. Synthesis of SG-6-ST3

Using the similar procedure for SG-6-ST, (E)-6,6'-dibromo-1,1'-bis(2-hexyldecyl)-[3,3'-biindolinylidene]-2,2'-dione (146 mg, 0.17 mmol), (4,8-didodecylbenzo[1,2-*b*:4,5-*b'*]dithiophene-2,6-diyl)bis(trimethylstannane) (143 mg, 0.17 mmol), Pd₂(dba)₃ (3.06 mg, 0.003 mmol), tri(*o*-tolyl)phosphine (4.06 mg, 0.01 mmol), freshly distilled toluene (1.7 mL) were added under inert atmosphere and polymerized after 24 hours mixing to give SG-6-ST3. Yield: 95 %

Mw: 176136 Da Mn: 54603 Da PDI: 3.23

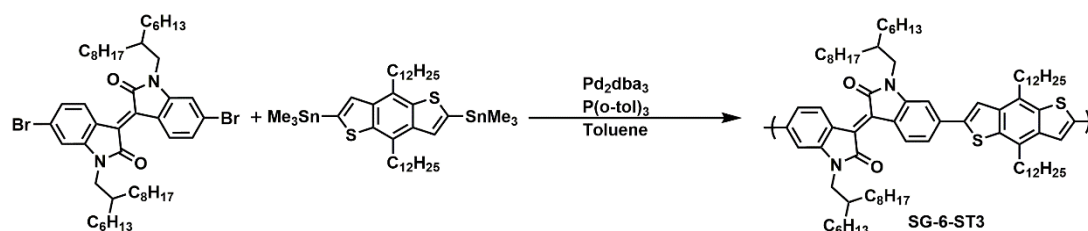


Figure 4.7. Synthetic route for SG-6-ST3

4.1.1.8. Synthesis of SG-7-ST

(E)-2,2'-dibromo-4,4'-bis(2-octyldodecyl)-[6,6'-bithieno[3,2-*b*]pyrrolylidene]-5,5'(4*H*,4'*H*)-dione (147 mg, 0.15 mmol), (4,8-didodecylbenzo[1,2-*b*:4,5-*b'*]dithiophene-2,6-diyl)bis(trimethylstannane) (126 mg, 0.15 mmol), Pd₂(dba)₃ (2.70 mg, 0.003 mmol), tri(*o*-tolyl)phosphine (3.60 mg, 0.01 mmol), freshly distilled toluene (1.5 mL) were added under inert atmosphere and polymerized after 1.5 hours mixing to give the corresponding polymer. Yield: 50 %

Mw: 96350 Da Mn: 27520 Da PDI: 3.50

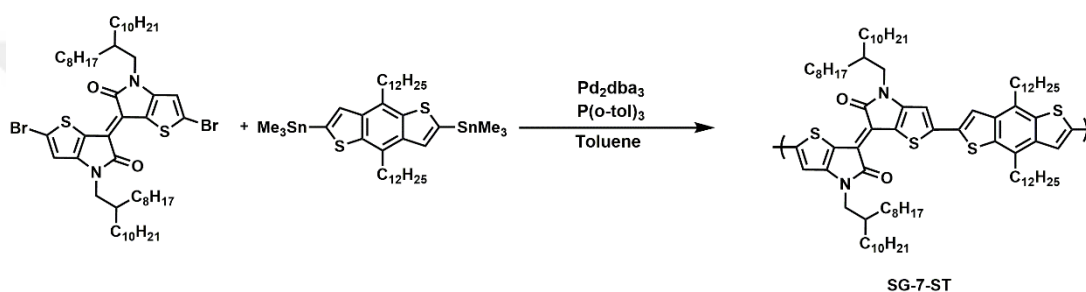


Figure 4.8. Synthetic route for SG-7-ST

4.1.1.9. Synthesis of SG-8-ST

4,7-Bis(5-bromothiopheno[3,2-*b*]thiophen-2-yl)-5,6-bis(octyloxy)benzo[*c*][1,2,5]oxadiazole (100 mg, 0.12 mmol), (4,8-didodecylbenzo[1,2-*b*:4,5-*b'*]dithiophene-2,6-diyl)bis(trimethylstannane) (105 mg, 0.12 mmol), Pd₂(dba)₃ (2.25 mg, 0.003 mmol), tri(*o*-tolyl)phosphine (3.00 mg, 0.01 mmol), freshly distilled toluene (1.25 mL) were mixed under inert atmosphere and polymerized for 1.5 hours to give the corresponding polymer. After 20 min. stirring total gelation occurred.

NMR spectra could not be recorded due to insolubility of the polymer. Very low molecular weight fractions as given by GPC result reported below.

Mw: 5320 Da Mn: 4120 Da PDI: 1.29

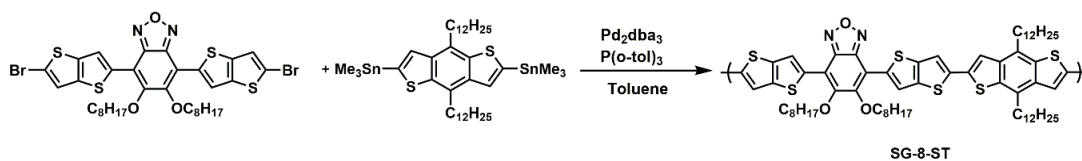


Figure 4.9. Synthetic route for SG-8-ST

4.1.1.10. Synthesis of SG-9-ST

Using the similar procedure explained above, 4,7-bis(5-bromofuran-2-yl)-5,6-bis(octyloxy)benzo[*c*][1,2,5]oxadiazole (80.0 mg, 0.12 mmol), (4,8-didodecylbenzo[1,2-*b*:4,5-*b'*]dithiophene-2,6-diyl)bis(trimethylstannane) (102 mg, 0.12 mmol), Pd₂(dba)₃ (2.20 mg, 0.002 mmol), tri(*o*-tolyl)phosphine (2.90 mg, 0.01 mmol), freshly distilled and degassed toluene (1.2 mL) were polymerized under nitrogen atmosphere for 3 hours to give the desired polymer.

ν_{max} (KBr, cm⁻¹): 3840-3740 (O-H), 2922 (C-H, alkane), 2852 (C-H), 2347 (O=C=O), 2050 (C=C), 1508 (N-O), 1459 (C-H, alkane), 1375 (S-O), 1299 (S-O), 1171 (S-O), 984 (C=C, alkene), 814 (C-H, substituted benzene), 784 (C-H, benzene derivative), 722 (C-H, benzene derivative), 560-517 (C-Br)

Mw: 101840 Da Mn: 61070 Da PDI: 1.66

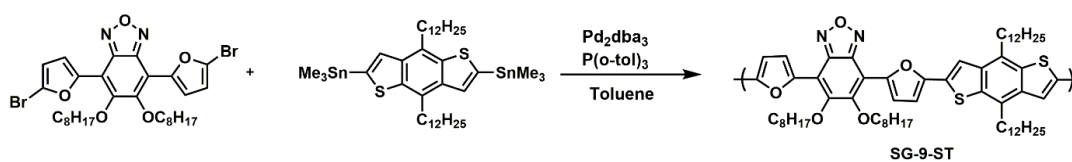


Figure 4.10. Synthetic route for SG-9-ST

4.1.2. Results and Discussion for PIIDDTP

Electrochemistry, spectroelectrochemistry and kinetic studies were done for PIIDDTP to characterize the polymer in terms of optoelectronic properties. Single scan cyclic voltammogram was recorded in 0.1 M TBAPF₆/ACN solution at a scan rate of 100 mV/s. The polymer has ambipolar characteristics. Since the polymer is both p and n dopable, frontier molecular orbital energy levels could be calculated from cyclic voltammetry studies. The oxidation potential of the polymer is at 0.89 V for p-doping region while the reduction potentials of the polymer are at -1.05 V and -1.40 V for n-doping region (Figure 4.11). The reason for having two reduction couples may be attributed to high electron density of the polymer coming from fused benzene rings in the isoindigo and strong electron donating ability of diethinopyrrole. HOMO energy level was found as -5.17 eV whereas LUMO energy level was found as -3.92 eV using onset values for oxidation and reduction respectively. The difference between those energy levels give the electronic band gap which was calculated as -1.28 eV. The polymer has low band gap. To investigate optical properties, electronic absorption spectra was recorded upon applied gradual potential. Figure 4.12 reveals that the absorption maximum of PIIDDTP was observed at 737 nm. The optical band gap was determined as 1.25 eV. Since dithienopyrrole is one of the strongest donor moieties, the combination of this unit with isoindigo throughout the backbone resulted in a low band gap polymer. High efficiency could be achieved in the solar cell applications due to broad absorption of the polymer which is close to NIR region. Table 4.1 summarizes the electronic properties.

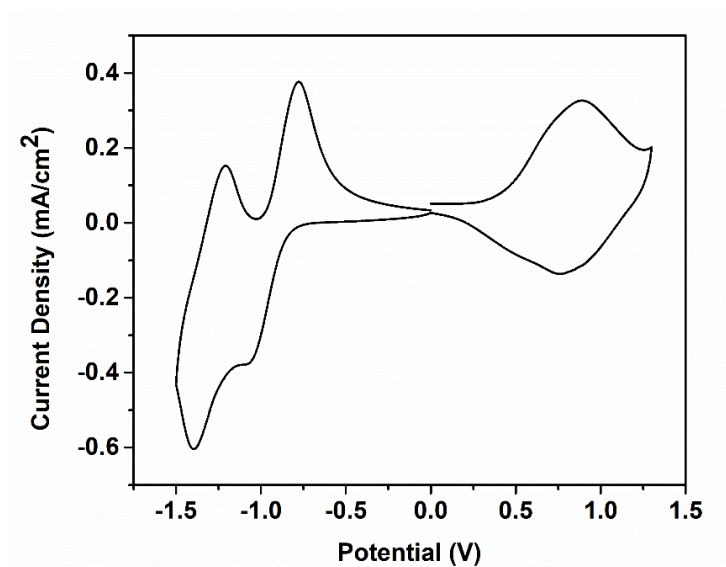


Figure 4.11. Single scan cyclic voltammogram of PIIDDTP in 0.1 M TBAPF₆/ACN solution at a scan rate of 100 mV/s.

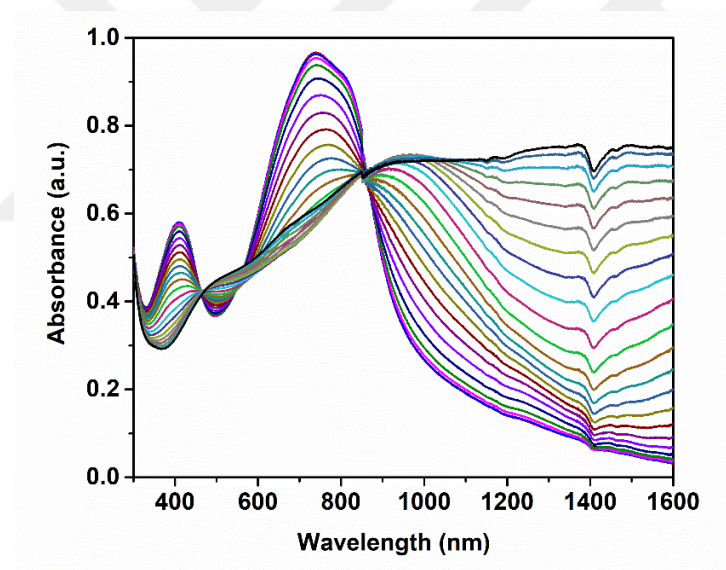


Figure 4.12. Electronic absorption spectra of the polymer upon applied gradual potential

In the kinetic studies, percent transmittance changes were recorded at the absorption maxima. Switching times and optical contrasts were calculated from kinetic studies in a 0.1 M TBAPF₆/ACN solution. The transmittance changes at dominant wavelengths are pointed out in Table 4.2. The optical contrasts were determined as 14 % at 400 nm, 13 % at 729 nm and 39 % at 1485 nm (Figure 4.13). The polymer has switching

times of 1.8 s and 1.7 s in the visible region (400 nm and 729 nm) and 1.8 s in the NIR region (1485 nm) PFBO is expected to have lower optical contrast in the visible region than PTTBO due to its extended absorption at around 600 nm. However, their optical contrasts are similar to each other. The polymer showed good stability, there is no decrease in percent transmittance change during measurements (Figure 4.13).

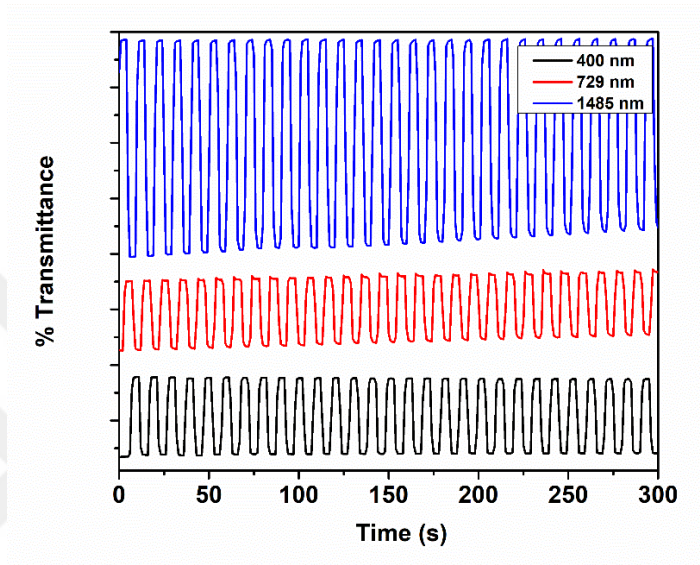


Figure 4.13. Percent transmittance change for polymer at absorption maxima

Table 4.1. Summary of electronic properties of polymer

Polymer	$E_{p,doping}$ (V)	$E_{n,doping}$ (V)	$E_{p^{de-}doping}$ (V)	$E_{n^{de-}doping}$ (V)	HOMO (eV)	LUMO (eV)	E_g^{el} (eV)
PIDDTP	0.89	-1.05/ -1.40	0.45	-0.78/ -1.22	-5.17	-3.92	1.28

Table 4.2. Summary of optical properties of polymer

Polymer	λ_{max} (nm)	$\lambda_{max,onset}$ (nm)	E_g^{op} (eV)	Optical Contrast (ΔT %)	λ (nm)	Switching Time(s)
PIDDTP	737	991	1.25	14	400 nm	1.80
				13	729 nm	1.70
				39	1485 nm	1.79

λ (nm) reveals the wavelength at which kinetic studies were performed.

4.2. Suzuki Coupling for Polymerizations of Alternating Copolymers

4.2.1. Syntheses

4.2.1.1. Synthesis of PIIDINDC

(E)-6,6'-dibromo-1,1'-diundecyl-[3,3'-biindolinylidene]-2,2'-dione (200 mg, 0.27 mmol), 5,11-bis(2-hexyldecyl)-3,9-bis(4,4,5,5-tetramethyl-1,3,2-dioxaborolan-2-yl)-5,11-dihydroindolo[3,2-*b*]carbazole (263 mg, 0.27 mmol), potassium carbonate (2M in H₂O), Pd(PPh₃)₄ (19.0 mg, 0.01 mmol) and Aliquat 336 (2 drops) were dissolved in anhydrous toluene (10 mL) and refluxed at 95 °C under argon atmosphere for 24 hours. The reaction was controlled by TLC. The solvent was removed under reduced pressure, chloroform was added and the mixture was washed with distilled water three times to remove alkaline solution. The organic layer was collected and dried over MgSO₄. After addition of methanol to crude product, the strongly complexing ligand; sodium diethyldithiocarbamate (10 mg) was added as a strong palladium scavenger, and the mixture was stirred for 1 hour. After filtration, the crude product was washed with methanol, acetone, and hexane using Soxhlet extractor to remove oligomers. Chloroform was used to extract the polymer. A black solid was obtained after precipitation with cold methanol. Yield: 26 %

Mw: 33300 Da, Mn: 24160 Da PDI: 1.38

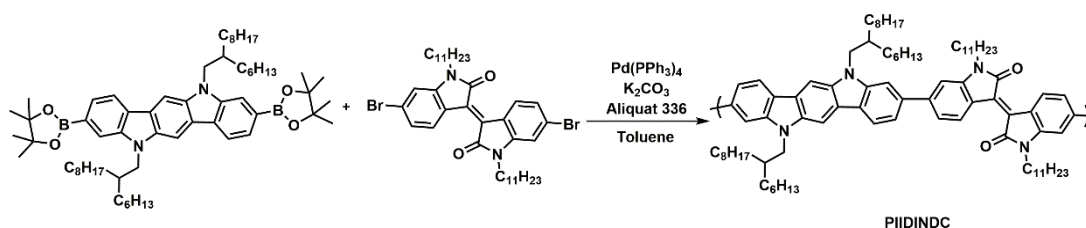


Figure 4.14. Synthesis of PIIDINDC

4.2.1.2. Synthesis of PSBSC

4,7-Bis(5-bromoselenophen-2-yl)-5,6-bis(octyloxy)benzo[*c*][1,2,5]oxadiazole (166 mg, 0.21 mmol), 9-(9-heptadecanyl)-9H-carbazole-2,7-diboronic acid bis(pinacol) ester (138 mg, 0.21 mmol), potassium carbonate (2M in H₂O), Pd(PPh₃)₄ (12.1 mg, 0.02 mmol) and Aliquat 336 (2-3 drops) were dissolved in anhydrous toluene (30 mL) and refluxed at 110 °C under argon atmosphere for 50 hours. The reaction was controlled by TLC. The solvent was removed under reduced pressure, chloroform was added and the mixture was washed with distilled water three times to remove alkaline solution. The organic layer was collected and dried over MgSO₄. After addition of methanol to crude product, the strongly complexing ligand; sodium diethyldithiocarbamate (10 mg) was added as a strong palladium scavenger, and the mixture was stirred for 1 hour. After filtration, the crude product was washed with methanol, acetone, and hexane using Soxhlet extractor to remove oligomers. Chloroform was used to extract the polymer. A dark pink solid was obtained after precipitation with cold methanol. Yield: 70%

¹H NMR (400 MHz, CDCl₃) δ: 8.75-7.64 (Carbazole), 7.22-6.93 (selenophene), 4.21 (-OCH₂), 3.68 (-CH), 1.79-1.09 (-CH₂), 0.84-0.73 (-CH₃).

Mw: 31000 Da, Mn: 17000 Da PDI: 1.81

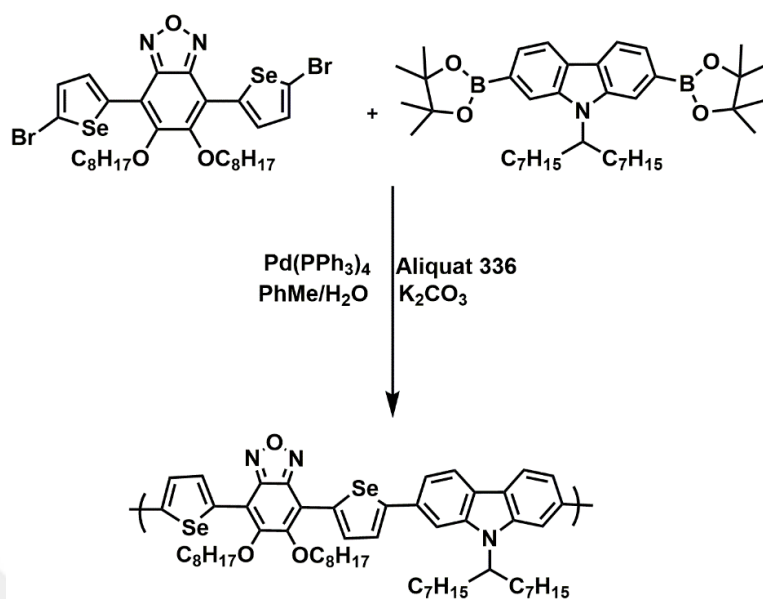


Figure 4.15. Synthetic route for PSBSC

4.2.1.3. Synthesis of PFBFC

Using a polymerization procedure similar to that described above for PSBSC, a mixture of 4,7-bis(5-bromofuran-2-yl)-5,6-bis(octyloxy)benzo[c][1,2,5]oxadiazole (174 mg, 0.26 mmol) and 9-(9-heptadecanyl)-9H-carbazole-2,7-diboronic acid bis(pinacol) ester (172 mg, 0.26 mmol) were dissolved in anhydrous toluene (30 mL) and polymerized to give PFBFC. Yield: 40 %

^1H NMR (400MHz, CDCl_3) δ : 8.25-7.70 (Carbazole), 7.50-6.96 (furan), 4.19 (-OCH₂), 3.67 (-CH), 1.98 (-CH₂), 0.82-0.68 (-CH₃)

M_w: 12000 Da, M_n: 10000 Da, PDI: 1.20

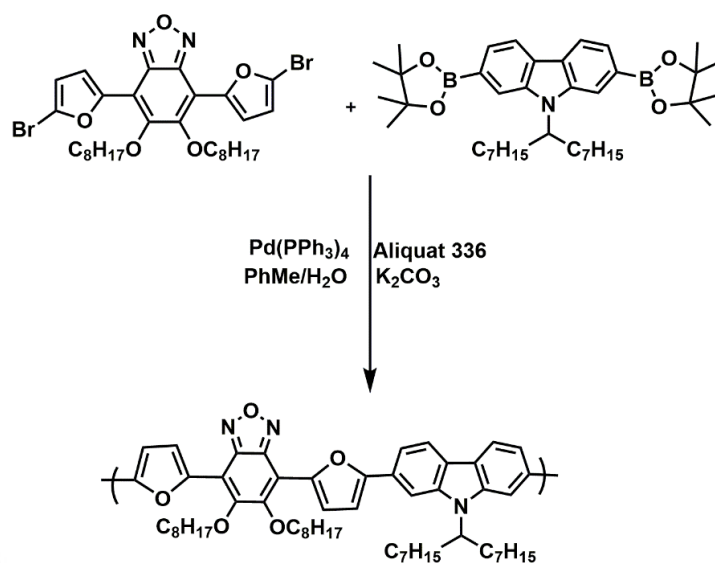


Figure 4.16. Synthetic route for PFBFC

4.2.1.4. Synthesis of PSBSFL

A mixture of 4,7-bis(5-bromoselenophen-2-yl)-5,6-bis(octyloxy)benzo[c][1,2,5]oxadiazole (104 mg, 0.13 mmol), and 9,9-dioctylfluorene-2,7-diboronic acid bis(1,3-propanediol) ester (73.2 mg, 0.13 mmol) were dissolved in anhydrous toluene (30 mL) and polymerized to give PSBSFL. Yield: 60 %

^1H NMR (400MHz, CDCl_3) δ : 8.25-7.70 (Carbazole), 7.22-6.93 (selenophene), 4.15 ($-\text{OCH}_2$), 1.97-1.00 ($-\text{CH}_2$), 0.83-0.73 ($-\text{CH}_3$)

Mw: 27000 Da, Mn: 16000 Da PDI:1.69

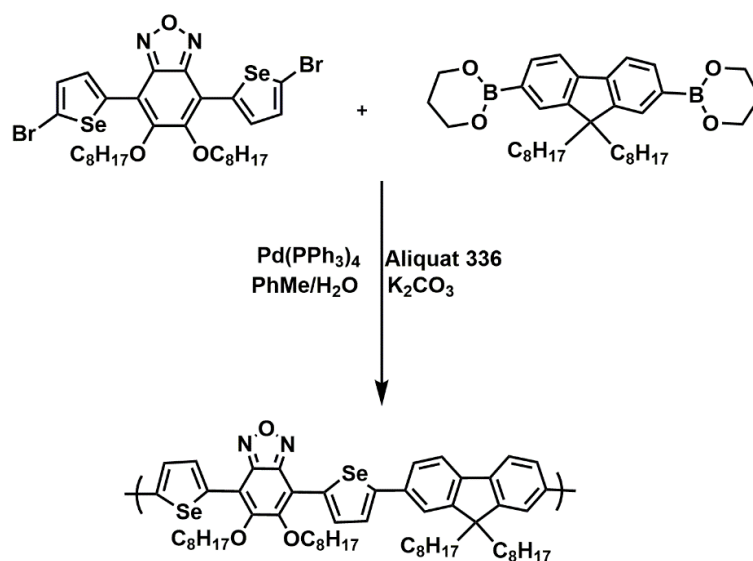


Figure 4.17. Synthetic route for PSBSFL

4.2.1.5. Synthesis of PFBFFL

Similarly a mixture of 4,7-bis(5-bromofuran-2-yl)-5,6-bis(octyloxy)benzo[c][1,2,5]oxadiazole (175 mg, 0.26 mmol), and 9,9-dioctylfluorene-2,7-diboronic acid bis(1,3-propanediol)ester (146 mg, 0.26 mmol) were dissolved in anhydrous toluene (30 mL) and polymerized to give PFBFFL. Yield: 35 %

^1H NMR (400MHz, CDCl_3) δ : 7.86-7.75 (fluorene), 7.50-6.92 (furan), 4.17 ($-\text{OCH}_2$), 1.97-1.01 ($-\text{CH}_2$), 0.83-0.69 ($-\text{CH}_3$)

Mw: 10000 Da, Mn: 6000 Da PDI: 1.67

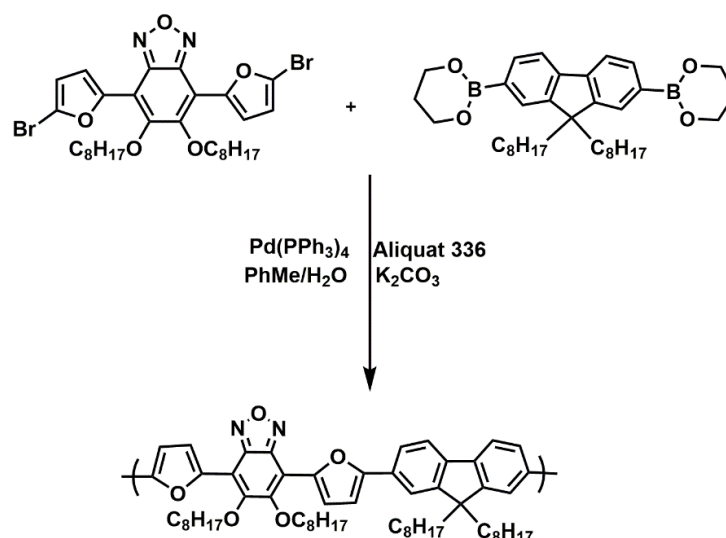


Figure 4.18. Synthetic route for PFBFFL

4.2.2. Results and Discussion

4.2.2.1. Electrochemical Studies

Cyclic voltammetry was used to investigate the electrochemical properties of the selenophene and furan bridged fluorene, carbazole/BO-based copolymers. Polymers were dissolved in chloroform to a concentration of 5 mg mL^{-1} and then spray coated on ITO coated glass electrode. Single scan cyclic voltammograms were performed in a 0.1 M solution of TBAPF_6 in acetonitrile at room temperature with a scan rate of 100 mV/s (Figure 4.19). The electrochemical properties of the polymers were summarized in Table 1. The onset oxidation and reduction potentials obtained from single scan cyclic voltammograms correspond to the HOMO and LUMO energy levels, respectively. The oxidation (doping/dedoping) potentials were $1.31 \text{ V} / 1.05 \text{ V}$ for PSBSC, $1.40 \text{ V} / 0.97 \text{ V}$ for PSBSFL, $1.10 \text{ V} / 0.98 \text{ V}$ for PFBFC and $1.26 \text{ V} / 1.01 \text{ V}$ for PFBFFL in the positive potential region. As given in the literature, furan substitution into a polymer backbone compare to selenophene, reduces the oxidation potential since oxygen-containing furan is richer in terms of electrons. Solubility, film morphology and convenient band gap of the polymer are not the only parameters for

solar cell applications. The highest occupied molecular orbital (HOMO) and the lowest unoccupied molecular orbital (LUMO) energy levels of the conducting polymers play a crucial role for fabrication of organic solar cell. To understand the electronic structures of the polymers, it is necessary to determine the energy levels of the conjugated polymers. To calculate the HOMO levels of the polymers, the onset potentials of the polymers were determined by utilizing the oxidation peak in anodic region of the cyclic voltammogram. HOMO energy levels were estimated from these values according to the energy level of the ferrocene reference (4.8 eV below vacuum level). HOMO energy levels were calculated as -5.42 eV for PSBSC, -5.33 eV for PSBSFL, -5.51 eV for PFBFC and -5.45 eV for PFBFFL according to equation (1). The polymers that exhibit n-type doping are less commonly obtained due to practically inaccessible reduction potentials and instability of organic anions, especially to water and oxygen. A rare property, n-doping, for conjugated polymer systems were clearly observed by CV studies for polymer films. The reduction (doping/dedoping) potentials were -1.50 /-1.15 V for PSBSC, -1.50/ -1.25 V for PSBSFL, -1.53/ -1.39 V for PFBFC and -1.53 /-1.12 V for PFBFFL in the negative potential region. According to equation (2), LUMO energy levels for PSBSC, PSBSFL, PFBFC, PFBFFL were -3.38 eV, -3.18 eV, -3.33 eV, -3.43 eV, respectively.

$$\text{HOMO: } - (4.75 + E_{\text{ox,onset}}) \text{ eV} \quad (1)$$

$$\text{LUMO: } - (4.75 + E_{\text{red,onset}}) \text{ eV} \quad (2)$$

Electronic band gaps of the polymers were calculated from the difference between HOMO and LUMO energy levels and were found as 2.04 eV for PSBSC, 2.15 eV for PSBSFL, 2.18 eV for PFBFC, 2.02 eV for PFBFFL. Copolymers based on carbazole, fluorene and benzooxadiazole units were synthesized by Cao and coworkers and revealed very poor reversibility for redox processes. Wei and coworkers also synthesized copolymers having same donor and acceptor moieties but with different alkyl chains. The polymers possessed irreversible doping/dedoping (reduction/reoxidation) processes in the negative potential range. [36, 37] In this

study, selenophene and furan bridges provide copolymers ambipolar character. Selenophene has chemical and physical properties similar to those of thiophene; the relatively lower aromaticity of selenophene increases the ground-state quinoid resonance character of its resulting polymers with improved planarity, increased effective conjugation length, and lower band-gap energy. [38] Selenophene comprising polymers have lower band gap than corresponding thiophene based polymers which were previously synthesized by Wei and coworkers. The electron-stabilizing effect of selenophene moieties due to larger size of Se atom than either an S or O atom resulted in narrowing of the band gap. On the other hand, furan and thiophene have similar energy levels with a comparable degree of aromaticity hence furan based copolymers possess also poor stability and similar oxidation potentials. Polymers having lower HOMO energy level can be achieved by introducing furan moiety into the polymer backbone due to high electronegativity of oxygen compare to sulfur atom. Woo et al. synthesized furan based polymers as an alternative to thiophene based ones and the results revealed increased solubility and slight difference in aromaticity.[39] When furan was introduced to polymer backbone as a π bridge, oxidation potential of the polymers were higher than expected hence higher HOMO energy levels resulted in low oxidative stability and lower Voc. The electron donating ability of the N atom is much stronger than that of C atom; hence lower band gap and higher HOMO energy levels were expected for these polymers. However, HOMO energy levels and band gap of four polymers were very similar to each other. Carbazole unit is fully aromatic and has stronger chemical and air stability than fluorene. [36] Air stability of carbazole comprising polymers (PSBSC and PFBFC) was greater than fluorene based polymers (PSBSFL and PFBFFL).

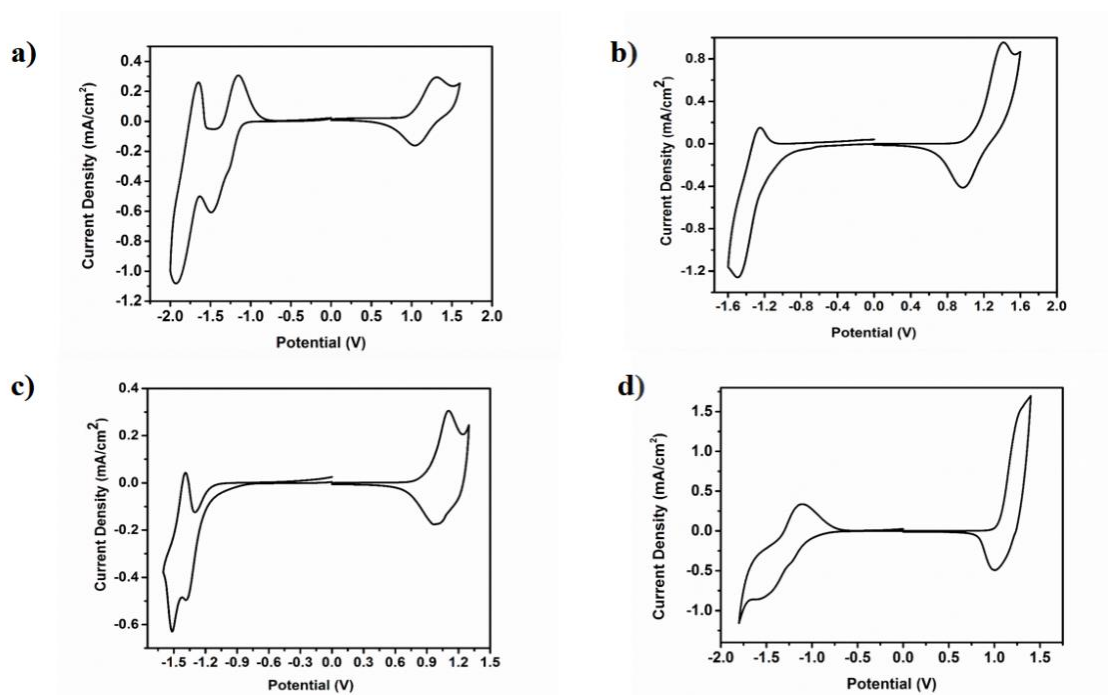


Figure 4.19. Single scan cyclic voltammograms of polymers a) PSBSC b) PSBSFL c) PFBFC d) PFBFFL on ITO in 0.1 M TBAPF₆/ACN electrolyte/solvent couple at a scan rate of 100 mV/s

Table 4.3. The comparison of optoelectronic properties of all polymers

Polymers	$E_{ox,doping}$ (V)	$E_{ox,dedoping}$ (V)	$E_{red,doping}$ (V)	$E_{red,dedoping}$ (V)	HOMO (eV)	LUMO (eV)	E_g (eV)
PSBSC	1.31	1.05	-1.50	-1.15	-5.42	-3.38	2.04
PFBFC	1.40	0.97	-1.50	-1.25	-5.51	-3.33	2.18
PSBSFL	1.10	0.98	-1.53	-1.39	-5.33	-3.18	2.15
PFBFFL	1.26	1.01	-1.53	-1.12	-5.45	-3.43	2.02

4.2.2.2. Spectroelectrochemical Studies

Spectroelectrochemistry studies were performed to explore the change in the optical properties of conducting polymer. These experiments disclose key properties of conjugated polymers such as band gap (E_g) and the intergap states that appear upon doping process. Spectroscopic measurements were performed in 0.1 M TBAPF₆/acetonitrile (ACN) solvent medium with same electrodes used in

electrochemical studies. For in situ spectroelectrochemical studies, spray coated polymer films were stepwise oxidized and spectral responses were recorded using UV-Vis-NIR spectroscopy. Figure 4.20 displays the absorption spectra of PSBSC, PSBSFL, PFBFC and PFBFFL recorded in a monomer free 0.1 M ACN/TBAPF₆ solution. The optical data including band gap (E_g), the absorption peak wavelengths (λ_{max}), the intergap states that appear upon doping and polaronic and bipolaronic band formations were obtained from spectroelectrochemistry studies. In 0.1 M ACN/TBAPF₆ solution, potential was swept between 0.0 V and 1.3 V for PSBSC, 0.0 V and 1.4 V for PSBSFL and 0.0 V to 1.1 V for PFBFC and 0.0 V and 1.1 V for PFBFFL. The increase in absorbance demonstrates the formation of polaron and bipolaron in the electronic absorption spectra. From 430 to 730 nm, broader absorption arise from intramolecular charge transfer between the acceptor (BO) and donor units. The absorption maximum revealed at 520 nm for PSBSC, at 495 nm for PSBSFL, at 550 nm for PFBFC and at 490 nm for PFBFFL corresponds to localized π - π^* transitions. The optical band gap of the polymers were calculated from those transitions as 1.98, 1.90, 1.77, 1.94 eV for PSBSC, PSBSFL, PFBFC and PFBFFL respectively. Polaronic and bipolaronic bands appear at 860 nm and 1510 nm for PSBSC. In Table 4.3, optical properties of the polymers were summarized. Color change of the polymer films observed during stepwise oxidation and needs to be defined precisely for an application in display devices (Figure 4.21). For that reason, in situ colorimetric analysis of the polymer films were studied by colorimetry analysis, which enables the determination of color coordinates. CIE (Commission Internationale de l'Eclairage) coordinates were used to point out the colors more scientifically. In the colorimetric measurements, the brightness of the color was represented as 'L', the color between red/magenta and green was represented as 'a' and the color between yellow and blue was represented as 'b'. The polymer films revealed multichromic character upon doping/dedoping and L,a,b results were reported in Table 4.4. While most of the conjugated polymers display two colors during doping/dedoping process, all polymers synthesized in this study revealed multi-coloration ranging.

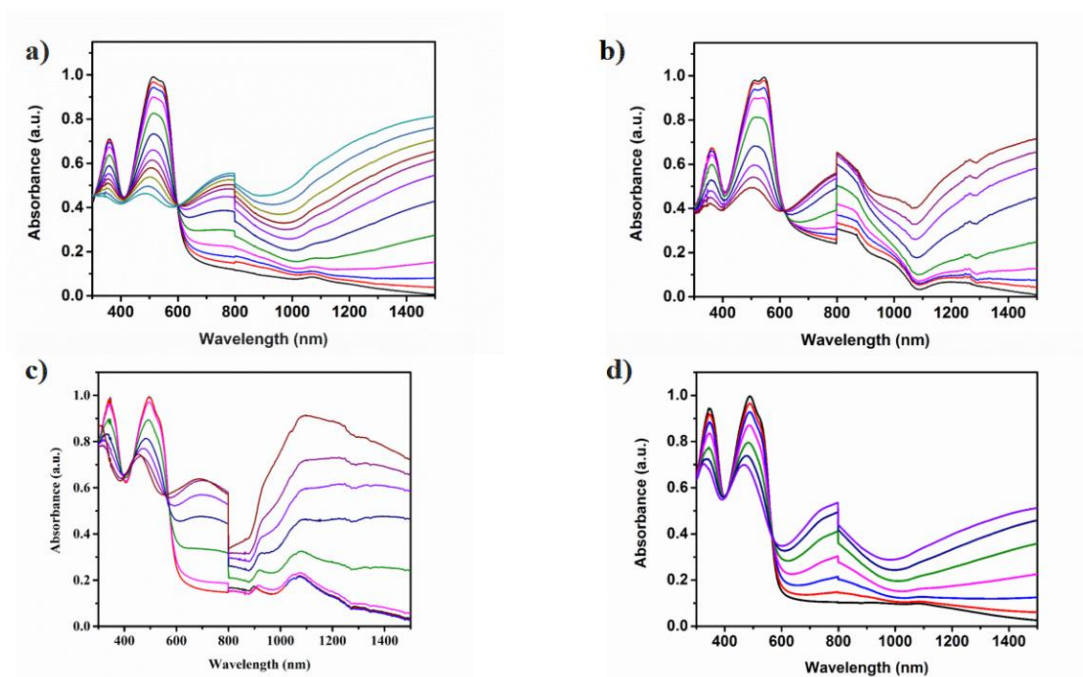


Figure 4.20. Change in the electronic absorption spectra of polymers in 0.1 M TBAPF₆/ACN solution between 0.0 V and 1.2 V for PSBSC (a), 0.0 V and 1.2 V for PSBSFL (b), 0.0 V and 1.1 V for PFBFC (c), and 0.0 V and 1.1 V for PFBFFL (d)

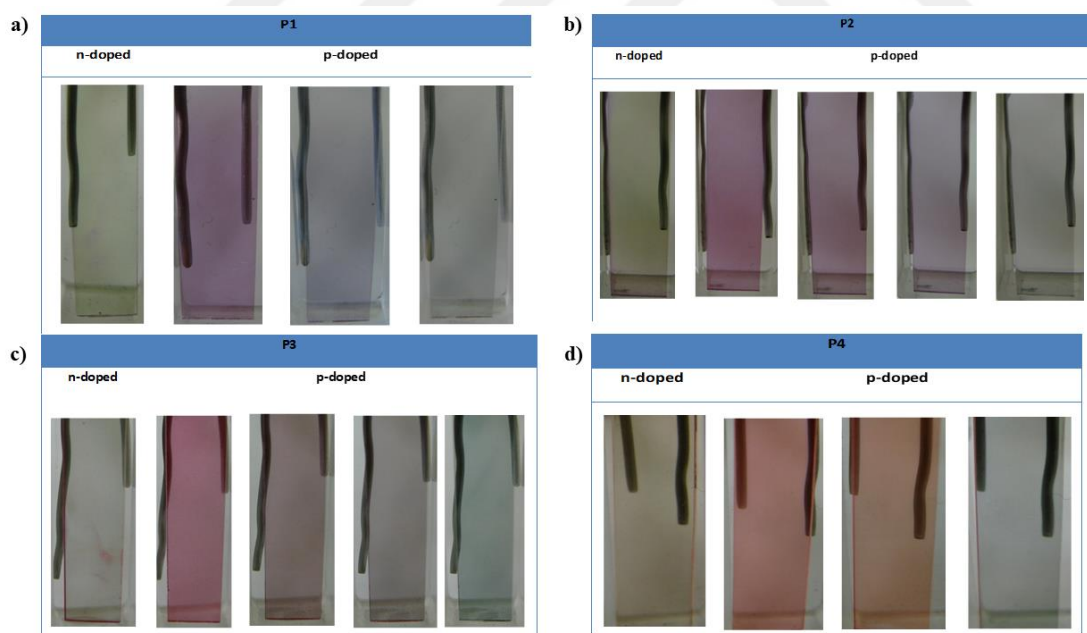


Figure 4.21. Colors of polymers. (a) PSBSC, (b) PSBSFL, (c) PFBFC, and (d) PFBFFL on ITO coated glass electrode

Table 4.4 Summary of colorimetry studies according to CIE

Polymer	Doping region	<i>L</i>	<i>a</i>	<i>b</i>
PSBSC	n-doping	69.09	-8.390	20.67
		60.18	16.23	-11.20
	p-doping	64.69	1.660	-1.187
		72.26	-5.759	6.049
PSBSFL	n-doping	60.72	-11.71	30.35
		47.37	26.69	10.78
	p-doping	53.26	15.79	4.323
		54.48	5.691	0.850
PFBFC	n-doping	69.94	-5.007	10.95
		77.75	-6.334	11.36
	p-doping	59.12	19.84	1.790
		59.59	2.422	18.64
PFBFFL	n-doping	63.87	0.412	7.203
		66.28	-5.850	4.999
	p-doping	78.98	-8.970	27.01
		62.41	18.20	24.18
		68.04	8.232	32.18
		67.62	-2.935	4.794

4.2.2.3. Photovoltaic Studies

Photovoltaic properties of the polymers in BHJ solar cells were investigated with the device stack; ITO/PEDOT:PSS/ polymer:PC₇₁BM/LiF/Al. Polymer PCBM blends were prepared at different ratios. J–V curves for the best performance cells for each polymer were represented in Figure 4.22, photovoltaic parameters were summarized in Table 4.5. Among all polymers, the highest performance was obtained with the device based on PSBSC. It exhibited a value of PCE of 1.89 % with a V_{OC} of 0.62 V, J_{SC} of 7.63 mAcm⁻², FF of 40 %, under the illumination of AM 1.5 G, 100 mWcm⁻². In order to investigate the nanoscale morphology of the polymer PCBM blends, AFM

analysis was carried out. Surface roughness values were determined as 2.60, 0.47, 15.1, and 10.1 nm for PSBSC [Fig. 4.23(a)], PSBSFL [Fig. 4.23(b)], PFBFC [Fig. 4.23(c)], and PFBFFL [Fig. 4.23(d)] blend films. Agglomerates and high root mean square roughness values obtained in PFBFC and PFBFFL PCBM blend films adversely affect the transport of charge carriers. The coarse phase separation observed in PFBFC and PFBFFL blends may be the reason of lower PCE values. As depicted in Figure 4.18(a) PSBSC PCBM blend formed continuous film morphology which is desired for high PCE values. IPCE measurements were carried out to determine the fraction of photons converted to electrons. As seen in Figure 4.24 the maximum IPCE values obtained with devices based on PSBSC, PSBSFL, PFBFC, and PFBFFL were measured 38 %, 26 %, 17 %, and 13 %, respectively.

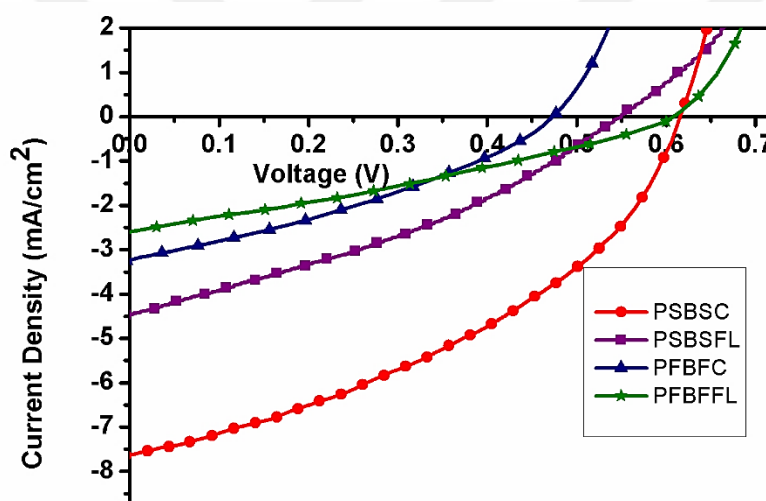


Figure 4.22. I-V curves for the photovoltaic devices

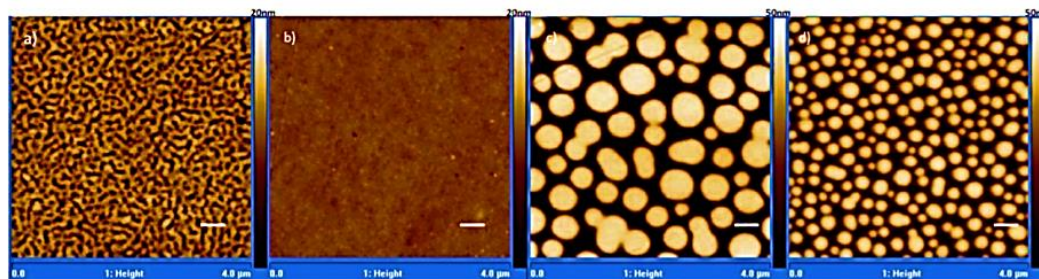


Figure 4.23. AFM images of the polymer PCBM blends (scale bar is 400 nm).

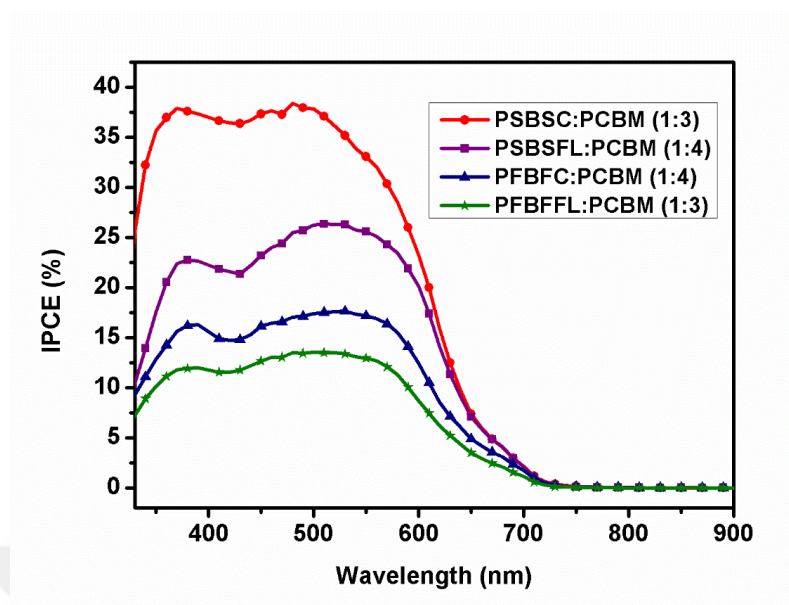


Figure 4.24. IPCE curves of the photovoltaic devices based on PSBSC:PC₇₁BM, PSBSFL:PC₇₁BM PFBFC: PC₇₁BM, and PFBFFL: PC₇₁BM blends

Table 4.5. Summary of the Photovoltaic Parameters

Polymers	V _{oc} (V)	J _{sc} (mAcm ⁻²)	FF (%)	PCE (%)
PSBSC: PCBM (1:3)	0.62	7.63	40	1.89
PFBFC: PCBM (1:4)	0.47	3.22	34	0.51
PSBSFL: PCBM (1:4)	0.55	4.46	33	0.81
PFBFFL: PCBM (1:3)	0.61	2.60	30	0.48

CHAPTER 5

RANDOM COPOLYMERS via TERPOLYMER APPROACH

5.1. Terpolymer Approach

Terpolymers which are composed of three different moieties throughout the polymer backbone are promising candidates as highly efficient electron donors for organic solar cells. Via adding a third component to donor-acceptor alternating copolymers it is possible to have synergetic effects on various important properties like absorption ability, charge mobility, and solubility. This approach has been explored as a tool to control the optoelectronic properties of donor-acceptor type polymers. New combinations of the reported donor (D) and acceptor (A) units have shown high efficiencies, exceeding 7–8 %, demonstrating great potential of terpolymers as alternative donors for solar cells. [40] Unlike normal donor–acceptor polymers with one electron-deficient segment in their repeating unit, two electron rich (or electron poor) moieties are combined with one electron poor (or electron rich) building block (Figure 5.1) which could lead to broadening of their absorption spectra and harvesting of photons efficiently. Another opportunity is to tune the HOMO and LUMO energy levels and molecular packing. [41-44]

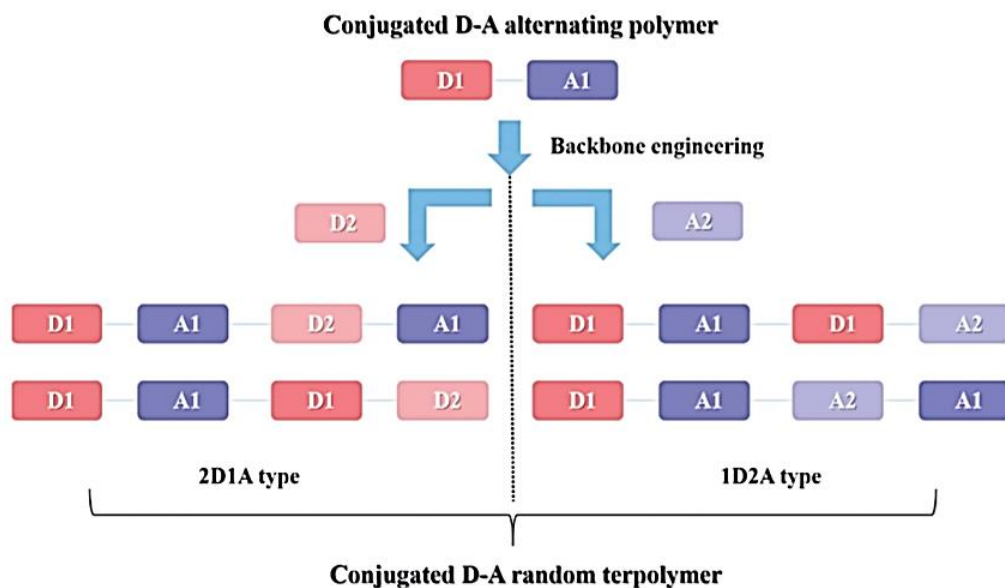


Figure 5.1. General structure of conjugated D–A random terpolymers

Polymer Journal volume 50, pages 21–31 (2018)

5.2. Syntheses

5.2.1. The Impact of Donor Moieties on the Polymer Backbone

5.2.1.1. Synthesis of P1

In a 50 mL three-necked flask, 4,7-dibromo-5,6-bis(octyloxy)-benzo[*c*][1,2,5]oxadiazole (160 mg, 0.30 mmol), 2,5-bis(tributylstannyl)thiophene (99.3 mg, 0.15 mmol) and 2,6-bis(trimethylstannyl)-4,8-bis(2-ethylhexyloxy)benzo[1,2-*b*:4,5-*b'*]dithiophene (116 mg, 0.15 mmol) were added and purged with argon for 1 hour. After addition of THF (20 mL), the mixture was stirred and purged with argon for another 30 min. Then, bis(triphenylphosphine)palladium(II) dichloride (5 mol %) was added to the solution and the mixture was heated at 90 °C for 48 hours. The polymer was end-capped after successful polymerization with phenyl end-groups to remove reactive trimethyltin or bromide groups which cause charge trapping. The solvent was evaporated under reduced pressure. After addition of methanol to the crude product, the strongly

complexing ligand; sodium diethyldithiocarbamate (10 mg) was added to remove residual palladium and the solution was stirred for 1 hour. After filtration, the crude product was washed with methanol, acetone, and hexane using a Soxhlet extractor to remove low molecular weight fractions. Chloroform was used to extract the polymer to give a dark blue solid. Yield: 50 %

^1H NMR (400 MHz, CDCl_3) δ : 8.57, 4.34, 3.67, 2.16, 1.92–1.14, 1.04, 0.91

Mw: 22000 Da Mn: 18000 Da PDI: 1.24

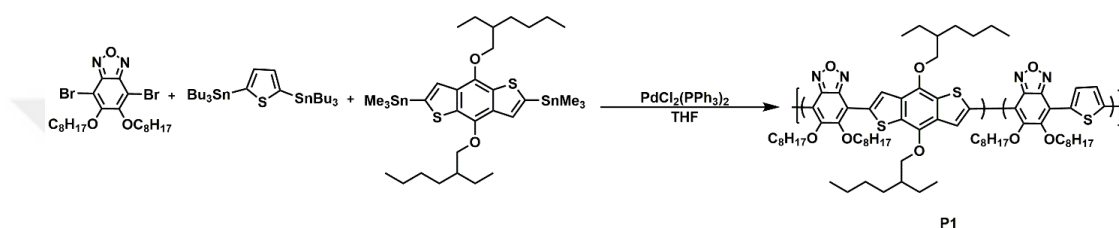


Figure 5.2. Synthetic route for P1

5.2.1.2. Synthesis of P2

A polymerization procedure similar to that described above for P1 was used for the preparation of P2. A mixture of 4,7-bis(5-bromothiophen-2-yl)-5,6-bis(octyloxy)benzo[c][1,2,5]oxadiazole (200 mg, 0.29 mmol), 2,5-bis(tributylstannyl)thiophene (94.7 mg, 0.14 mmol), 2,6-bis(trimethylstannyl)-4,8-bis(2-ethylhexyloxy)benzo[1,2-*b*:4,5-*b'*]dithiophene (110 mg, 0.19 mmol), and bis(triphenylphosphine)palladium(II) dichloride (5 mol %) was dissolved in anhydrous THF (25 mL) and polymerized to give P2. Yield: 85 %

^1H NMR (400 MHz, CDCl_3) δ : 7.30–7.24, 7.50–6.96, 4.14, 3.68, 1.80, 1.37–1.19, 0.94

Mw: 20000 Da Mn: 17000 Da PDI: 1.15

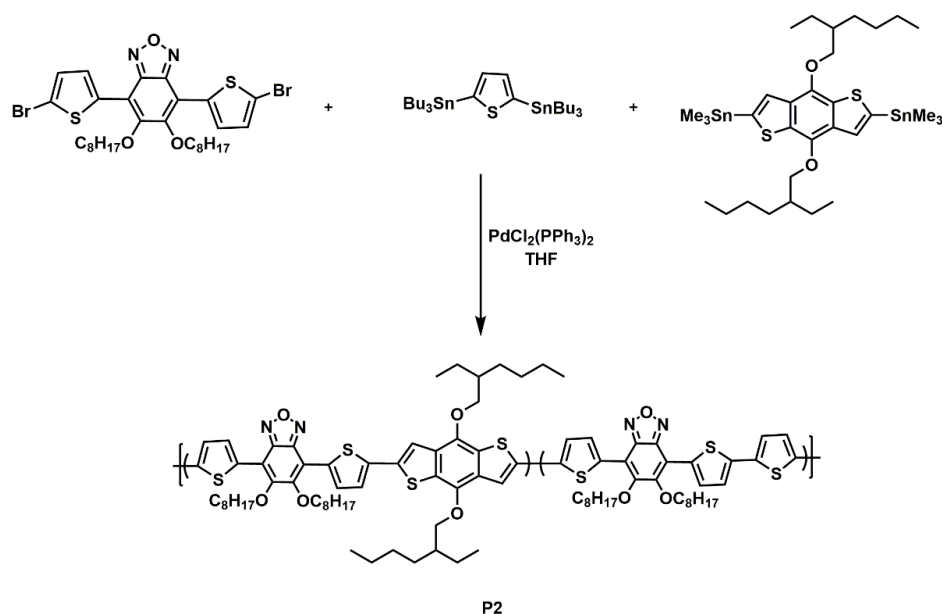


Figure 5.3. Synthetic route for P2

5.2.1.3. Synthesis of P3

Using a polymerization procedure similar to that described above for P1, P2 was synthesized. A mixture of 4,7-bis(5-bromothiophen-2-yl)-5,6-bis(octyloxy)benzo[*c*][1,2,5]oxadiazole (100 mg, 0.12 mmol), 2,5-bis(tributylstannyl)thiophene (41.0 mg, 0.06 mmol), 2,6-bis(trimethylstannyl)-4,8-bis(2-ethylhexyloxy)benzo[1,2-*b*:4,5-*b'*]dithiophene (47.6 mg, 0.06 mmol) and bis(triphenylphosphine)palladium(II) dichloride (5 mol %) was dissolved in anhydrous THF (20 mL) and polymerized to give P3. Yield: 44 %.

^1H NMR (400 MHz, CDCl_3) δ : 7.45, 6.93, 4.14, 3.68, 1.97–1.18, 0.84

Mw: 48000 Da Mn: 45000 Da PDI: 1.06

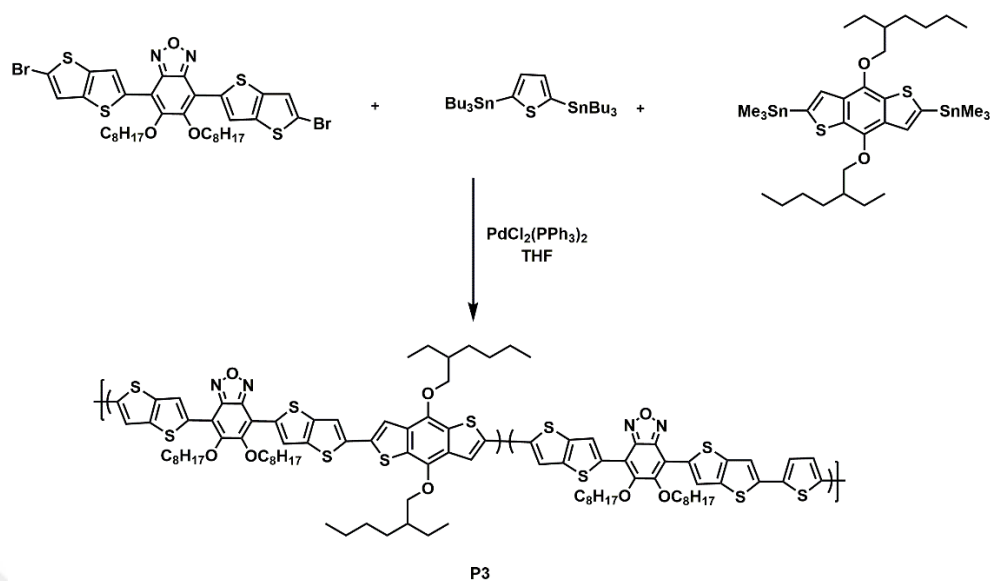


Figure 5.4. Synthetic route for P3

5.3. Results and Discussion

5.3.1. Electrochemical Studies

Electronic and optical properties of polymers play a crucial role in the application areas of polymers. Low oxidation potentials, low band gaps or broad absorption spectrum are some of the requested qualifications for polymers for several applications especially in organic photovoltaics. [31] Cyclic voltammetry was used to investigate the redox behaviors of polymers. It is performed via a three electrode system where the potential is scanned at a working electrode relative to a known reference electrode while recording the resulting current. System has a potentiostat and a cell consisting of a silver wire as the reference electrode, an indium tin oxide (ITO) coated glass as the working electrode and a platinum wire as the counter electrode. A solution of polymers with a 5 mg mL^{-1} concentration in chloroform solvent was spray coated on to the working electrode using a spray gun. Cyclic voltammetry studies were performed in a $0.1 \text{ M NaClO}_4\text{-LiClO}_4/\text{ACN}$ supporting electrolyte/solvent system at a scan rate of 100 mV/s . It is a fact that n-type doping is a rare property for conducting polymers since organic anions are very sensitive to water and oxygen. For conjugated polymers P₁ and P₂, n-doping was observed in the cyclic voltammetry studies. The

solutions were degassed with nitrogen before each measurement in order to have an inert system.

As shown in Figure 5.5, P1 and P2 have ambipolar characteristics while P3 has only p-dopable character. Single scan cyclic voltammetry runs were performed in the range of -2.00 V / 1.30 V for P1, -1.90 V / 1.30 V for P2 and 0.00 V / 1.75 V for P3, respectively. Corresponding oxidation/reduction potentials in p-doped state were recorded as 1.15 V / 0.75 V for P1, 0.90 V / 0.80 V for P2 and 1.10 V / 0.90 V for P3 whereas the doping/dedoping potentials in n-doped state were observed as -1.80 V / -1.60V for P1 and -1.70 V / -1.50 V for P2, respectively (Table 5.1). Recently, the insertion of π -bridges between donor-acceptor units is a straightforward way in structural modifications of polymers which leads to enhance the electronic and optical properties of polymers.⁴⁰ In this study, thiophene and thieno[3,2-*b*]thiophene linkages eliminate the torsion angle and allow the polymer to adopt a planar structure. In addition, overall aromaticity of the system is decreased and hence polymers with lower band gaps can be obtained. As seen in Figure 5.5, P2 has a lower oxidation potential than P1 as a consequence of more efficient intramolecular charge transfer (ICT) between donor-acceptor units through thiophene unit. Trang et al. stated that as the number of thiophene rings in the polymer backbone increases oxidation potential of the polymers comprising 2,1,3-benzooxadiazole unit decreases.[32] Although it seems that P₃ has a higher oxidation peak than P1 and P2, it starts to get oxidized around 0.8 V and shows a broad redox behavior compared to P1 and P2. Thus, introducing thieno[3,2-*b*]thiophene unit rather than thiophene as a π -linker enhances the intermolecular charge transfer and doping/dedoping processes can be performed more easily. Due to its more rigid and fused structure, thienothiophene provides more π -electron delocalization on polymer chain and higher charge mobilities. [33] The oxidation potentials of P1 and P2 in the n-doped states cannot be observed clearly; however, they show a reversible color change during the n-type doping/dedoping processes. Cyclic voltammetry studies were also performed at different scan rates to prove electroactivity of polymer films (Figure 5.6). This study also showed that

polymers were well adhered to the working electrode. As the scan rate increases, current response of the polymers increases as supported by the Randles-Sevcik equation. [34] The linear dependence of anodic/cathodic current peak as a function of the scan rate proves the non-diffusion controlled mass transfer during the redox processes. Scan rate studies of P1 could not be performed since it is not as stable as P2 and P3. Due to the lack of π -bridge unit in P1, the intermolecular interactions of alkyl chains on benzodithiophene and benzooxadiazole units decrease the ICT between donor-acceptor units. HOMO/LUMO energy levels were calculated from the onset values of the oxidation/reduction potentials of the polymers from the cyclic voltammetry studies. NHE was taken as -4.75 eV against vacuum level. Accordingly, HOMO/LUMO energy levels ($E_{\text{HOMO}}/E_{\text{LUMO}}$) were calculated using equations 1 and 2 respectively.

$$\text{HOMO} = -(4.75 + E_{ox}^{onset}) \text{ (eV)} \quad (1)$$

$$\text{LUMO} = -(4.75 + E_{red}^{onset}) \text{ (eV)} \quad (2)$$

HOMO energy levels were calculated as -5.55 eV, -5.35 eV and -5.15 eV while corresponding LUMO energy levels were calculated as -3.35 eV, -3.55 eV and -3.43 eV for P1, P2, and P3, respectively. P2 has lower band gap compared to similar studies in literature with benzodithiophene and benzooxadiazole units. [35] Thus, it was shown that coupling of strong electron donor and acceptor units with efficient bridging agents can produce polymers with lower band gaps. HOMO energy levels of polymers increased as the electron transporting ability of π -bridge unit increases. It was shown that thienothiophene unit is richer in electron density compare to thienyl substituent [45], and thienothiophene containing polymers show high lying HOMO energy levels compared to thiophene containing ones. [46] Thus P3 has a higher HOMO energy level than P2 and P1 due to conjugation and charge transport between D-A units.

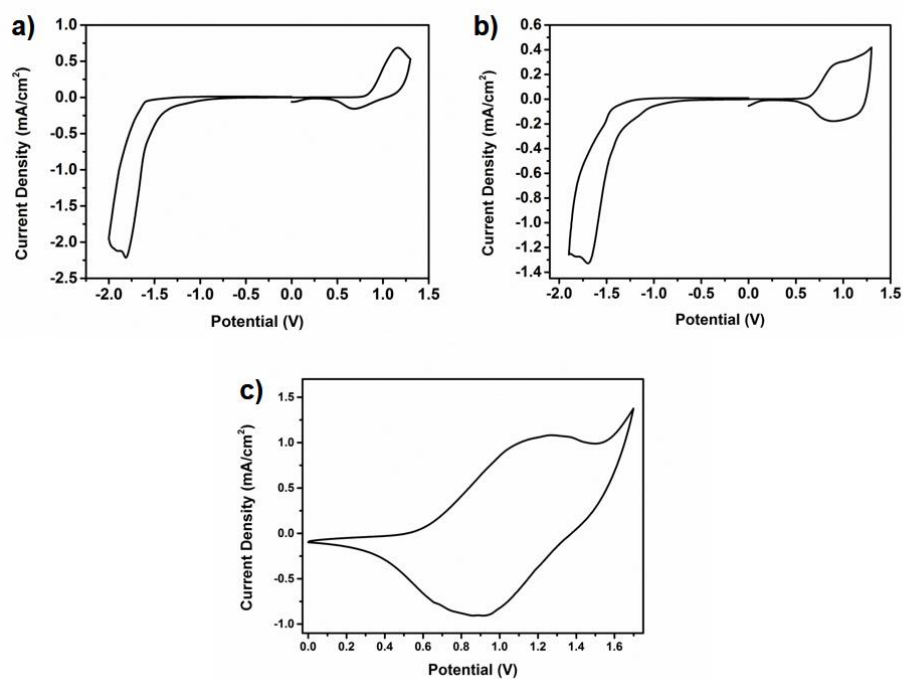


Figure 5.5. Single scan cyclic voltammograms of polymers a) P1 b) P2 c) P3

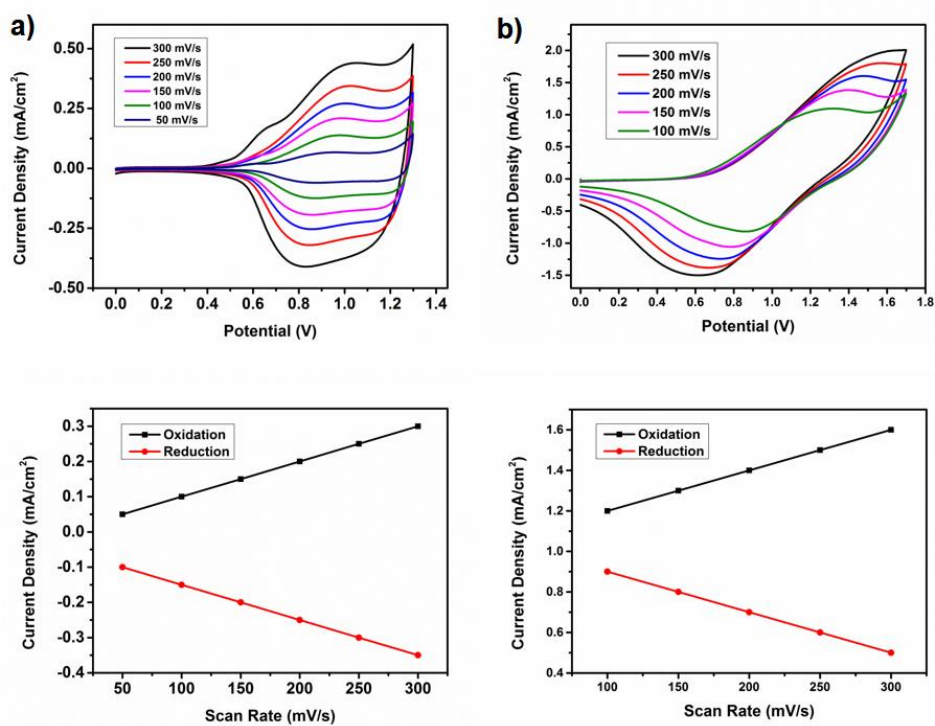


Figure 5.6. Scan rate studies polymers a) P1 b) P2

5.3.2. Optical Studies

Spectroelectrochemical studies were performed to observe the optical properties of polymers such as maximum absorption wavelength of the neutral polymer film which is correlated with its neutral state color and used to calculate the optical band gaps of polymers. Formation of polaron/bipolaron bands are regarded as the charge carriers on polymer backbone. In order to investigate optical properties, polymers were dissolved in chloroform and then spray coated on the ITO coated glass electrode. All experiments were performed in 0.1 M NaClO₄-LiClO₄/ACN supporting electrolyte/solvent system. Starting from the neutral state absorption spectra were scanned through Visible-NIR region up to the most oxidized state of polymers by step wise increasing the potential. As shown in Figure 5.7, P1 and P2 have absorption peaks around 350-400 nm in the visible range presumably due to the π - π^* transition in the conjugated polymer back bone. The maximum absorption bands of polymers were observed around 610 nm with a 560 nm shoulder for P1, around 560 nm for P2 and 520 nm for P3, which can be attributed to the intramolecular charge transfer (ICT) between benzodithiophene (donor) and benzooxadiazole (acceptor) segments. The neutral state colors of polymers were similar to each other, and they reveal λ_{max} values in the visible region. Optical band gaps of polymers were calculated using the onset value of these maximum absorption wavelengths which are 680 nm for P1, 700 nm for P2 and 720 nm for P3. Corresponding optical band gaps were calculated as the 1.82 eV for P1, 1.77 eV for P2 and 1.72 eV for P3, respectively. Lower band gaps could be achieved via introducing stronger π -bridges into the polymer backbone. Optical properties of three polymers were summarized in Table 5.1. The difference between electronic and optical band gaps may arise due to creation of free ions instead of neutral excited state in the electrochemical studies. Hence, optical band gaps are found lower than that of electronic ones. As seen from Figure 3a, polaron/bipolaron band formations could not be observed clearly for P1 compared to P2 and P3. This might be due to the fact that the polymer cannot be fully oxidized as the neutral band

could not be depleted completely via applying a higher potential than 1.0 V (Figure 5.7a-P1).

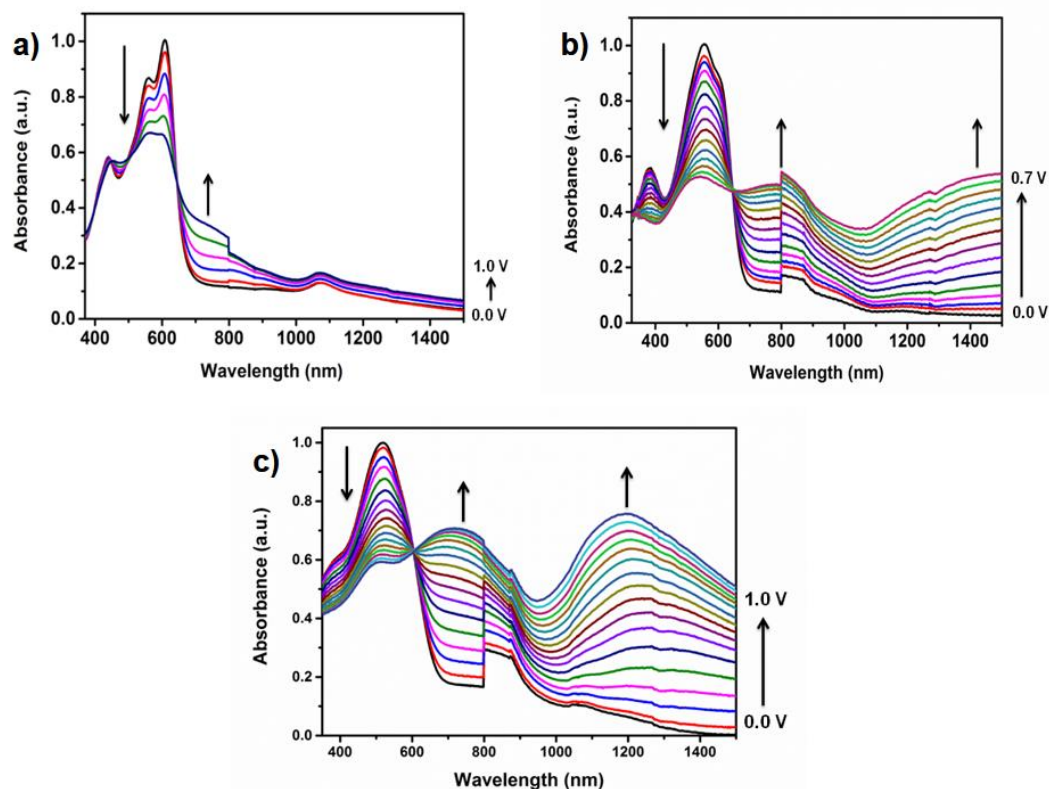


Figure 5.7. Electronic absorption spectra of polymers in 0.1 M NaClO₄-LiClO₄/ACN solution
a) P1 b) P2 c) P3

P1 and P2 exhibit a light blue color whereas P3 has a light purple color in their neutral states (Figure 5.8). Upon applied potential, polymers revealed a gray-transparent color in their oxidized states. For further characterizations, colorimetry studies were performed and scientific color results were summarized in Table 5.2 according to the CIE (Commission Internationale de l'Eclairage) standards. In CIE coordinates, L represents the luminescence (brightness) of a color, a represents the color between red/magenta and green, b represents the color between yellow and blue.

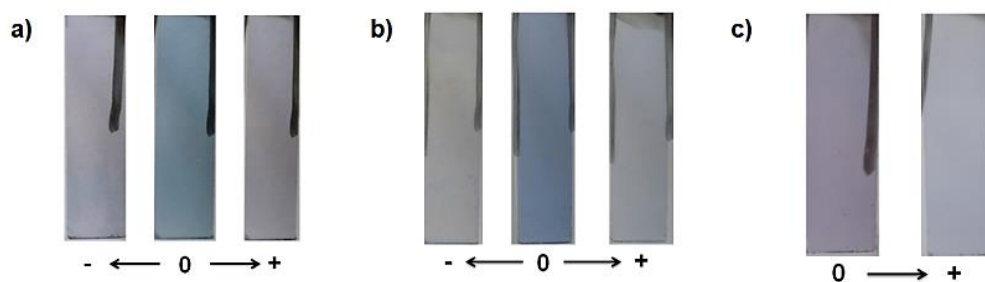


Figure 5.8. Colors of polymers upon applied potential a) P1 b) P2 c) P3

Table 5.1 Comparison of optical and electronic properties of random copolymers

Polymer	$E_{ox/red}$ (V)	E_{ox}^{onset} (V)	λ_{max} (nm)	λ_{max}^{onset} (nm)	E_{gop} (eV)	$HOMO$ (eV)	$LUMO$ (eV)
P1	1.15/0.75	0.80	610	680	1.82	-5.55	-3.73
P2	0.90/0.80	0.60	560	700	1.77	-5.35	-3.58
P3	1.10/0.90	0.40	520	720	1.72	-5.15	-3.43

Table 5.2 Summary of colorimetry studies according to CIE

Polymer	Applied Potential (V)	L	a	b
P1	0.0	67.46	-7.33	-10.09
	1.0	72.58	0.01	-0.01
	-1.7	82.87	-0.99	-1.48
P2	0.0	69.83	-3.89	-15.88
	0.7	76.34	-0.96	-2.63
	-1.6	78.93	-0.81	-1.99
P3	0.0	67.19	9.61	-15.28
	1.0	76.59	2.01	-3.28

5.3.3. Kinetic Studies

Kinetic studies were performed to investigate percent transmittance change (ΔT %) and switching time of the polymers. Switching time can be defined as the time required switching between the two extreme states i.e. neutral and oxidized/reduced states of

the polymer at a 95 % optical contrast. The measurements were done between neutral and fully oxidized/reduced states by applying a square-wave potential within a 5 s time interval at wavelengths in which maximum absorption values were obtained in Vis-NIR regions. The wavelengths for neutral, polaron and bipolaron regions were chosen from the spectroelectrochemical studies. Corresponding percent transmittance values were recorded as 10 % at 560 nm, 6 % at 800 nm and 24 % at 1265 nm for P2 whereas P3 revealed an optical contrast of 27 % at 520 nm and 17 % 1230 nm for P3, respectively. Since P1 is not strongly as stable as P2 and P3 kinetic studies of P₁ cannot be performed. Results were calculated from Figure 5.9 and summarized in Table 5.3.

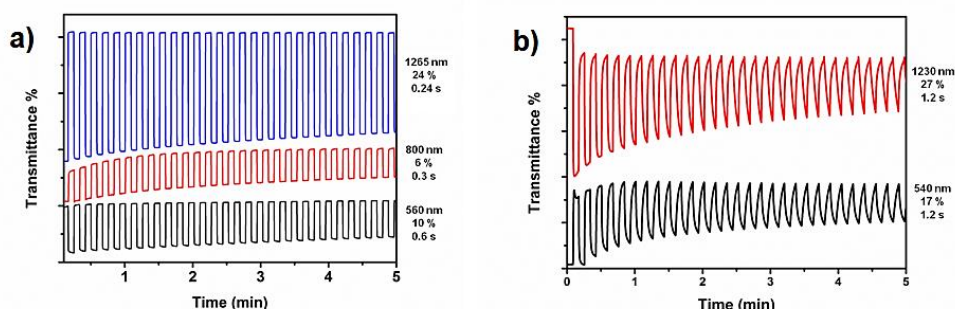


Figure 5.9. Percent transmittance change and electrochromic switching times of a) P2 and b) P3 when switched between neutral and oxidized states in 0.1 M NaClO₄-LiClO₄/ACN

Table 5.3 Summary of results of kinetic studies for P2 and P3

Polymer	Wavelength (nm)	Transmittance %	Switching time (s)
P2	560	10	0.6
	800	6	0.3
	1265	24	0.2
P3	540	17	1.2
	1230	27	1.2

5.3.4. Photovoltaic Studies

The photovoltaic properties of the polymer was investigated in BHJ solar cells with the device structure of ITO/PEDOT:PSS/Polymer:PC₇₁BM/LiF/Al. Active layers were obtained from dichlorobenzene, in order to optimize the morphology of the active layer high boiling point additive DIO (1,8-diiodooctane) was added. Polymer:PC₇₁BM weight ratio was optimized between 1:1 and 1:3. 1:1 weight ratio with 3.0 % weight concentration gives the highest efficiency. Device current density-voltage (J–V) characteristics are depicted in Figure 5.10 and photovoltaic parameters are summarized in Table 5.4. Without any post-treatment, P2 incorporated device spin-coated from dichlorobenzene exhibited power conversion efficiency (PCE) of 4.48 % with a J_{sc} value of 8.88 mA cm⁻², Voc of 0.79 V, FF of 64 %. 0.5 vol% DIO addition improved the device performance to 4.79 % through a rise in current density. DIO dissolves PC₇₁BM selectively hence PC₇₁BM can intercalate into the polymer rich domains, promoting the donor acceptor interfacial area, resulting in interpenetrated networks. [48,49] Further optimizations in the DIO amount were carried out; 1.0 vol % DIO was found as the optimum amount. The use of 1.0 vol % DIO led to an improvement to 5.17 % PCE with an open circuit voltage of 0.79 V, a short-circuit current density of 10.24 mA cm⁻², and a fill factor of 64 %.

The nanoscale morphologies of the active layers were investigated with AFM in tapping mode. Active layer root mean square roughnesses (rms) were determined as 1.97 nm and 2.60 nm for the active layers spin coated from DCB and DCB with 1.0 % DIO, respectively. Due to volatilization of the DIO, PC₇₁BM molecules tend to aggregate near the top surface leading to increase in roughness.[47] For further understanding of the active layer morphologies, TEM (transmission electron microscopy) analysis were carried out. Fiber-like domains with enhanced donor acceptor interfacial area which is crucial for charge separation and charge transport are seen in the TEM image of P2:PC₇₁BM (1:1) films spin coated from dichlorobenzene with 1.0 % DIO (Figure 5.11).

By using incident photon to current efficiency (IPCE) method, the ratio of number of charges collected by electrodes to the number of incident photons was investigated. 57 % IPCE was obtained at 530 nm for the best performance solar cell as depicted in Figure 5.12.

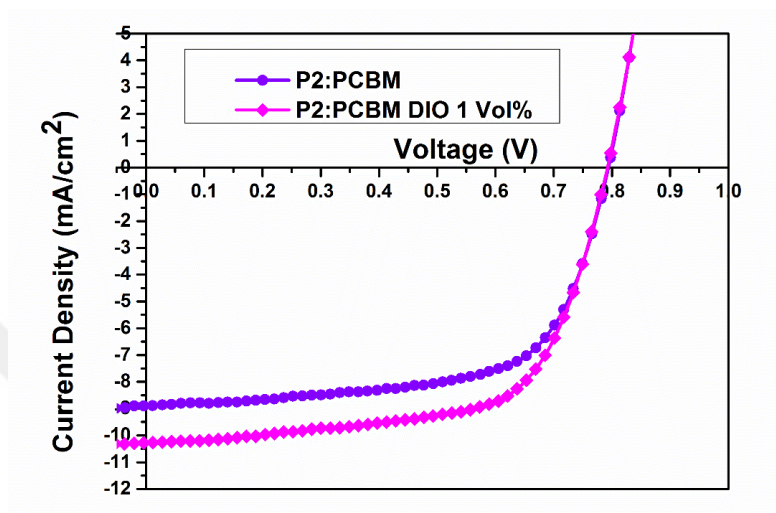


Figure 5.10. Current density - voltage curves of the optimized P2:PC₇₁BM (1:1) devices with and without 1.0 vol % DIO.

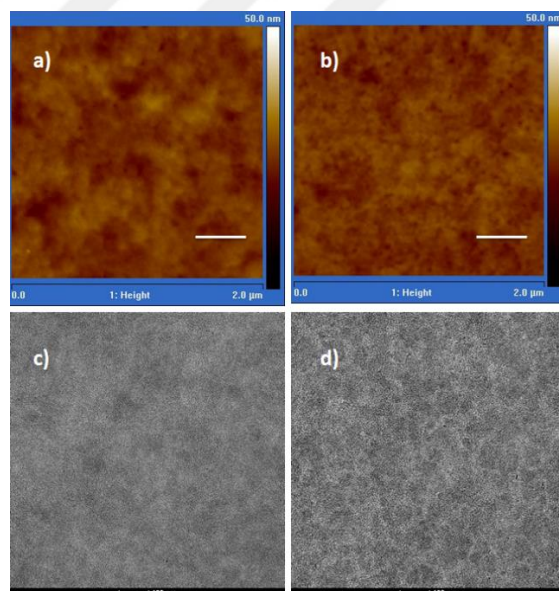


Figure 5.11. AFM images of P2:PC₇₁BM (1:1) films spin coated (a) from dichlorobenzene without additive (b) from dichlorobenzene with 1.0 % DIO. (Scale bar is 400 nm) TEM images of P2:PC₇₁BM (1:1) films spin coated (c) from dichlorobenzene without additive (d) from dichlorobenzene with 1.0 % DIO

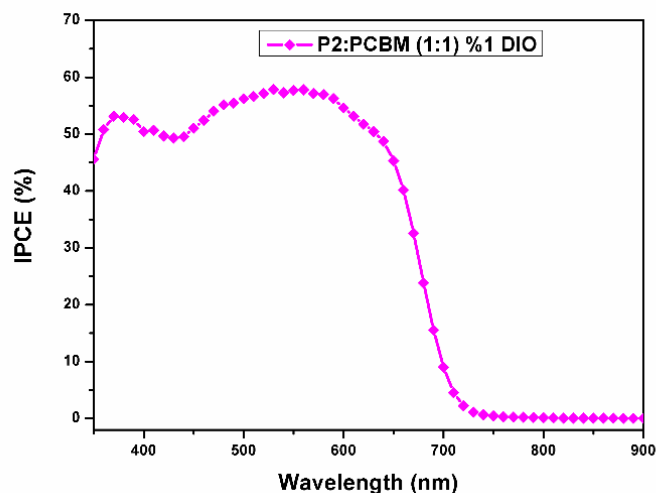


Figure 5.12. IPCE curve of the photovoltaic device based on P2:PC₇₁BM (1:1) spin coated from dichlorobenzene with 1.0 % DIO

Table 5.4 Summary of the photovoltaic parameters for P2

Polymer:PC ₇₁ BM	V _{oc} (V)	J _{sc} (mAcm ⁻²)	FF (%)	PCE (%)	Additive (DIO)
1:3	0.80	4.20	67	2.25	-
1:2	0.80	6.29	66	3.32	-
1:1	0.79	8.88	64	4.48	-
1:1	0.80	9.52	63	4.79	0.5 vol %
1:1	0.79	10.24	64	5.17	1.0 vol %
1:1	0.78	9.12	65	4.62	2.0 vol%

2,1,3-Benzooxadiazole, thiophene and benzodithiophene based random copolymers were synthesized *via* Stille polycondensation reaction. Thiophene and thieno[3,2-*b*]thiophene were used as π -conjugated linkers. P1 and P2 exhibit a light blue color whereas P3 has a light purple color in their neutral states. P1 has an optical band gap of 1.82 eV whereas optical band gaps of P2 and P3 are 1.77 eV and 1.72 eV, respectively. Incorporation of conjugated linkers into polymer backbone provided us to obtain lower band gap polymers due to increase in the π -electron density. Without any post-treatment, the blend of P2 and PC₇₁BM ([6,6]-phenyl-C₇₁-butyric acid

methyl ester), exhibited a value of PCE of 4.48 % with a J_{sc} value of 8.88 mA cm^{-2} , V_{oc} of 0.79 V, FF of 64 % under the illumination of AM 1.5 G, 100 mW cm^{-2} . The addition of DIO improved the device performance to 5.17 % through a rise in current density. P3 has very low solubility in common solvents due to its high molecular weight, hence device construction of this polymer could not be achieved. For ease of device construction, monomers possessing solubilizing alkoxy chains were used to synthesize random copolymers. However, P1 has no π bridge between the donor and acceptor moieties and the alkyl chains may lead to very low interaction between PC₇₁BM and the polymer. This may as well be the reason for not getting proper film coating on the substrate. Therefore, we could not obtain an I-V curve from the devices of this polymer. The reason for P3 not revealing I-V characteristics may arise from β -branching which may be seen for thienothiophene unit. Hence, the polymer would not be soluble in common solvent even it does not have very high molecular weight.

5.4. The Impact of Acceptor Moieties on the Polymer Backbone

5.4.1. Syntheses

5.4.1.1. Synthesis of RP1

4,7-Dibromo-5,6-bis(octyloxy)benzo[c][1,2,5]oxadiazole (74.1 mg, 0.14 mmol), 4,7-dibromo-5,6-difluorobenzo[c][1,2,5]thiadiazole (45.7 mg, 0.14 mmol), (4,8-bis(5-(2-ethylhexyl)thiophen-2-yl)benzo[1,2-*b*:4,5-*b'*]dithiophene-2,6-diyl)bis(trimethylstannane) (251 mg, 0.28 mmol), tetrakis(triphenylphosphine)palladium(0) (8.00 mg, 0.01 mmol) and freshly distilled toluene (2 mL) were added to a 10 mL schlenk tube purged with argon for 1 hour. The mixture was placed into a pre-heated oil bath which was 95 °C and stirred for 20 hours. The polymerization was controlled by TLC and stopped by the addition of 5 mL of *o*-dichlorobenzene (*o*-DCB) and stirred for an additional 20 min. The polymer was precipitated in methanol and washed with acetone and hexane in a Soxhlet apparatus to remove the oligomers and catalyst residue. The polymer was collected using

chloroform. After solvent evaporation, cold methanol and the strongly complexing ligand; sodium diethyldithiocarbamate (10 mg) were added to remove residual palladium and the solution was stirred for 1 hour. The polymer was filtered and collected as a dark purple. Yield: 35 %

ν_{\max} (KBr, cm^{-1}): 3839-3740 (O-H), 2923 (C-H, alkane), 2855 (C-H), 2646 (S-H), 2347 (O=C=O), 1455 (C-H, alkane), 1375 (C-H), 1199 (C-O), 1088 (S-O), 992 (C=C, alkene), 848 (C-H, substituted benzene), 799-725 (C-H, benzene derivative), 531-448 (C-Br)

^1H NMR (400 MHz, CDCl_3) δ : 8.76, 7.65, 7.45, 6.91, 6.81, 6.75, 4.09, 3.93, 2.93, 1.33, 1.30, 0.95

Mw: 27000 Da Mn: 10000 Da PDI: 2.70 RP1-os

Mw: 12300 Da Mn: 5700 Da PDI: 2.15 RP1-ss

The abbreviations reveal the polymers with the same chemical structure. However, the only difference between two reactions were the catalytic system. tetrakis(triphenylphosphine)palladium(0) (8.00 mg, 0.01 mmol) was used for RP1-os and tris(dibenzylideneacetone)dipalladium(0) (6.76 mg, 0.02 mmol) and triphenylarsine (24.5 mg, 0.08 mmol) were used for RP1-ss.

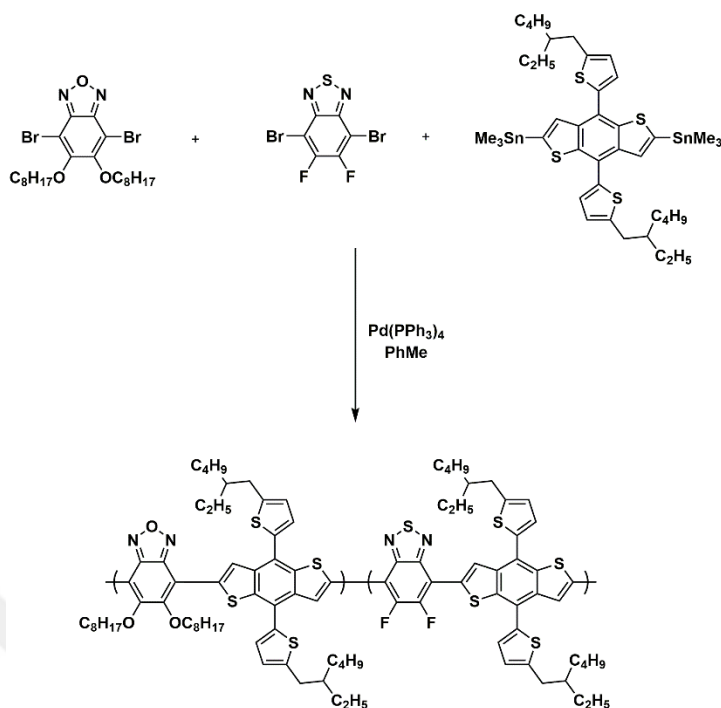


Figure 5.13. Synthetic route for RP1

5.4.1.2. Synthesis of RP2

Polymerization procedure similar to that described above for RP1 was used for the preparation of RP2. A mixture of 4,7-dibromobenzo[*c*][1,2,5]oxadiazole (77.5 mg, 0.28 mmol), 4,7-dibromo-5,6-difluorobenzo[*c*][1,2,5]thiadiazole (92.1 mg, 0.28 mmol), (4,8-bis(5-(2-ethylhexyl)thiophen-2-yl)benzo[1,2-*b*:4,5-*b'*]dithiophene-2,6-diyl)bis(trimethylstannane) (505 mg, 0.56 mmol) and tetrakis(triphenylphosphine)palladium(0) (16.1 mg, 0.02 mmol) were dissolved in anhydrous toluene (3 mL) in a 10 mL schlenk tube under inert atmosphere and polymerized to give RP2. Yield: 30 %

ν_{max} (KBr, cm^{-1}): 3840-3741 (O-H), 2955-2922 (C-H, alkane), 2855 (C-H), 2650 (S-H), 2285 (C-N), 1596 (C=C, conjugated alkene), 1475-1455 (C-H, alkane), 1375 (C-H, alkane), 1300 (S-N), 1100 (C-O), 897 (C-H, substituted benzene), 797-725 (C-H, benzene derivative), 661 (C-Br), 531-447 (C-Br)

^1H NMR could not be recorded due to low solubility of the polymer.

Mw:6000 Da Mn: 5000 Da PDI: 1.20

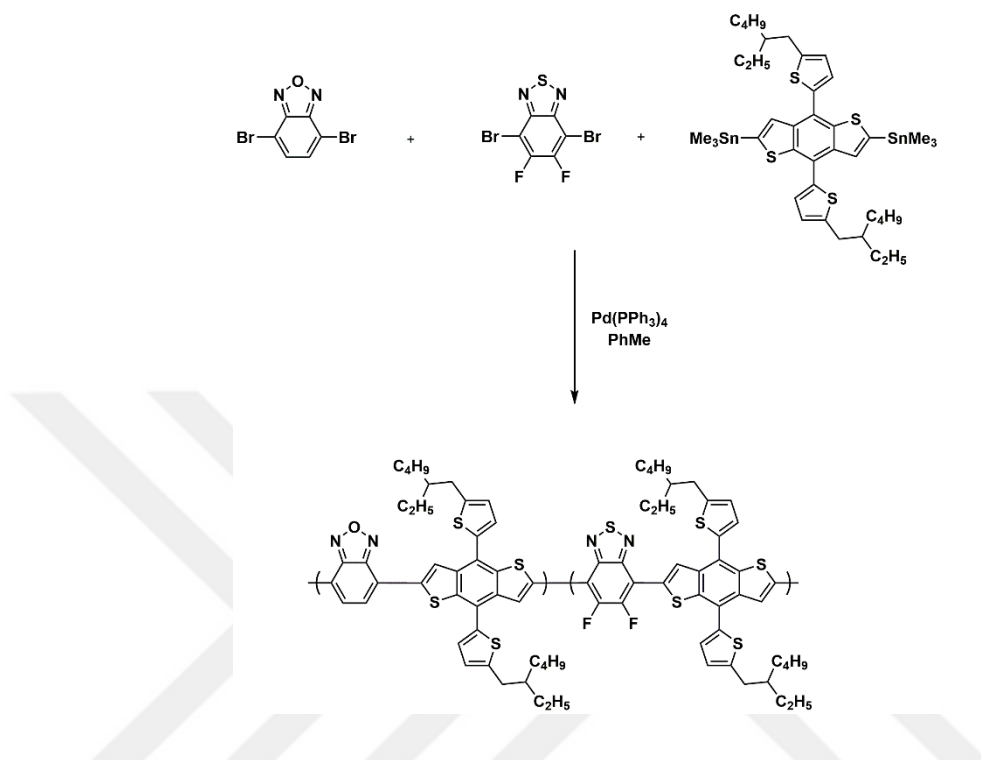


Figure 5.14. Synthetic route for RP2

5.4.1.3. Synthesis of RP3

Polymerization procedure similar to that described above for RP1 and RP2 was performed to obtain RP3. A mixture of (E)-6,6'-dibromo-1,1'-bis(2-hexyldecyl)-[3,3'-biindolinyldiene]-2,2'-dione (92.5 mg, 0.11 mmol), 4,7-dibromo-5,6-difluorobenzo[c][1,2,5]thiadiazole (35.0 mg, 0.11 mmol), (4,8-bis(5-(2-ethylhexyl)thiophen-2-yl)benzo[1,2-*b*:4,5-*b'*]dithiophene-2,6-diyl)bis(trimethylstannane) (193 mg, 0.21 mmol) and tetrakis(triphenylphosphine)palladium(0) (6.15 mg, 0.01 mmol) were dissolved in

anhydrous toluene (2 mL) in a 10 mL schlenk tube under inert atmosphere and polymerized to give RP3. Yield: 67 %

ν_{max} (KBr, cm^{-1}): 3840-3740 (O-H), 2955 (N-H), 2922 (C-H, alkane), 2854 (C-H), 2646 (S-H), 1608 (C=C, conjugated alkene), 1508 (N-O), 1453 (C-H, alkane), 1376 (S-O), 1173 (S-O), 1111 (C-O), 814 (C-H, substituted benzene), 722 (C-H, benzene derivative), 529 (C-Br), 447 (C-Br)

^1H NMR (400 MHz, CDCl_3) δ : 8.94, 7.58, 7.40, 6.91, 2.90, 1.34, 1.15, 0.75

Mw:64000 Da Mn: 25000 Da PDI: 2.56

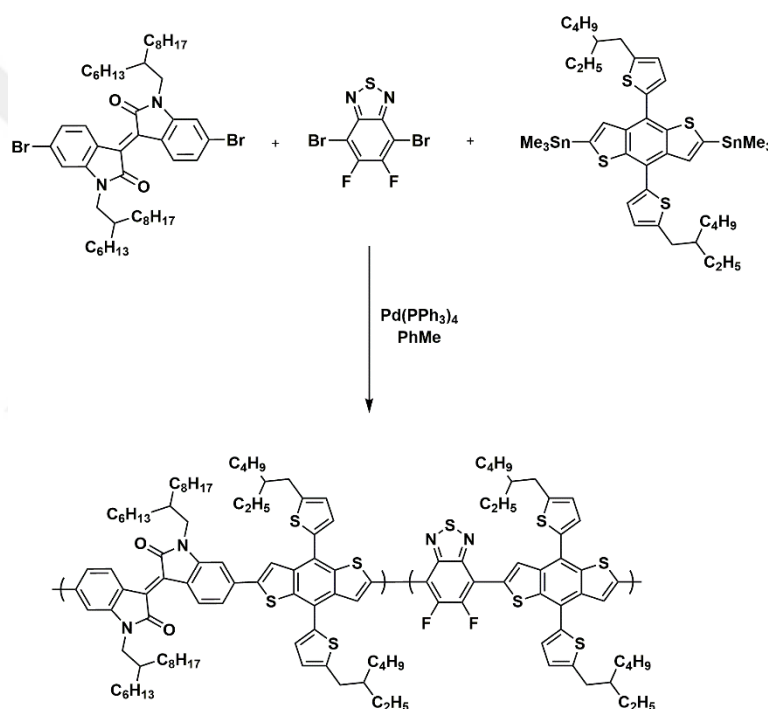


Figure 5.15. Synthetic route for RP3

5.4.2. Results and Discussion

5.4.2.1. Electrochemistry Studies

Cyclic voltammetry was used to investigate the electrochemical properties of the random copolymers. Polymers were dissolved in chloroform to a concentration of 5 mg.mL⁻¹ and then spray coated on ITO coated glass electrode. Single scan cyclic voltammograms were performed in a 0.1 M solution of TBAPF₆ in acetonitrile at room temperature with a scan rate of 100 mV/s (Figure 5.16). The electrochemical properties of the polymers were summarized in Table 1. The onset oxidation and reduction potentials obtained from single scan cyclic voltammograms correspond to the HOMO energy levels. The oxidation (doping/dedoping) potentials were 1.20 V / 0.80 V for RP1-os, 1.13 V / 0.85 V for RP1-ss, 1.15 V / 0.93 V for RP2 and 1.08 V / 0.89 V for RP3 in the positive potential region. The lowest oxidation potential was recorded for RP3 which comprise isoindigo as one of the acceptors in the polymer backbone. Richer electron density of isoindigo could lead to lower oxidation than other polymers. The molecular weights of RP1-os and RP1-ss were different from each other, electronic properties were similar. To calculate the HOMO levels of the polymers, the onset potentials of the polymers were determined by utilizing the oxidation peak in anodic region of the cyclic voltammogram. HOMO energy levels were estimated from these values according to the energy level of the ferrocene reference (4.8 eV below vacuum level). The onset potential of the polymers were 0.83 V, 0.90 V, 0.91 V and 0.92 V for RP1-os, RP1-ss, RP2 and RP3, respectively. HOMO energy levels were calculated as -5.58 eV for RP1-os, -5.65 eV for RP1-ss, -5.90 eV for RP2, -5.67 eV for RP3. The polymers did not exhibit n-type doping. LUMO energy levels were found -4.08 eV, -4.11 eV, -4.40 eV, -4.20 eV for RP3.

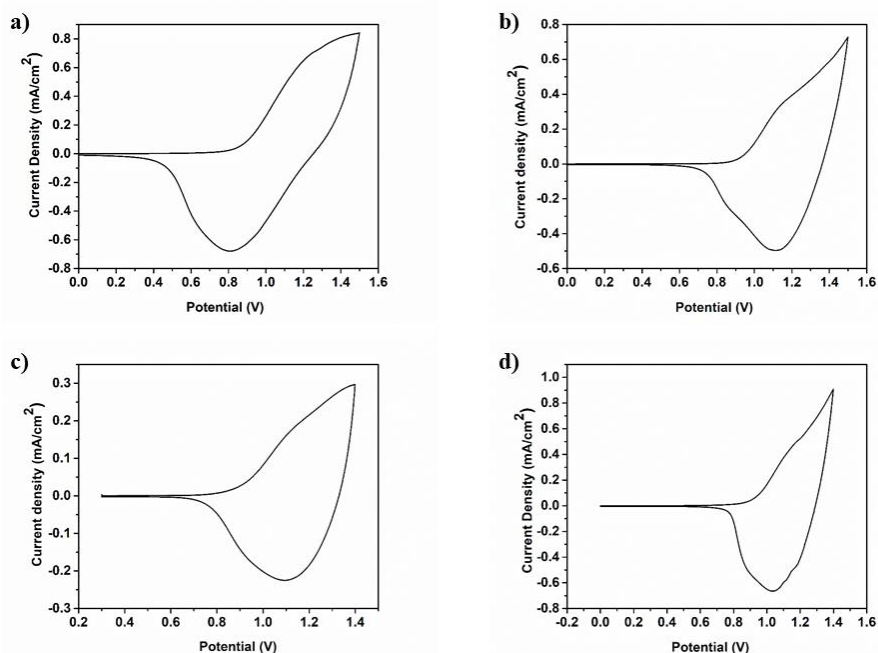


Figure 5.16. Single scan cyclic voltammograms of a) RP1-os b)RP1-ss c) RP2 and d) RP3

5.4.2.2. Spectroelectrochemistry Studies

Spectroelectrochemistry measurements were performed in 0.1 M TBAPF₆/acetonitrile (ACN) solvent medium. Spray coated polymer films were stepwise oxidized and spectral responses were recorded using UV-Vis-NIR spectroscopy. Figure 5.17 displays the absorption spectra of RP1-os, RP1-ss, RP2 and RP3 which were achieved in 0.1 M ACN/TBAPF₆ solution. The increase in absorbance demonstrates the formation of polaron and bipolaron in the electronic absorption spectra. The absorption maximum revealed at 655 nm for RP1-os, at 660 nm for RP1-ss, at 665 nm for RP2 and at 680 nm for RP3 corresponds to localized π - π^* transitions. The onset values for maximum absorptions were found as 825 nm for RP1-os, 805 nm for RP1-ss, 825 nm for RP2, 847 nm for RP3. The optical band gap of the polymers were calculated from those transitions as 1.50 eV for RP1-ss, 1.54 eV for RP1-ss, 1.50 eV for RP2, 1.47 eV for RP3. The lowest band gap was calculated for RP3 having the

highest molecular weight resulting in red-shift in the absorption. All the band gaps were found very similar. Figure 5.18 reveals the colors of RP3 with L, a, b values.

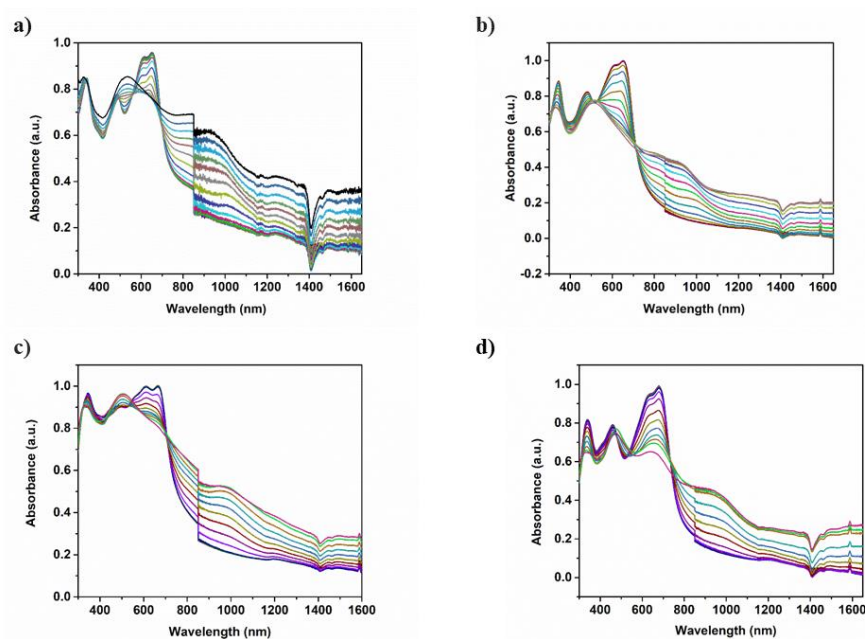


Figure 5.17. Electronic absorption spectra of a) RP1-os b)RP1-ss c) RP2 and d) RP3

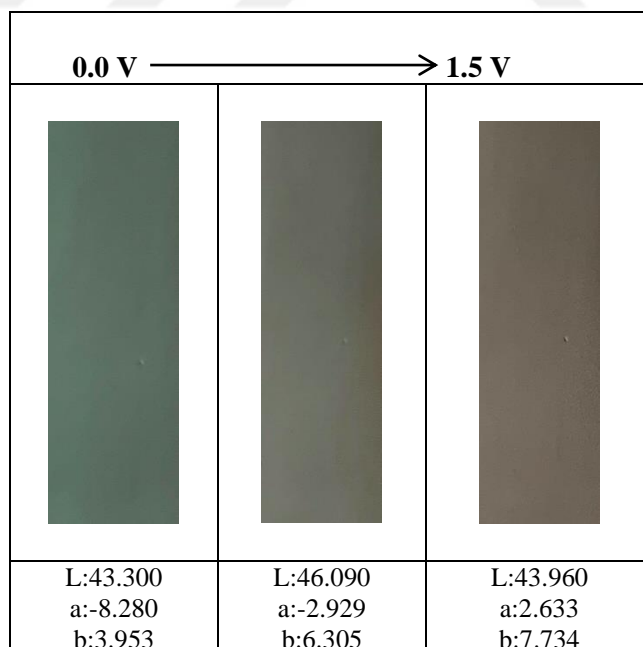


Figure 5.18. The colors of the RP3 a) Hexane phase b) Chloroform phase

Table 5.5. The comparison of optoelectronic properties of random copolymers

Polymers	$E_{ox,doping}$ (V)	$E_{ox,dedoping}$ (V)	HOMO (eV)	LUMO (eV)	E_g (eV)
RP-os	1.20	0.80	-5.58	-4.08	1.50
RP1-ss	1.13	0.85	-5.65	-4.11	1.54
RP2	1.15	0.93	-5.90	-4.40	1.50
RP3	1.08	0.89	-5.67	-4.20	1.47

Since all the copolymers have only p-dopable characteristics, LUMO energy levels were estimated using optical band gaps. Optoelectronic properties of random copolymers were summarized in Table 5.5.

5.4.2.3. Preliminary Photovoltaic Studies

Photovoltaic properties of the some polymers with bulk heterojunction device structure were investigated with the device structure; ITO/PEDOT:PSS/polymer:PC₇₁BM/LiF/Al. The blend ratio for Polymer: PCBM were aimed to be optimized via increasing PCBM ratio in the solutions. Solvent screening was done to obtain the best results in terms of photovoltaic characteristics of the polymer which was represented in Figure 5.19. For RP1, J–V curves for the best performance cells for were represented in Figure 5.20, photovoltaic parameters were summarized in Table 5.6. Apart from acceptor (PCBM) and donor (polymers) ratio in the blends, different solvents were used to obtain the best morphology to increase the short circuit current. Chlorobenzene gave better results than o-dichlorobenzene. The highest values obtained were PCE of 1.37 % with a V_{oc} of 0.79 V, J_{sc} of 4.22 mAcm⁻², FF of 41 %, under the illumination of AM 1.5 G, 100 mW cm⁻². The rate was adjusted as 500 rpm for each optimization to obtain the active layer thicknesses around 100 nm.

For RP3, photovoltaic parameters were summarized in Table 5.7 and Figure 5.21 shows current density - voltage curves of the optimized RP3:PC₇₁BM devices with different polymer:PCBM ratios. Similar optimizations like solvent screening and % concentration of the blends were done. Chlorobenzene gave better results than o-

dichlorobenzene. The highest values obtained were PCE of 0.93 % with a V_{OC} of 0.75 V, J_{SC} of 2.22 mAcm^{-2} , FF of 56 %, under the illumination of AM 1.5 G, 100 mWcm^{-2} . The rate was adjusted as 500 rpm for each optimization to obtain the active layer thicknesses around 100 nm. The lower PCE in photovoltaics may arise due to higher tendency to agglomerate for isoindigo derivatives. Agglomeration of polymer could block charges to reach corresponding electrodes hence exciton recombination may occur leading to much lower current in the solar cell. To observe any agglomerates which adversely affect the morphology so that the transport of charge carriers, AFM studies will be performed after all the parameters obtained.

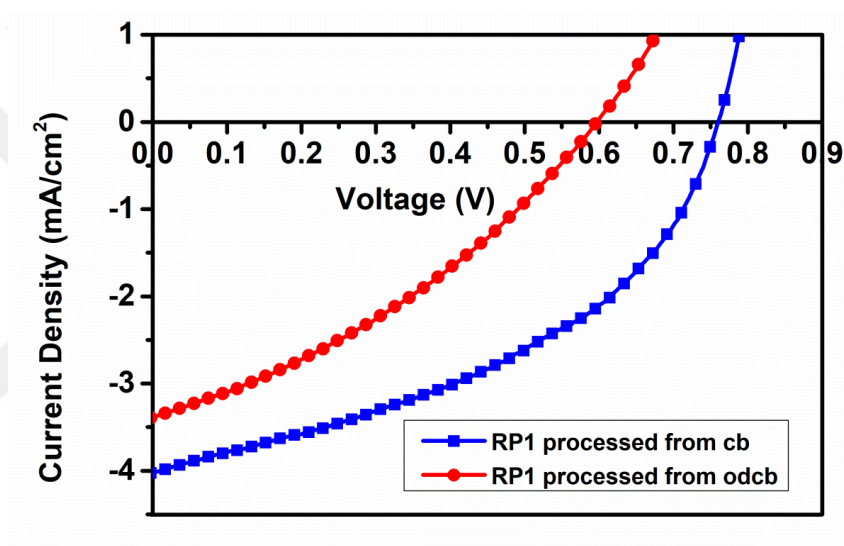


Figure 5.19. Current density - voltage curves for RP1 using different chlorinated solvents

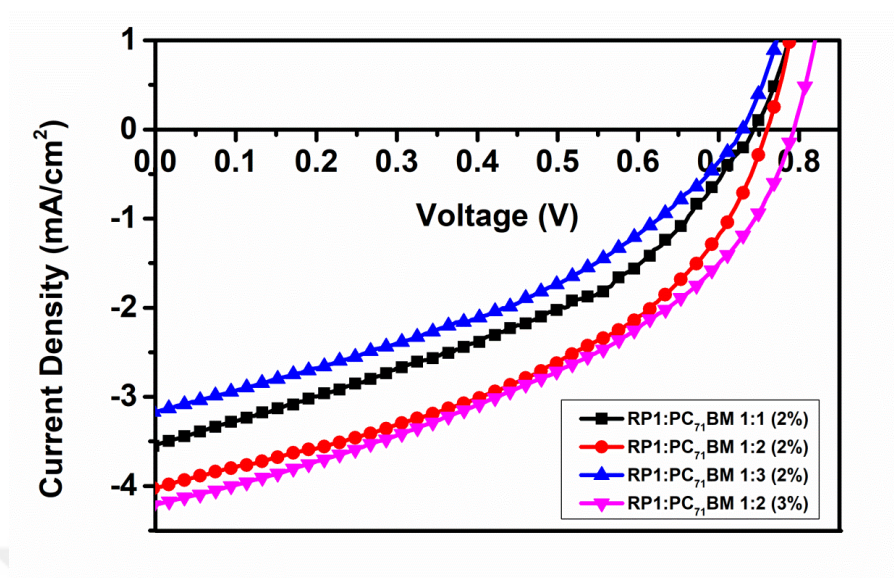


Figure 5.20. Current density - voltage curves of the optimized RP1:PC₇₁BM devices with different polymer:PCBM ratios

Table 5.6 Summary of the preliminary photovoltaic studies for RP1

RP1:PC ₇₁ BM (solvent)	V _{oc} (V)	J _{sc} (mAcm ⁻²)	FF (%)	PCE (%)	% (concentration)
1:1 (cb)	0.78	1.02	39	1.02	2
1:2 (cb)	0.76	4.03	43	1.31	2
1:3 (cb)	0.73	3.20	38	0.88	2
1:2 (cb)	0.79	4.22	41	1.37	3
1:2 (o-dcb)	0.60	3.39	34	0.69	2

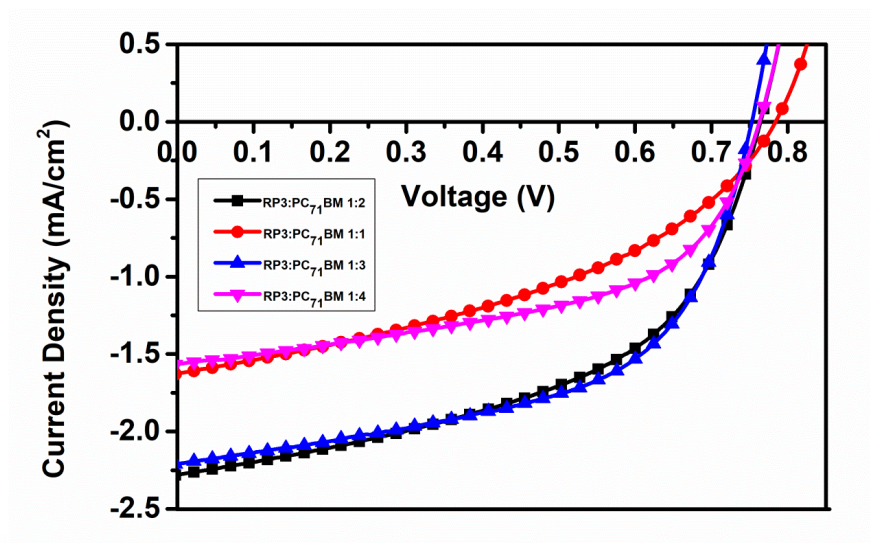


Figure 5.21. Current density - voltage curves of the optimized RP3:PC₇₁BM devices with different polymer:PCBM ratios

Table 5.7 Summary of the preliminary photovoltaic studies for RP3

RP3:PC ₇₁ BM (solvent)	V _{oc} (V)	J _{sc} (mAcm ⁻²)	FF (%)	PCE (%)	% (concentration)
1:1 (cb)	0.78	1.63	41	0.52	2
1:2 (cb)	0.76	2.29	51	0.88	2
1:3 (cb)	0.75	2.22	56	0.93	2
1:4 (cb)	0.76	1.56	53	0.63	2
1:2 (o-dcb)	0.68	2.35	42	0.67	2

CHAPTER 6

DIRECT HETEROARYLATION POLYMERIZATION (DHAP)

6.1. General Information

To become a useful approach, Direct Heteroarylation Polymerization (DHAP or sometimes called DArP) must be at least comparable or with superior performance to those obtained using the classical polymerization methods such as Stille or Suzuki polymerizations to produce materials. Hence, polymers were synthesized via both Stille coupling and DHAP to compare the polymerization types in terms of molecular weight and optoelectronic properties of the polymers. Gel permeation chromatography (GPC) was performed to determine number-average (M_n) and weight-average (M_w) molecular weights with a high temperature Varian Polymer Laboratories GPC220 equipped with an RI detector and a PL BV400 HT Bridge Viscometer. The column set consists of 2PL gel Mixed C (300 x 7.5 mm) columns and a PL gel Mixed C guard column. In general, since conjugated polymers could have strong aggregation properties, care must be taken to fully solubilize them because aggregates would cause gross overestimation of both molecular weights and molar mass dispersity. To achieve more accurate GPC results for such materials, high temperature analysis with solvents such as 1,2-dichlorobenzene and 1,2,4-trichlorobenzene are recommended. The eluent 1,2,4-trichlorobenzene (TCB) (with 0.0125% BHT w/v) flow rate was fixed to 1.0 mL/min. All measurements were done at 110 °C. Polymer solutions were prepared at concentrations of 1.0 mg/mL in 1,2,4-trichlorobenzene. Dissolution was done using a Varian Polymer Laboratories PL-SP 260VC sample preparation system. To achieve complete dissolution of polymers, the vials were held at 110 °C while shaking for 1 hour. Through a 2 mm porous stainless steel filter used with the 0.40 μ m glass filter into a 2 mL chromatography vial all the samples were filtered to remove insoluble residue. The calibration method was the classical polystyrene method using

polystyrene narrow standards Easi-Vials PS-M from Varian Polymer Laboratories dissolved in TCB.

6.2. Syntheses of Polymers

6.2.1. Synthesis of SG-1

In a microwave vial, 4,7-dibromo-5,6-bis(octyloxy)benzo[*c*][1,2,5]oxadiazole (133 mg, 0.25 mmol), 4,8-didodecylbenzo[1,2-*b*:4,5-*b'*]dithiophene (131 mg, 0.25 mmol), Pd(OAc)₂ (2.80 mg, 0.01 mmol), tri(*o*-tolyl)phosphine (13.0 mg, 0.04 mmol), Cs₂CO₃ (243 mg, 0.75 mmol) and pivalic acid (25.4 mg, 0.25 mmol) were added. The vial was sealed with a cap and purged with nitrogen three times to remove oxygen. Freshly distilled and degassed toluene was added (0.5 mL) to the reaction medium and the mixture was placed to a pre-heated oil bath at 120 °C. The solution was stirred until gelation occurs. After cooling to room temperature, the solution was poured in methanol/acidified water (10 % HCl) (9:1). Polymer was recovered through filtration using a 0.45 µm nylon filter and washed using a Soxhlet apparatus with acetone and hexane, respectively. Later, the polymer was extracted with chloroform. The chloroform fraction was evaporated (~10 mL) and then poured in methanol. The polymer was recovered using a 0.45 µm nylon filter and dried under vacuum. Yield: 31 %

Mw: 6058 Da Mn: 5348 Da PDI: 1.13

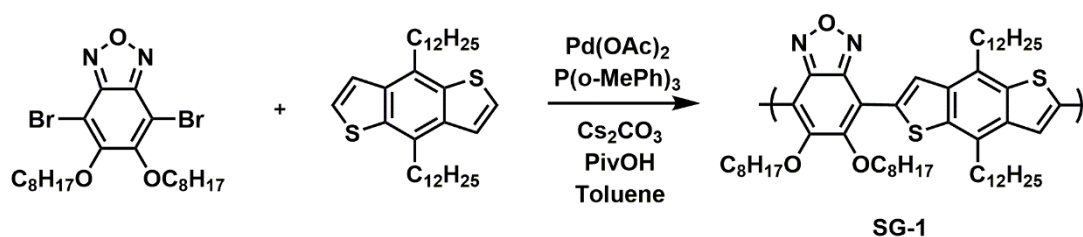


Figure 6.1. Synthetic route for SG-1

6.2.2. Synthesis of SG-2

Using a polymerization procedure similar to that described above for SG-1, 4,7-dibromo-5,6-bis(octyloxy)benzo[*c*][1,2,5]oxadiazole (153 mg, 0.29 mmol), 4,8-didodecylbenzo[1,2-*b*:4,5-*b'*]dithiophene (151 mg, 0.29 mmol), Pd(OAc)₂ (3.21 mg, 0.01 mmol), tri(*o*-tolyl)phosphine (15.1 mg, 0.04 mmol), Cs₂CO₃ (280 mg, 0.86 mmol) and pivalic acid (28.9 mg, 0.29 mmol) were added in a vial was then sealed with a cap under nitrogen atmosphere. Freshly distilled and degassed THF was added (0.8 mL) to the reaction medium and the mixture was placed to a pre-heated oil bath at 120 °C. The solution was stirred for 5 hours. Acidic methanol solution was prepared and the reaction mixture was poured into this solution. Polymer was recovered through filtration using a 0.45 µm nylon filter and washed using a Soxhlet apparatus with acetone and hexane, respectively. After extraction of the polymer with chloroform, solvent was evaporated (~10 mL). The polymer was added drop wise to cold methanol and recovered using a 0.45 µm nylon filter and dried under vacuum. Yield: 45 %

ν_{\max} (KBr, cm⁻¹): 2921 (C-H, alkane), 2851 (C-H), 1589 (C=C stretching, conjugated alkene), 1528 (N-O), 1376-1300 (S-O), 1297 (N-O), 1199 (C-O), 1058 (C-O, alkoxy group), 998 (C=C, alkene), 838 (C=C, alkene), 721 (C-H, benzene derivative), 577-481 (C-Br)

Mw: 8715 Da Mn: 6501 Da PDI: 1.34

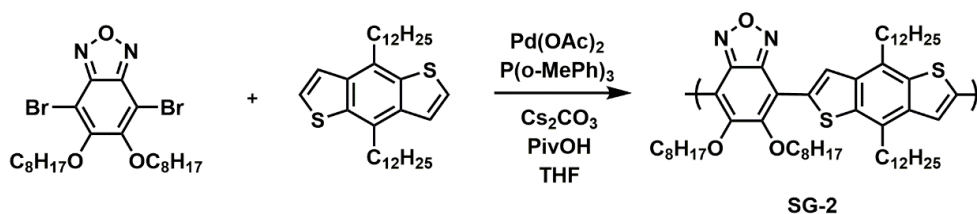


Figure 6.2. Synthetic route for SG-2

6.2.3. Synthesis of SG-3

(E)-6,6'-dibromo-1,1'-diundecyl-[3,3'-biindolinylidene]-2,2'-dione (109 mg, 0.26 mmol), 4,8-didodecylbenzo[1,2-*b*:4,5-*b'*]dithiophene (137 mg, 0.26 mmol), Pd(OAc)₂ (2.91 mg, 0.01 mmol), tri(*o*-tolyl)phosphine (13.7 mg, 0.04 mmol), Cs₂CO₃ (254 mg, 0.78 mmol) and pivalic acid (26.2 mg, 0.26 mmol) were added in a vial sealed with a cap under inert atmosphere. Then, freshly distilled toluene (1.3 mL) was added to the vial and the mixture was heated to reflux for 2 hours. The reaction mixture was poured into acidic methanol solution and recovery of polymer was achieved through filtration with a 0.45 µm nylon filter. The polymer was washed with acetone and hexane in a Soxhlet apparatus, respectively. Extraction of the polymer was done using chloroform. The solvent was evaporated (~10 mL). The polymer was added drop wise to cold methanol and recovered using a 0.45 µm nylon filter and dried under vacuum. Yield: 58 %

ν_{\max} (KBr, cm⁻¹): 2920 (C-H, alkane), 2850 (C-H), 1691 (C-O). 1608 (α,β -unsaturated ketone, C=C), 1538 (N-O), 1455 (C-H, alkane), 1359 (S-O), 1245 (C-N), 1171 (C-O), 1109 (C-O), 868 (C-H, substituted benzene), 815 (C-H, substituted benzene), 721 (C-H, benzene derivative), 520-460 (C-Br)

Mw: 60480 Da Mn: 37355 Da PDI: 1.44

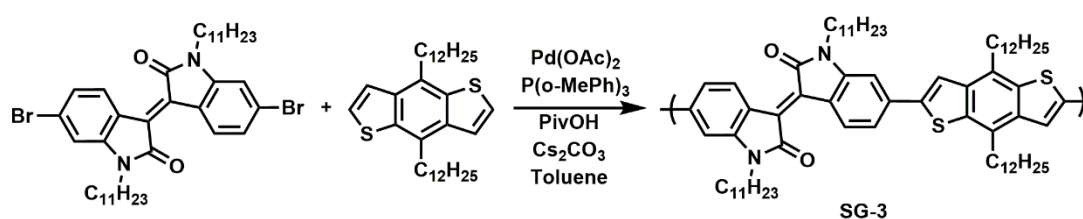


Figure 6.3. Synthetic route for SG-3

6.2.4. Synthesis of SG-4

In a microwave vial, 4,7-bis(5-bromoselenophen-2-yl)-5,6-bis(octyloxy)benzo[c][1,2,5]oxadiazole (208 mg, 0.26 mmol), 4,8-didodecylbenzo[1,2-*b*:4,5-*b'*]dithiophene (139 mg, 0.26 mmol), Pd(OAc)₂ (2.95 mg, 0.01 mmol), tri(*o*-tolyl)phosphine (13.9 mg, 0.04 mmol), Cs₂CO₃ (257 mg, 0.79 mmol) and pivalic acid (26.5 mg, 0.26 mmol) were added. The vial was sealed with a cap and purged with nitrogen three times to remove oxygen. Freshly distilled and degassed toluene was added (0.75 mL) to the reaction medium and the mixture was placed to an oil bath pre-heated at 120 °C. The solution was stirred for 5 hours. Then, the solution was allowed to cool and poured in acidic methanol. The polymer was washed with acetone and hexane in a Soxhlet apparatus, respectively. Extraction of the polymer was done using chloroform. The solvent was evaporated (~10 mL). The polymer was added dropwise to cold methanol and recovered using a 0.45 µm nylon filter and dried under vacuum. Yield: 55 %

ν_{\max} (KBr, cm⁻¹): 3840-3740 (O-H), 2920 (N-H), 2851 (N-H), 2286 (S-H), 2050 (C-H, aromatic), 1747 (C-O), 1432 (O-H), 1387 (S-O), 1280 (C-O), 1193 (C-O), 1054 (C-O, alkoxy group), 987 (C=C, alkene), 788-720 (C-H, benzene derivative), 560-441 (C-Br).

Mw: 14539 Da Mn: 8902 Da PDI: 1.63

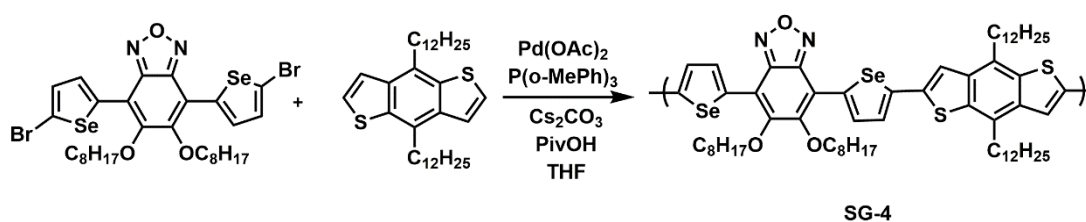


Figure 6.4. Synthetic route for SG-4

6.2.5. Synthesis of SG-5

In a microwave vial, 4,7-dibromo-5,6-bis(octyloxy)benzo[*c*][1,2,5]selenadiazole (174 mg, 0.29 mmol), 4,8-didodecylbenzo[1,2-*b*:4,5-*b'*]dithiophene (154 mg, 0.29 mmol), Pd(OAc)₂ (3.27 mg, 0.02 mmol), tri(*o*-tolyl)phosphine (15.4 mg, 0.04 mmol), Cs₂CO₃ (285 mg, 0.87 mmol) and pivalic acid (29.5 mg, 0.29 mmol) were added. After sealing the vial with a cap and purging with nitrogen, freshly distilled and degassed toluene was added (0.5 mL) to the reaction medium. The mixture was placed to an oil bath pre-heated at 120 °C. The solution was stirred overnight. After cooling to room temperature, the solution was poured in methanol/acidified water (10 % HCl) (9:1). No precipitate formed after recrystallization from cold methanol. Polymerization could not be achieved.

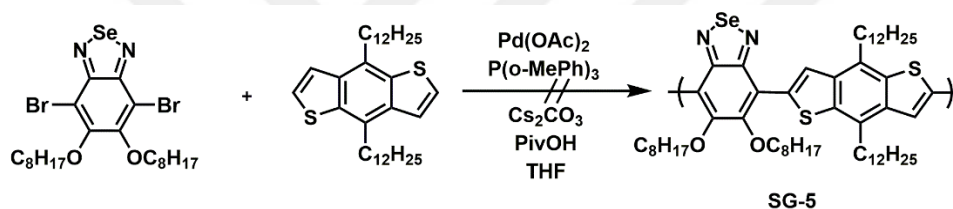


Figure 6.5. Synthetic route for SG-5

6.2.6. Synthesis SG-6

(*E*)-6,6'-dibromo-1,1'-bis(2-hexyldecyl)-[3,3'-biindolinylidene]-2,2'-dione (288 mg, 0.33 mmol), 4,8-didodecylbenzo[1,2-*b*:4,5-*b'*]dithiophene (175 mg, 0.33 mmol), Pd(OAc)₂ (3.75 mg, 0.02 mmol), tri(*o*-tolyl)phosphine (17.6 mg, 0.05 mmol), Cs₂CO₃ (325 mg, 0.99 mmol) and pivalic acid (33.5 mg, 0.33 mmol) were added in a vial sealed with a cap under inert atmosphere. Degassed and anhydrous toluene (1.7 mL) was added to the mixture and the solution was polymerized for 24 hours. Yield: 89 %
 ν_{max} (KBr, cm⁻¹): 3840-3741 (O-H), 2921 (C-H, alkane), 2852 (C-H), 2285 (C-N), 2050 (C=C), 1689 (CO, δ -lactam), 1608 (C=C, conjugated alkene), 1458 (C-H, alkane), 1356 (S-O), 1220 (C-O), 1169 (C-O), 1111 (S-O), 868-815 (C-H, substituted benzene), 768-721 (C-H, benzene derivative), 622-521 (C-Br), 460 (C-Br)

Mw: 44466 Da Mn: 17163 Da PDI: 2.59

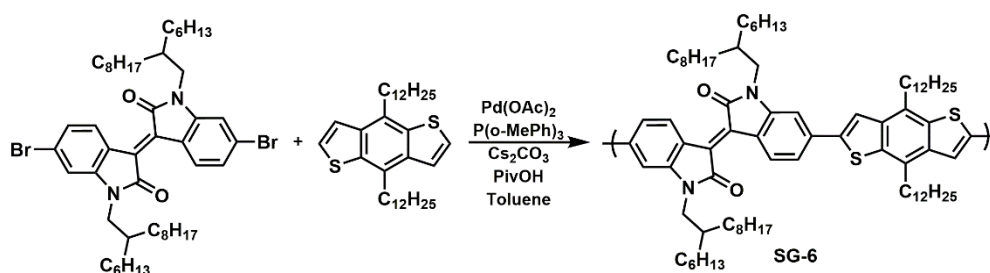


Figure 6.6. Synthetic route for SG-6

6.2.7. Synthesis of SG-6-2

(E)-6,6'-dibromo-1,1'-bis(2-hexyldecyl)-[3,3'-biindolinylidene]-2,2'-dione (281 mg, 0.32 mmol), 4,8-didodecylbenzo[1,2-*b*:4,5-*b'*]dithiophene (170 mg, 0.32 mmol), Herrmann-Beller catalyst (15.1 mg, 0.02 mmol), tri(*o*-anisyl)phosphine (17.0 mg, 0.05 mmol), Cs₂CO₃ (315 mg, 0.97 mmol) and pivalic acid (32.5 mg, 0.32 mmol) were added in a vial sealed with a cap under inert atmosphere. Degassed and anhydrous toluene (1.6 mL) was used for polymerization. The mixture was stirred for 24 hours. Yield: 80 %

Mw: 33707 Da Mn: 13187 Da PDI: 2.55

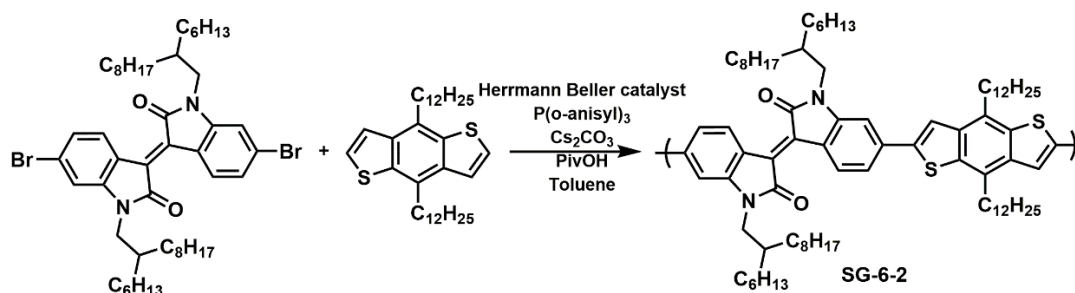


Figure 6.7. Synthetic route for SG-6-2

6.2.8. Synthesis of SG-6-3

(E)-6,6'-dibromo-1,1'-bis(2-hexyldecyl)-[3,3'-biindolinylidene]-2,2'-dione (250 mg, 0.29 mmol), 4,8-didodecylbenzo[1,2-*b*:4,5-*b'*]dithiophene (151 mg, 0.29 mmol), Pd₂(dba)₃ (15.2 mg, 0.04 mmol), tri(*o*-tolyl)phosphine (17.0 mg, 0.05 mmol), Cs₂CO₃ (281 mg, 0.86 mmol) and pivalic acid (29.0 mg, 0.28 mmol) were added in a vial sealed with a cap under inert atmosphere. Degassed and anhydrous toluene (1.4 mL) was added to the solid mixture. Then polymerization was kept until gelation occurs. Yield: 80 %

M_w: 26617 Da M_n: 13523 Da PDI: 1.97

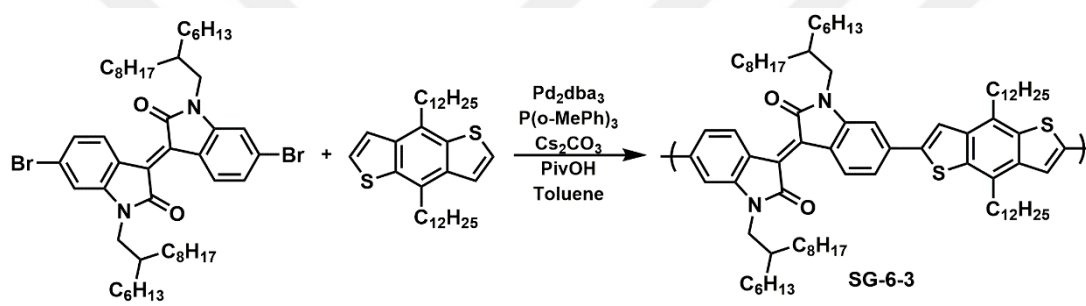


Figure 6.8. Synthetic route for SG-6-3

6.2.9. Synthesis of SG-7

(E)-2,2'-dibromo-4,4'-bis(2-octyldodecyl)-[6,6'-bithieno[3,2-*b*]pyrrolylidene]-5,5'-(4H,4'H)-dione (127 mg, 0.13 mmol), 4,8-didodecylbenzo[1,2-*b*:4,5-*b'*]dithiophene (67.4 mg, 0.13 mmol), tris(dibenzylideneacetone)dipalladium(0)-chloroform adduct (1.32 mg, 0.001 mmol), tri(*o*-tolyl)phosphine (1.80 mg, 0.01 mmol), Cs₂CO₃ (135 mg, 0.38 mmol), pivalic acid (13.0 mg, 0.13 mmol) and anhydrous N,N,N',N'-tetramethylethylenediamine (4.46 mg, 0.04 mmol) were added to a microwave vial which was sealed with a cap under argon atmosphere. The mixture was held under argon atmosphere for 30 min. Then, freshly distilled and degassed toluene (1.3 mL) was added to the reaction mixture. The solution was heated to reflux.

The reaction was controlled with TLC during 5 days. Polymerization could not be achieved probably due to β -branching of starting material.

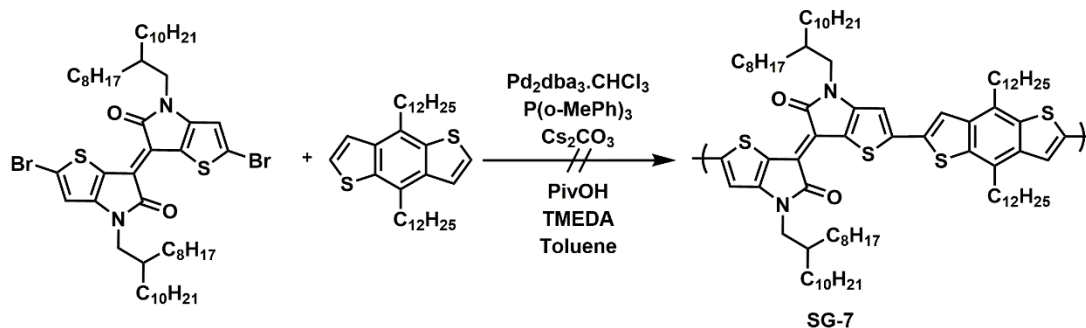


Figure 6.9. Synthetic route for SG-7

6.2.10. Synthesis of SG-8

The same reaction conditions for SG-7 were applied for polymerization of 4,7-bis(5-bromothiopheno[3,2-b]thiophen-2-yl)-5,6-bis(octyloxy)benzo[c][1,2,5]oxadiazole. Polymerization could not be achieved.

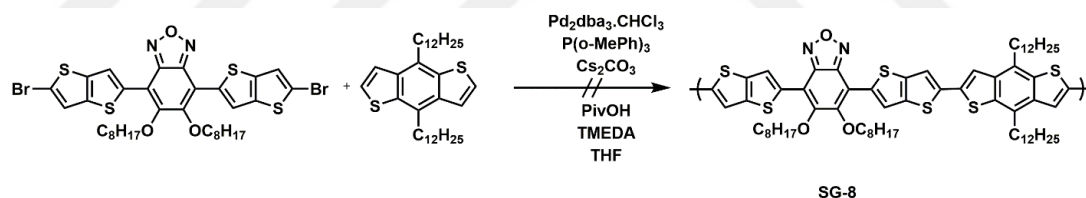


Figure 6.10. Synthetic route for SG-8

6.2.11. Synthesis of SG-9

The same reaction conditions for SG-7 were applied for polymerization of 4,7-bis(5-bromofuran-2-yl)-5,6-bis(octyloxy)benzo[c][1,2,5]oxadiazole. Polymerization could not be achieved.

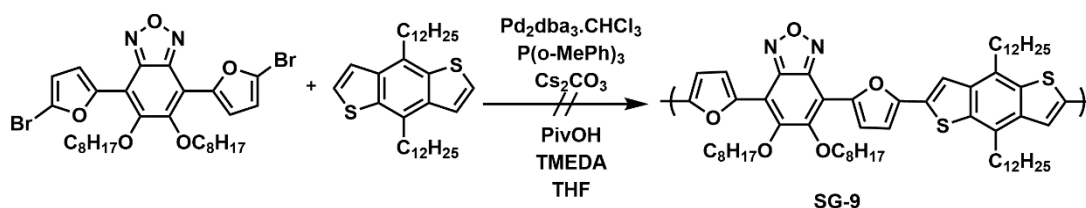


Figure 6.11. Synthetic route for SG-9

6.2.12. Synthesis of SG-10

(E)-6,6'-dibromo-1,1'-bis(2-hexyldecyl)-[3,3'-biindolinylidene]-2,2'-dione (113 mg, 0.13 mmol), 5-(2-ethylhexyl)-1,3-bis(thieno[3,2-b]thiophen-2-yl)-4H-thieno[3,4-c]pyrrole-4,6(5H)-dione (70.4 mg, 0.13 mmol), Herrmann-Beller catalyst (mg, mmol), Cs_2CO_3 (135 mg, 0.38 mmol) and pivalic acid (13.0 mg, 0.13 mmol) were added to a microwave vial which was sealed with a cap under argon atmosphere. Then, freshly distilled and degassed toluene (1.3 mL) was added to the reaction mixture. The solution was heated to reflux in the pre-heated oil bath. Suddenly gelation occurred. After cooling to room temperature and pouring the solution into cold methanol gave the polymer. Soxhlet apparatus was used to wash the polymer with acetone and hexane to remove low molecular weight fractions. Chloroform was used to extract the polymer. However, the obtained polymer was insoluble in chloroform. Chlorobenzene was also used to extract the polymer from Soxhlet thimble. The synthesized polymer was insoluble in most of organic solvents most probably due to crosslinking.

Molecular weights and NMR spectra could not be recorded due to insolubility of the polymer.

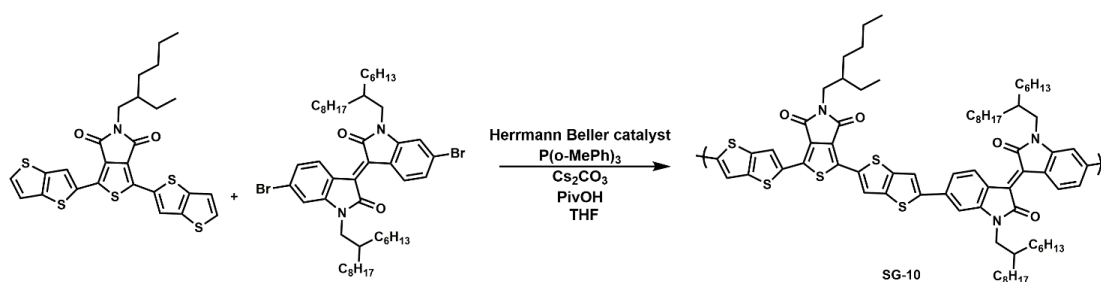


Figure 6.12. Synthetic route for SG-10

6.3. Results and Discussion

6.3.1. Electrochemistry and Spectroelectrochemistry of SG-2-ST and SG-9-ST

Two polymers were characterized to determine electronic properties. Figure 6.13 illustrates single scan cyclic voltammograms of SG-2-ST and SG-9-ST. The oxidation potential, onset values for redox couples and HOMO-LUMO energy levels were calculated from these voltammograms. SG-2-ST is only p-dopable. The much higher molecular weight of SG-9-ST may lead to gain the polymer n-doping characteristics. The onset values for oxidation peaks were found as 1.01 V and 0.98 V for SG-2-ST and for SG-9-ST, respectively. For SG-9-ST, the onset values reduction peak was found as -0.99 V. HOMO levels are calculated as -5.76 eV for SG-2-ST and -5.73 eV for SG-9-ST. LUMO energy levels was calculated as -3.76 eV for SG-9-ST using onset value of reduction peak. Yet, for SG-2-ST LUMO energy level was estimated using optical band gap and calculated -4.13 eV. The electronic band gap is 1.97 eV for SG-9-ST (Table 6.1). In addition, the difference between those polymers is incorporation of a π bridge between acceptor and donor groups which results in decrease in steric hindrance. Even the optical band gaps were calculated very similar, absorption maxima of two polymers are very different. The effect of a π bridge and also molecular weight resulted in a drastic change in the absorption. Red shift in the absorption was around 25 nm. Optical band gaps were found as 1.63 eV for SG-2-ST and 1.72 eV for SG-9-ST. The lower band gap for SG-2-ST could probably resulted

from a broad absorption which could affect the onset value. Kinetic studies could be recorded for both polymers. The results were illustrated in Table 6.2.

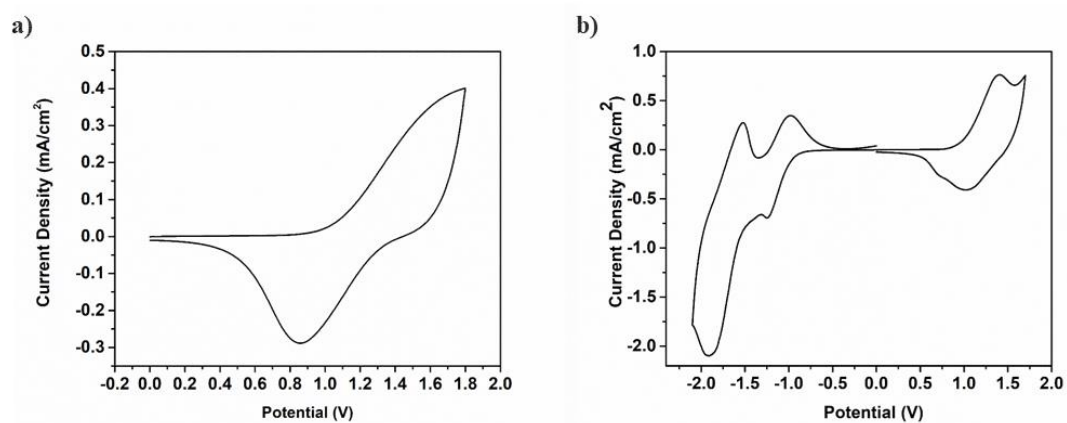


Figure 6.13. Cyclic voltammograms of some polymers a) SG-2-ST b) SG-9-ST

Table 6.1. Summary of electronic properties for some polymers

Polymer	$E_{p,doping}$ (V)	$E_{n,doping}$ (V)	$E_{p^{de-doping}}$ (V)	$E_{n^{de-doping}}$ (V)	HOMO (eV)	LUMO (eV)	E_g^{el} (eV)
SG-2-ST	1.45	-	0.86	-	-5.76	-4.13	-
SG-9-ST	1.40	-1.90/ -1.24	0.71	-1.52/ -0.99	-5.73	-3.76	1.97

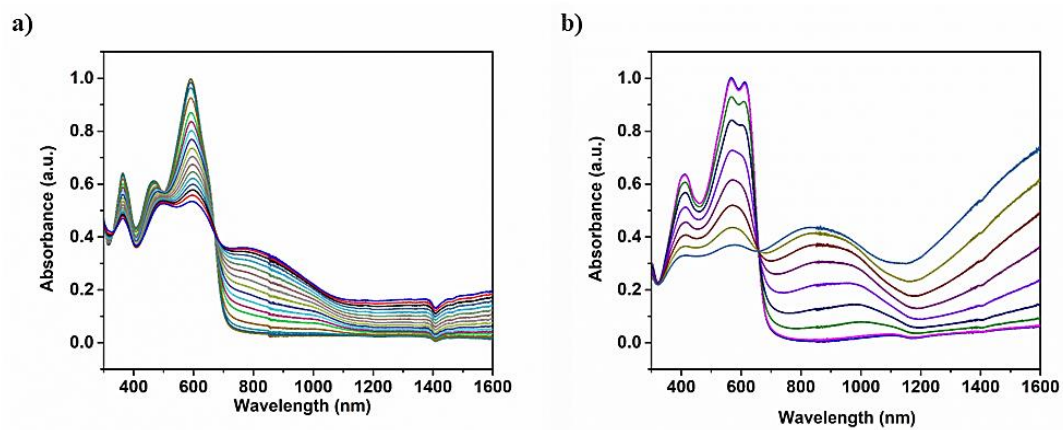


Figure 6.14. Electronic absorption spectra of a) SG-2-ST b) SG-9-ST

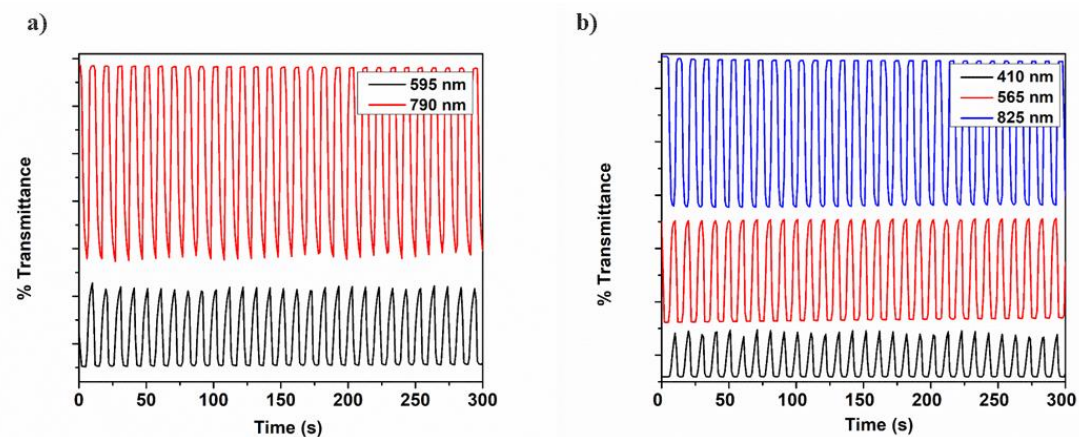


Figure 6.15. Change in percent transmittances a) SG-2-ST and b) SG-9-ST

Table 6.2. Summary of optical properties of polymers

Polymer	λ_{max} (nm)	$\lambda_{max,onset}$ (nm)	E_g^{op} (eV)	Optical Contrast (ΔT %)	λ (nm)	Switching Time(s)
SG-2-ST	590	762	1.63	15	595	-
				40	790	
SG-9-ST	615	720	1.72	7	410	1.7
				38	565	3.0
				55	825	1.7

6.3.2. Optical Properties of Some Polymers Synthesized via DHAP and Stille Coupling

Absorption of all polymers were recorded in chloroform. Figure 6.16 illustrates the differences of absorbance intensity and maximum wavelength values for polymers which were both synthesized via DHAP and Stille Coupling. Absorption behaviors of polymers having similar molecular weights are very similar for both polymerization types proving that DHAP could be alternative route to Stille coupling in terms of optical properties.

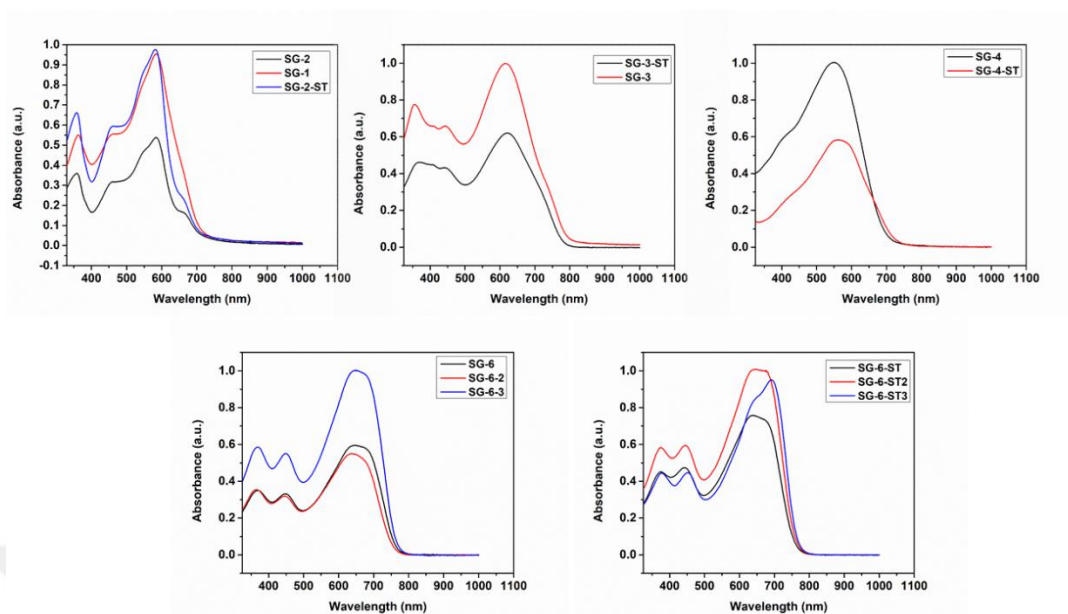


Figure 6.16. Comparison of UV-Vis absorption of polymers synthesized via Stille reaction and DHAP (in solution)

On the other hand, Figure 6.17 shows normalized UV-Vis absorption of polymers synthesized via Stille reaction. Apart from those solution absorption spectra, the polymers will be used for characterization upon applied potential gradually. Kinetic studies will also be recorded later on.

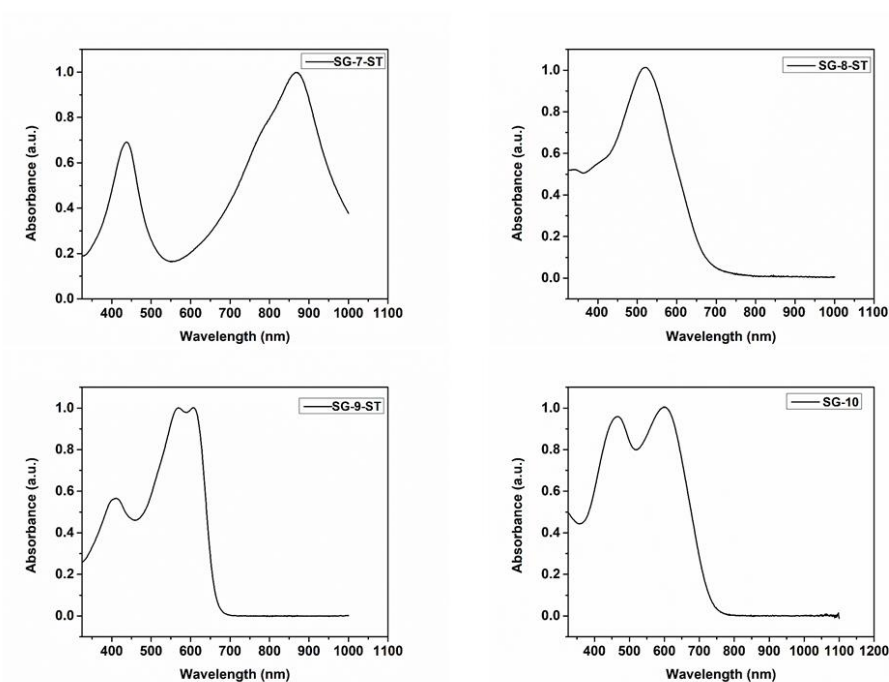


Figure 6.17. Normalized UV-Vis absorption of polymers synthesized via Stille reaction (in solution)

6.3.3. Photovoltaic Studies/Preliminary Results for SG-4

Photovoltaic properties of the some polymers with bulk heterojunction device structure were investigated with the device structure; ITO/PEDOT:PSS/polymer:PC₇₁BM/LiF/Al. The blend ratio for Polymer: PCBM were aimed to be optimized via increasing PCBM ratio in the solutions. For SG-4, J–V curves for the best performance cells for were represented in Figure 6.19, photovoltaic parameters were summarized in Table 6.2. Different from acceptor (PCBM) and donor (polymers) ratio in the blends, the effect of solvent additive was also investigated to obtain higher device performance via better morphology. Host solvents dissolve effectively both electron donor and acceptor molecules whereas solvent additives have generally selective solubility to one of the molecules (mostly the acceptor). PCBM aggregates could be dissolved in the additives and this could lead to smaller domains with improved Polymer: PCBM interpenetration network. Besides, additives could increase

domain sizes for maximizing charge separation and minimizing charge recombination. The better morphology would eventually increase PCE. On the other hand, the low vapor pressure solvent additives could sometimes lead to coarser domains and lower charge carrier mobility. Hence, power conversion efficiency may be decreased. Diphenyl ether (DPE) was used as the additive. For this polymer, solvent additive resulted in lower short circuit current which may be attributed to reduced absorption strength. The highest value obtained was PCE of 1.34 % with a V_{OC} of 0.74 V, J_{SC} of 4.27 mAcm^{-2} , FF of 42 %, under the illumination of AM 1.5 G, 100 mWcm^{-2} with solvent additive amount of 3 %. The rate was adjusted as 500 rpm for each optimization to obtain the active layer thicknesses around 100 nm. Thermal annealing was applied at 100°C for 10 minutes however the PCE values were decreased dramatically. The active layer compositions indicated were processed from the solvent o-DCB for each optimization step. (Table 6.3.)

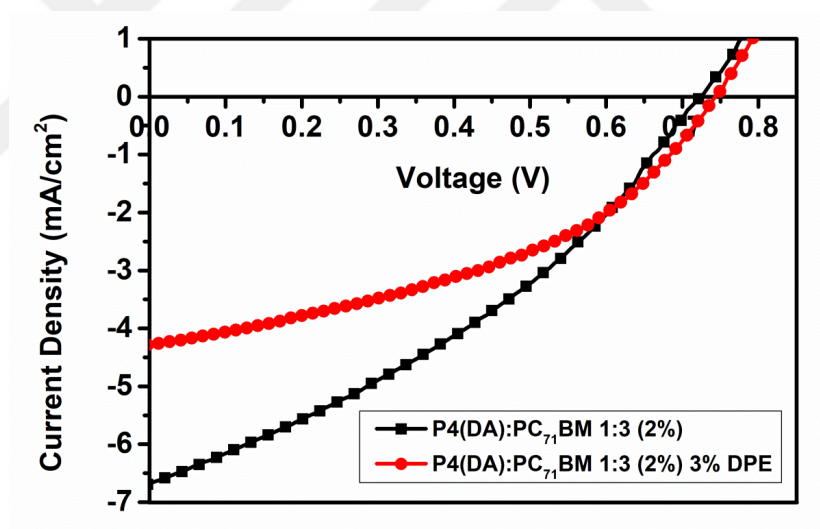


Figure 6.18. Current density - voltage curves of the optimized SG-4:PC₇₁BM (1:1) devices with and without 3.0 vol % DPE

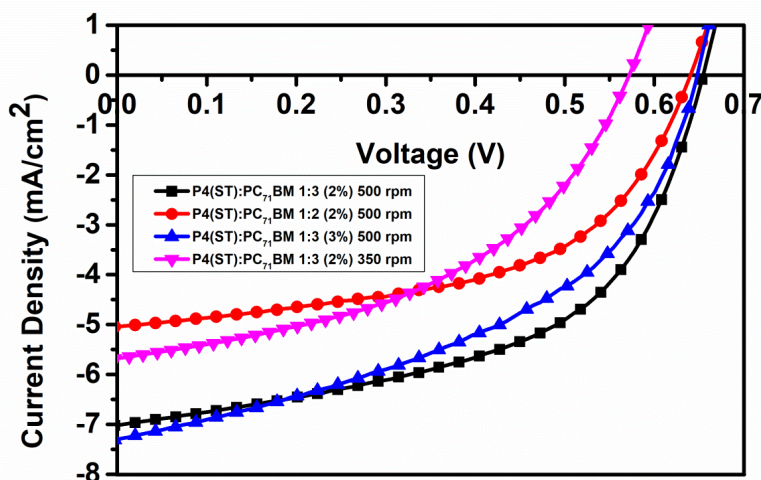


Figure 6.19. Current density - voltage curves of the optimized SG-4-ST:PC₇₁BM (1:1) devices with different blend ratios

Table 6.3. Summary of photovoltaic parameters for optimization studies of SG-4

SG-4: PC ₇₁ BM (w:w)	V _{oc} (V)	J _{sc} (mAcm ⁻²)	FF (%)	PCE (%)	Additive	Spin coating rate (rpm)	% (conc.)
1:2	0.53	5.03	30	0.79	-	500	2
1:3	0.73	6.71	34	1.67	-	500	2
1:3	0.65	5.41	30	1.04	-	500	3
1:3	0.55	6.24	29	1.00	-	750	2
1:3	0.72	5.07	35	1.27	-	350	2
1:3	0.74	4.27	42	1.34	3 % DPE	500	2
1:3	0.79	3.34	44	1.16	2 % DIO	500	2

Solvent, time, catalyst screening were achieved to optimize reaction conditions to synthesize high molecular weight polymers which result in red-shift in the absorption hence lower band gap and better photon harvesting. Therefore in terms of their chemical structures, same polymers were synthesized with different reaction conditions. The higher molecular weight polymers resulted in red shift in the absorption as expected.

Table 6.4 shows properties of polymers which were obtained via two different synthetic methodologies i.e. Stille coupling and Direct Heteroarylation Polymerization (DHAP).

Table 6.4. Comparison of maximum absorption and molecular weights of polymers synthesized via DHAP and Stille reaction

Polymers	M_w (Da)	M_n (Da)	PDI	λ_{max} (nm)
SG-1	6057	5348	1.13	582
SG-2	8715	6501	1.34	584
SG-2-ST	8737	6508	1.34	582
SG-3	60480	37355	1.44	619
SG-3-ST	28388	19926	1.42	618
SG-4	14539	8902	1.63	549
SG-4-ST	14577	8812	1.65	568
SG-6	44466	17163	2.59	651
SG-6-2	33707	13187	2.55	639
SG-6-3	26617	13523	1.97	653
SG-6-ST	27657	16414	1.69	641
SG-6-ST2	19902	11699	1.70	653
SG-6-ST3	176136	54603	3.23	692
SG-10	4710	3240	1.45	600

Table 6.5. Comparison of maximum absorption and molecular weights of polymers synthesized via Stille reaction

Polymers	M_w (Da)	M_n (Da)	PDI	λ_{max} (nm)
SG-7-ST	96350	27520	3.50	868
SG-8-ST	5320	4120	1.29	520
SG-9-ST	101840	61070	1.66	610



CHAPTER 7

CONCLUSIONS

For syntheses and characterization of homopolymers and random copolymers, generally two different approaches were used which were the impact of electron donors on the polymer backbone and the impact of electron acceptors on the polymer backbone.

Firstly a series of monomers were synthesized via Stille coupling reaction to obtain low-band gap conjugated polymers-PSBO, PFBO and PTTBO comprising electron-rich selenophene, furan, and thieno[3,2-*b*]thiophene (TT) as donor units in conjugation with electron-deficient 2,1,3-benzoxadiazole (BO) moiety as the acceptor unit. Potentiodynamically synthesized polymers on ITO coated glass slides were examined to investigate electrochemical and spectroelectrochemical properties. Spectroelectrochemical studies revealed that stepwise oxidation results in multicolored electrochromic polymers. Thiophene, 3-hexylthiophene, 3,4-ethylenedioxythiophene comprising homopolymers of benzoxadiazole moiety were synthesized earlier in our group. Comparison among all polymers revealed that EDOT based homopolymer has smallest band gap with best optical and kinetic results due to strong electron donating ability of EDOT unit on the polymer backbone. Additionally, two different monomers comprising isoindigo and thienopyrrolodione were synthesized to observe the impact of the donor moiety on the polymer backbone. Thienothiophene was used as the donor moiety. The potentiodynamically synthesized homopolymers were characterized in terms of HOMO-LUMO energy levels via cyclic voltammetry studies since they reveal ambipolar characteristics and optical band gap was calculated via spectroelectrochemistry studies. Both polymers were used as the active layers for biosensor applications which is about developing highly sensitive, inexpensive, practical and selective biological devices for the detection of glucose, cholesterol, alcohol, urea and pesticides. In this very novel biosensor construction,

yarn would be converted into a device and used for detection of analytes mentioned above. Conductive yarn surface are modified with different thickness values of polymers. Besides, conventional biosensor are also being constructed using those homopolymers.

Moreover, various alternating copolymers were synthesized via Stille polycondensation reactions to be used in organic solar cells as active layers. Some of the polymers were characterized to determine the frontier molecular orbital energy levels via electrochemistry studies. The other aim of synthesizing those polymers (except for PIIDDTP) was to compare two different synthetic methodologies which are Stille and Direct Heteroarylation polymerizations. Polymers with the same structures synthesized by those reactions were compared in terms of molecular weights and optoelectronic properties. Moreover, polymers with the suitable energy levels are now being used in the construction of solar cells. ^1H NMR results of the polymers could not be recorded since high temperature analyses are required to see the defects and also get high resolution spectra. However the polymers were characterized using Fourier Transform Infrared Spectroscopy (FTIR), elemental analyses and thermal analyses which are thermogravimetric analysis (TGA) and differential scanning calorimetry (DSC). Apart from those polymers, PIDDTTP was synthesized and characterized in terms of optoelectronic properties. Optical and electronic properties were investigated. Besides, PSBSC, PFBFC, PSBSFL and PFBFFL were synthesized via Suzuki coupling. Among all polymers, the highest performance was obtained with the device based on PSBSC. It exhibited a value of PCE of 1.89 % with a V_{oc} of 0.62 V, J_{sc} of 7.63 mA cm^{-2} , FF of 40 %, under the illumination of AM 1.5 G, 100 mW cm^{-2} Air stability of carbazole comprising polymers (PSBSC and PFBFC) was greater than fluorene based polymers (PSBSFL and PFBFFL). The molecular weights of polymers were not so high most probably due to using biphasic system in the reaction medium for Suzuki coupling. Hence, the polymers did not give high power conversion efficiencies in the

solar cells especially due to low short circuit current which may arise from limited absorption.

Conventional donor–acceptor polymers have one electron-deficient and one electron-rich segments in their repeating units. Unlike from normal donor-acceptor polymers, two electron rich (or electron poor) moieties are combined with one electron poor (or electron rich) building block which could lead to broadening of their absorption spectra and harvesting of photons efficiently. Hence, polymers using terpolymer approach were synthesized and characterized using two opposite aspects which were the impact of electron rich unit in the polymer and the impact of electron poor unit through the polymer backbone. To investigate the impact of π bridge and donor moiety on the polymer backbone P1, P2 and P3 were synthesized. P3 has very low solubility in common solvents such as chloroform or tetrahydrofuran on account of its high molecular weight, device construction using P3 could not be achieved. For solution processability and further applications, monomers possessing solubilizing alkoxy chains were used to synthesize random copolymers. P1 with no π bridge between the donor and acceptor moieties did not reveal any I-V characteristics. The long carbon chains may lead to very low interaction between PC₇₁BM and the polymer. This may as well be the reason for not getting proper film coating on the substrate. For P3 with no I-V characteristics, β -branching which may be seen for thienothiophene unit could cause no result in solar cells. Hence, the polymer would not be soluble in common solvent even it does not have very high molecular weight. Also, RP1, RP2 and RP3 were synthesized. The difference between those polymers were various acceptor units keeping the same donor group on the polymer backbone. As the strength of acceptor moieties change, optoelectronic properties and solar cell characteristics would change. Benzodithiophene was the donor in all polymers whereas acceptors were alkoxy substituted benzoxadiazole for RP1, benzoxadiazole for RP2 and isoindigo for RP3. RP1 and RP3 were used as the active layers in solar cells. The preliminary results revealed that RP3 gave lower PCE in photovoltaics which may arise due to higher tendency to agglomerate for isoindigo derivatives.

Agglomeration of polymer could block charges to reach corresponding electrodes hence exciton recombination may occur leading to much lower current in the solar cell. RP2 will be used for organic photovoltaics.

In addition, polymers were obtained via two different synthetic methodologies i.e. Stille coupling and Direct Heteroarylation Polymerization (DHAP). Since performance of compounds should be comparable or even superior for these polymerization techniques, molecular weights and absorption maxima were compared for polymers. As seen from the table, number average and weight average molecular weights are very similar for both Stille and DHAP reactions. Besides, maximum absorption of polymers gave also similar results. The advantage of DHAP is the possibility to obtain polymers with less or no structural defects like branching, crosslinking, and homocoupling depending on the reaction condition. It is not possible to remove those defects via various purification processes since they are chemically embedded throughout the polymer chains. Hence, polymers obtained via DHAP can have better solubility even their molecular weights are much higher as in the case of SG-3 which may result from less defects in the polymer backbone. Polymers must also be compared in terms of device performance for solar cells and electronic properties like frontier molecular orbital energy levels and band gap. For future studies, those characterizations will be achieved. To observe the structural defects, high temperature NMR should be used. The polymers will be characterized in terms of ^1H NMR using high temperature measurements since taken results were not in high resolution with defined peaks. Apart from those, polymers abbreviated as SG-7-ST, SG-8-ST, SG-9-ST, SG-10-ST were also compared in terms of their absorbance in UV-Vis-NIR region. Sunlight covers a broad spectrum from UV to IR and around 51 % of sunlight is present in NIR region of solar spectrum. For better harvesting of photons, absorption in the NIR region is very crucial. SG-7-ST is a NIR absorbing material. This polymer can easily be a promising candidate for solar cell application especially for ternary solar cells which combines three different materials via matching suitable maximum absorptions to obtain maximum efficiency in the solar

cell. The other polymers abbreviated as SG-8-ST and SG-10 were mostly insoluble in common organic solvents hence they could not be characterized. After heating in a chlorinated solvent for solubility, only absorption spectra could be recorded. Most fraction of the polymers left inside PTFE syringe filters due to their insolubility in the solvent for SG-8-ST and SG-10 before GPC measurements, the results for molecular weights are very low for those polymers. The aim to synthesize SG-10 was obtaining an acceptor-acceptor type polymer rather than donor-acceptor type polymers used in the solar cells. If the polymer could be soluble and its energy levels were suitable, it was aimed to be used instead of fullerene in the active layer. The most probable reason for insolubility of the polymer may arise from crosslinking which could be observed for thienothiophene derivatives in direct heteroarylation reaction. For SG-8-ST, the reaction was so quick hence the polymer suddenly precipitated in the reaction medium. Therefore, a very high polymer may be synthesized hence it could be insoluble. The other factor for insolubility could again be attributed to crosslinking. For furan based polymers, it is not so easy to synthesize very high molecular weight due to instability of furan based monomers. However, a high molecular weight polymer, SG-9-ST, could be synthesized successfully. This polymer would be a great candidate for photovoltaics.

On the other hand, non-fullerene acceptors with rhodanine end groups were aimed to be synthesized for organic solar cells. Synthesis of non-fullerene acceptors via direct heteroarylation reaction was achieved for the first time in literature. After purification of those materials, rhodanine flanking will be achieved via Knoevenagel condensation reaction. For the construction of solar cells, contrary to the conventional structure, inverted structures will be constructed for fullerene-free organic photovoltaics. Since those molecules are highly sensitive to acidic compounds and PEDOT:PSS was used as the interface layer in a solar cell, inverted solar cell structures would protect the small molecules from degradation via cutting direct contact to acidic layer hence high efficiency photovoltaics could be obtained.

The polymers were synthesized and characterized in terms of optoelectronic properties. Furthermore, thermogravimetric analysis (TGA) and differential scanning calorimetry (DSC) were carried out to investigate both thermal stability and thermal transitions for some of polymers which could show suitability of materials for organic photovoltaics since stability affects shelf life of devices. Perkin Elmer Differential Scanning Calorimetry was used to sweep the temperature to determine heat capacity change (ΔC_p), glass transition temperature (T_g) and melting temperature (T_m) for polymers. Thermogravimetric analyses (TGA) of polymers were performed to see the specific weight loss using Perkin Elmer Pyris 1 TGA. During the experiment a heating rate of 10 °C/min, the polymer films were heated up to 350 °C under nitrogen atmosphere. Weight loss of the polymers were recorded as 19 % after 325 °C for SG-2, 31 % for SG-2-ST while the temperature was gradually increased. SG-3 revealed nearly no degradation. For SG-3-ST, nearly 1.5 % was recorded after 250 °C. 11 % weight loss was obtained for SG-4 after 250 °C, around 10 % weight loss was recorded after 250 °C. For RP1-ss the weight loss was around 7 % after 300 °C whereas the weight loss was around 5 % after 300 °C for RP1-os. For RP3, the weight loss was around 1 % after 380 °C whereas the weight loss was around 3 % after 350 °C for RP2. For the same polymer obtained from hexane phase the weight loss was around 4 % after 200 °C. The longer chains with higher molecular weight polymer resulted in higher thermal stability. For SG-6, nearly no degradation was observed. SG-9-ST resulted in a weight loss of 5 % after 300 °C. For PIIDDTP, the weight loss was recorded as 22 % while the temperature was gradually increased. The polymers were mostly designated as stable up to 300 °C.

Since metals could cause detrimental effects in solar cells, elemental analyses were done to observe any residual catalyst (i.e. Pd(0)) in the polymers after polycondensation reactions and purifications. The results revealed that no metal exists as a residue or structural defect through the polymer backbone.

Synthesized polymers were aimed to be used as the active layers for several applications such as biosensors and organic photovoltaics. Some of homopolymers

obtained via electropolymerizations were used in biosensors. Donor–acceptor terpolymers were synthesized to broaden the optical absorption and hence improve the light-harvesting properties. Some copolymers synthesized via classical polymerization reactions and DHAP are still being used for solar cell constructions.



REFERENCES

- [1] Strom, E. T. and Rasmussen S. C., (2011) 100 Years of Plastics Leo Baekeland and Beyond Retrieved from <https://pubs.acs.org/doi/full/10.1021/bk-2011-1080.ch010>
- [2] Shirakawa, H. In Les Prix Nobel. The Nobel Prizes 2000; Frängsmyr, T., Ed.; Nobel Foundation: Stockholm, 2001
- [3] Shirakawa, H., Louis, E. J., MacDiarmid, A. G., Chiang, C. K., Heeger, A. J. J. Synthesis of electrically conducting organic polymers: halogen derivatives of polyacetylene, (CH)_x, Chem. Soc., Chem. Commun., 1977, 578-580.
- [4] The Nobel Prize in Chemistry 2000 (2019, August 5) Retrieved from <https://www.nobelprize.org/prizes/chemistry/2000/summary/>
- [5] a) Fredrickson G. H., in Encyclopedia of Materials: Science and Technology, 2002 Retrieved from <https://www.sciencedirect.com/topics/engineering/homopolymers>
- b) Hagiopol C., in Reference Module in Materials Science and Materials Engineering, 2016 Retrieved from <https://www.sciencedirect.com/topics/materials-science/copolymer>
- [6] Hamielec A. E., Macgregor J. F., Penlidis A., (1989) Comprehensive Polymer Science and Supplements: The Synthesis, Characterization, Reactions & Applications of Polymers Oxford, England; New York : Pergamon Press.
- [7] Sadki S., Schottland P., Brodie N., Sabourau G., The mechanisms of pyrrole electropolymerization, Chem. Soc. Rev., 2000, 29, 283–293.
- [8] Cosnier S., Karyakin A., (2010) Electropolymerization: Concepts, Materials and Applications, Weinheim, Mechanisms of Electropolymerization and Redox Activity: Fundamental Aspects, Wiley.
- [9] X. Ling, (1998) Formation of Polymer Coatings by Electropolymerization, Chemical Engineering, University of Waterloo.
- [10] Anand J., Palaniapan S., Sathyanarayana D., Conducting polyaniline blends and composites. Prog. Polym. Sci., 1998, 23, 993–1018.
- [11] Heinze J., Rasche A., Pagels M., Geschke B., On the origin of the so-called nucleation loop during electropolymerization of conducting polymers. J. Phys. Chem. B, 2007, 111, 989-997.
- [12] Otero T., DeLaretta E., Electrochemical control of the morphology, adherence, appearance and growth of polypyrrole films. Synth. Met., 1988, 26, 79-88.

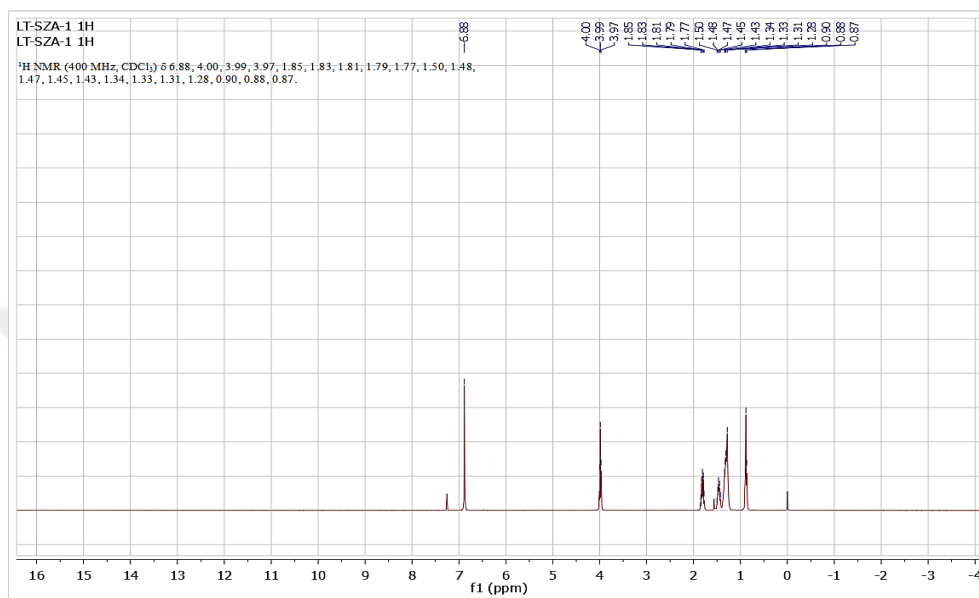
- [13] Sanchez D., Diaz R., Herrasti P., Ocon P., Electrogenation and characterization of poly(3-methylthiophene). *Polym. J.*, 2001, 33, 514-521.
- [14] Beletskaya I. P., Cheprakov A. V., The Heck Reaction as a sharpening stone of palladium catalysis, *Chem. Rev.*, 2000, 100, 3009-3066.
- [15] Corbet, J. P., Mignani G., Selected, patented cross coupling reaction technologies, *Chem Rev.*, 2006, 106, 2651-2710.
- [16] Azarian D., Dua S. S., Eaborn C., Walton D. R. M. J., Reactions of organic halides with R_3MMR_3 compounds ($M=Si, Ge, Sn$) in the presence of tetrakis(triarylphosphine)palladium, *Organomet. Chem.*, 1976, 117, C55-C75.
- [17] Cordovilla C., Bartolomé C., Ilarduya J. M. M., Espinet P., The Stille Reaction, 38 Years Later, *ACS Catal.*, 2015, 5, 3040-3053.
- [18] Leclerc M., Morin J. F. (2017). *Synthetic methods for conjugated polymers and carbon materials*. Weinheim, Germany: Wiley.
- [19] Miyaura N., Suzuki A., Palladium-Catalyzed Cross-Coupling Reactions of Organoboron Compounds, *Chem. Rev.*, 1995, 95, 2457-2483.
- [20] Carsten B., He F., Son H. J., Xu T., Yu L., Stille polycondensation for synthesis of functional materials, *Chem. Rev.*, 2011, 111, 1493-1528
- [21] Yan C., Barlow S., Wang Z., Yan H., Jen A. K.-Y., Marder S. R., Zhan X., Non-fullerene acceptors for organic solar cells, *Nat. Rev. Mater.*, 2018 3, 18003-18022.
- [22] Yao H., Ye L., Zhang H., Li S., Zhang S., Hou J., Molecular design of benzodithiophene based organic photovoltaic materials, *Chem. Rev.*, 2016, 116, 7397-7457.
- [23] Huang H., Huang J. (2014) *Organic and Hybrid Solar Cells*, Switzerland: Springer.
- [24] Eftaiha A. F., Sun J.-P., Hill I. G., Welch G. C., Recent advances of non-fullerene, small molecular acceptors for solution processed bulk heterojunction solar cells, *J. Mater. Chem. A*, 2014, 2, 1201-1213.
- [25] Wadsworth A., Moser M., Marks A., Little M. S., Gasparini N., Brabec C. J., Baran D., McCulloch I., Critical review of the molecular design progress in non-fullerene electron acceptors towards commercially viable organic solar cells, *Chem. Soc. Rev.*, 2019, 48, 1596-1625.
- [26] Zhan C., Yao J., More than conformational “Twisting” or “Coplanarity”: molecular strategies for designing high-efficiency nonfullerene organic solar cells, *Chem. Mater.*, 2016, 28, 1948-1964.

- [27] Holliday S., Ashraf R. S., Nielsen C. B., Kirkus M., Röhr J. A., Tan C.-H., Fregoso E. C., Knall A.-C., Durrant J. R., Nelson J., McCulloch I., Organic photovoltaics, *J. Am. Chem. Soc.*, 2015, 137, 898–904.
- [28] Srivani D., Agarwal A., Bhosale S. V., Puyad A. L., Xiang W., Evans R. A., Gupta A., Bhosale S.V., Naphthalene diimide-based non-fullerene acceptors flanked by open-ended and aromatizable acceptor functionalities, *Chem. Commun.*, 2017, 53, 11157–11160.
- [29] McCulloch I., Heeney M., Bailey C., Genevicius K., MacDonald I., Shkunov M., Sparrowe D., Tierney S., Wagner R., Zhang W., Chabinyc M. L., Kline R.M.D., McGehee R. J., Toney M. F., Liquid-crystalline semiconducting polymers with high charge-carrier mobility, *Nat. Mater.* 2006, 5, 328–333.
- [30] Xu J., Hou J., Zhang S., Nie G., Pu S., Shen L., Xiao Q., Electrosyntheses of high quality freestanding polyselenophene films in boron trifluoride diethyl etherate, *J. Electroanal. Chem.*, 2005, 578, 345–355.
- [31] Jiang J. M., Raghunath P., Lin Y. C., Lin H. K., Ko C. L., Su W C.-Y, Lin M. C., Wei K. H., Linear solubilizing side chain substituents enhance the photovoltaic properties of two-dimensional conjugated benzodithiophene-based polymers, *Polymer*, 2015, 79, 262–270.
- [32] Do T. T., Ha Y. E., Kim J. H., Effect of the number of thiophene rings in polymers with 2,1,3-benzooxadiazole core on the photovoltaic properties, *Org. Electron.*, 2013, 14, 2673–2681.
- [33] Li Z., Huo L., Guo X., Yong W., Zhang S., Fan H., Synthesis and photovoltaic properties of D- π -A copolymers based on thieno[3,2-*b*]thiophene bridge unit, *Polymer*, 2013, 54, 6150–6157.
- [34] Gau V., Ma S. C., Wang H., Tsukuda J., Kibler J., Haake D. A., Electrochemical Molecular Analysis Without Nucleic Acid Amplification, *Methods*, 2005, 37, 73–83.
- [35] Liu B., Chen X., He Y., Li Y., Xu X., Xiao L., Li L., Zou Y., New alkylthienyl substituted benzo[1,2-*b*:4,5-*b'*]dithiophene-based polymers for high performance solar cells, *J. Mater. Chem A*, 2013, 1, 570–577.
- [36] Jiang J. M., Yang P. A., Lan S. C., Yu C. M., Wei K. H., Benzooxadiazole-based donor/acceptor copolymers imparting bulk-heterojunction solar cells with high open-circuit voltages, *Polymer*, 2013, 54, 155–161.
- [37] Ding P., Zhong C., Zou Y., Pan C., Wu H., Cao Y., 5,6-Bis(decyloxy)-2,1,3-benzooxadiazole-Based Polymers with Different Electron Donors for Bulk-Heterojunction Solar Cells, *J. Phys. Chem. C* 2011, 115, 16211–16219.
- [38] Chen H. Y., Yeh S. C., Chen C. T., Chen C. T., Comparison of thiophene- and selenophene-bridged donor–acceptor low band-gap copolymers used in bulk-heterojunction organic photovoltaics, *J. Mater. Chem.* 2012, 22, 21549–21559.

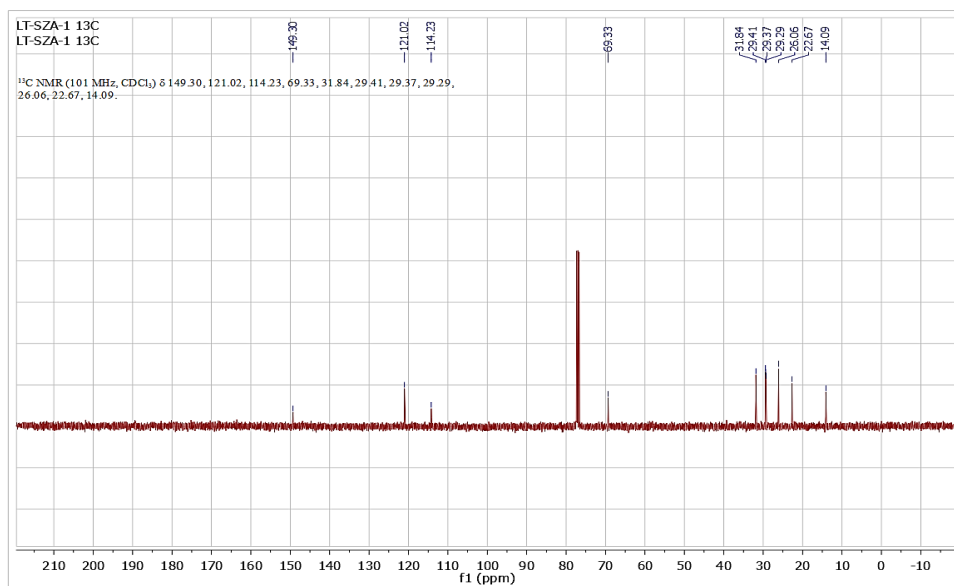
- [39] Wang X., Chen S., Sun Y., Zhang M., Li Y., Li X., Wang H., A furan-bridged D- π -A copolymer with deep HOMO level: synthesis and application in polymer solar cells, *Polym. Chem.* 2011, 2, 2872–2877.
- [40] T. E. Kang, K.-H. Kim, B. J. Kim, Design of terpolymers as electron donors for highly efficient polymer solar cells, *J. Mater. Chem. A*, 2014, 2, 15252–15267.
- [41] Hendriks K. H., Heintges G. H. L., Wienk M. M., Janssen R. A. J., Comparing random and regular diketopyrrolopyrrole–bithiophene–thienopyrrolodione terpolymers for organic photovoltaics, *J. Mater. Chem. A*, 2014, 2, 17899–17905.
- [42] Fang L., Zhou Y., Yao Y.-X., Diao Y., Lee W.-Y., Appleton A. L., Allen R., Reinspach J., Mannsfeld S. C. B., Bao Z., Side-Chain Engineering of Isoindigo-Containing Conjugated Polymers Using Polystyrene for High-Performance Bulk Heterojunction Solar Cells, *Chem. Mater.*, 2013, 25, 4874–4880.
- [43] Chang W.-H., Gao J., Dou L., Chen C.-C., Liu Y., Yang Y., Side-Chain Tunability via Triple Component Random Copolymerization for Better Photovoltaic Polymers, *Adv. Energy Mater.*, 2014, 4, 1300864.
- [44] Chen C. H., Cheng Y. J., Chang C. Y., Hsu C. S., Donor–Acceptor Random Copolymers Based on a Ladder-Type Nonacyclic Unit: Synthesis, Characterization, and Photovoltaic Applications, *Macromolecules*, 2011, 44, 8415–8424.
- [45] a) Kim H., Lee H., Seo D., Jeong Y., Cho K., Lee J., Lee Y., Regioregular Low Bandgap Polymer with Controlled Thieno[3,4-b]thiophene Orientation for High-Efficiency Polymer Solar Cells, *Chem. Mater.*, 2015, 27, 3102–3107. b) Kleinhenz N., Yang L., Zhou H., Price S. C., You W., Low-Band-Gap Polymers That Utilize Quinoid Resonance Structure Stabilization by Thienothiophene: Fine-Tuning of HOMO Level, *Macromolecules*, 2011, 44, 872–877.
- [46] Kim H., Lee H., Jeong Y., Park J. U., Seo D., Heo H., Lee D., Ahn Y., Lee Y., Donor–acceptor polymers with a regioregularly incorporated thieno[3,4-b]thiophene segment as a π -bridge for organic photovoltaic devices, *Synth. Met.*, 2016, 211, 75–83.
- [47] Suna Q., Zhanga F., Wang J., Ana Q., Zhaob C., Lia L., Tenga F., Hua B., Toward high efficiency organic photovoltaic devices with enhanced thermal stability utilizing P3HT-b-P3PHT block copolymer additives, *J. Mater. Chem. A*, 2015, 3, 18432–18443.
- [48] Liao H. C., Ho C. C., Chang C. Y., Jao M. H., Darling S. B., Su W. F., Additives for morphology control in high-efficiency organic solar cells, *Mat. Today*, 2013, 16, 326–336.
- [49] Peet J., Kim J. Y., Coates N. E., Ma W. Doses M., Heeger A. J., Bazan G. C., Efficiency enhancement in low-bandgap polymer solar cells by processing with alkane dithiols, *Nat. Mat.*, 2007, 6, 497–500.

APPENDICES

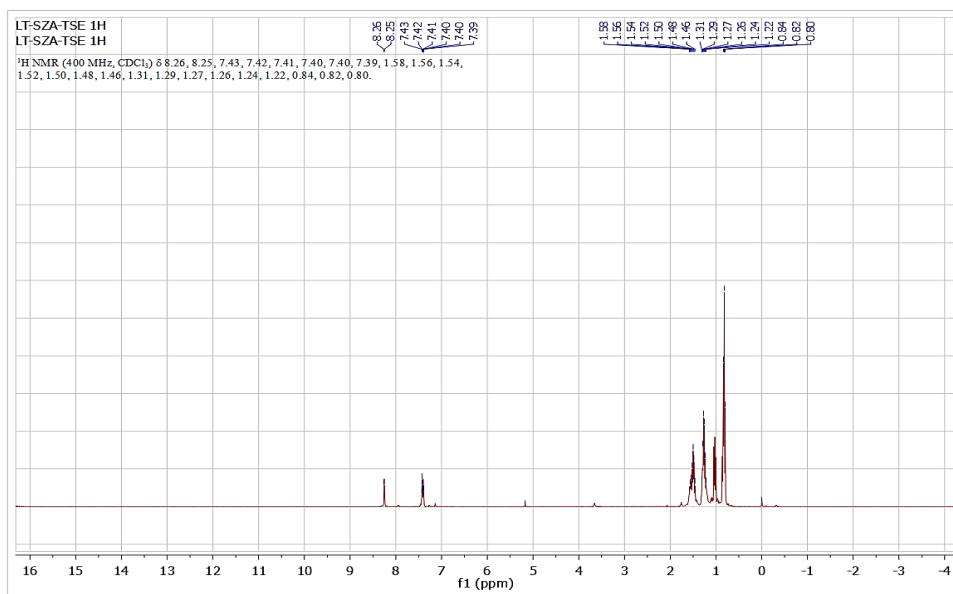
A. NMR Spectra of Materials



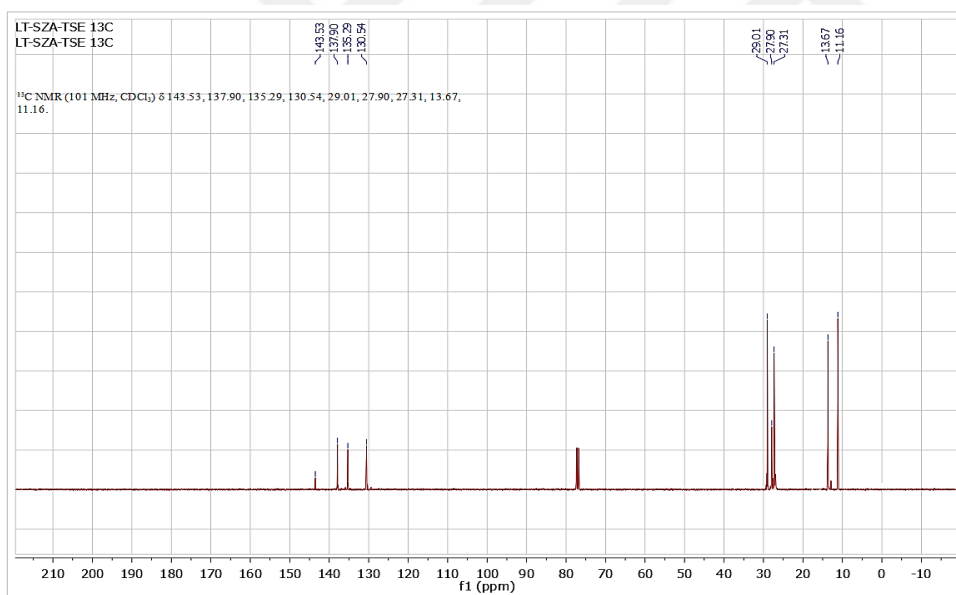
^1H NMR spectrum of 1,2-bis(octyloxy)benzene



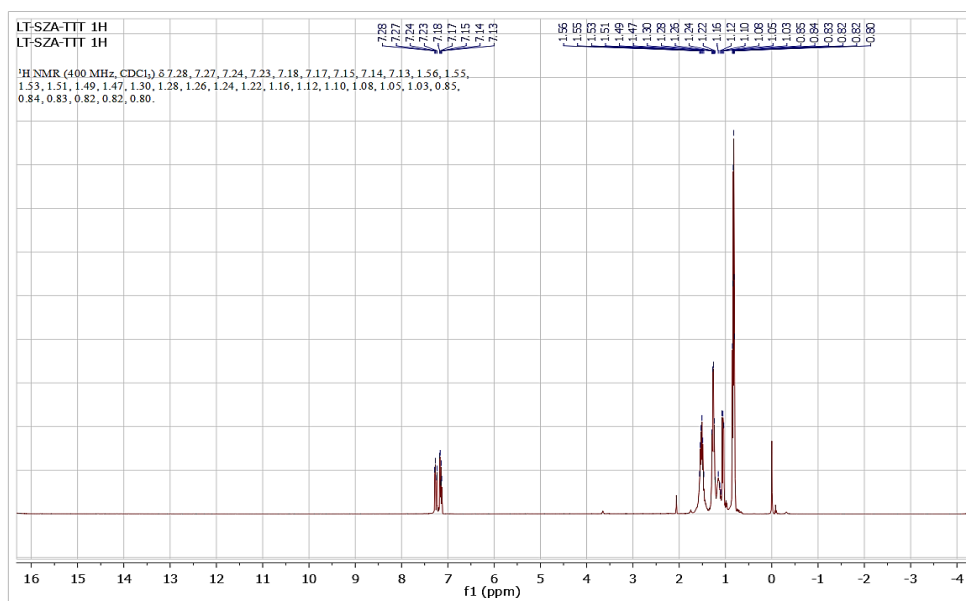
^{13}C NMR spectrum of 1,2-bis(octyloxy)benzene



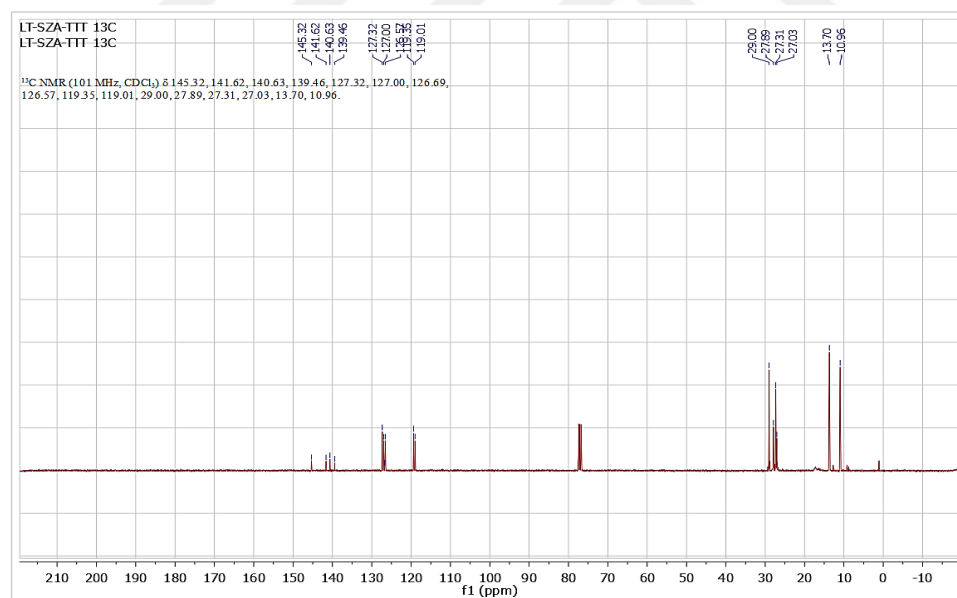
¹H NMR spectrum of tributyl(selenophen-2-yl)stannane



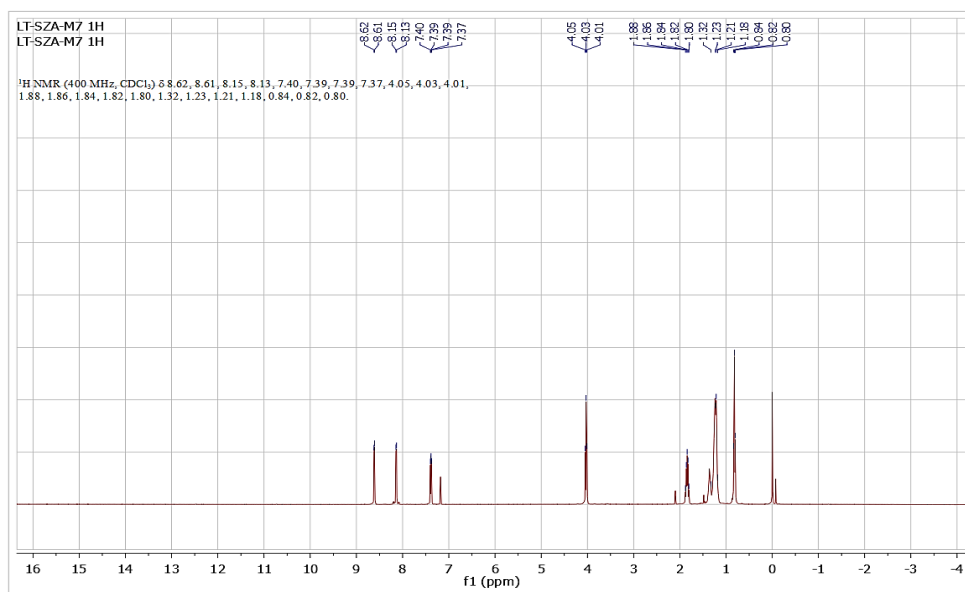
¹³C NMR spectrum of tributyl(selenophen-2-yl)stannane



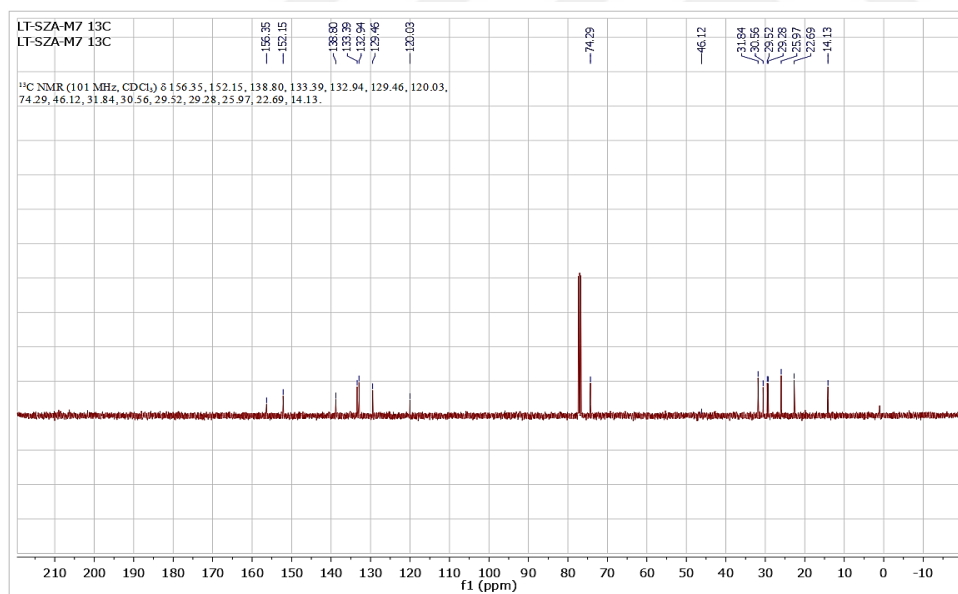
¹H NMR spectrum of tributyl(thieno[3,2-b]thiophen-2-yl)stannane



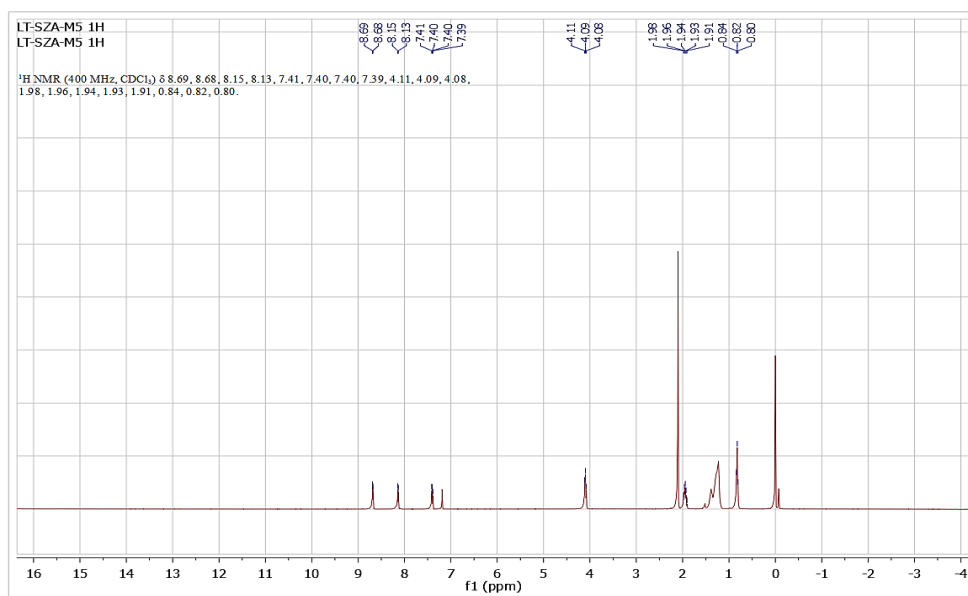
¹³C NMR spectrum of tributyl(thieno[3,2-b]thiophen-2-yl)stannane



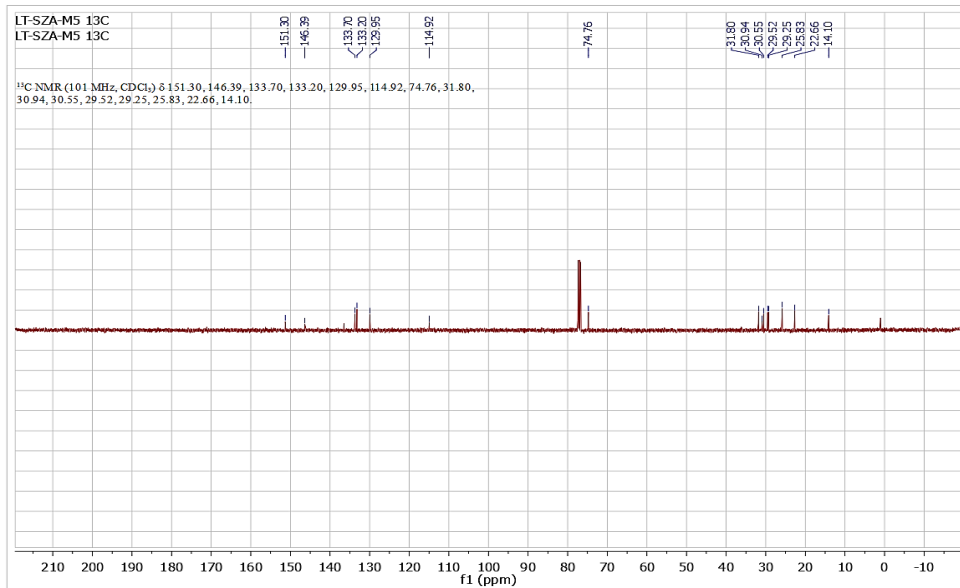
¹H NMR spectrum of 5,6-bis(octyloxy)-4,7-di(selenophen-2-yl)benzo[c][1,2,5]selenadiazole (M7)



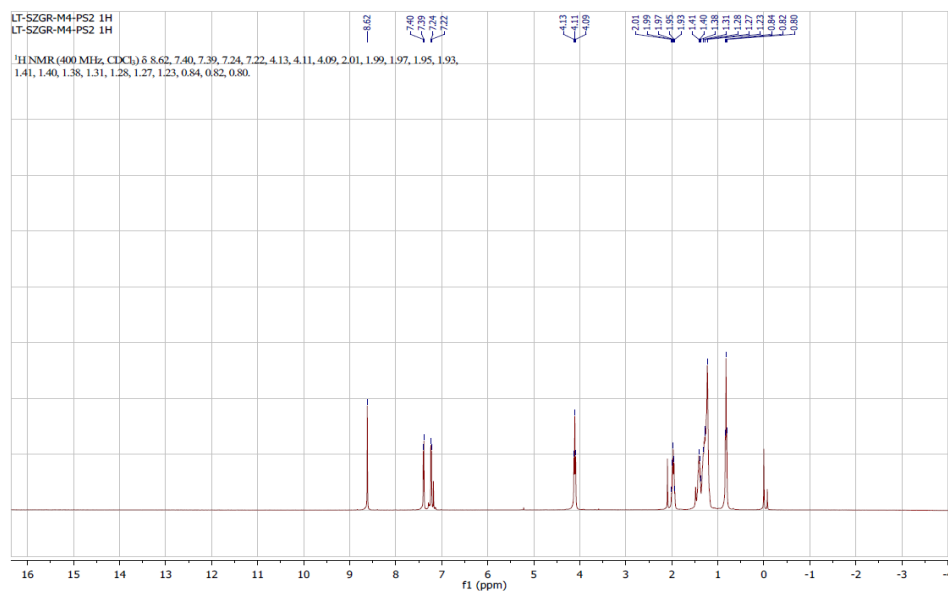
¹³C NMR spectrum of 5,6-bis(octyloxy)-4,7-di(selenophen-2-yl)benzo[c][1,2,5]selenadiazole (M7)



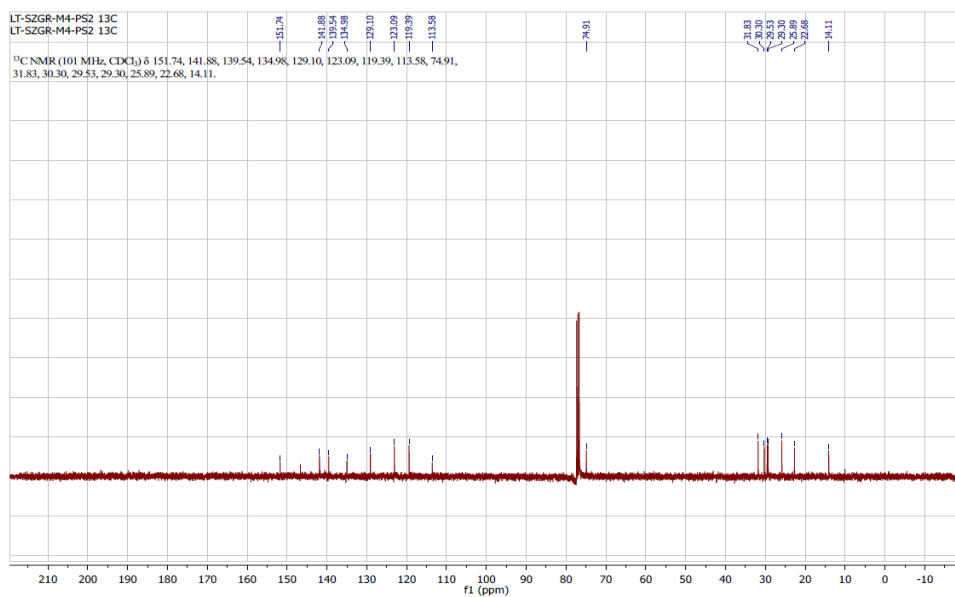
¹H NMR spectrum of 5,6-bis(octyloxy)-4,7-di(selenophen-2-yl)benzo[c][1,2,5]oxadiazole (M5)



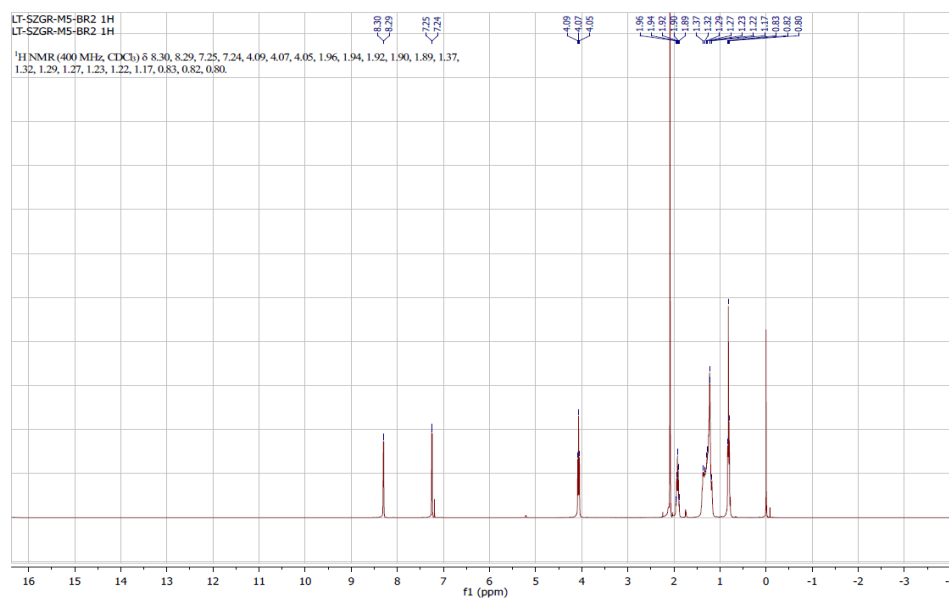
¹³C NMR spectrum of 5,6-bis(octyloxy)-4,7-di(selenophen-2-yl)benzo[c][1,2,5]oxadiazole (M5)



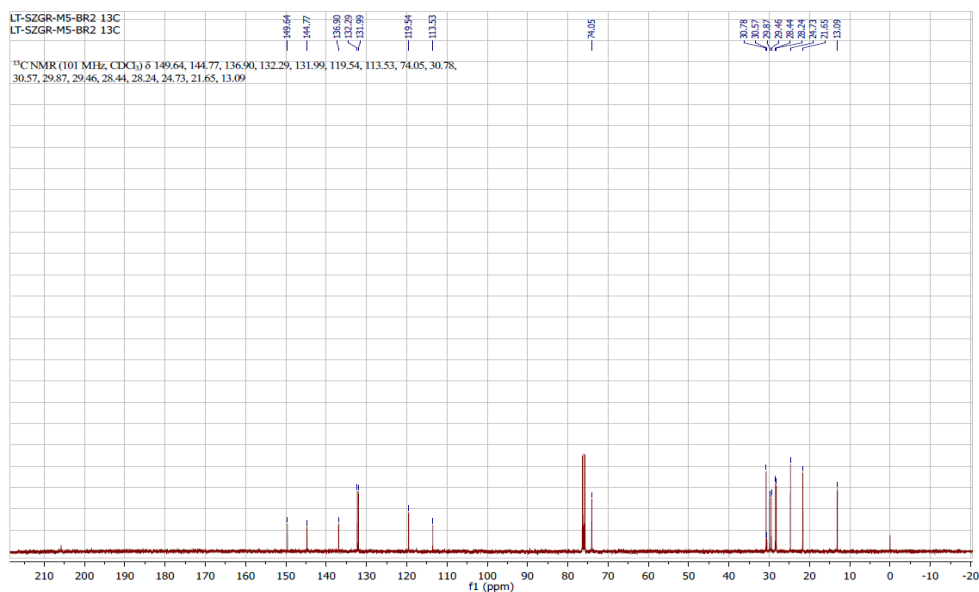
¹H NMR spectrum of 5,6-bis(octyloxy)-4,7-bis(thieno[3,2-b]thiophen-2-yl)benzo[c][1,2,5]oxadiazole (M4)



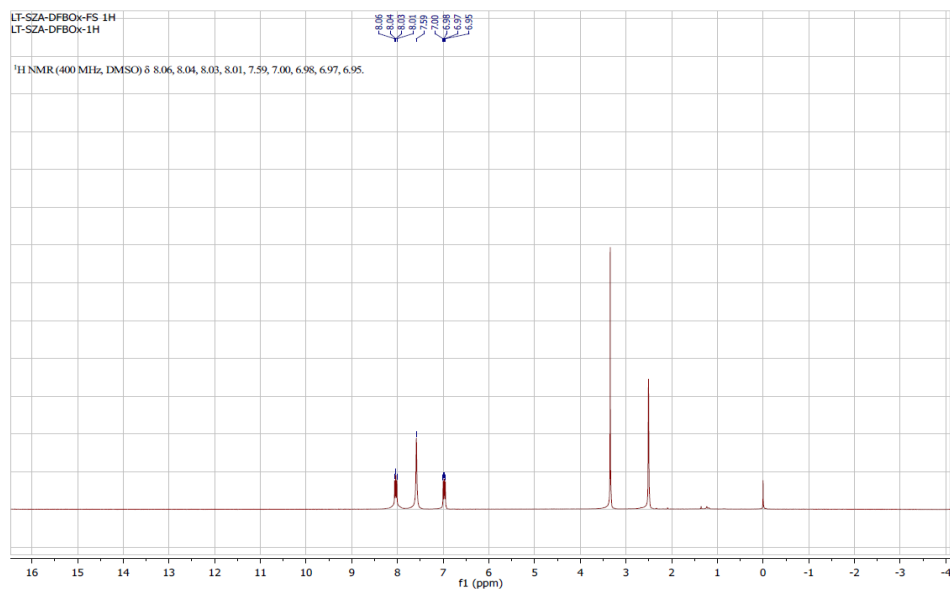
¹³C NMR spectrum of 5,6-bis(octyloxy)-4,7-bis(thieno[3,2-b]thiophen-2-yl)benzo[c][1,2,5]oxadiazole (M4)



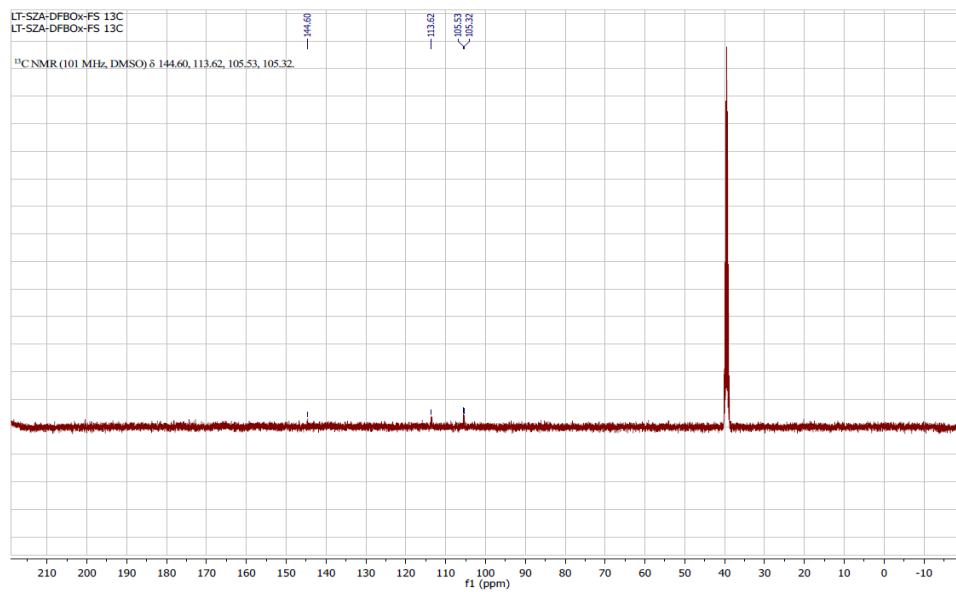
¹H NMR spectrum of 4,7-bis(5-bromoselenophen-2-yl)-5,6-bis(octyloxy)benzo[c][1,2,5]oxadiazole (M5-Br)



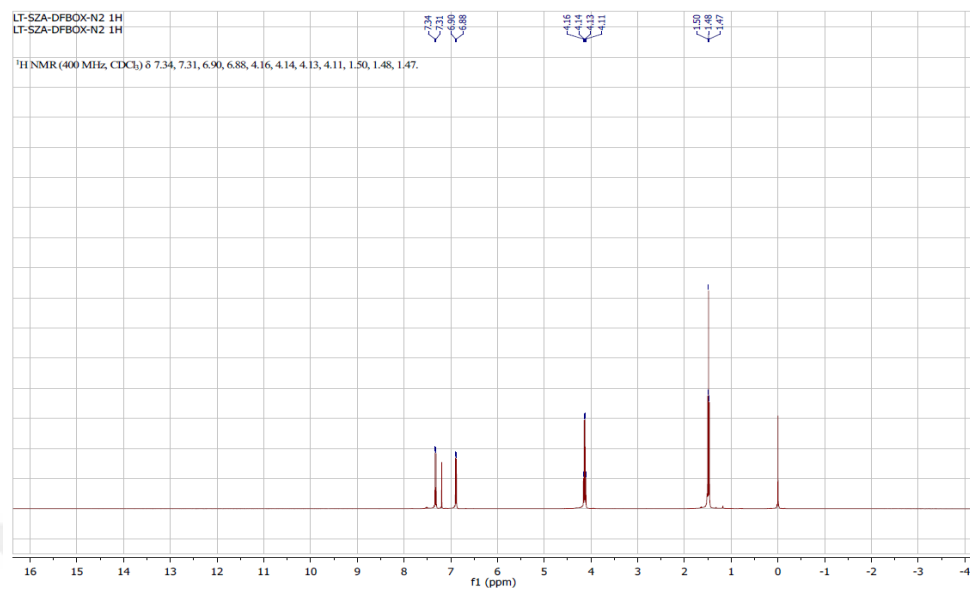
¹³C NMR spectrum of 4,7-bis(5-bromoselenophen-2-yl)-5,6-bis(octyloxy)benzo[c][1,2,5]oxadiazole (M5-Br)



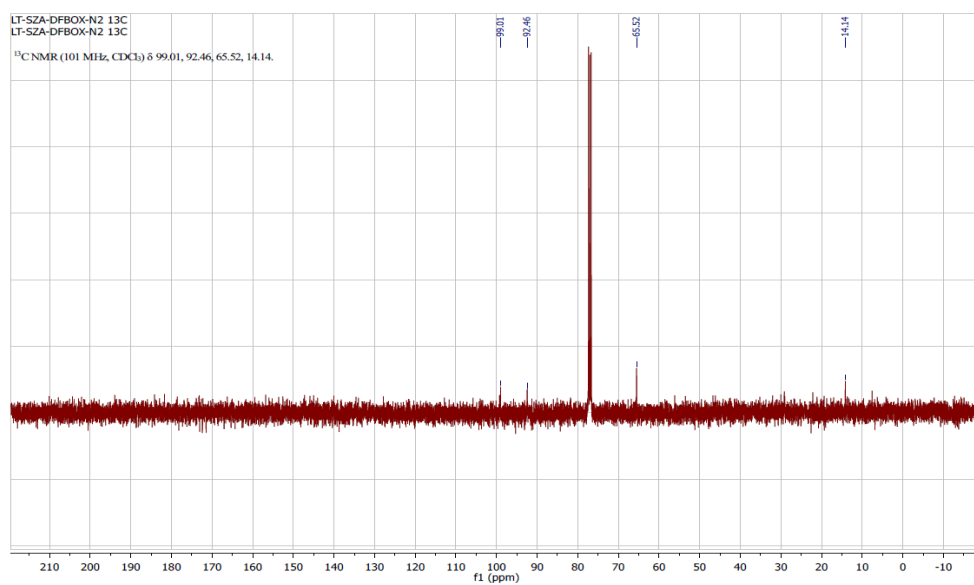
¹H NMR spectrum of 5,6-difluorobenzo[c][1,2,5]oxadiazole 1-oxide (DFBO-1)



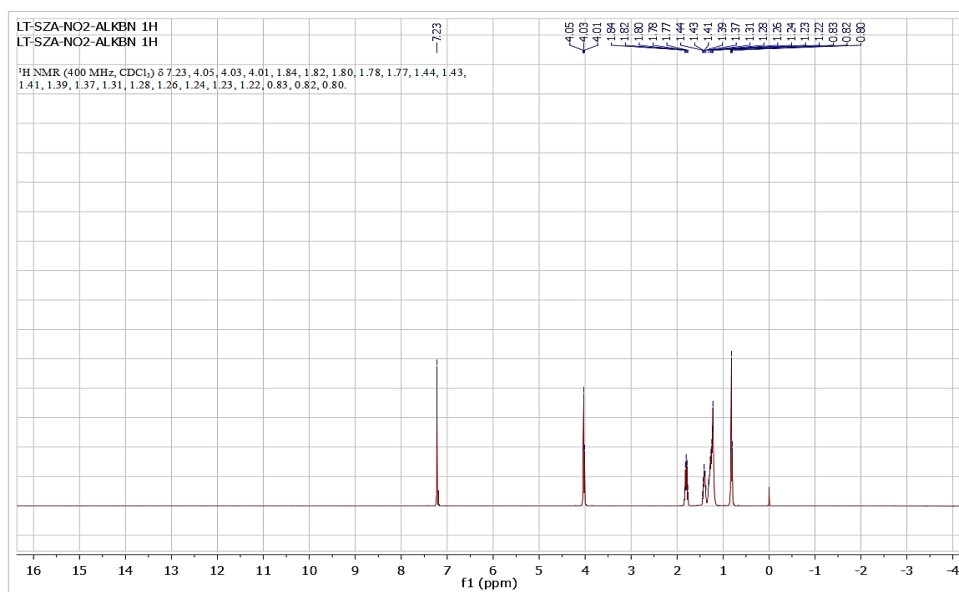
¹³C NMR spectrum of 5,6-difluorobenzo[c][1,2,5]oxadiazole 1-oxide (DFBO-1)



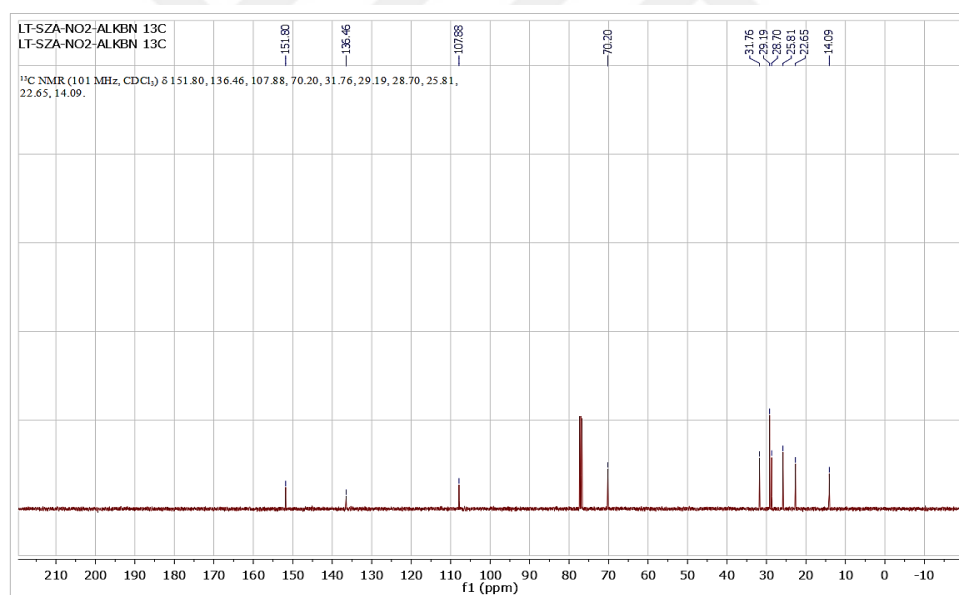
¹H NMR spectrum of 5,6-difluorobenzo[c][1,2,5]oxadiazole (DFBO-2)



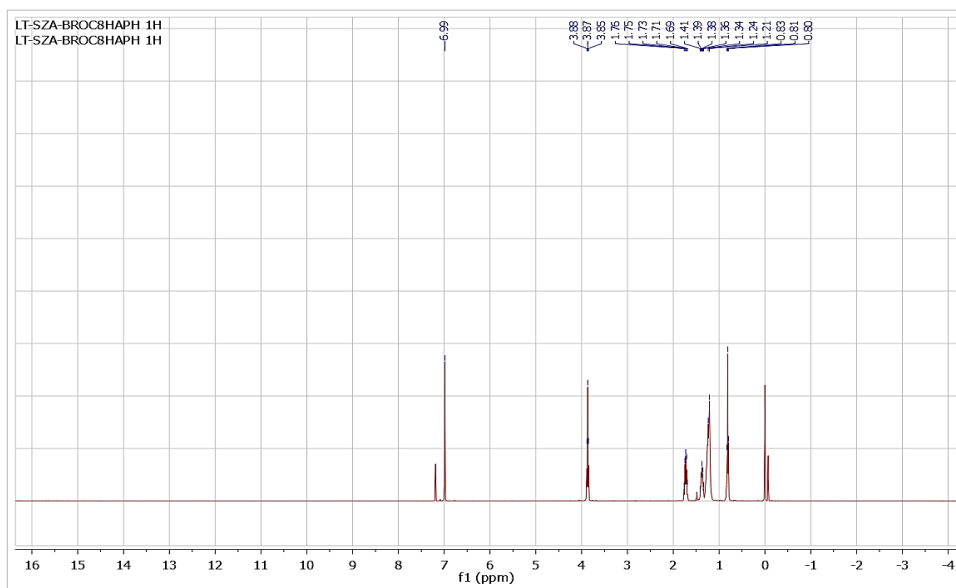
¹³C NMR spectrum of 5,6-difluorobenzo[c][1,2,5]oxadiazole (DFBO-2)



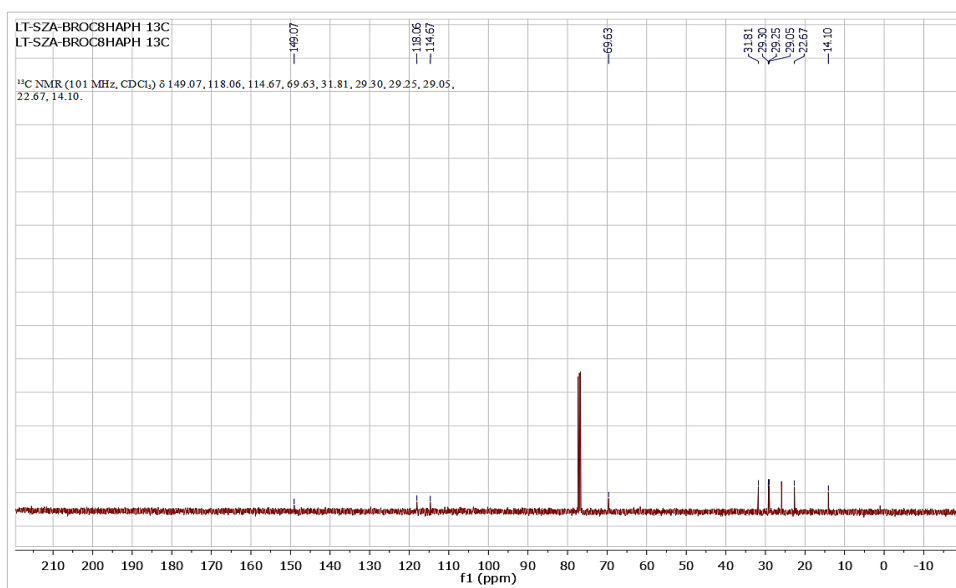
¹H NMR spectrum of 1,2-dinitro-4,5-bis(octyloxy)benzene



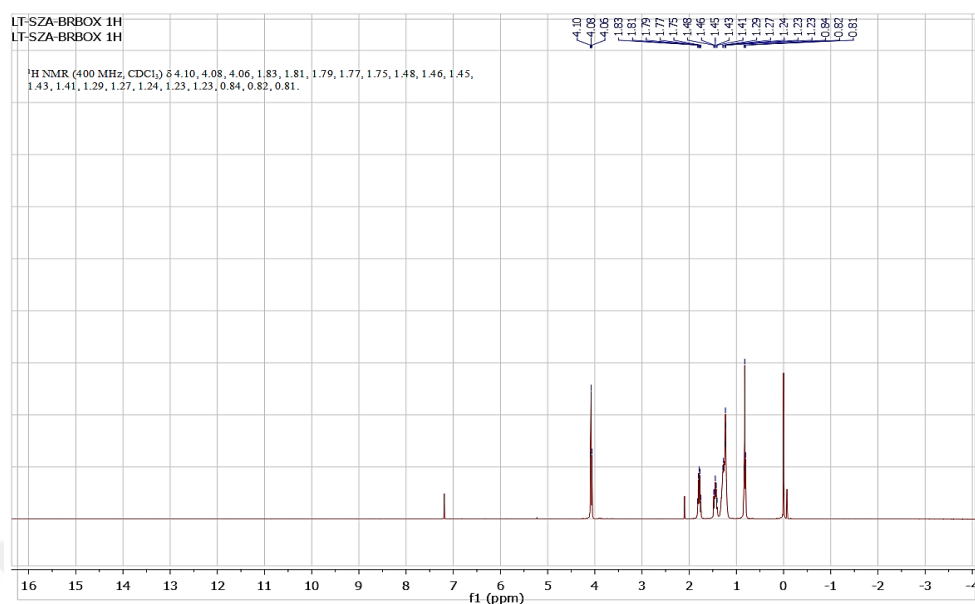
¹³C NMR spectrum of 1,2-dinitro-4,5-bis(octyloxy)benzene



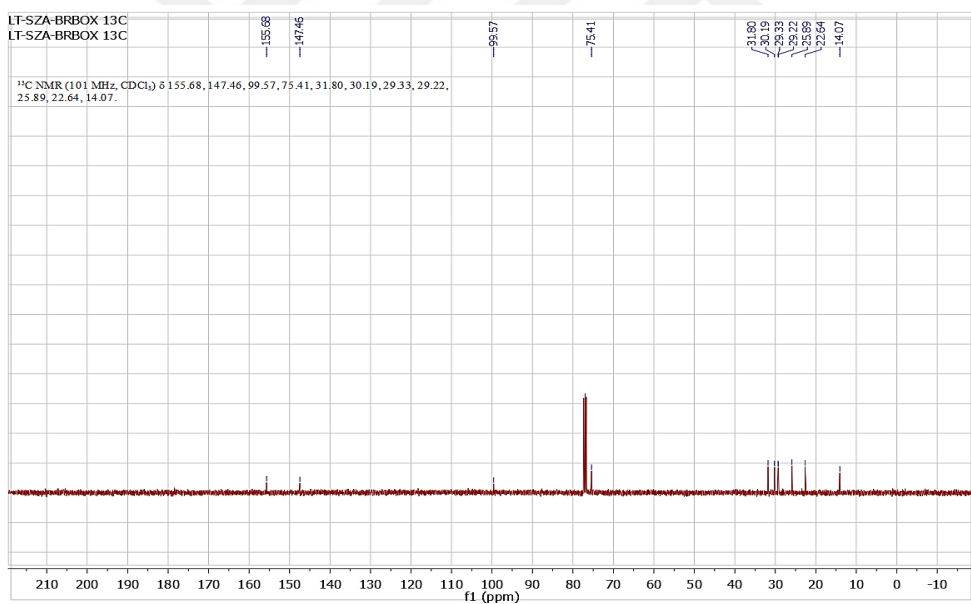
^1H NMR spectrum of 1,2-dibromo-4,5-bis(octyloxy)benzene



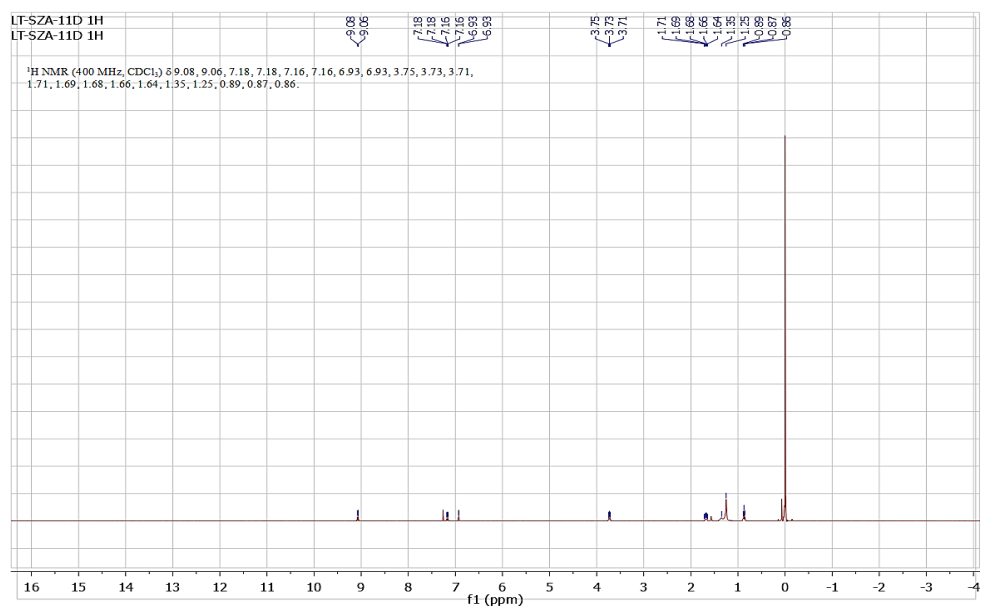
^{13}C NMR spectrum of 1,2-dibromo-4,5-bis(octyloxy)benzene



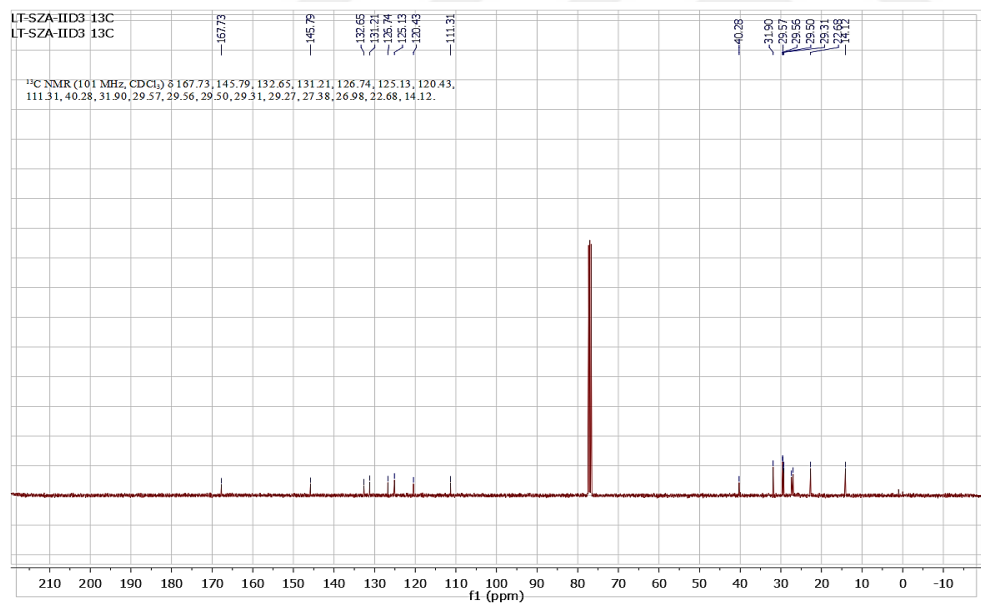
¹H NMR spectrum of 4,7-dibromo-5,6-bis(octyloxy)benzo[c][1,2,5]oxadiazole



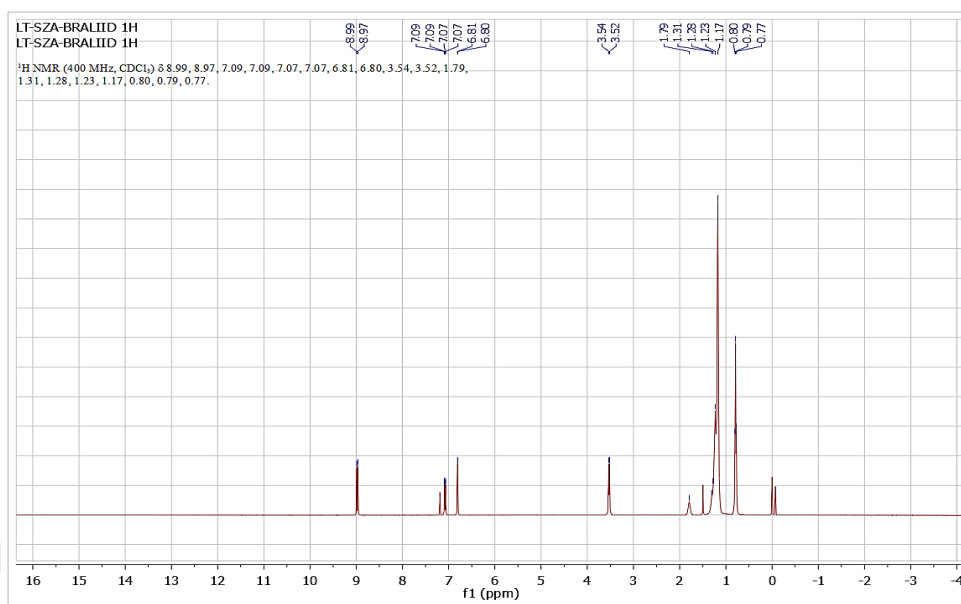
¹³C NMR spectrum of 4,7-dibromo-5,6-bis(octyloxy)benzo[c][1,2,5]oxadiazole



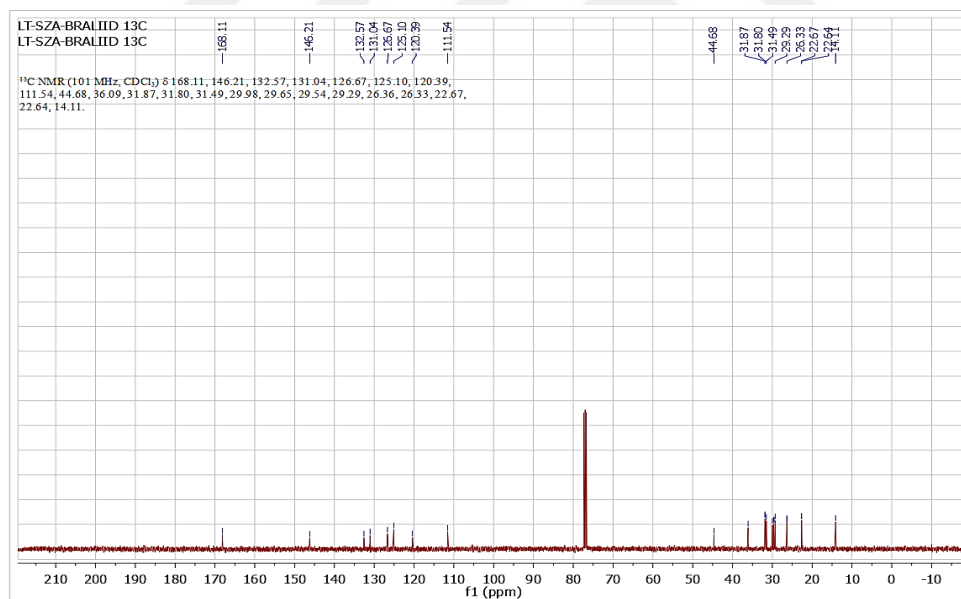
¹H NMR spectrum of (E)-6,6'-dibromo-1,1'-diundecyl-[3,3'-biindolinylidene]-2,2'-dione (IID)



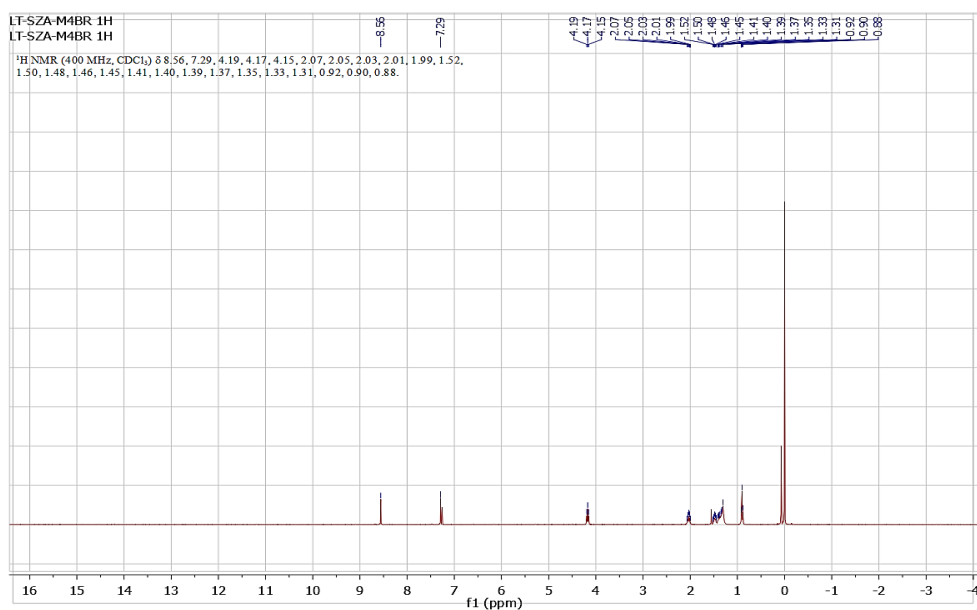
¹³C NMR spectrum of (E)-6,6'-dibromo-1,1'-diundecyl-[3,3'-biindolinylidene]-2,2'-dione (IID)



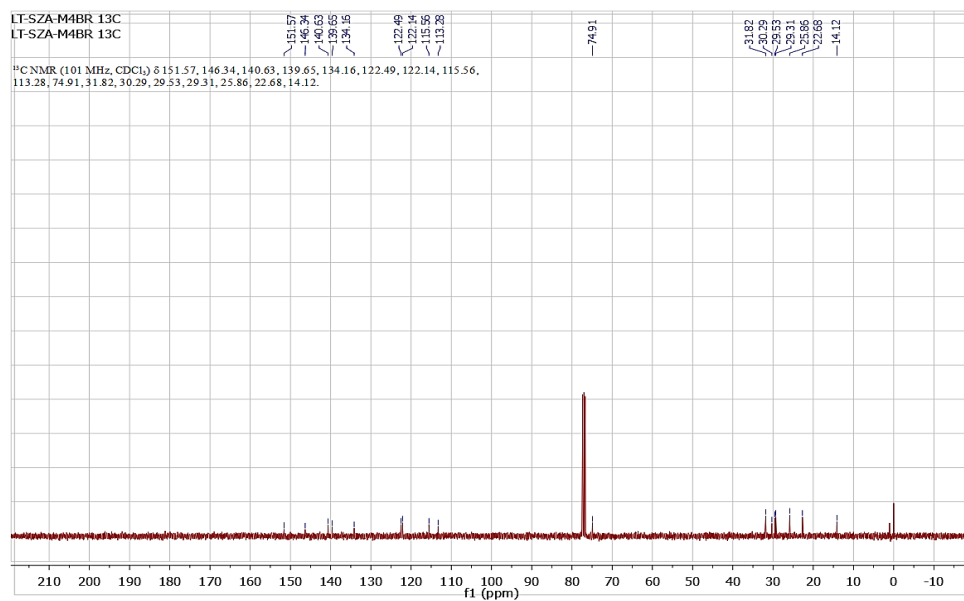
¹H NMR spectrum of (E)-6,6'-dibromo-1,1'-bis(2-hexyldecyl)-[3,3'-biindolinylidene]-2,2'-dione (Branched-IIID)



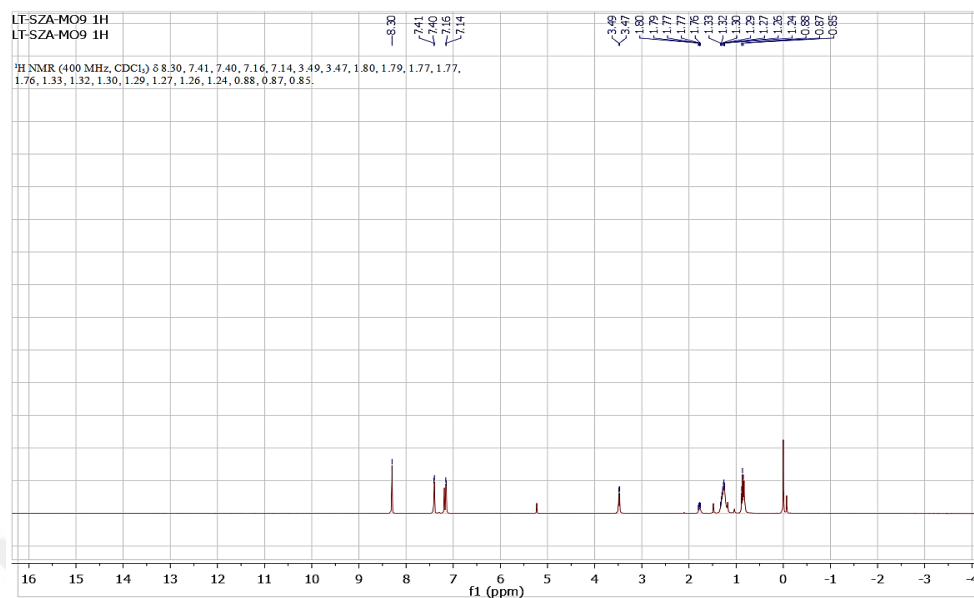
¹³C NMR spectrum of (E)-6,6'-dibromo-1,1'-bis(2-hexyldecyl)-[3,3'-biindolinylidene]-2,2'-dione (Branched-IIID)



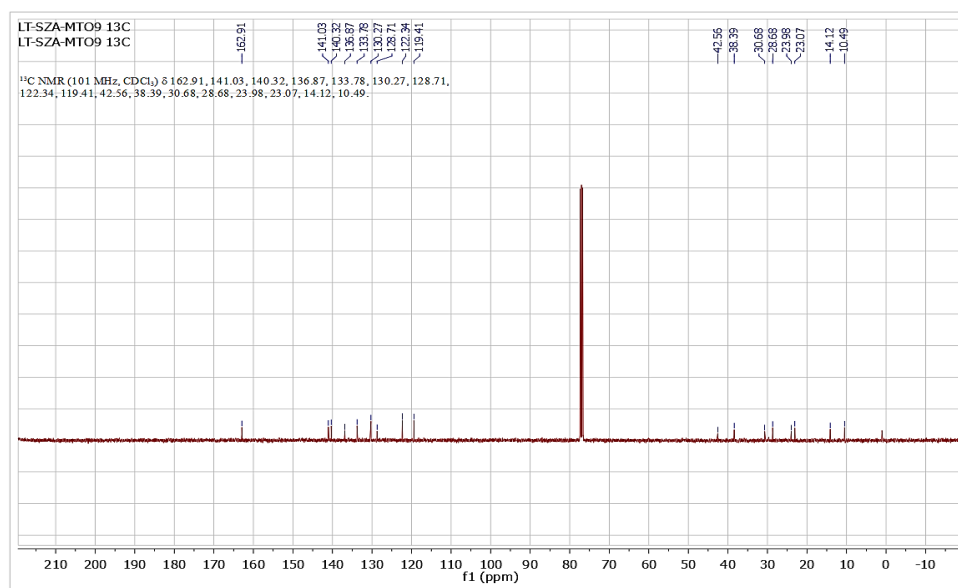
¹H NMR spectrum of 4,7-bis(5-bromothiopheno[3,2-*b*]thiophen-2-yl)-5,6-bis(octyloxy)benzo[*c*][1,2,5]oxadiazole



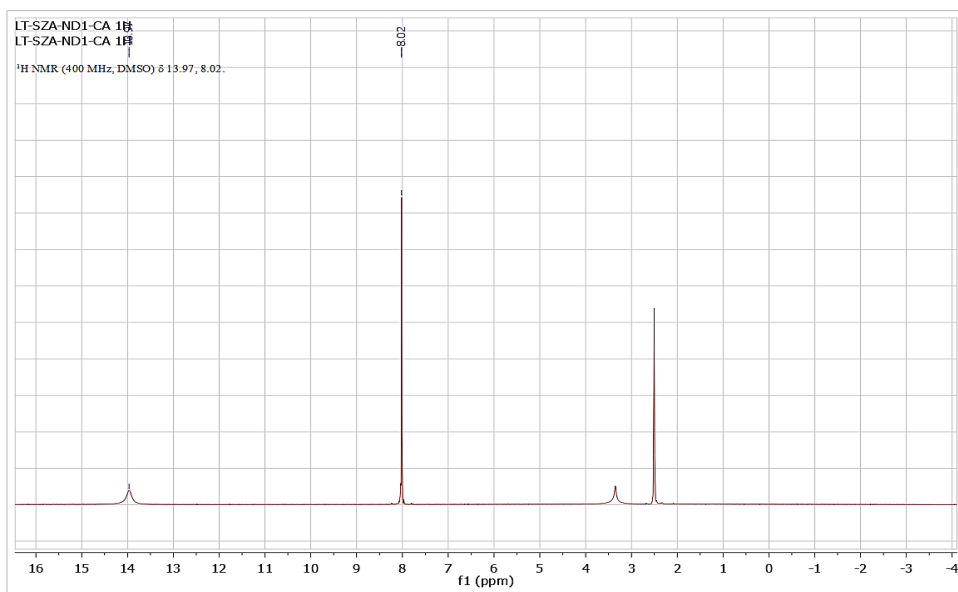
¹³C NMR spectrum of 4,7-bis(5-bromothiopheno[3,2-*b*]thiophen-2-yl)-5,6-bis(octyloxy)benzo[*c*][1,2,5]oxadiazole



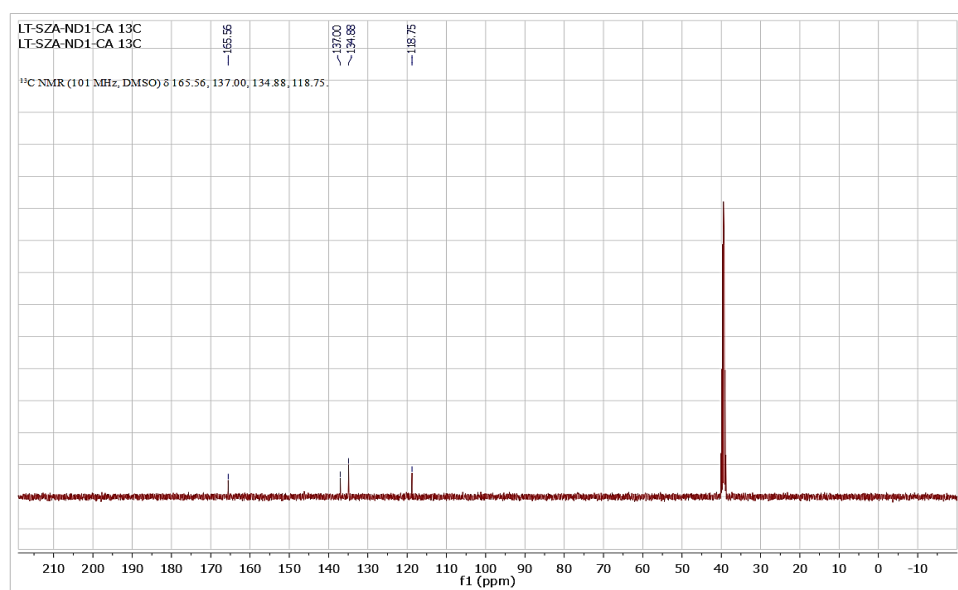
¹H NMR spectrum of 5-(2-ethylhexyl)-1,3-bis(thieno[3,2-*b*]thiophen-2-yl)-4H-thieno[3,4-*c*]pyrrole-4,6(5H)-dione (M9)



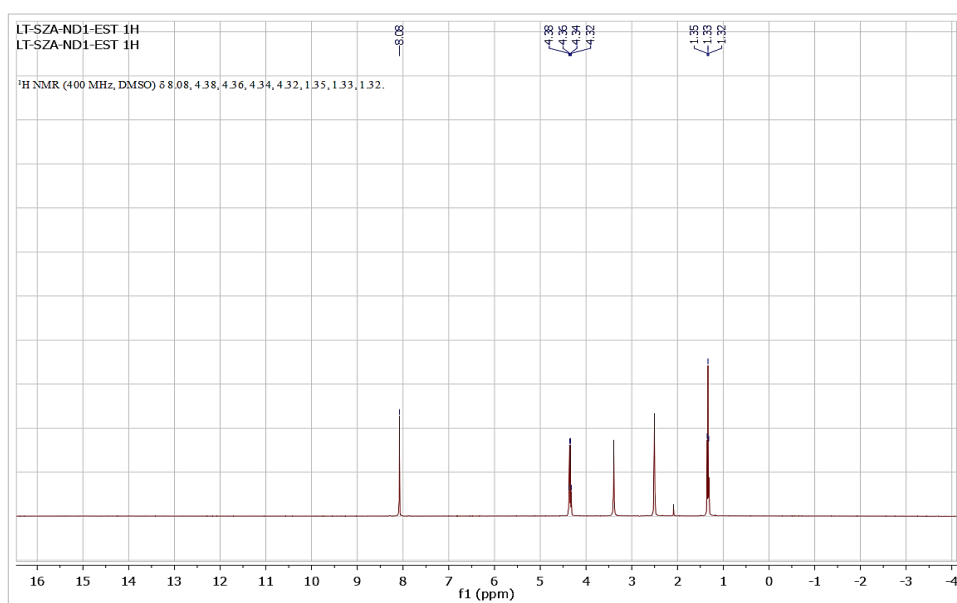
¹³C NMR spectrum of 5-(2-ethylhexyl)-1,3-bis(thieno[3,2-*b*]thiophen-2-yl)-4H-thieno[3,4-*c*]pyrrole-4,6(5H)-dione (M9)



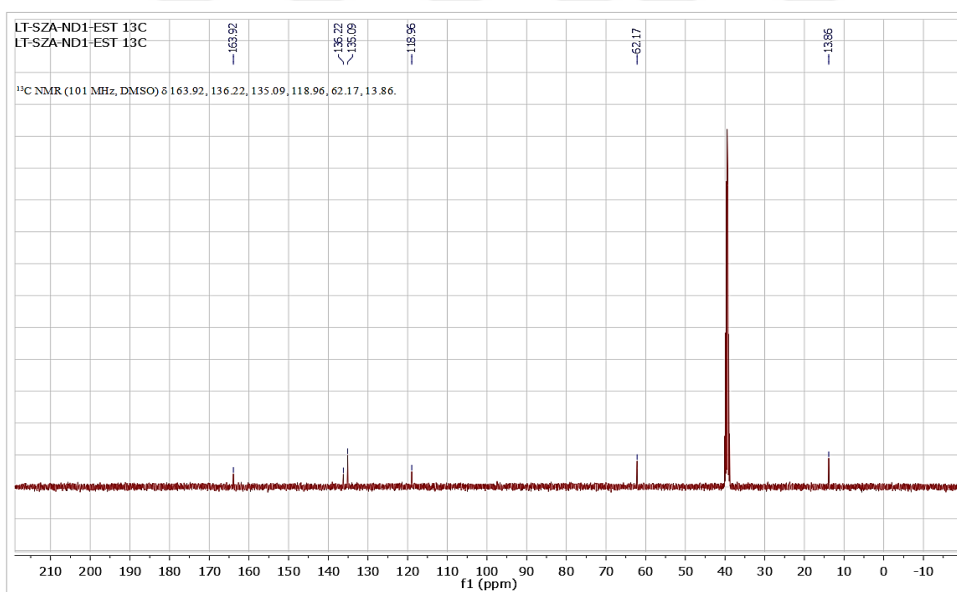
¹H NMR spectrum of 2,5-dibromoterephthalic acid (ND1-CA)



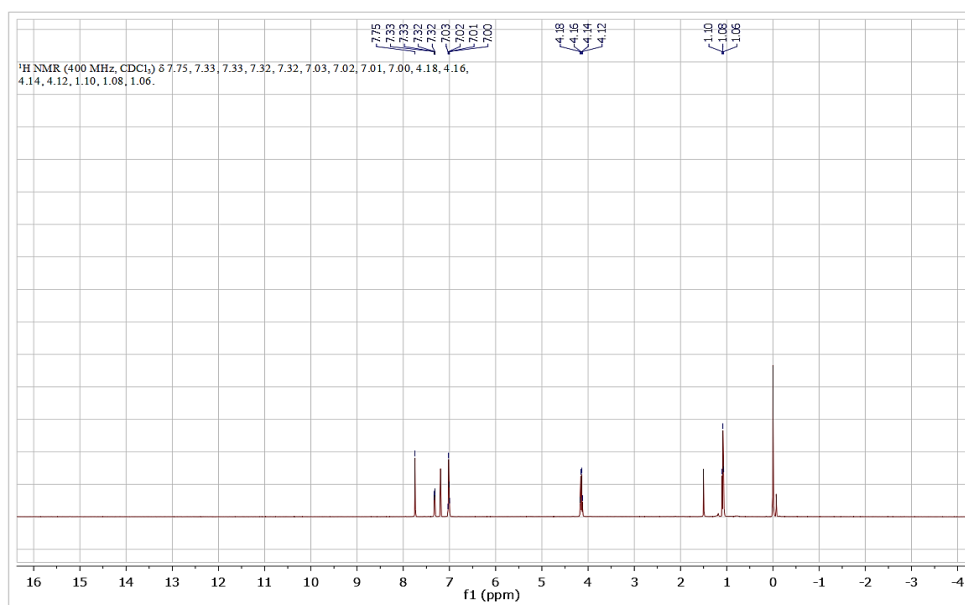
¹³C NMR spectrum of 2,5-dibromoterephthalic acid (ND1-CA)

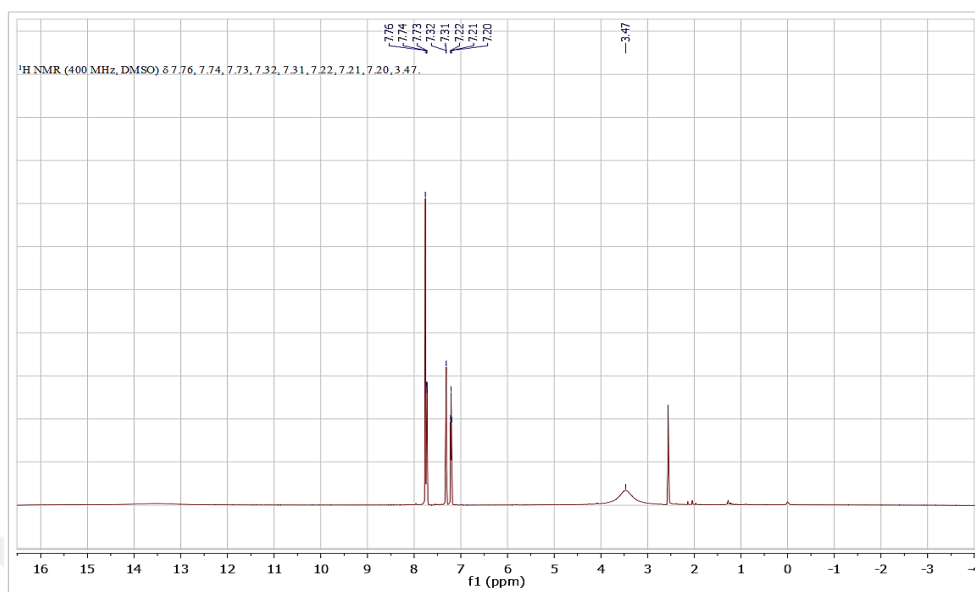


¹H NMR spectrum of diethyl 2,5-dibromoterephthalate (ND1-Est)

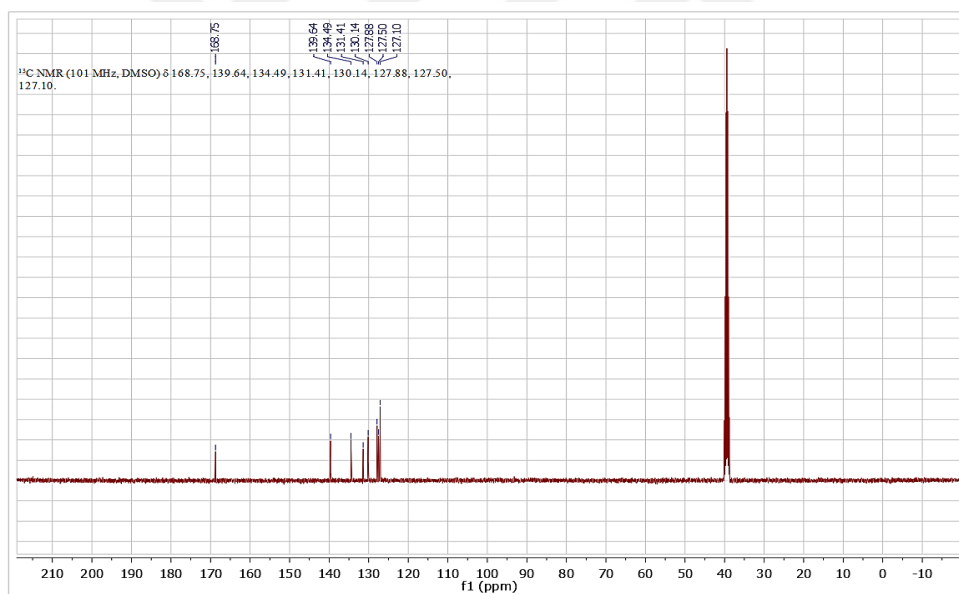


¹³C NMR spectrum of diethyl 2,5-dibromoterephthalate (ND1-Est)

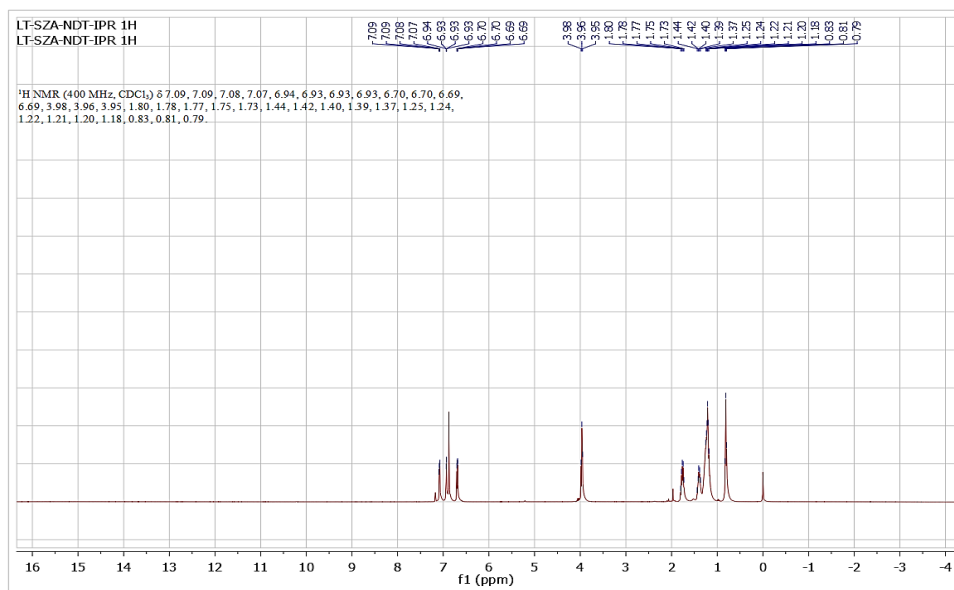




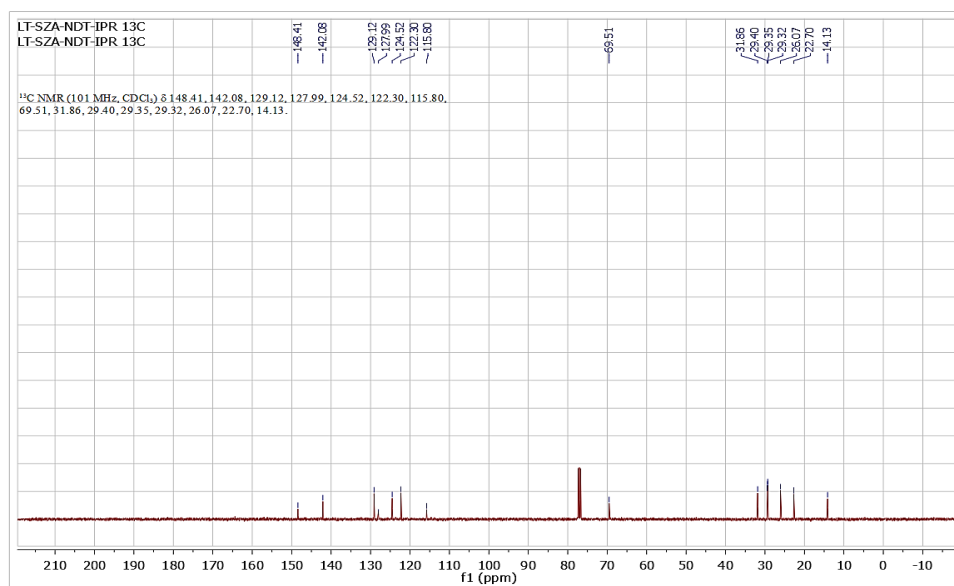
¹H NMR spectrum of 2,5-di(thiophen-2-yl)terephthalic acid (ND1-Th-CA)



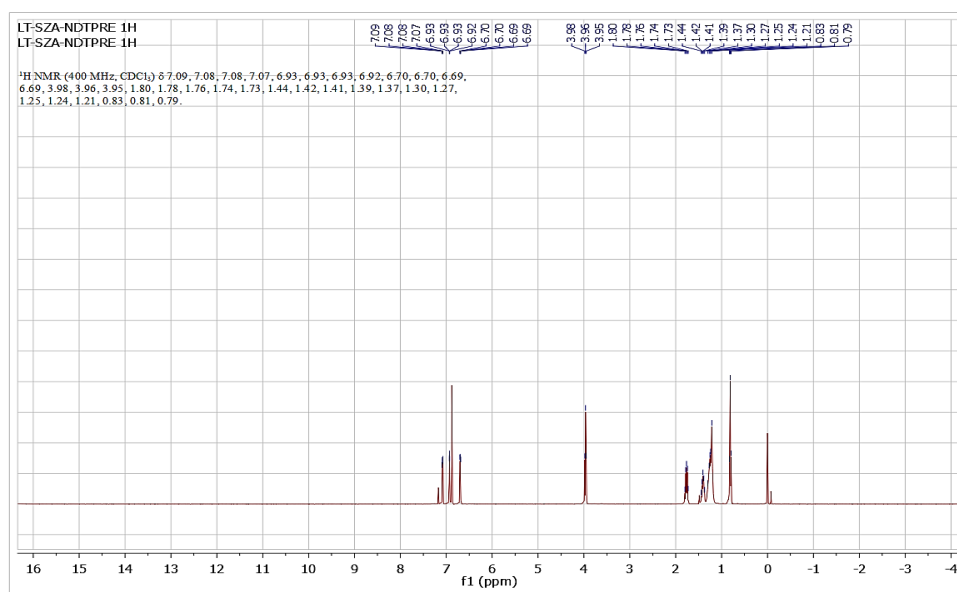
¹³C NMR spectrum of 2,5-di(thiophen-2-yl)terephthalic acid (ND1-Th-CA)



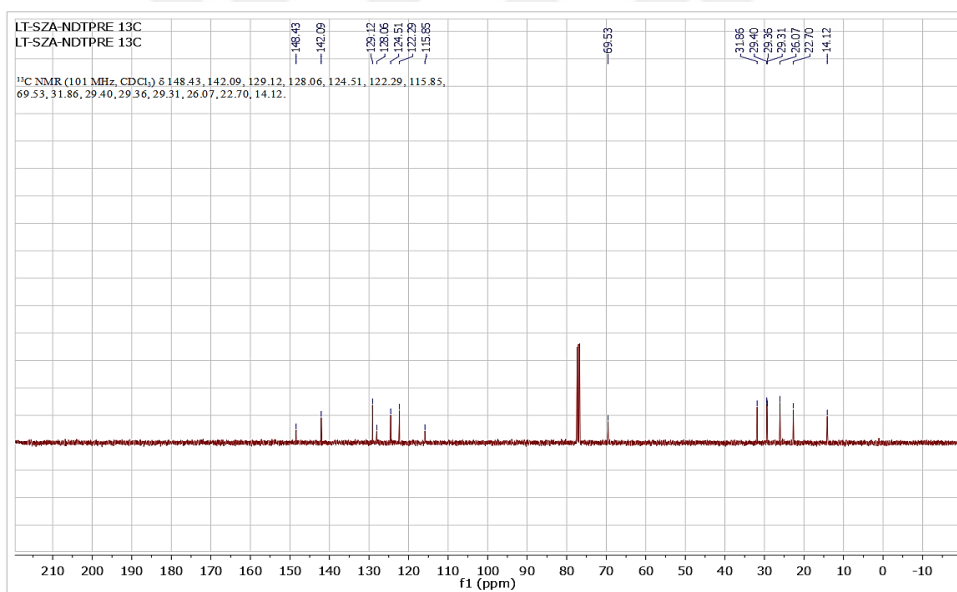
¹H NMR spectrum of 5,6-bis(octyloxy)naphtho[2,1-*b*:3,4-*b'*]dithiophene (NDT)



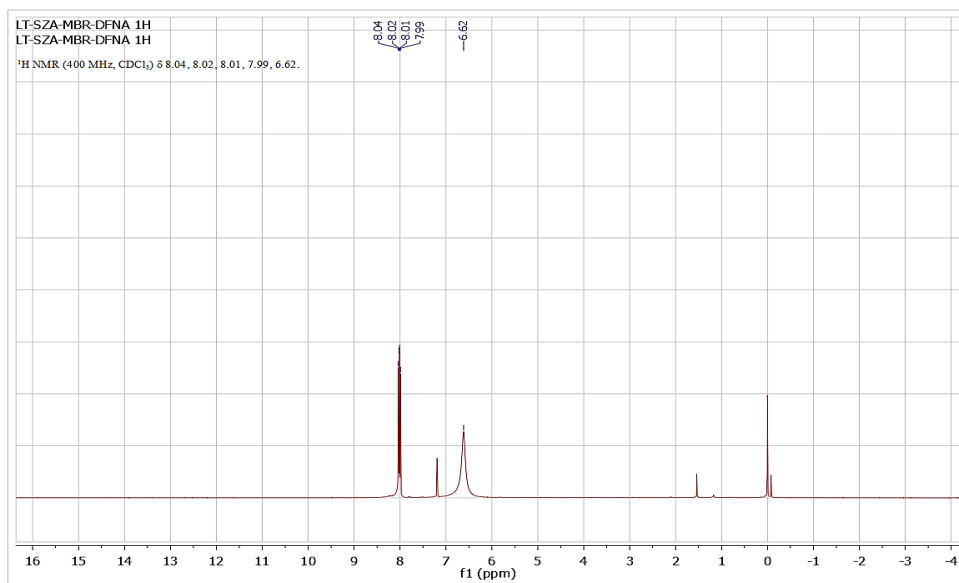
¹³C NMR spectrum of 5,6-bis(octyloxy)naphtho[2,1-*b*:3,4-*b'*]dithiophene (NDT)



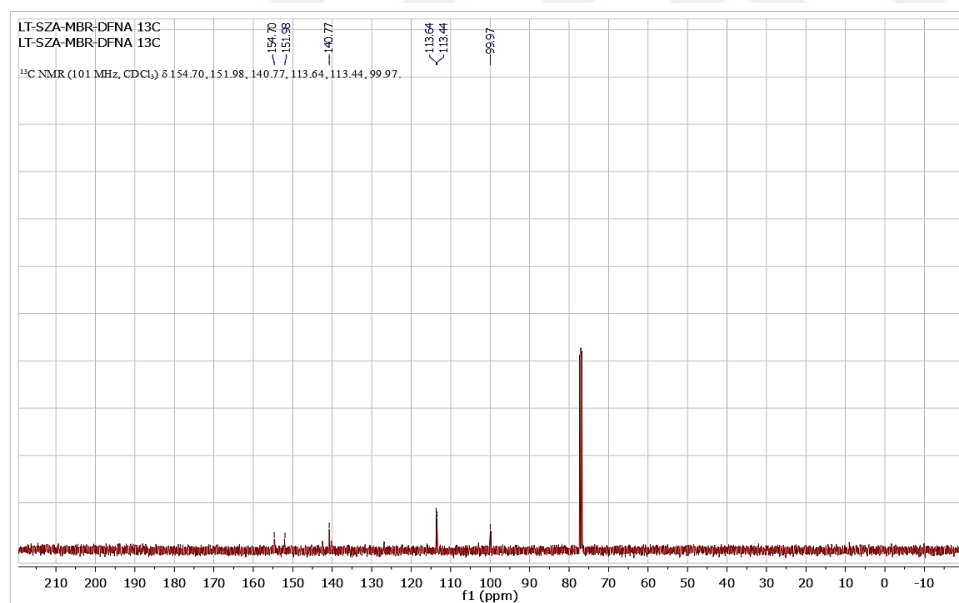
¹H NMR spectrum of 3,3'-(4,5-bis(octyloxy)-1,2-phenylene)dithiophene (NDT-Pre)



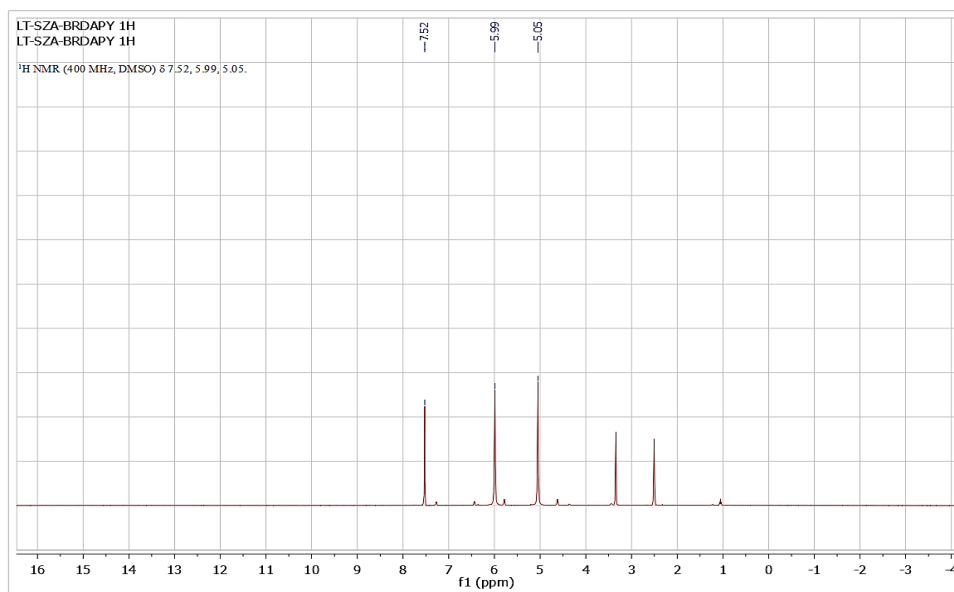
¹³C NMR spectrum of 3,3'-(4,5-bis(octyloxy)-1,2-phenylene)dithiophene (NDT-Pre)



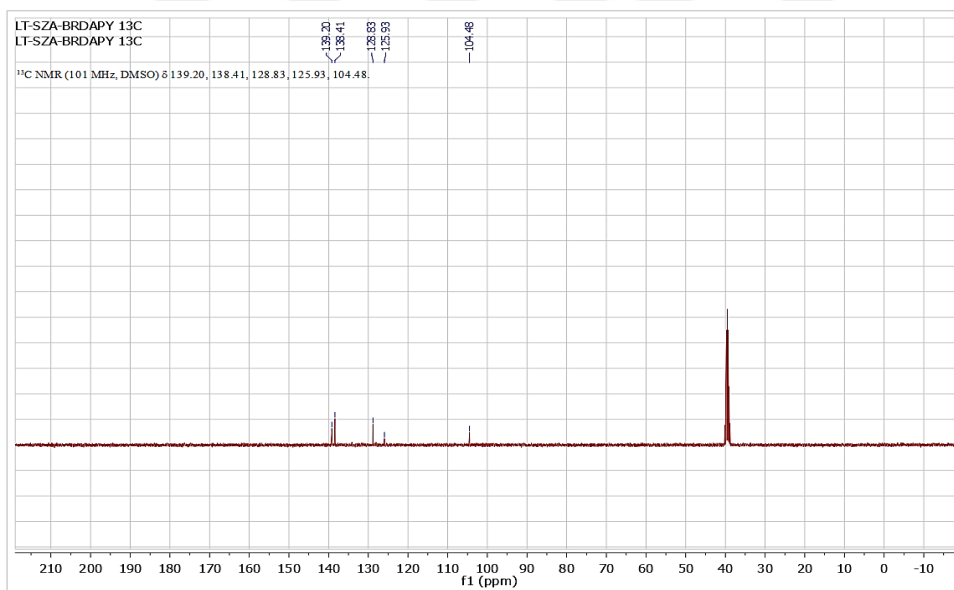
¹H NMR spectrum of 2-bromo-3,4-difluoro-6-nitroaniline (MBR-DFNA)



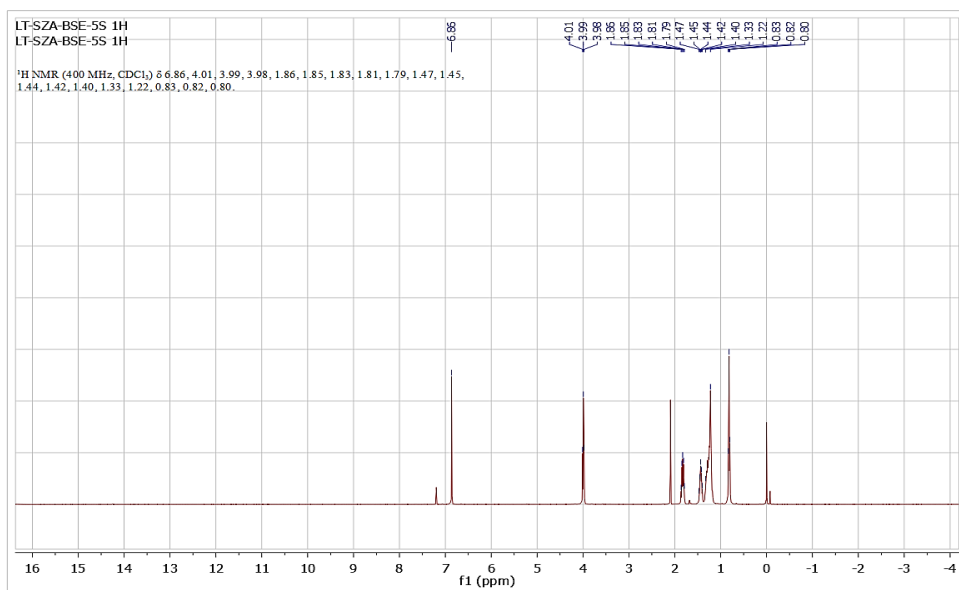
¹³C NMR spectrum of 2-bromo-3,4-difluoro-6-nitroaniline (MBR-DFNA)



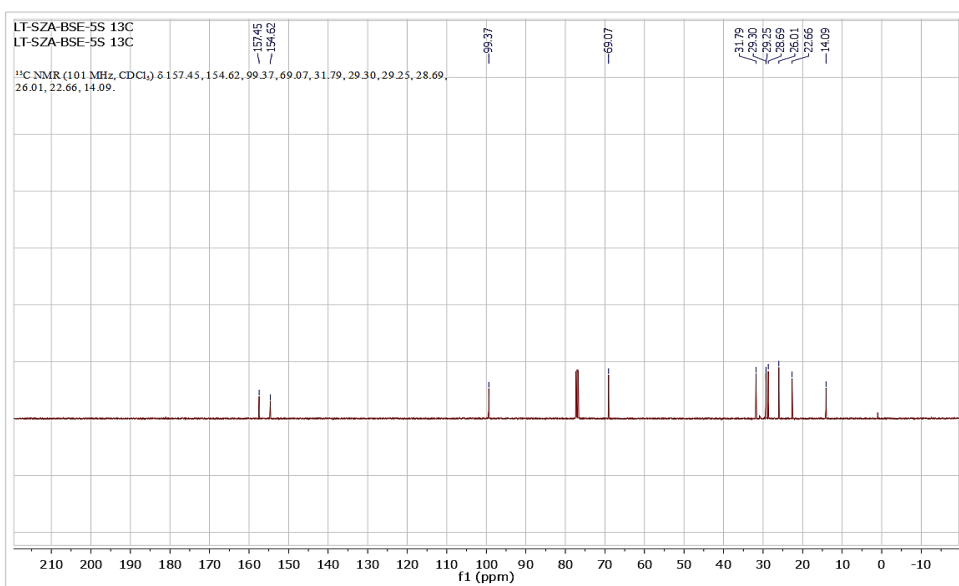
¹H NMR spectrum of 2,5-dibromopyridine-3,4-diamine



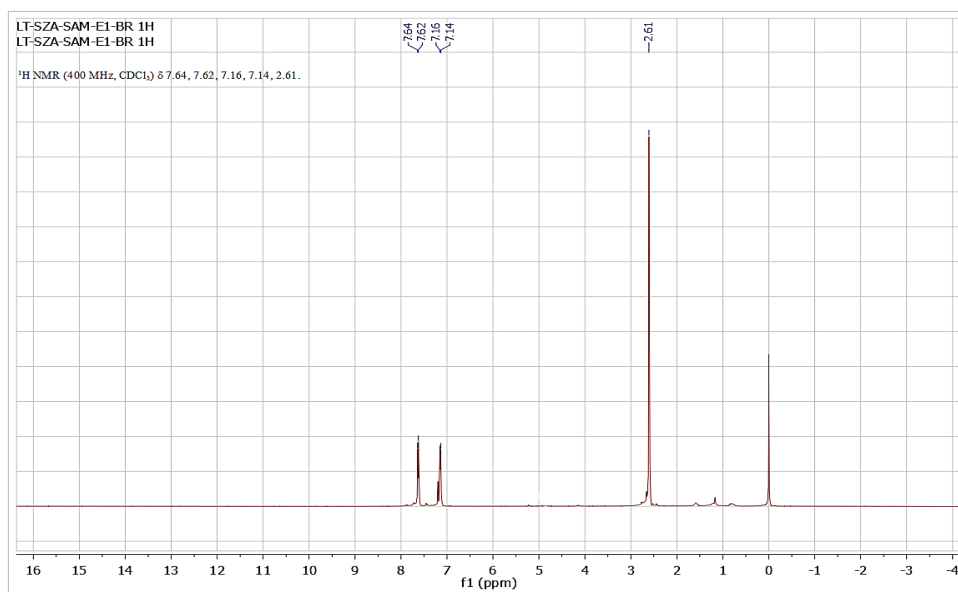
¹³C NMR spectrum of 2,5-dibromopyridine-3,4-diamine



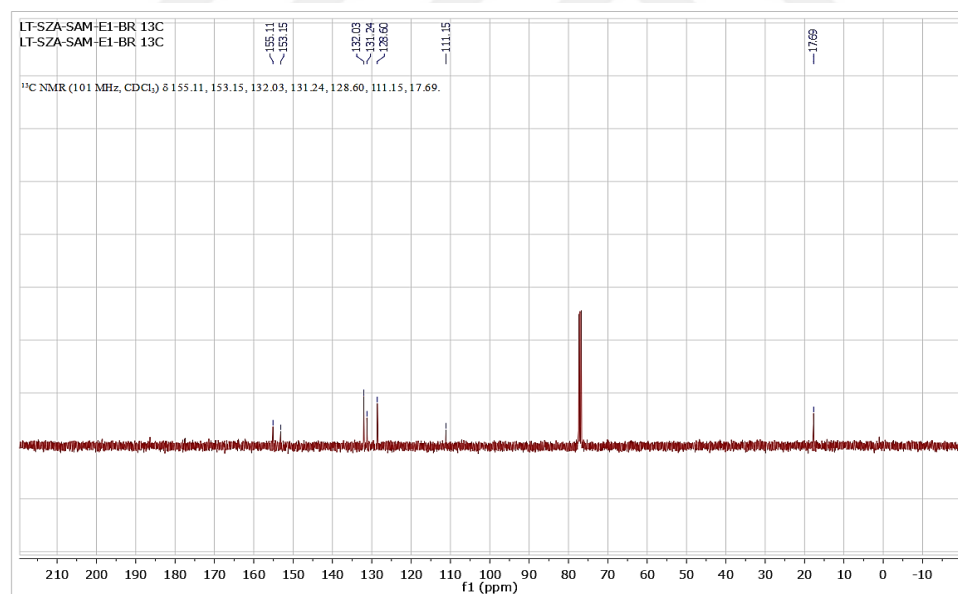
¹H NMR spectrum of 5,6-bis(octyloxy)benzo[c][1,2,5]selenadiazole (BSe)



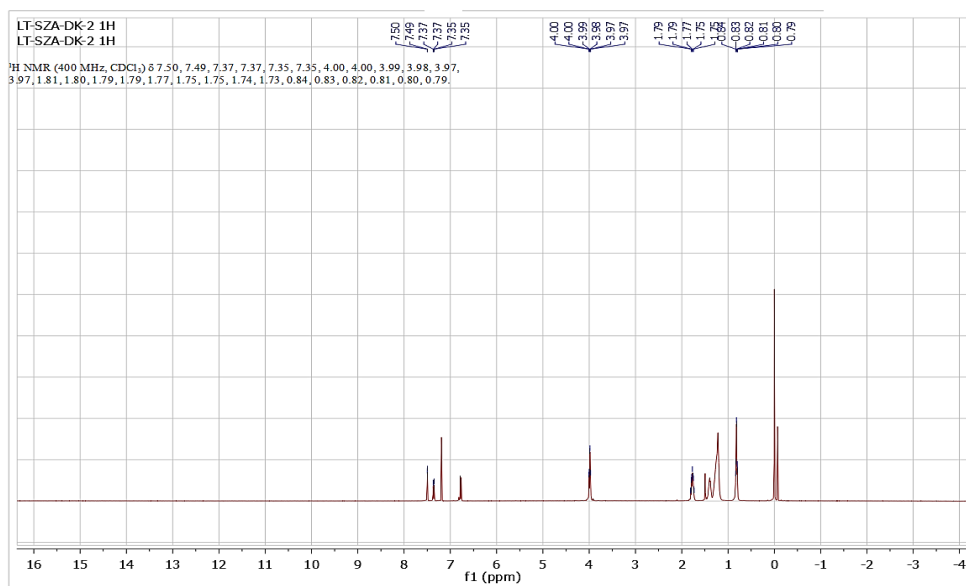
¹³C NMR spectrum of 5,6-bis(octyloxy)benzo[c][1,2,5]selenadiazole (BSe)



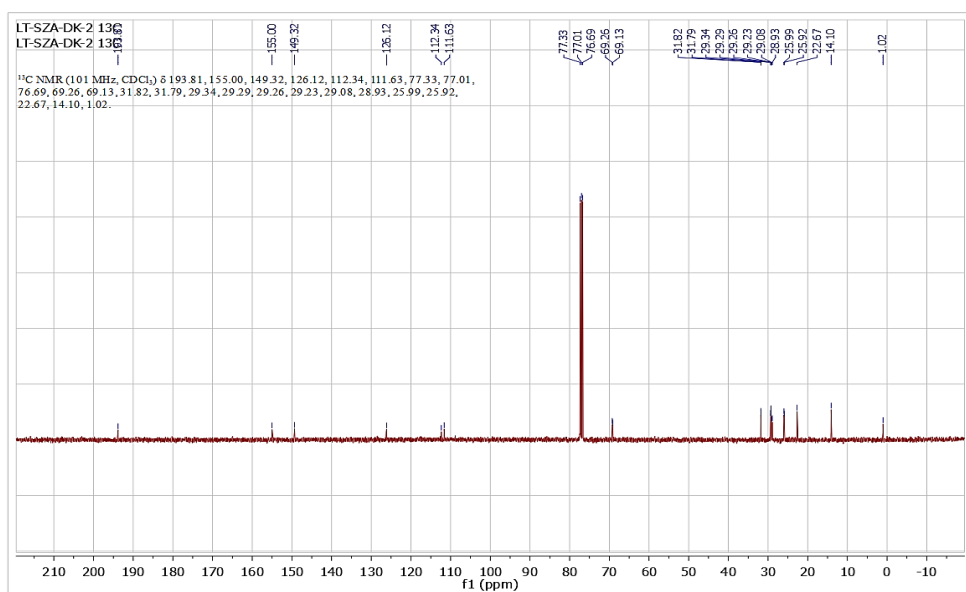
¹H NMR spectrum of 4-bromo-7-methylbenzo[c][1,2,5]thiadiazole (SAM-E1-Br)



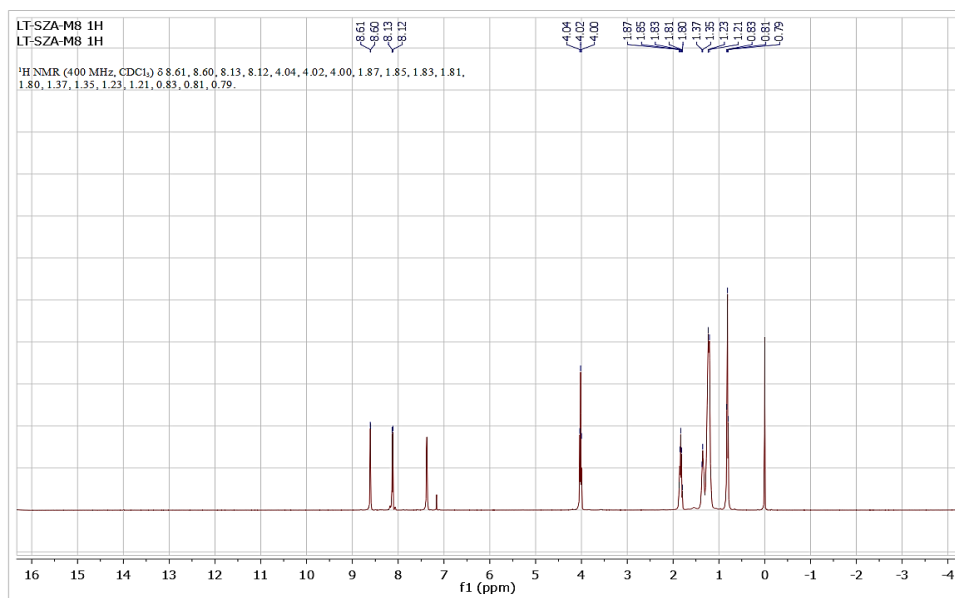
¹³C NMR spectrum of 4-bromo-7-methylbenzo[c][1,2,5]thiadiazole (SAM-E1-Br)



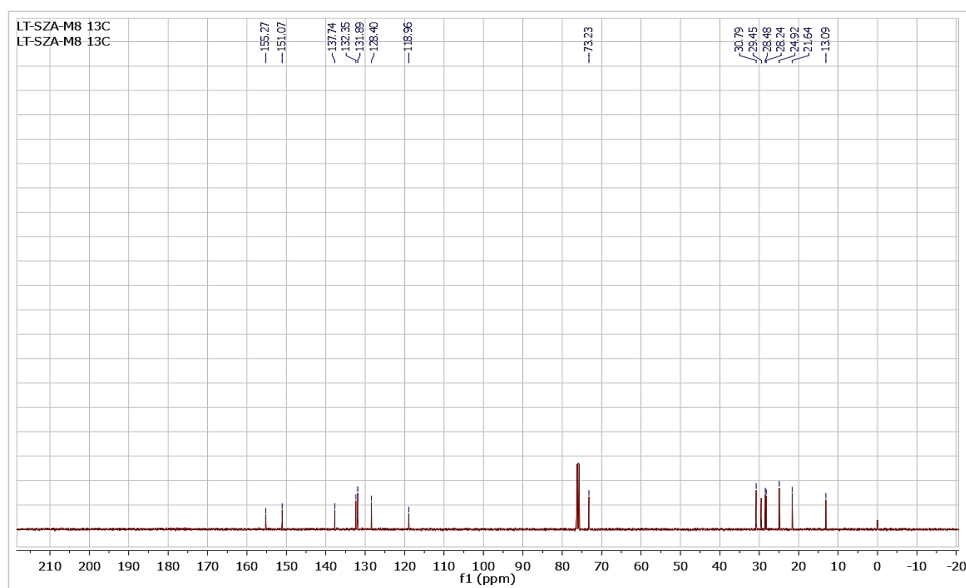
¹H NMR spectrum of 1,2-bis(3,4-bis(octyloxy)phenyl)ethane-1,2-dione



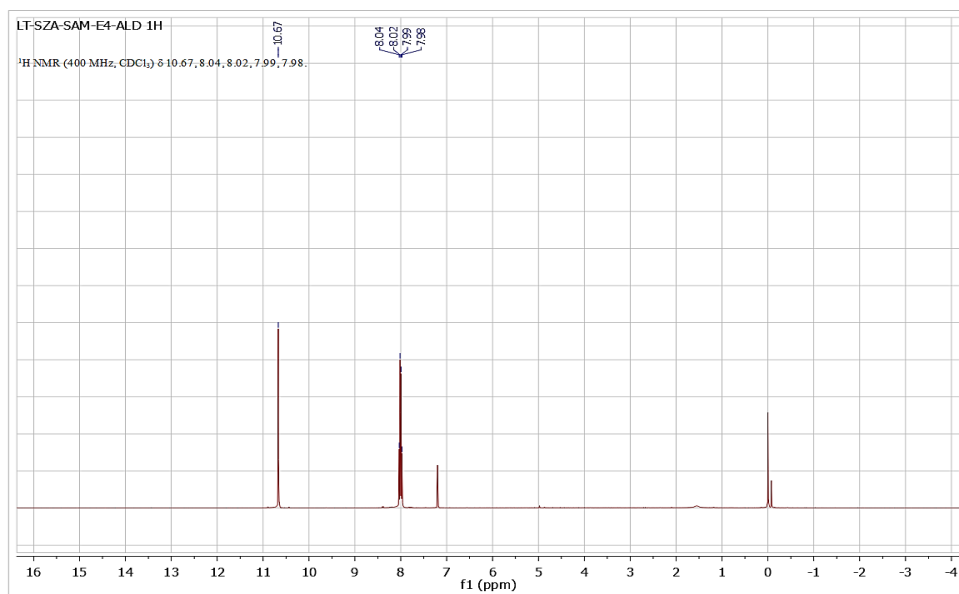
¹³C NMR spectrum of 1,2-bis(3,4-bis(octyloxy)phenyl)ethane-1,2-dione



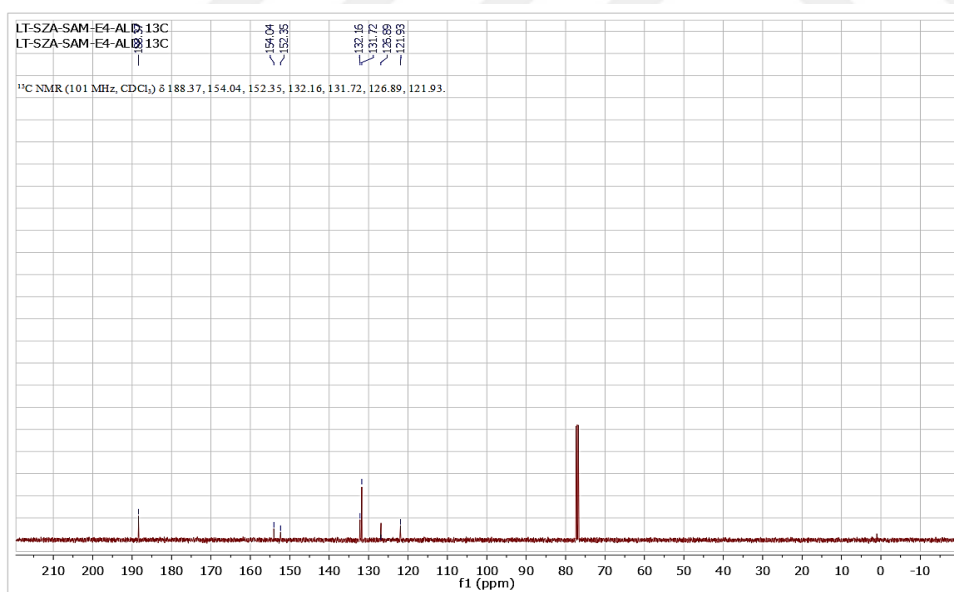
¹H NMR spectrum of 5,6-bis(octyloxy)-4,7-bis(thieno[3,2-b]thiophen-2-yl)benzo[c][1,2,5]selenadiazole (M8)



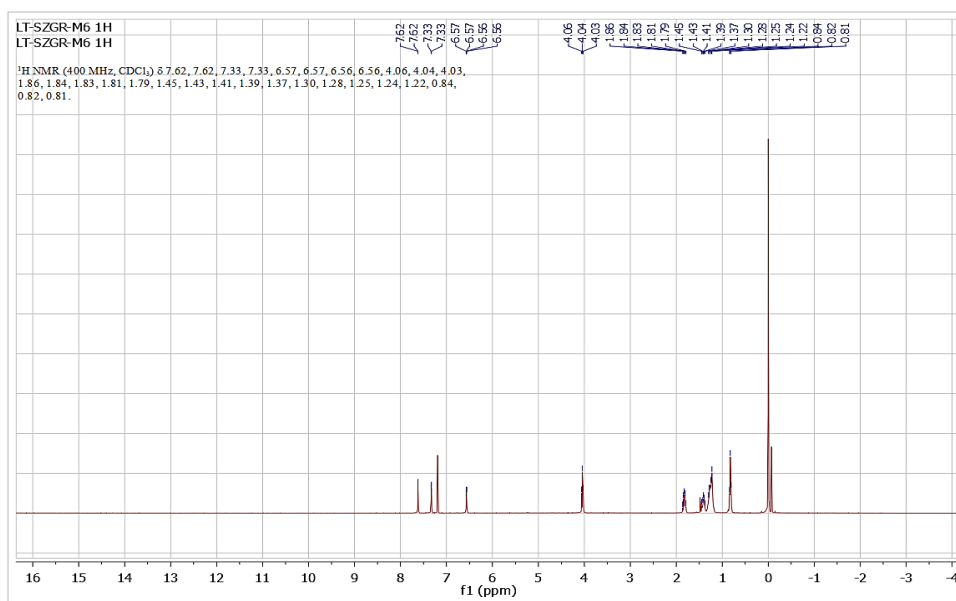
¹³C NMR spectrum of 5,6-bis(octyloxy)-4,7-bis(thieno[3,2-b]thiophen-2-yl)benzo[c][1,2,5]selenadiazole (M8)



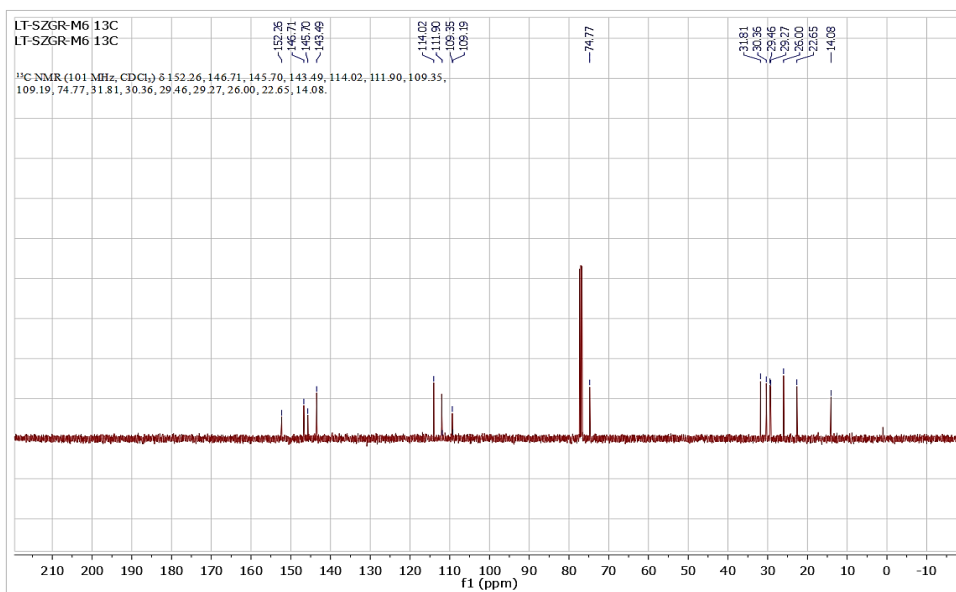
¹H NMR spectrum of 7-bromobenzo[c][1,2,5]thiadiazole-4-carbaldehyde (SAM-E4-Ald)



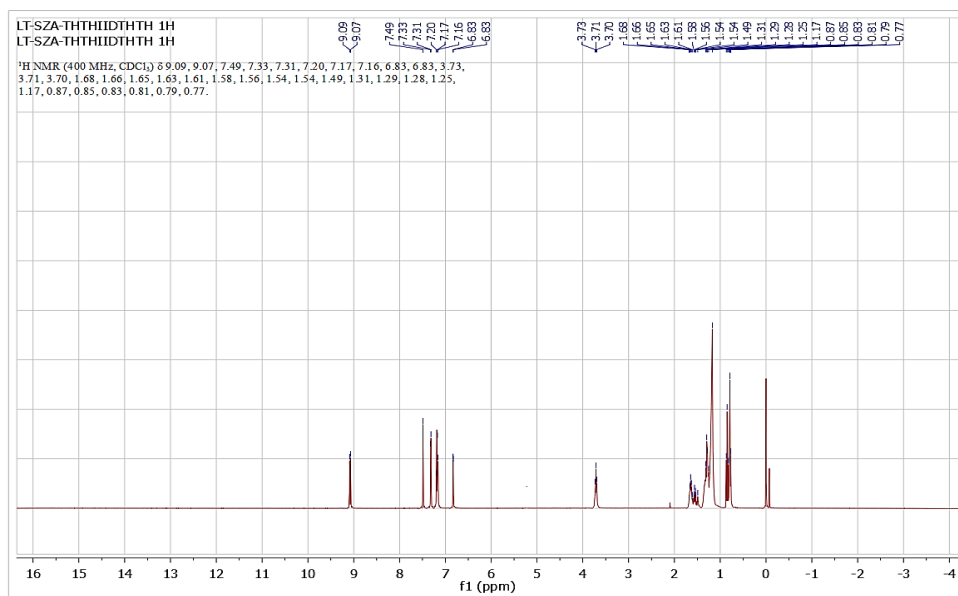
¹³C NMR spectrum of 7-bromobenzo[c][1,2,5]thiadiazole-4-carbaldehyde (SAM-E4-Ald)



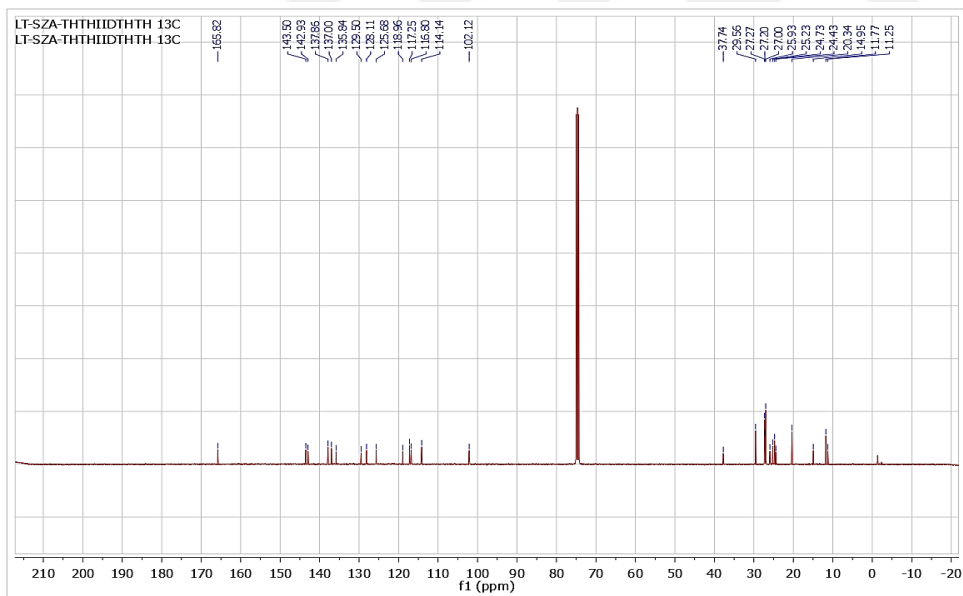
¹H NMR spectrum of 4,7-di(furan-2-yl)-5,6-bis(octyloxy)benzo[c][1,2,5]oxadiazole



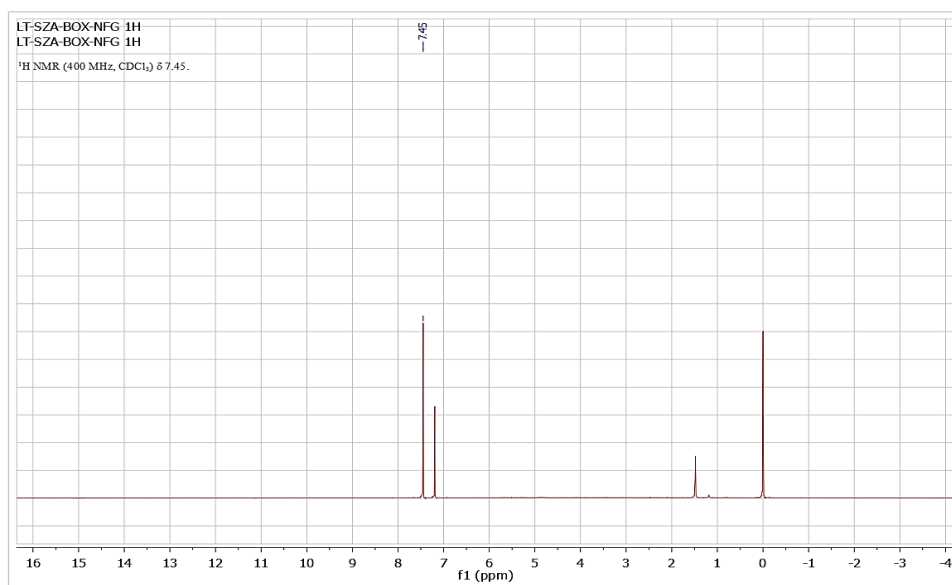
¹³C NMR spectrum of 4,7-di(furan-2-yl)-5,6-bis(octyloxy)benzo[c][1,2,5]oxadiazole



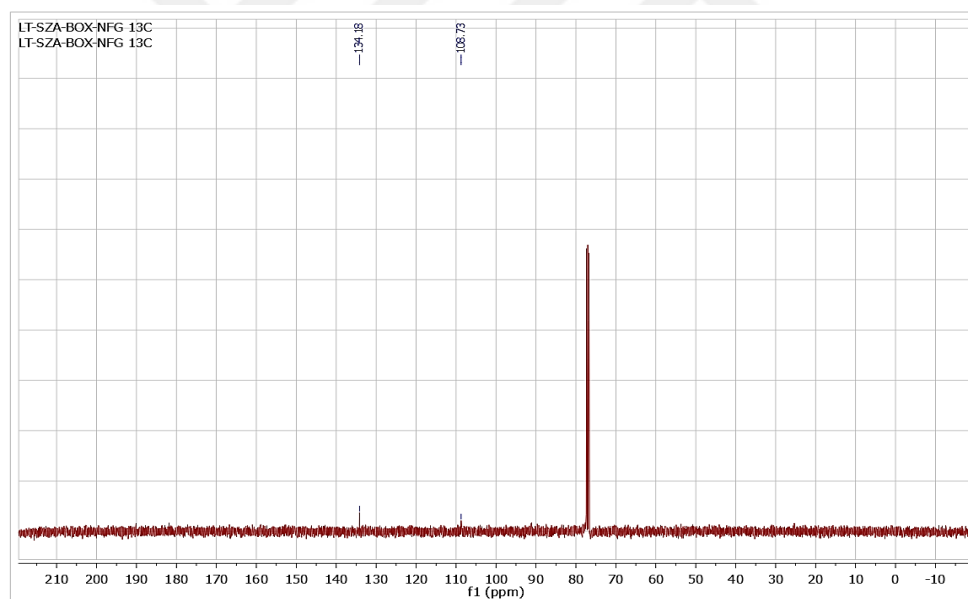
¹H NMR spectrum of (E)-6,6'-bis(thieno[3,2-b]thiophen-2-yl)-1,1'-diundecyl-[3,3'-biindolinylidene]-2,2'-dione (M10)



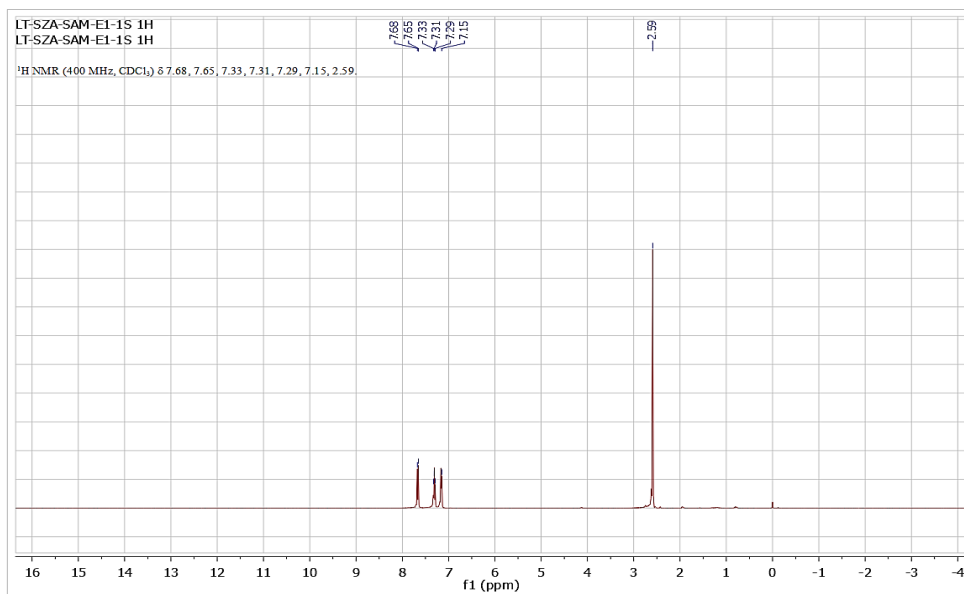
¹³C NMR spectrum of (E)-6,6'-bis(thieno[3,2-b]thiophen-2-yl)-1,1'-diundecyl-[3,3'-biindolinylidene]-2,2'-dione (M10)



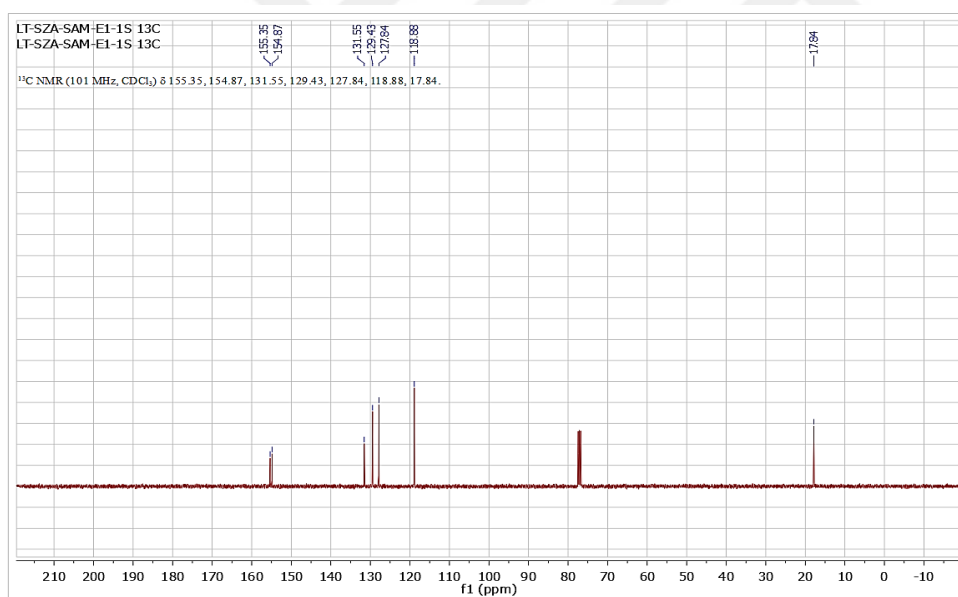
¹H NMR spectrum of 4,7-dibromobenzo[c][1,2,5]oxadiazole (BOx-NFG)



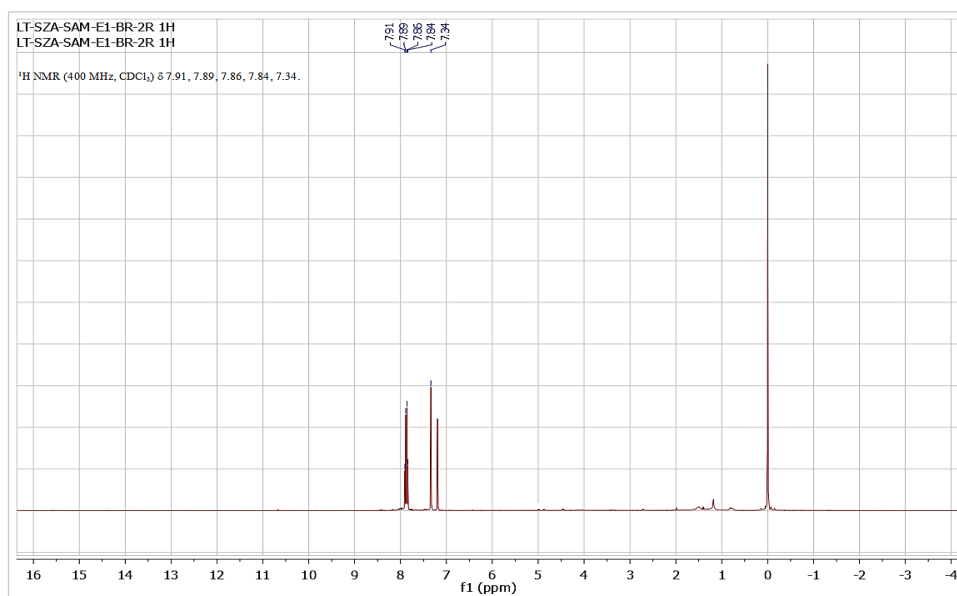
¹³C NMR spectrum of 4,7-dibromobenzo[c][1,2,5]oxadiazole (BOx-NFG)



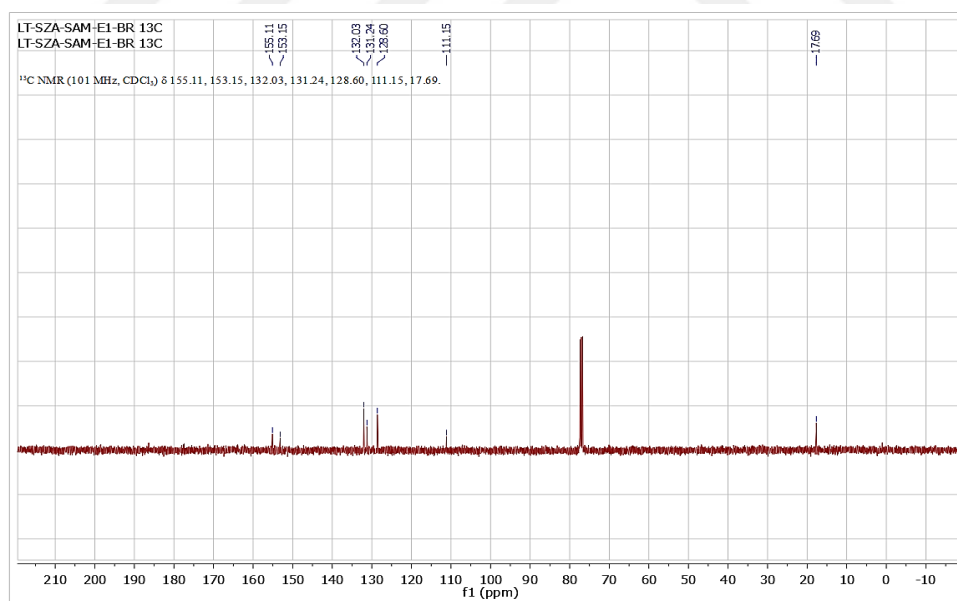
¹H NMR spectrum of 4-methylbenzo[c][1,2,5]thiadiazole (SAM-E1)



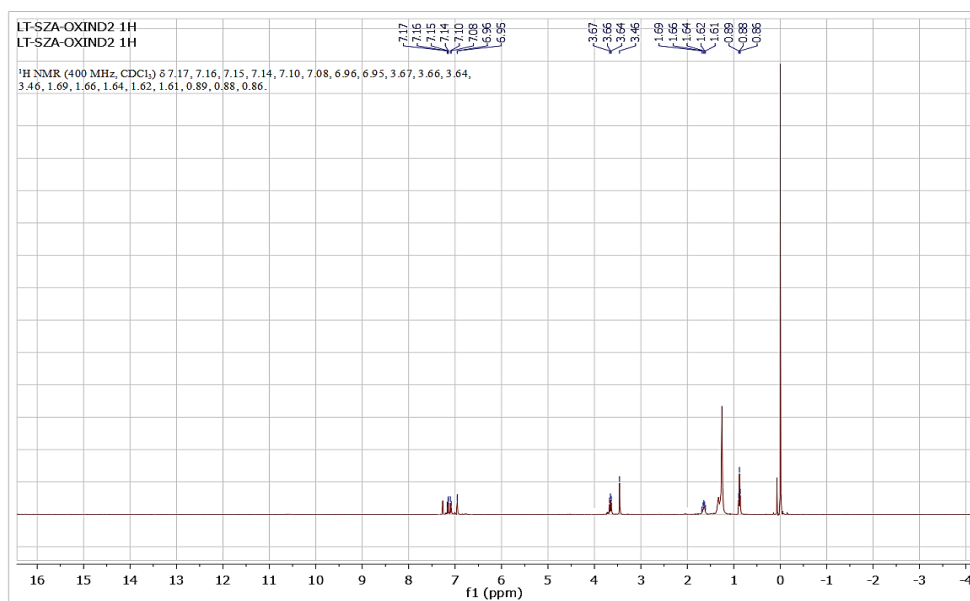
¹³C NMR spectrum of 4-methylbenzo[c][1,2,5]thiadiazole (SAM-E1)



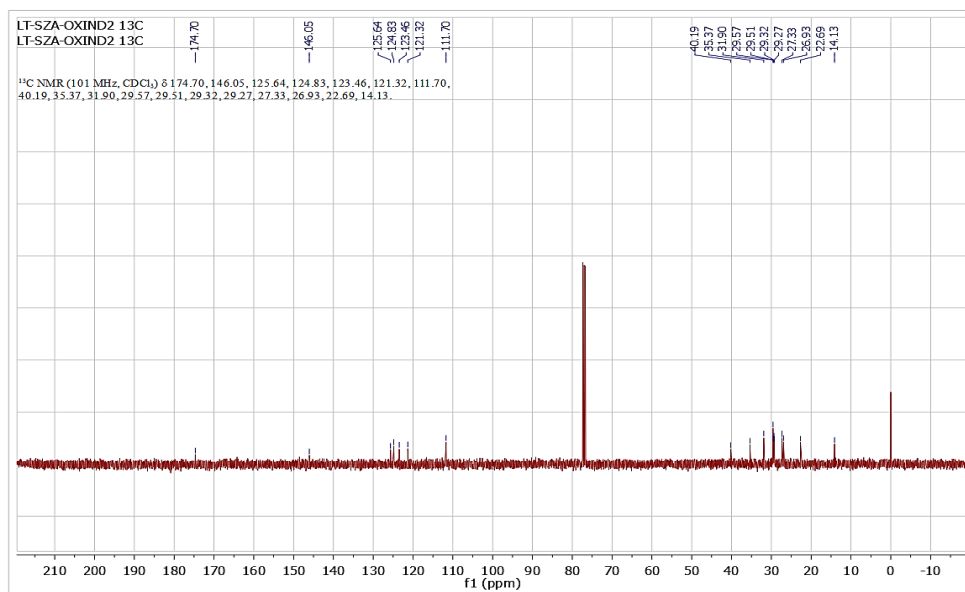
¹H NMR spectrum of 4-bromo-7-dibromomethyl-2,1,3-benzothiadiazole (SAM-E1-Br-2R)



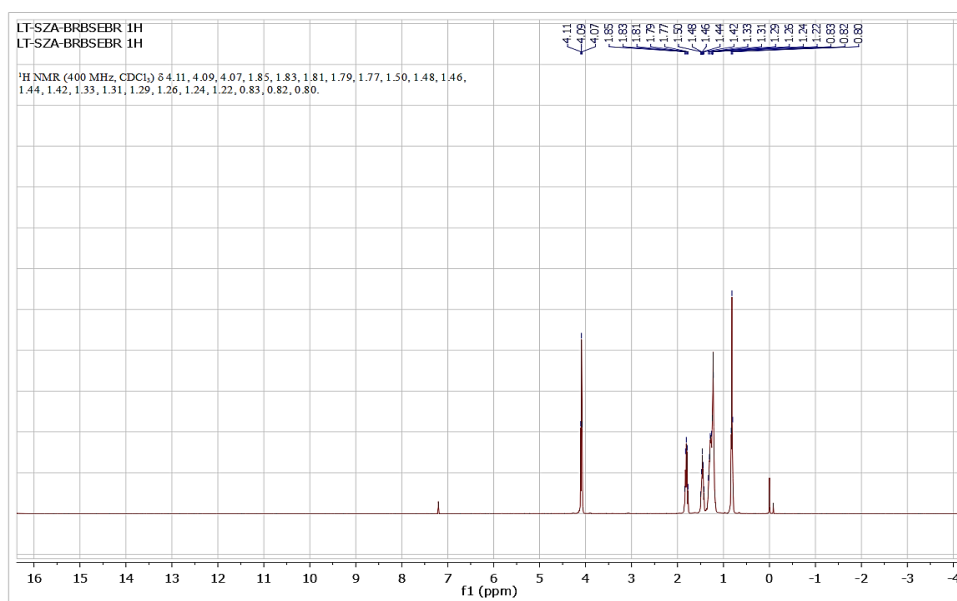
¹³C NMR spectrum of 4-bromo-7-dibromomethyl-2,1,3-benzothiadiazole (SAM-E1-Br-2R)



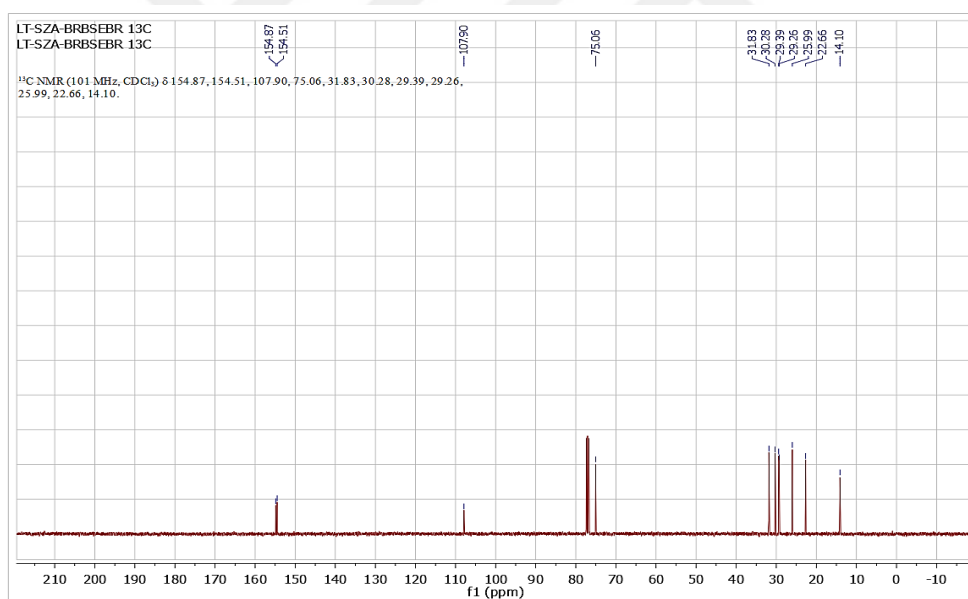
¹H NMR spectrum of 6-bromo-1-undecylindolin-2-one (oxindole)



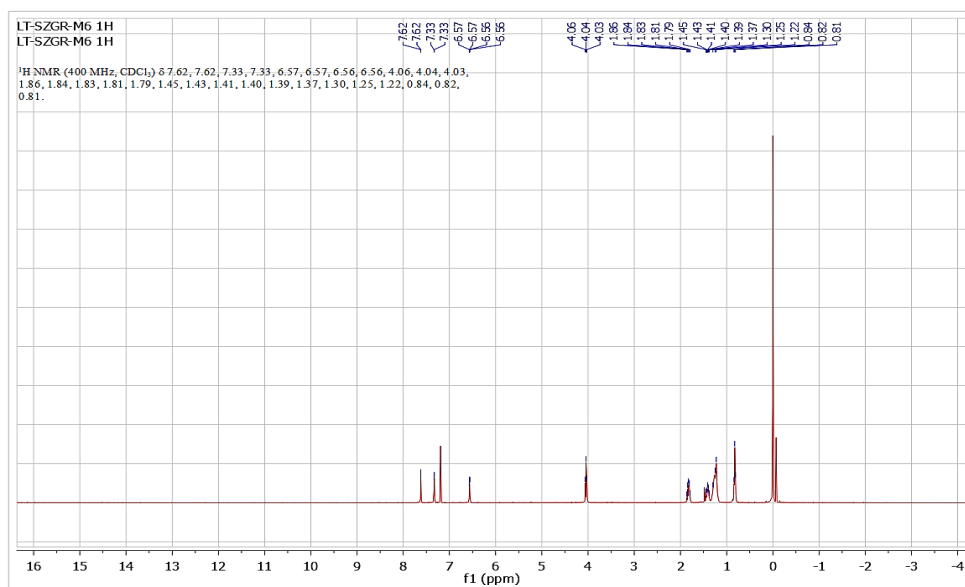
¹³C NMR spectrum of 6-bromo-1-undecylindolin-2-one (oxindole)



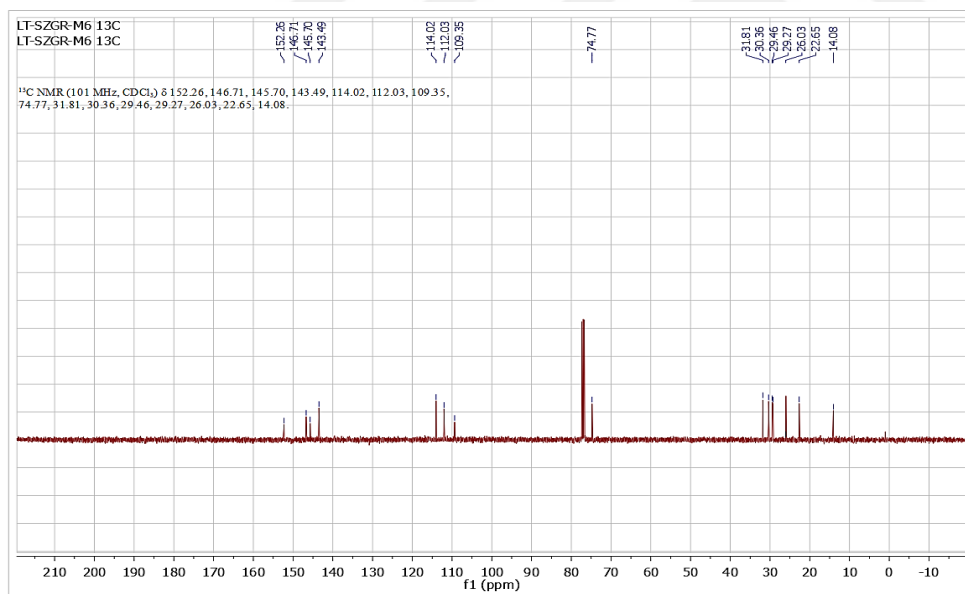
¹H NMR spectrum of 4,7-dibromo-5,6-bis(octyloxy)benzo[c][1,2,5]selenadiazole



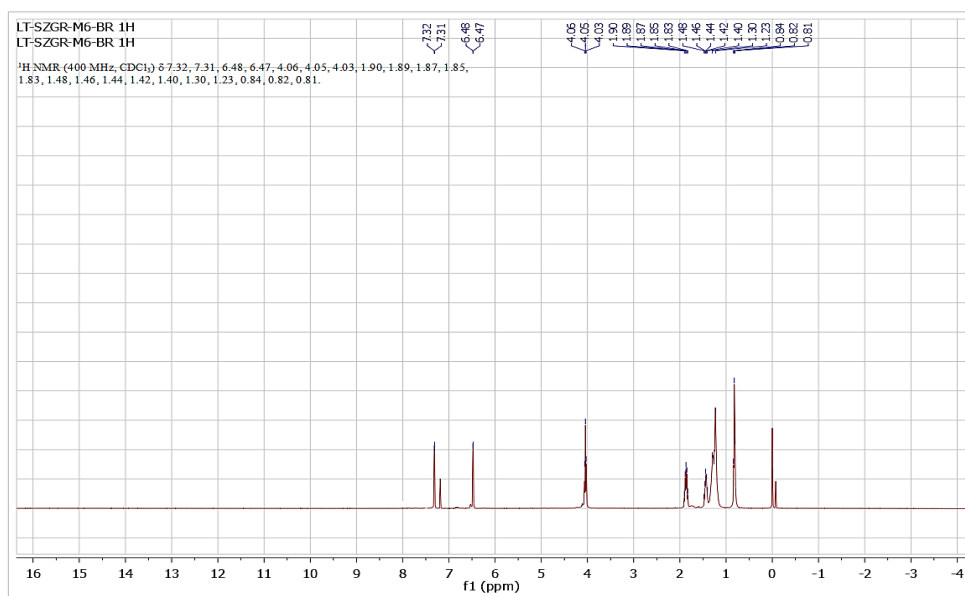
¹³C NMR spectrum of 4,7-dibromo-5,6-bis(octyloxy)benzo[c][1,2,5]selenadiazole



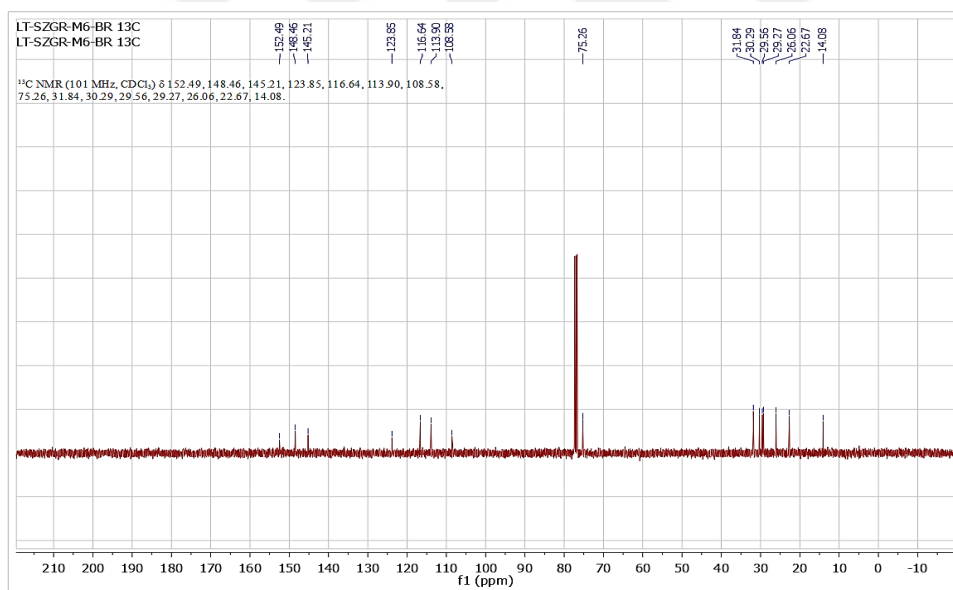
¹H NMR spectrum of 4,7-di(furan-2-yl)-5,6-bis(octyloxy)benzo[c][1,2,5]oxadiazole (M6)



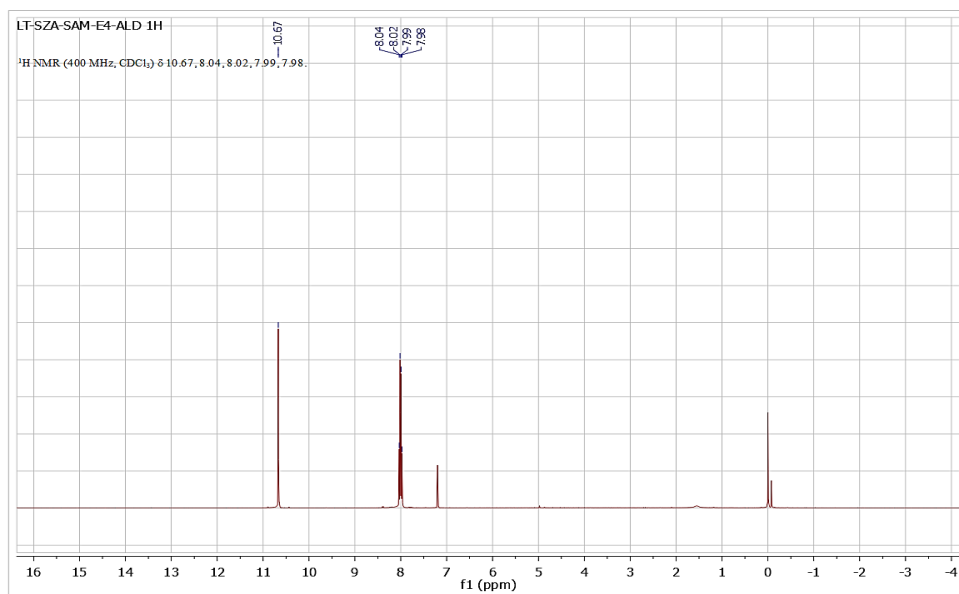
¹³C NMR spectrum of 4,7-di(furan-2-yl)-5,6-bis(octyloxy)benzo[c][1,2,5]oxadiazole (M6)



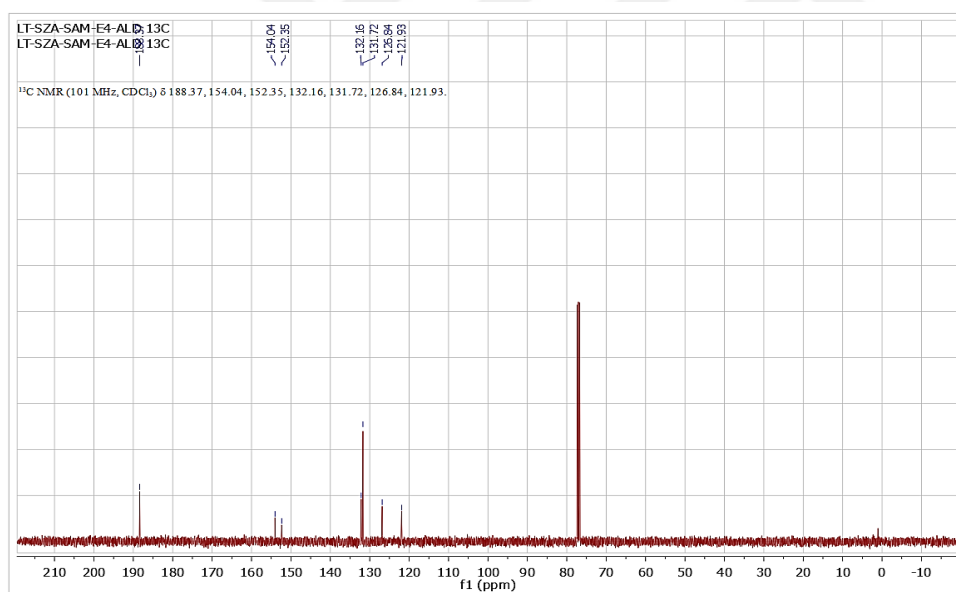
¹H NMR spectrum of 4,7-bis(5-bromofuran-2-yl)-5,6-bis(octyloxy)benzo[c][1,2,5]oxadiazole (M6-Br)



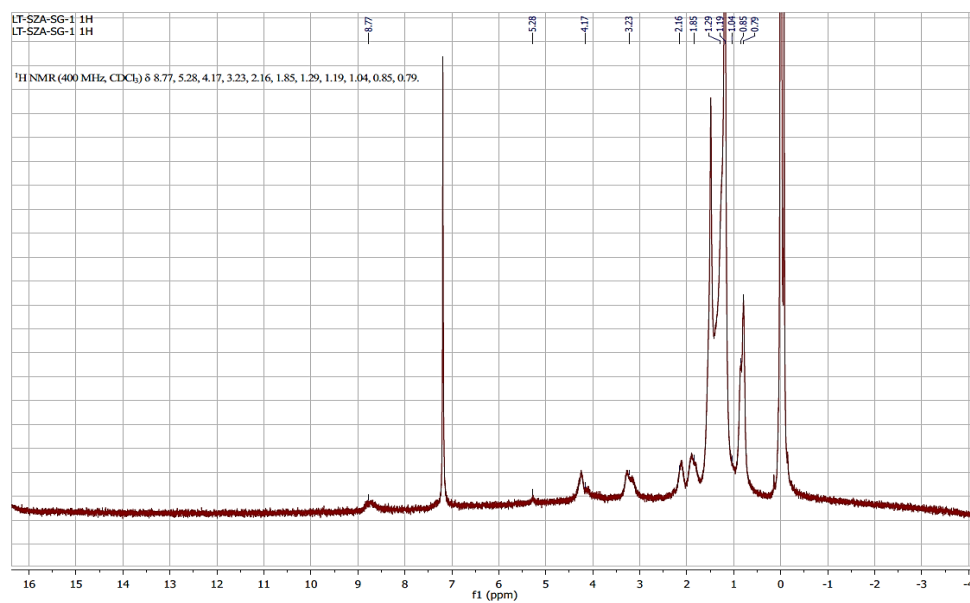
¹³C NMR spectrum of 4,7-bis(5-bromofuran-2-yl)-5,6-bis(octyloxy)benzo[c][1,2,5]oxadiazole (M6-Br)



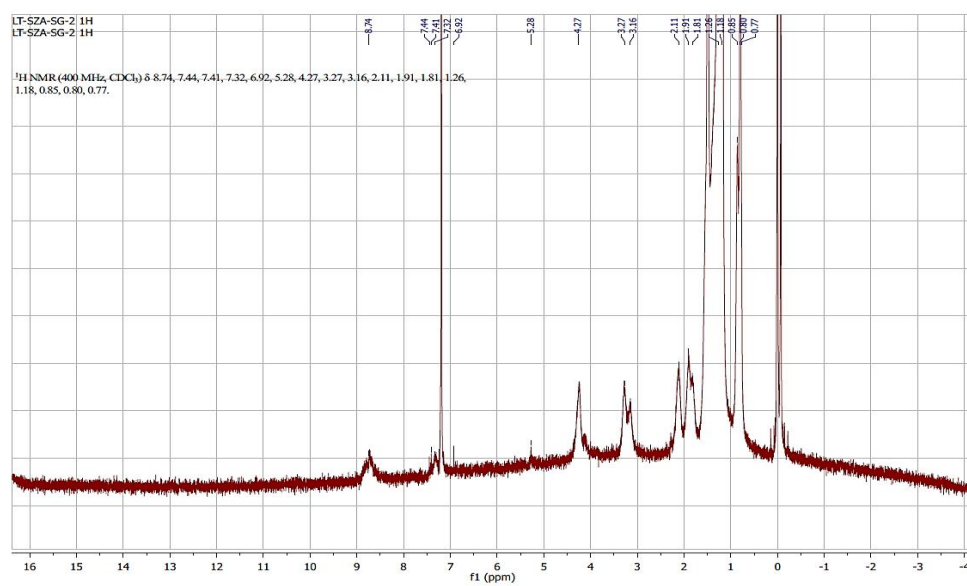
¹H NMR spectrum of SAM-E4-Br



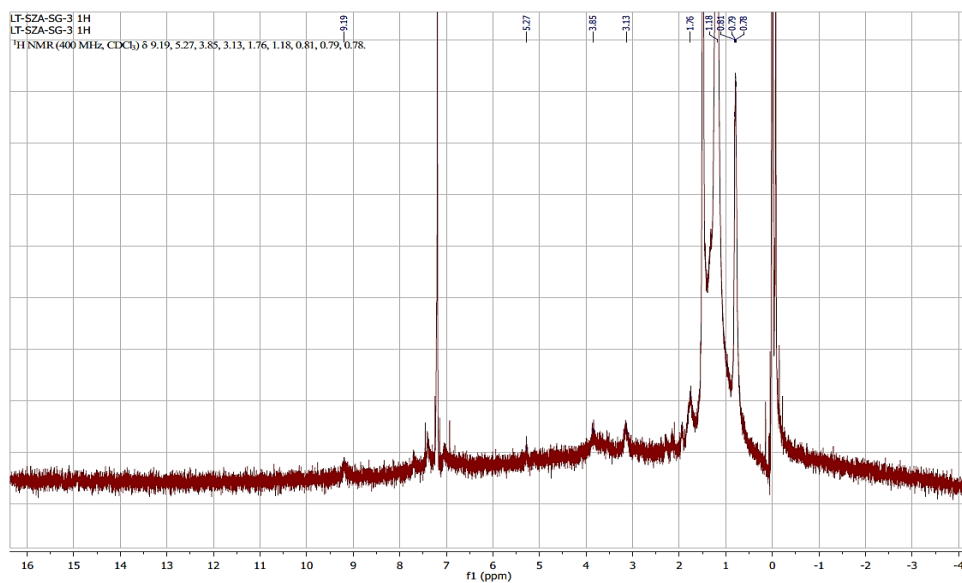
¹³C NMR spectrum of SAM-E4-Br



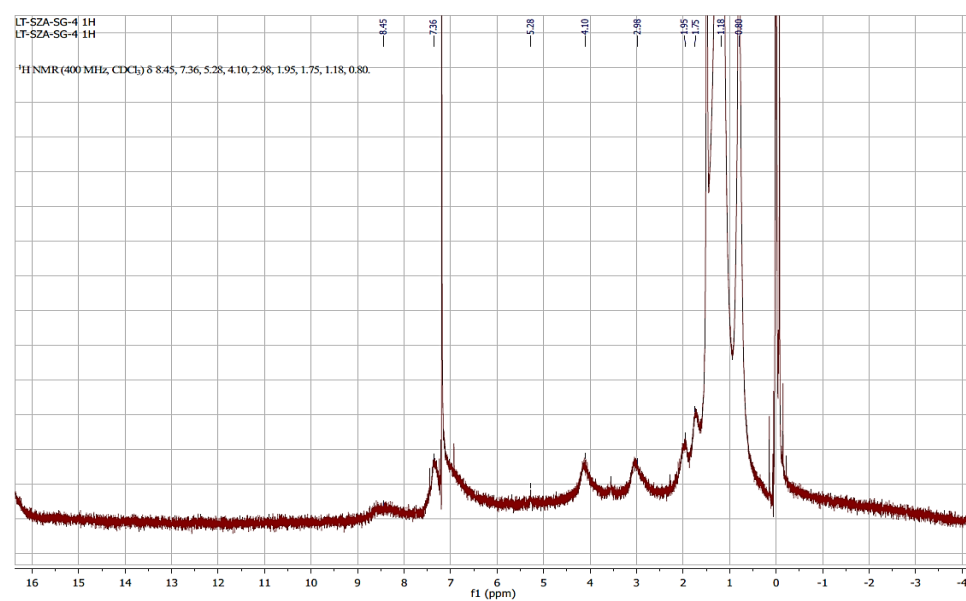
¹H NMR spectrum of SG-1



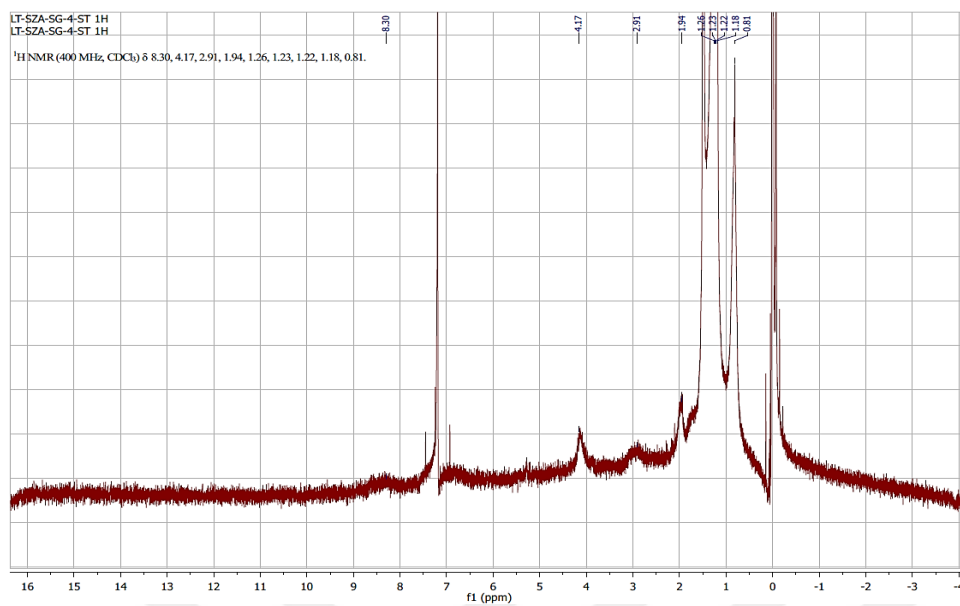
¹H NMR spectrum of SG-2



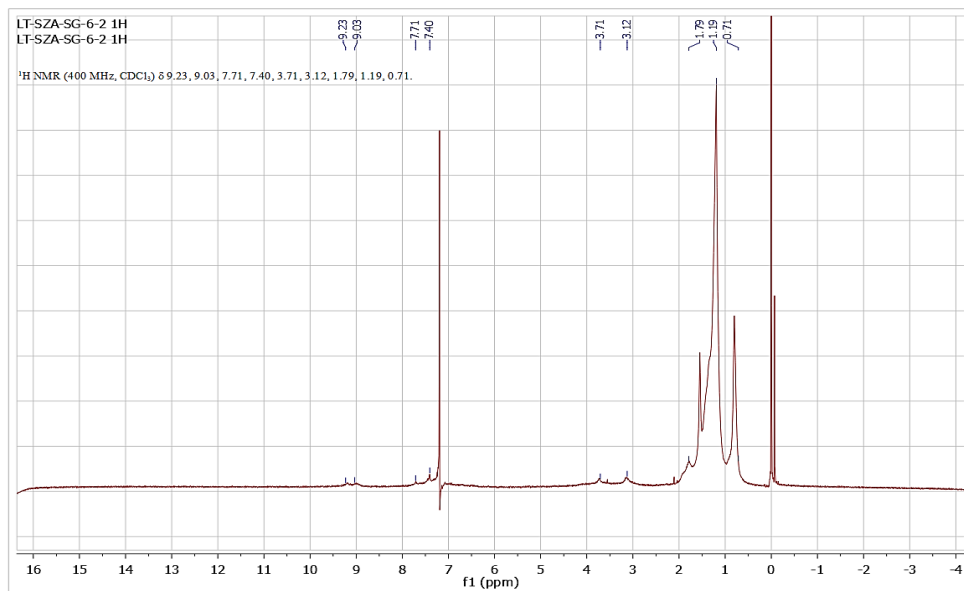
¹H NMR spectrum of SG-3



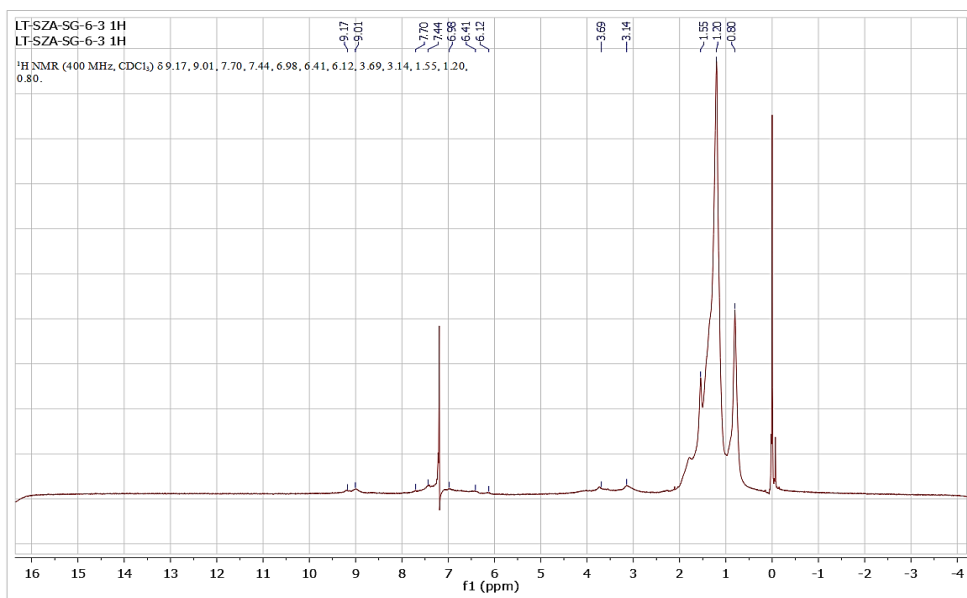
¹H NMR spectrum of SG-4



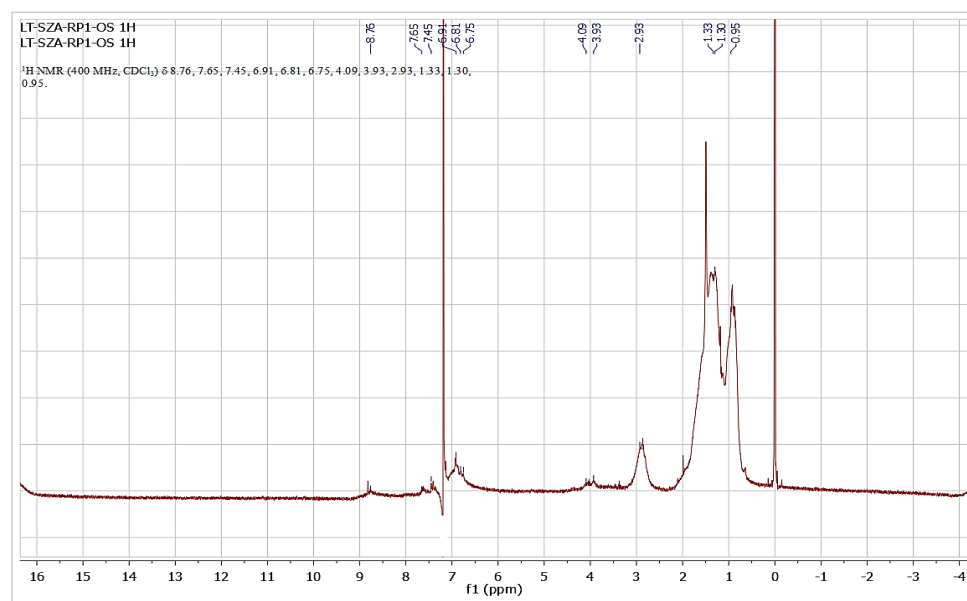
¹H NMR spectrum of SG-4-ST



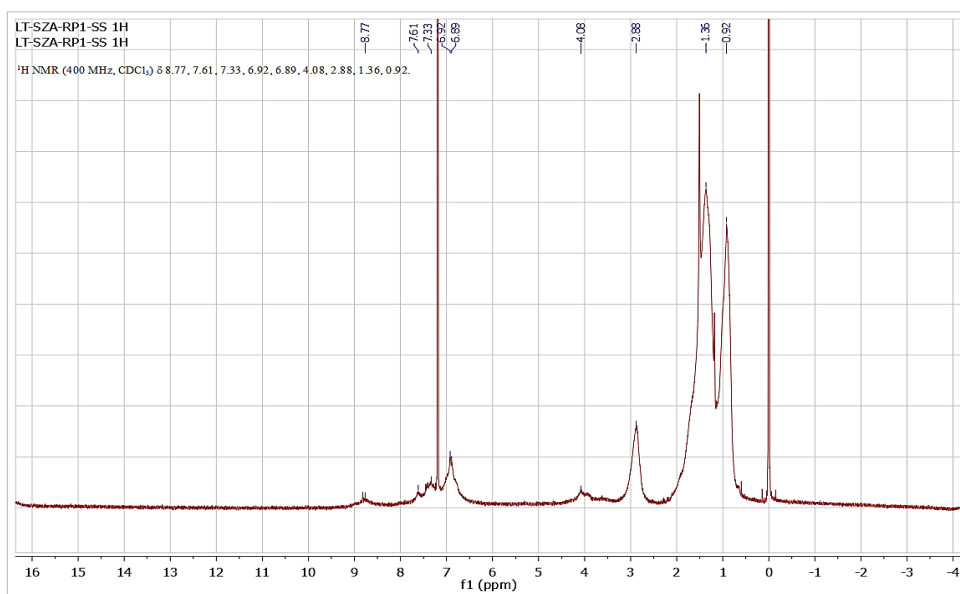
¹H NMR spectrum of SG-6-2



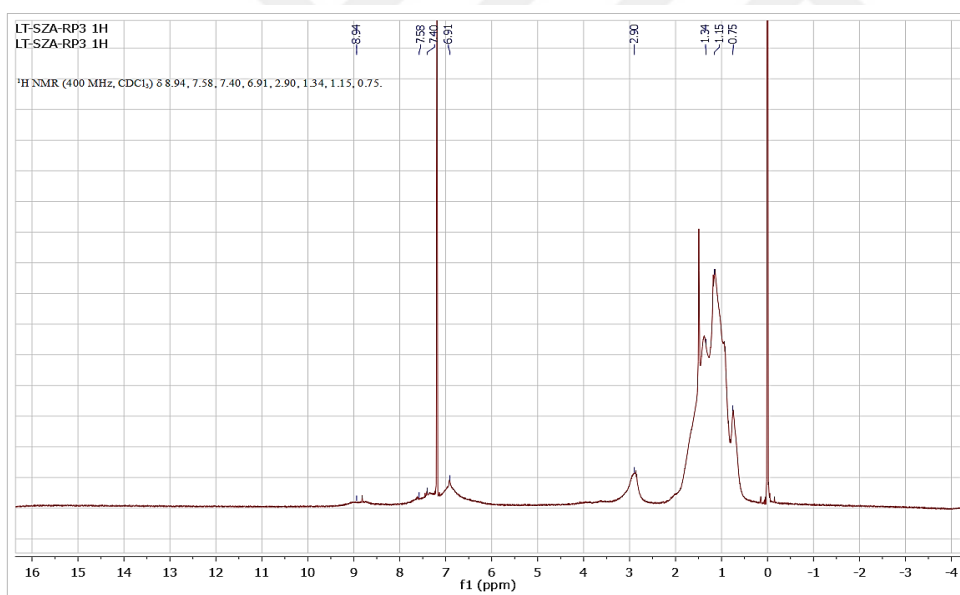
¹H NMR spectrum of SG-6-3



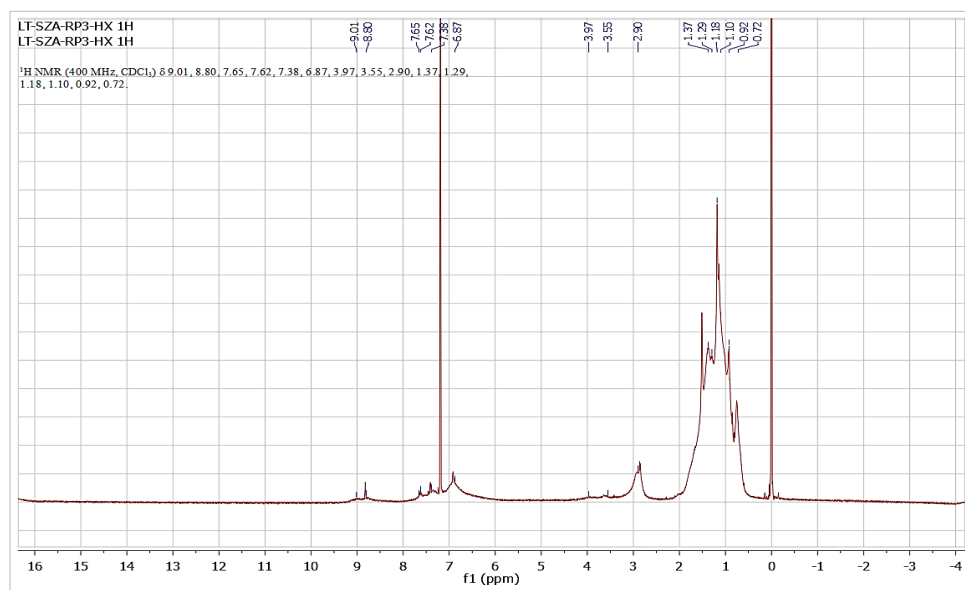
¹H NMR spectrum of RP1-os



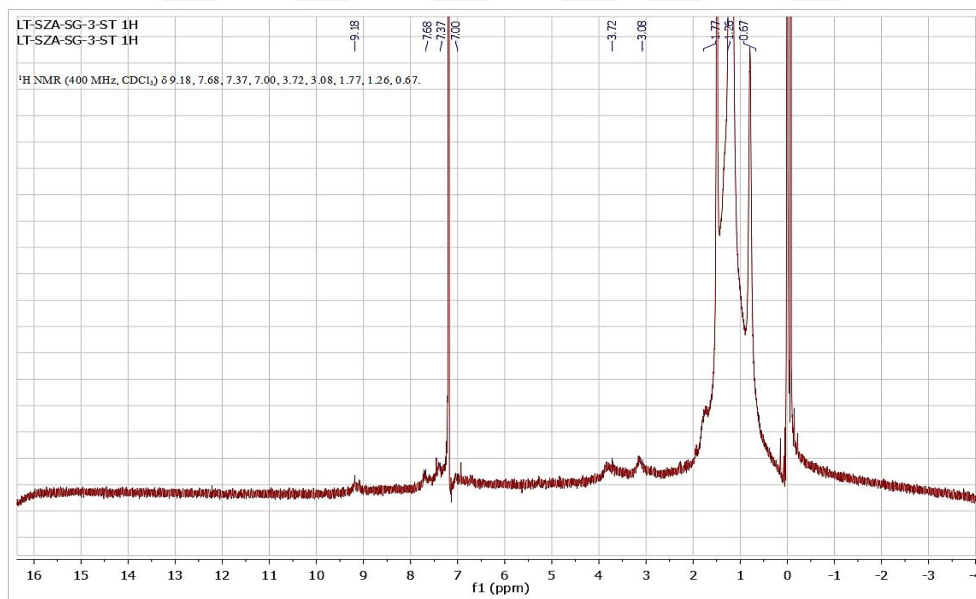
¹H NMR spectrum of RP1-ss



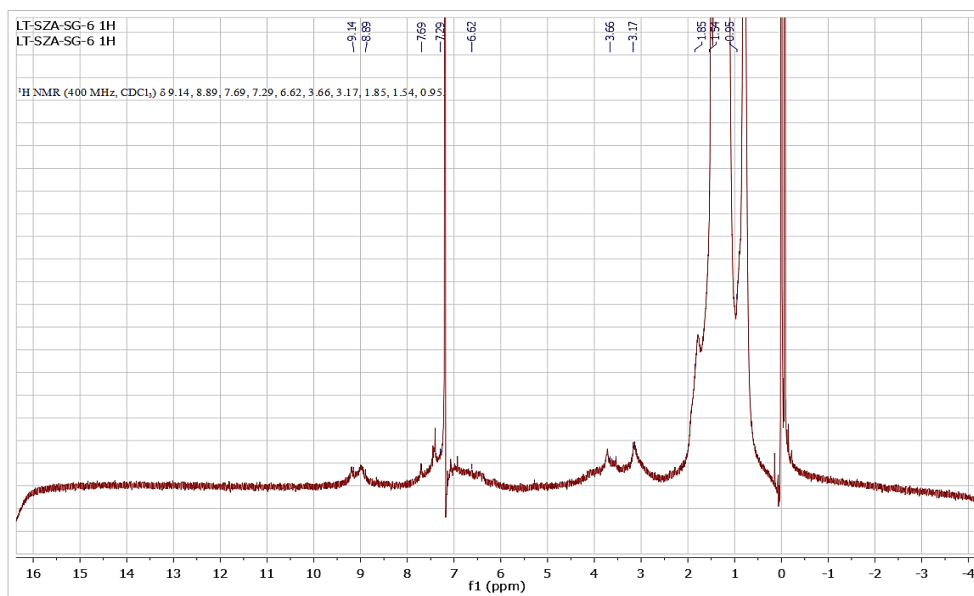
¹H NMR spectrum of RP3



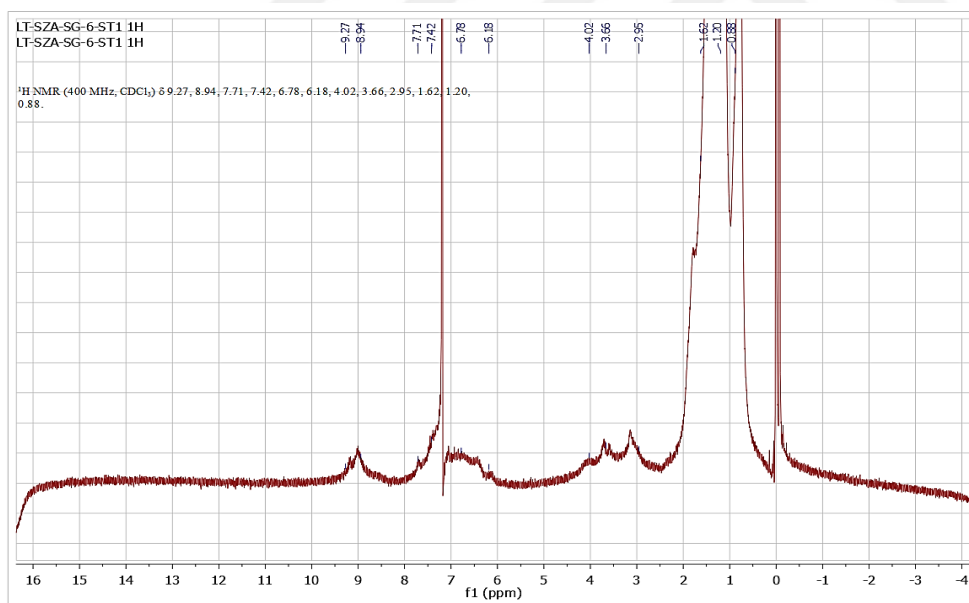
¹H NMR spectrum of RP3-Hx (Hexane Fraction)



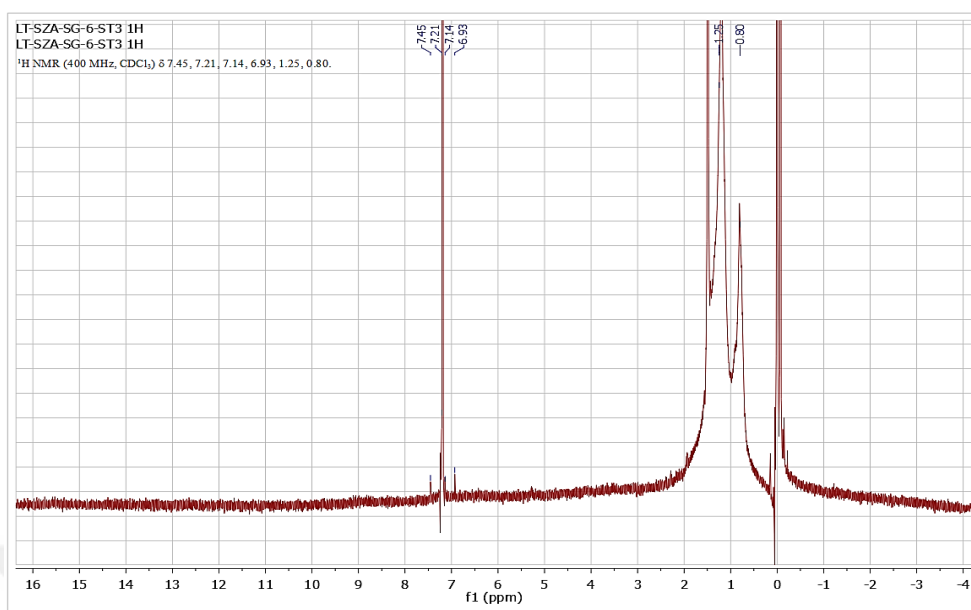
¹H NMR spectrum of SG-3-ST



¹H NMR spectrum of SG-6



¹H NMR spectrum of SG-6-ST1



¹H NMR spectrum of SG-6-ST3

B. The Results for Thermal Analyses and Elemental Analyses of Polymers



**ORTA DOĞU TEKNİK ÜNİVERSİTESİ****MERKEZ LABORATUVARI****AR-GE EĞİTİM VE ÖLÇME MERKEZİ**

Üniversiteler Mah. Dumlupınar Blv. No:1, 06800 Çankaya Ankara/TÜRKİYE
Tel: +90 312 210 64 21 Fax: +90 312 210 64 25 e-posta: merlab@metu.edu.tr <http://www.merlab.odtu.edu.tr>

DENEY RAPORU**ANALYSIS REPORT****DENEY SONUÇLARI – ANALYSIS RESULTS**

Numune Adı	%C	%H	%N	%s
SG-2	71.75	10.42	3.30	7.44
SG-2-ST	70.58	10.17	3.16	7.74
SG-3	75.24	10.07	2.93	5.71
SG-3-ST	74.36	9.96	2.80	5.84
SG-4	57.81	7.22	2.12	5.18
SG-4-ST	61.07	7.94	2.00	6.19
SG-6	75.14	10.76	2.48	5.48
SG-9-ST	70.90	9.49	2.97	6.70
PIID DTP	69.10	9.26	4.41	6.74
RP-1-OS	61.34	7.32	3.72	18.44

Bu rapor, MERLAB'ın yazılı izni olmadan kısmen de olsa kopyalanıp çoğaltılamaz. Sonuçlar sadece deneyi yapılan numuneye aittir. İmzasız raporlar geçersizdir. This report can not be partially copied or reproduced without official permission of MERLAB. The results only belong to the analysed sample. The reports without a signature are invalid.

FRM-NKB-03 Rev.No/Tarih: 00/-

2/2

Elemental analyses of polymers



ORTA DOĞU TEKNİK ÜNİVERSİTESİ
MERKEZ LABORATUVARI
AR-GE EĞİTİM VE ÖLÇME MERKEZİ

Üniversiteler Mah. Dumlupınar Blv. No:1, 06800 Çankaya Ankara/TÜRKİYE
Tel: +90 312 210 64 21 Fax: +90 312 210 64 25 e-posta: merlab@metu.edu.tr http://www.merlab.odtu.edu.tr

DENEY RAPORU
ANALYSIS REPORT

DENEY SONUÇLARI – ANALYSIS RESULTS

Numune Adı	%C	%H	%N	%S
01-RP-1-SS	64,91	6,74	3,04	16,90
	52,31	6,14	2,69	15,33
02-RP-2	49,56	5,85	3,28	17,96
03-RP-3	68,64	7,61	2,98	13,85
04-RP-3-Hex	56,69	7,53	2,38	11,50

Bu rapor, MERLAB'ın yazılı izni olmadan kısmen de olsa kopyalanıp çoğaltılamaz. Sonuçlar sadece deneyi yapılan numuneye aittir. İmzasız raporlar geçersizdir. This report can not be partially copied or reproduced without official permission of MERLAB. The results only belong to the analysed sample. The reports without a signature are invalid.

FRM-NKB-03 Rev.No/Tarih: 00/-

2/2

Elemental analyses of polymers



ORTA DOĞU TEKNİK ÜNİVERSİTESİ

MERKEZ LABORATUVARI

AR-GE EĞİTİM VE ÖLÇME MERKEZİ

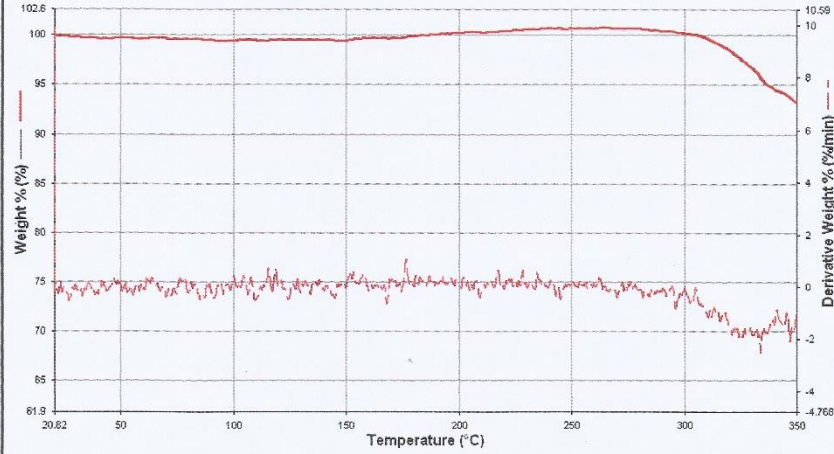
Üniversiteler Mah. Dumlupınar Blv. No:1, 06800 Çankaya Ankara/TÜRKİYE
Tel: +90 312 210 64 21 Fax: +90 312 210 64 25 e-posta: merlab@metu.edu.tr <http://www.merlab.odtu.edu.tr>

DENEY RAPORU

ANALYSIS REPORT

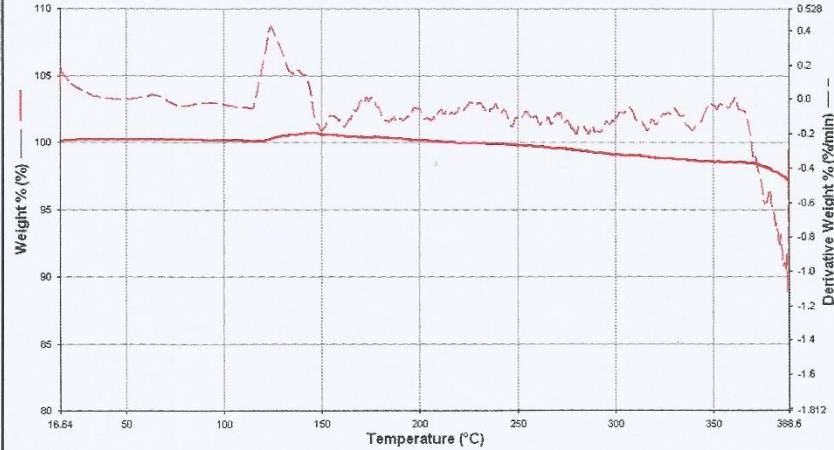
DENEY SONUÇLARI – ANALYSIS RESULTS

1. Numune: 27689-1= Rp-1-SS



%Kayıp= 6.702%

2. Numune: 27689-2= RP-2



%Kayıp= 2.841%

Bu rapor, MERLAB'ın yazılı izni olmadan kısmen de olsa kopyalanıp çoğaltılamaz. Sonuçlar sadece deneyi yapılan numuneye aittir. İmzasız raporlar geçersizdir. This report can not be partially copied or reproduced without official permission of MERLAB. The results only belong to the analysed sample. The reports without a signature are invalid.

FRM-NKB-03 Rev.No/Tarih: 00/-

2/3

TGA Curves of Polymers

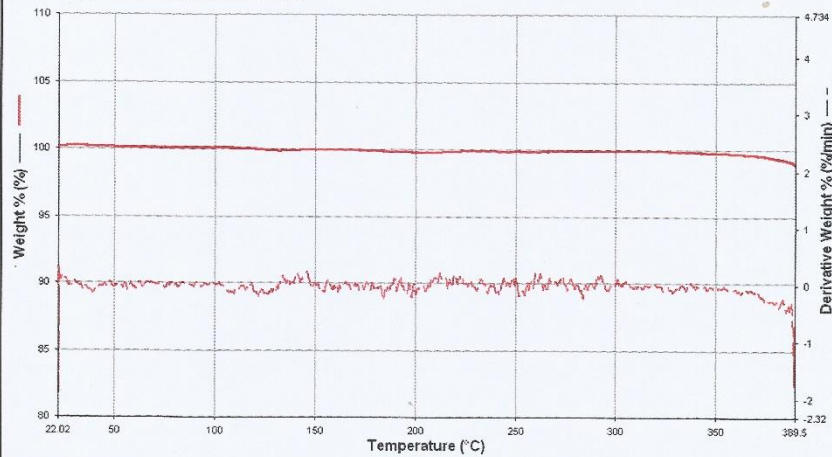


ORTA DOĞU TEKNİK ÜNİVERSİTESİ
MERKEZ LABORATUVARI
AR-GE EĞİTİM VE ÖLÇME MERKEZİ

Üniversiteler Mah. Dumlupınar Blv. No:1, 06800 Çankaya Ankara/TÜRKİYE
Tel: +90 312 210 64 21 Fax: +90 312 210 64 25 e-posta: merlab@metu.edu.tr http://www.merlab.odtu.edu.tr

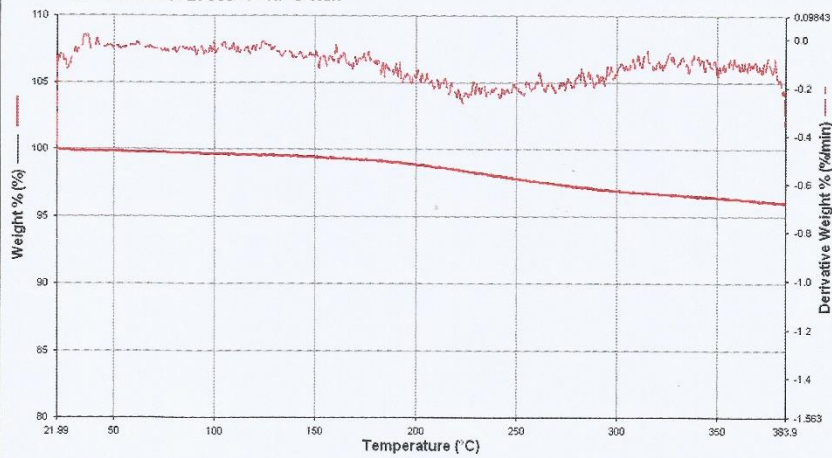
DENEY RAPORU
ANALYSIS REPORT

3. Numune: 27689-3= RP-3



%Kayıp= 1.161%

4. Numune: 27689-4= RP-3-Hex



%Kayıp= 4.089%

Bu rapor, MERLAB'ın yazılı izni olmadan kısmen de olsa kopyalanıp çoğaltılamaz. Sonuçlar sadece deneyi yapılan numuneye aittir. İmzasız raporlar geçersizdir. This report can not be partially copied or reproduced without official permission of MERLAB. The results only belong to the analysed sample. The reports without a signature are invalid.

FRM-NKB-03 Rev.No/Tarih: 00/-

3/3

TGA Curves of Polymers



ORTA DOĞU TEKNİK ÜNİVERSİTESİ

MERKEZ LABORATUVARI

AR-GE EĞİTİM VE ÖLÇME MERKEZİ

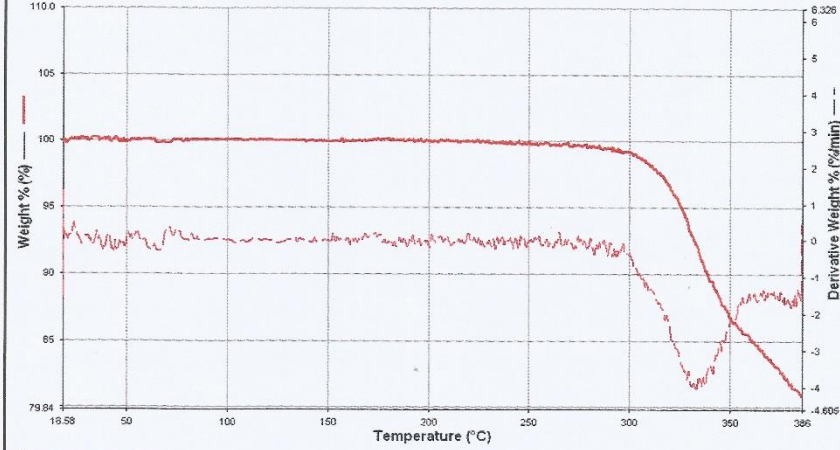
Üniversiteler Mah. Dumlupınar Blv. No:1, 06800 Çankaya Ankara/TÜRKİYE
Tel: +90 312 210 64 21 Fax: +90 312 210 64 25 e-posta: merlab@metu.edu.tr http://www.merlab.odtu.edu.tr

DENEY RAPORU

ANALYSIS REPORT

DENEY SONUÇLARI – ANALYSIS RESULTS

1. Numune: 27691-1=SG-2



%Kayıp=19.070 %

2. Numune: 27691-2=SG-2-ST



%Kayıp= 30.760%

Bu rapor, MERLAB' ın yazılı izni olmadan kısmen de olsa kopyalanıp çoğaltılamaz. Sonuçlar sadece deneyi yapılan numuneye aittir. İmzasız raporlar geçersizdir. This report can not be partially copied or reproduced without official permission of MERLAB. The results only belong to the analysed sample. The reports without a signature are invalid.

FRM-NKB-03 Rev.No/Tarih: 00/-

2/6

TGA Curves of Polymers

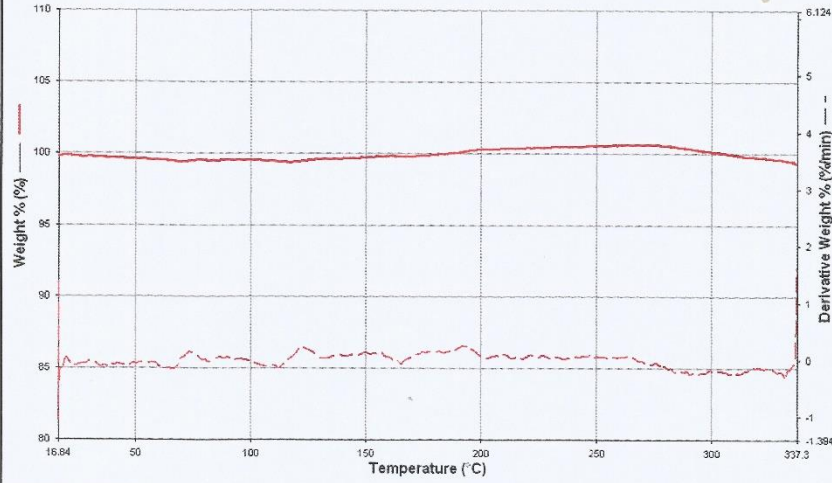


ORTA DOĞU TEKNİK ÜNİVERSİTESİ
MERKEZ LABORATUVARI
AR-GE EĞİTİM VE ÖLÇME MERKEZİ

Universiteler Mah. Dumlupınar Blv. No:1, 06800 Çankaya Ankara/TÜRKİYE
Tel: +90 312 210 64 21 Fax: +90 312 210 64 25 e-posta: merlab@metu.edu.tr http://www.merlab.odtu.edu.tr

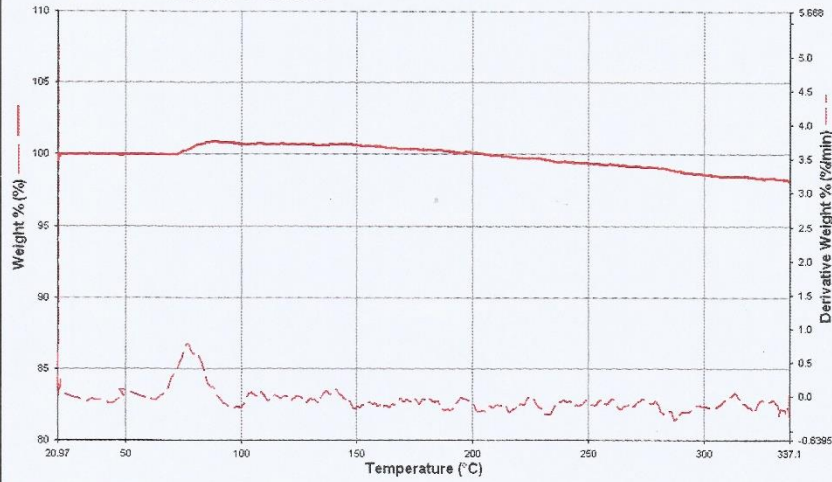
DENEY RAPORU
ANALYSIS REPORT

3. Numune: 27691-3= SG-3



%Kayıp= 0.568%

4. Numune: 27691-4= SG-3-ST



%Kayıp= 1.471%

Bu rapor, MERLAB'ın yazılı izni olmadan kısmen de olsa kopyalanıp çoğaltılamaz. Sonuçlar sadece deneyi yapılan numuneye aittir. İmzasız raporlar geçersizdir. This report can not be partially copied or reproduced without official permission of MERLAB. The results only belong to the analysed sample. The reports without a signature are invalid.

FRM-NKB-03 Rev.No/Tarih: 00/-

3/6

TGA Curves of Polymers



ORTA DOĞU TEKNİK ÜNİVERSİTESİ

MERKEZ LABORATUVARI

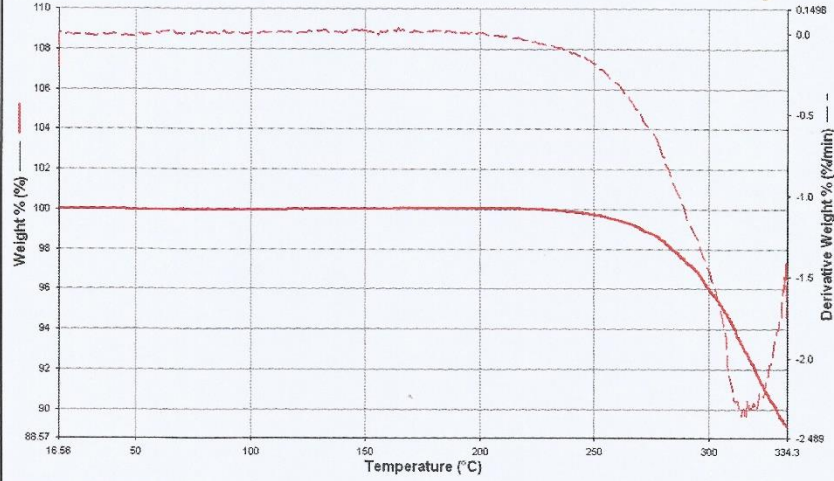
AR-GE EĞİTİM VE ÖLÇME MERKEZİ

Üniversiteler Mah. Dumlupınar Blv. No:1, 06800 Çankaya Ankara/TÜRKİYE
Tel: +90 312 210 64 21 Fax: +90 312 210 64 25 e-posta: merlab@metu.edu.tr http://www.merlab.odtu.edu.tr

DENEY RAPORU

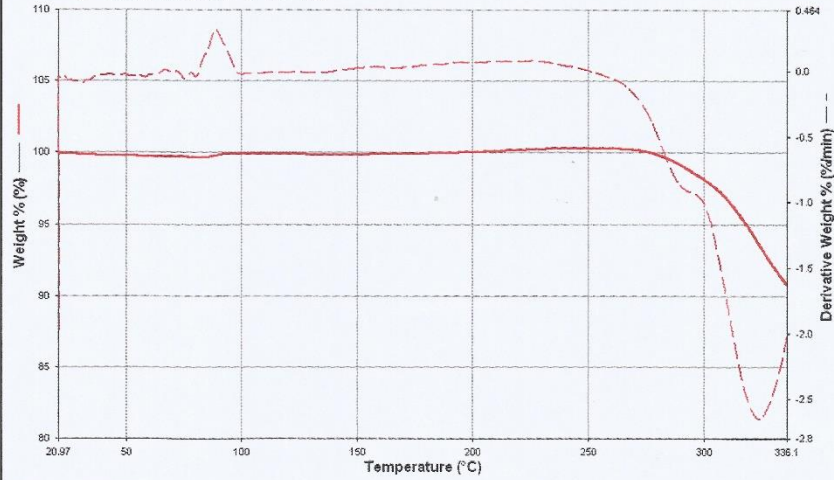
ANALYSIS REPORT

5. Numune: 27691-5= SG-4



%Kayıp=10.884 %

6. Numune: 27691-6= SG-4-ST



%Kayıp= 9.209%

Bu rapor, MERLAB' in yazılı izni olmadan kısmen de olsa kopyalanıp çoğaltılamaz. Sonuçlar sadece deneyi yapan numuneye aittir. İmzasız raporlar geçersizdir. This report can not be partially copied or reproduced without official permission of MERLAB. The results only belong to the analysed sample. The reports without a signature are invalid.

FRM-NKB-03 Rev.No/Tarih: 00/-

4/6

TGA Curves of Polymers

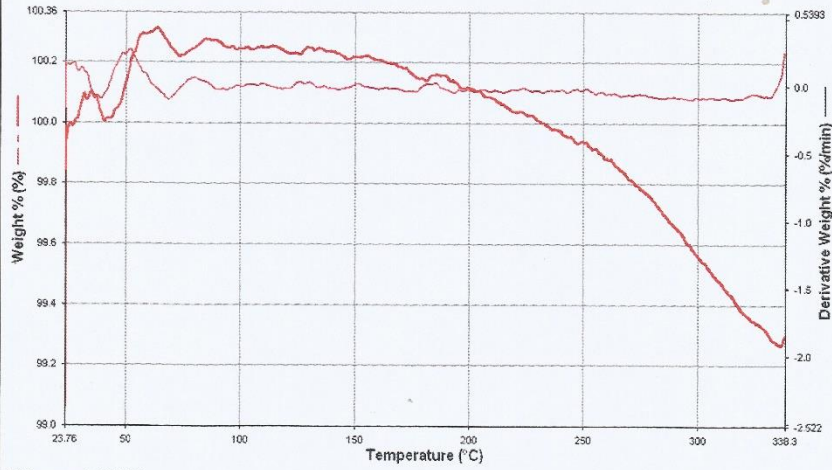


ORTA DOĞU TEKNİK ÜNİVERSİTESİ
MERKEZ LABORATUVARI
AR-GE EĞİTİM VE ÖLÇME MERKEZİ

Üniversiteler Mah. Dumlupınar Blv. No:1, 06800 Çankaya Ankara/TÜRKİYE
Tel: +90 312 210 64 21 Fax: +90 312 210 64 25 e-posta: merlab@metu.edu.tr http://www.merlab.odtu.edu.tr

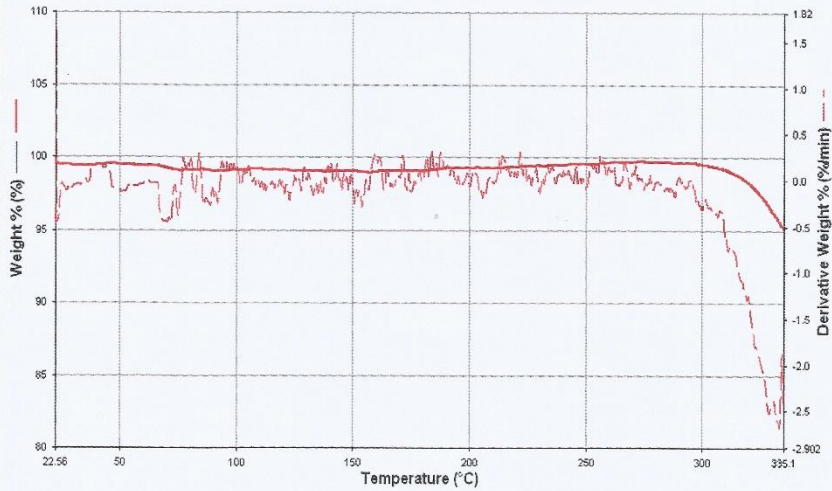
DENEY RAPORU
ANALYSIS REPORT

7. Numune: 27691-7= SG-6



%Kayıp= 0.690%

8. Numune: 27691-8= SG-9-ST



%Kayıp=4.634 %

Bu rapor, MERLAB' in yazılı izni olmadan kısmen de olsa kopyalanıp çoğaltılamaz. Sonuçlar sadece deneyi yapılan numuneye aittir. İmzasız raporlar geçersizdir. This report can not be partially copied or reproduced without official permission of MERLAB. The results only belong to the analysed sample. The reports without a signature are invalid.

FRM-NKB-03 Rev.No/Tarih: 00/-

5/6

TGA Curves of Polymers

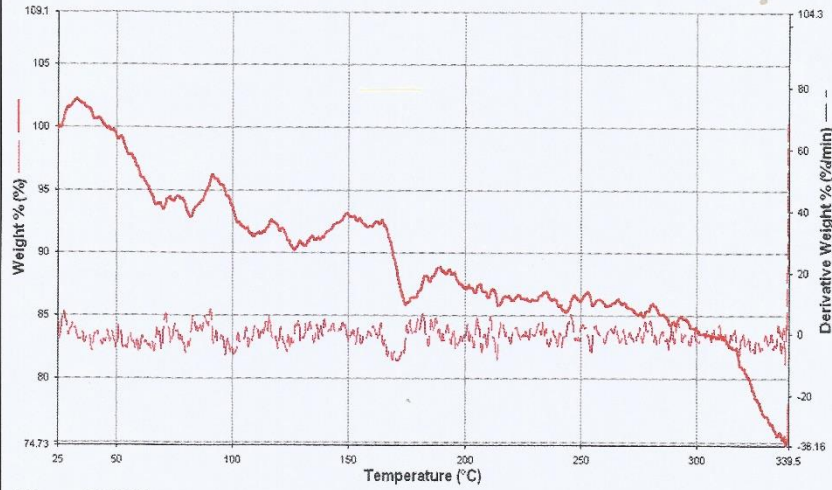


ORTA DOĞU TEKNİK ÜNİVERSİTESİ
MERKEZ LABORATUVARI
AR-GE EĞİTİM VE ÖLÇME MERKEZİ

Üniversiteler Mah. Dumlupınar Blv. No:1, 06800 Çankaya Ankara/TÜRKİYE
Tel: +90 312 210 64 21 Fax: +90 312 210 64 25 e-posta: merlab@metu.edu.tr http://www.merlab.odtu.edu.tr

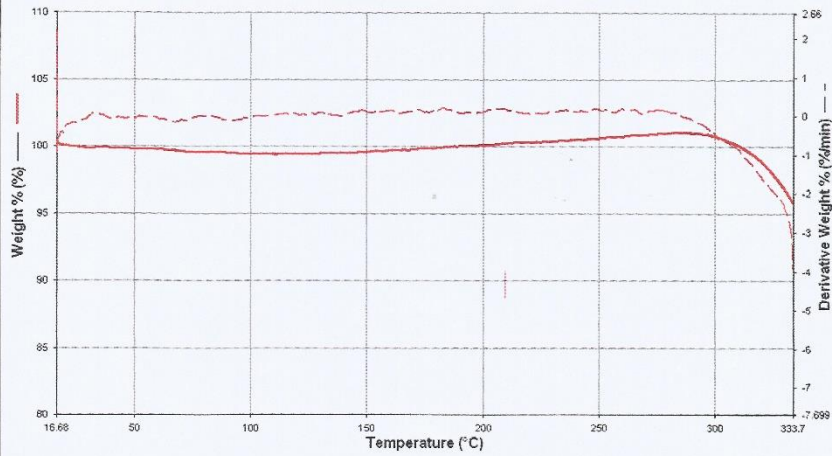
DENEY RAPORU
ANALYSIS REPORT

9. Numune: 27691-9= PIID DTP



%Kayıp=21.788 %

10. Numune: 27691-10= RP-1-ÖS



%Kayıp= 4.554%

Bu rapor, MERLAB' in yazılı izni olmadan kısmen de olsa kopyalanıp çoğaltılamaz. Sonuçlar sadece deneyi yapılan numuneye aittir. İmzasız raporlar geçersizdir. This report can not be partially copied or reproduced without official permission of MERLAB. The results only belong to the analysed sample. The reports without a signature are invalid.

FRM-NKB-03 Rev.No/Tarih: 00/-

6/6



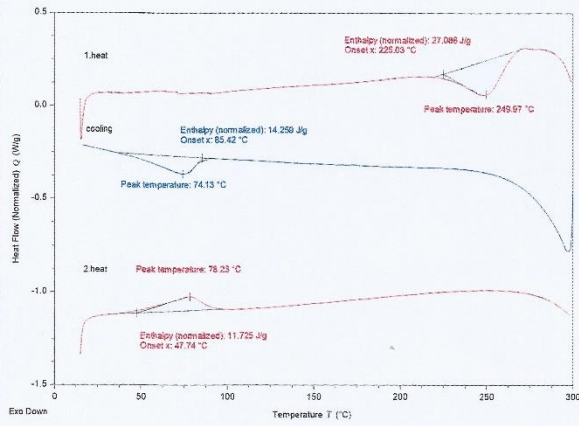
ORTA DOĞU TEKNİK ÜNİVERSİTESİ
MERKEZ LABORATUVARI
AR-GE EĞİTİM VE ÖLÇME MERKEZİ
Üniversiteler Mah. Dumlupınar Blv. No:1, 06800 Çankaya Ankara/TÜRKİYE
Tel: +90 312 210 64 21 Fax: +90 312 210 64 25 e-posta: merlab@metu.edu.tr http://www.merlab.odtu.edu.tr

DENEY RAPORU
ANALYSIS REPORT

DENEY SONUÇLARI – ANALYSIS RESULTS

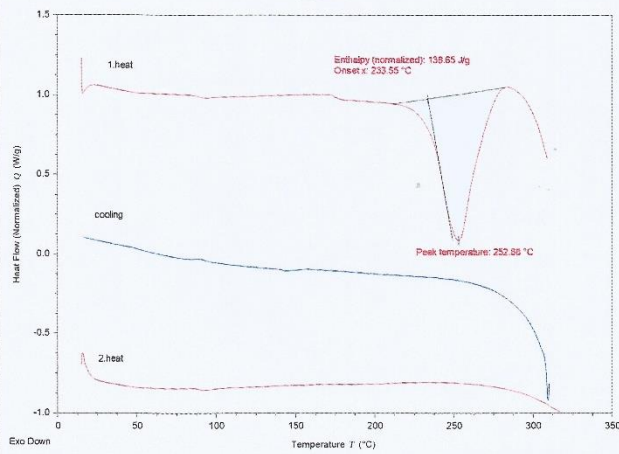
1. Numune: 27690-1

27690_1_05082019



2. Numune: 27690-2

27690_2_05082019



Bu rapor, MERLAB'ın yazılı izni olmadan kısmen de olsa kopyalanıp çoğaltılamaz. Sonuçlar sadece deneyi yapılan numuneye aittir. İmzasız raporlar geçersizdir. This report can not be partially copied or reproduced without official permission of MERLAB. The results only belong to the analysed sample. The results without a signature are invalid.
FRM-NKB-03 Rev.No/Tarih: 00/-

2/6



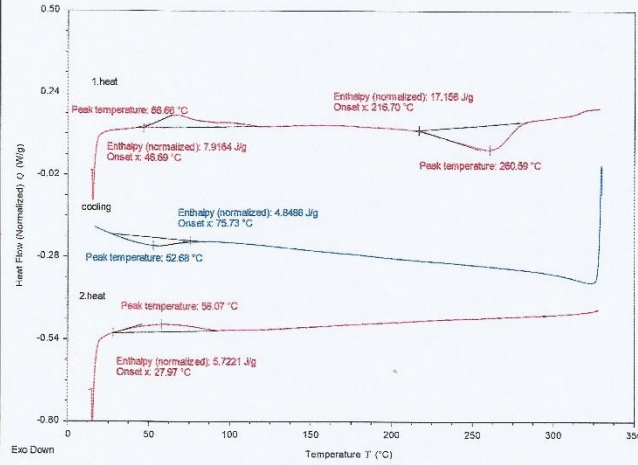
ORTA DOĞU TEKNİK ÜNİVERSİTESİ
MERKEZ LABORATUVARI
AR-GE EĞİTİM VE ÖLÇME MERKEZİ

Üniversiteler Mah. Dumlupınar Blv. No:1, 06800 Çankaya Ankara/TÜRKİYE
Tel: +90 312 210 64 21 Fax: +90 312 210 64 25 e-posta: merlab@metu.edu.tr http://www.merlab.odtu.edu.tr

DENEY RAPORU
ANALYSIS REPORT

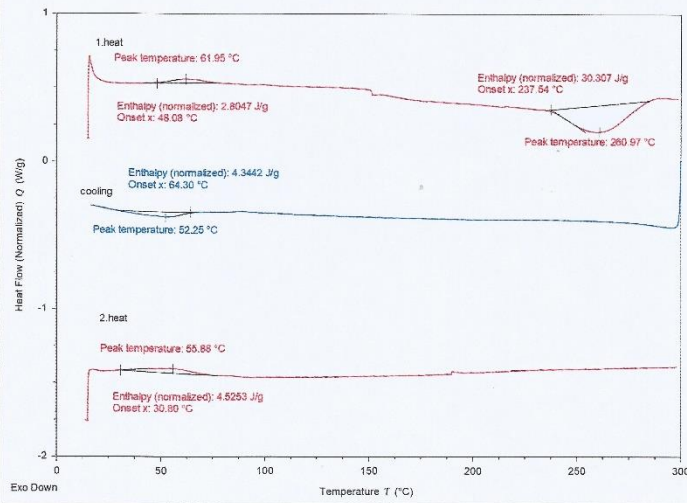
3. Numune: 27690-3

27690_3_05092019



4. Numune: 27690-4

27690_4_06092019



Bu rapor, MERLAB'ın yazılı izni olmadan kısmen de olsa kopyalanıp çoğaltılamaz. Sonuçlar sadece deneyi yapan numuneye aittir. İmzasız raporlar geçersizdir. This report can not be partially copied or reproduced without official permission of MERLAB. The results only belong to the analysed sample. The reports without a signature are invalid.

FRM-NKB-03 Rev.No/Tarih: 00/-

3/6



ORTA DOĞU TEKNİK ÜNİVERSİTESİ

MERKEZ LABORATUVARI

AR-GE EĞİTİM VE ÖLÇME MERKEZİ

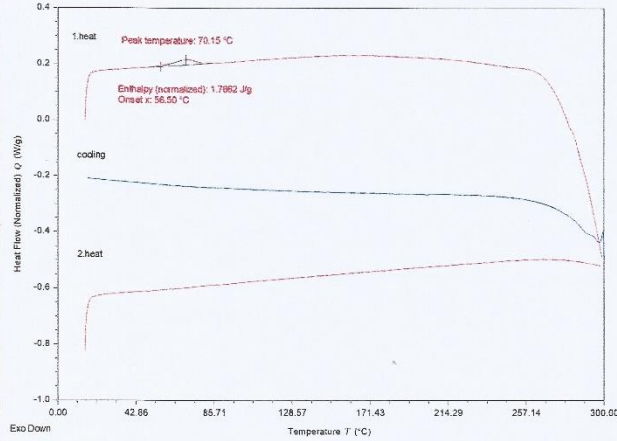
Üniversiteler Mah. Dumlupınar Blv. No:1, 06800 Çankaya Ankara/TÜRKİYE
Tel: +90 312 210 64 21 Fax: +90 312 210 64 25 e-posta: merlab@metu.edu.tr http://www.merlab.odtu.edu.tr

DENEY RAPORU

ANALYSIS REPORT

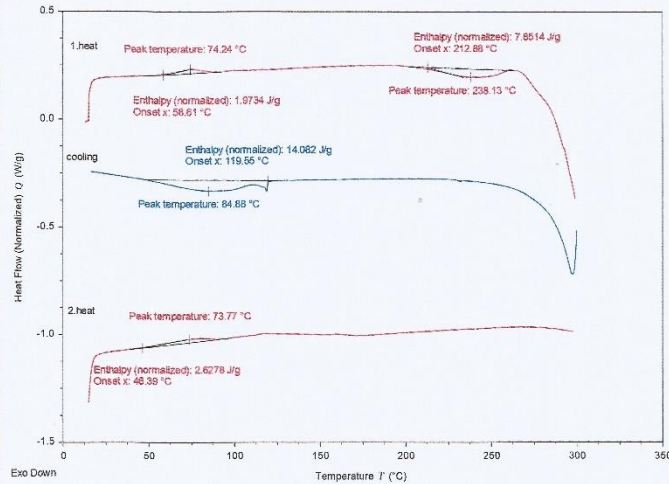
5. Numune: 27690-5

27690_5_06092019



6. Numune: 27690-6

27690_6_06092019



Bu rapor, MERLAB'ın yazılı izni olmadan kısmen de olsa kopyalanıp çoğaltılamaz. Sonuçlar sadece deneyi yapılan numuneye aittir. İmzasız raporlar geçersizdir. This report can not be partially copied or reproduced without official permission of MERLAB. The results only belong to the analysed sample. The reports without a signature are invalid.

FRM-NKB-03 Rev.No/Tarih: 00/-

4/6

DSC Curves of Polymers



ORTA DOĞU TEKNİK ÜNİVERSİTESİ

MERKEZ LABORATUVARI

AR-GE EĞİTİM VE ÖLÇME MERKEZİ

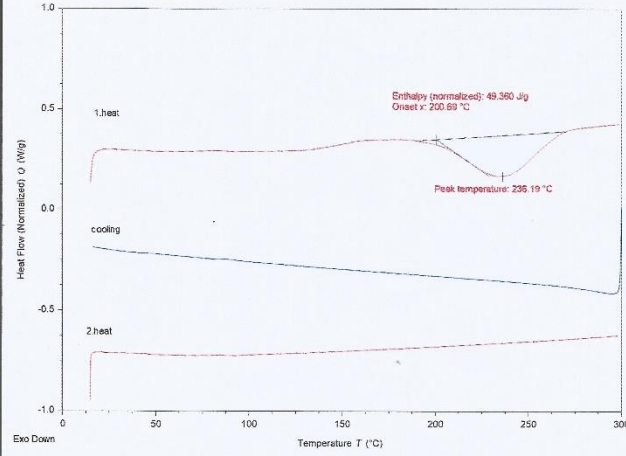
Üniversiteler Mah. Dumlupınar Blv. No:1, 06800 Çankaya Ankara/TÜRKİYE
Tel: +90 312 210 64 21 Fax: +90 312 210 64 25 e-posta: merlab@metu.edu.tr http://www.merlab.odtu.edu.tr

DENEY RAPORU

ANALYSIS REPORT

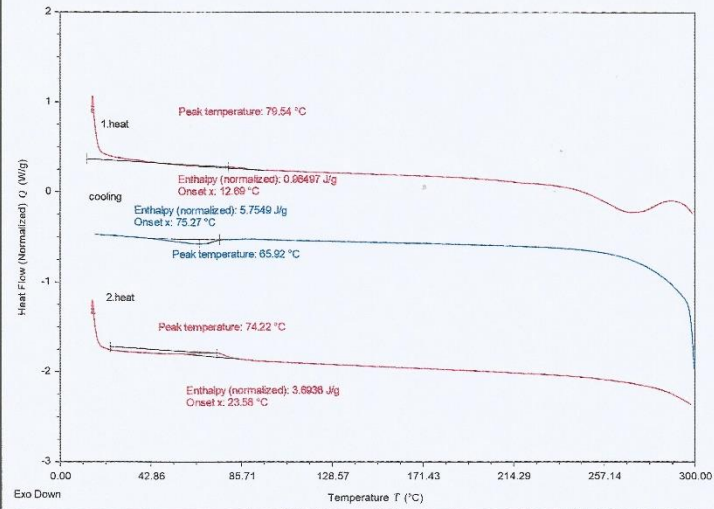
7. Numune: 27690-7

27690_7_09092019



8. Numune: 27690-8

27690_8_09092019



Bu rapor, MERLAB'ın yazılı izni olmadan kısmen de olsa kopyalanıp çoğaltılamaz. Sonuçlar sadece deneyi yapılan numuneye aittir. İmzasız raporlar geçersizdir. This report can not be partially copied or reproduced without official permission of MERLAB. The results only belong to the analysed sample. The reports without a signature are invalid.

FRM-NKB-03 Rev.No/Tarih: 00/-

5/6

DSC Curves of Polymers



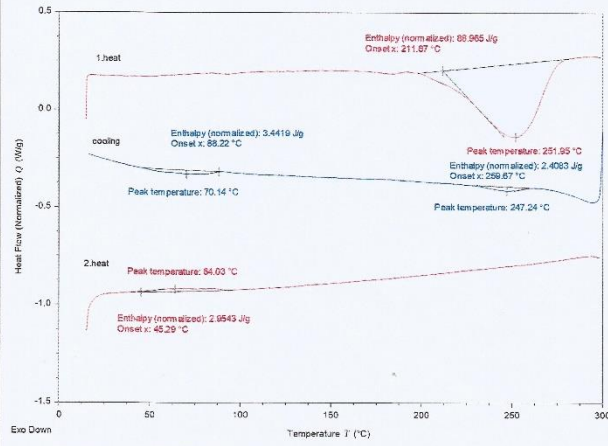
ORTA DOĞU TEKNİK ÜNİVERSİTESİ
MERKEZ LABORATUVARI
AR-GE EĞİTİM VE ÖLÇME MERKEZİ

Üniversiteler Mah. Dumlupınar Blv. No:1, 06800 Çankaya Ankara/TÜRKİYE
Tel: +90 312 210 64 21 Fax: +90 312 210 64 25 e-posta: merlab@metu.edu.tr http://www.merlab.odtu.edu.tr

DENEY RAPORU
ANALYSIS REPORT

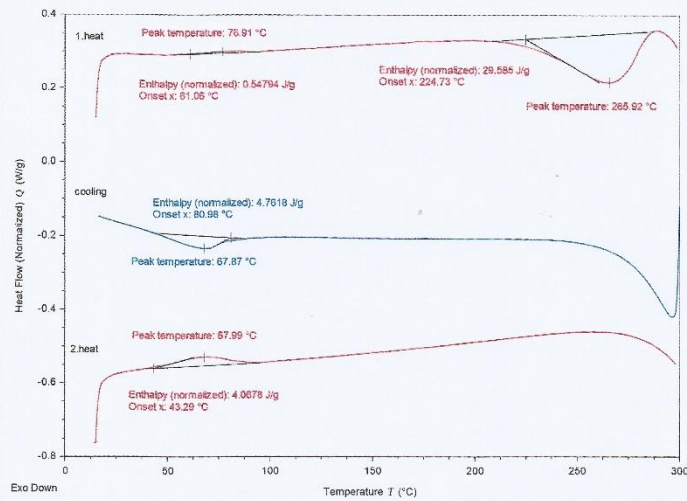
9. Numune: 27690-9

27690_9_09062019



10. Numune: 27690-10

27690_10_10092019



Bu rapor, MERLAB'ın yazılı izni olmadan kısmen de olsa kopyalanıp çoğaltılamaz. Sonuçlar sadece deneyi yapılan numuneye aittir. İmzasız raporlar geçersizdir. This report can not be partially copied or reproduced without official permission of MERLAB. The results only belong to the analysed sample. The reports without a signature are invalid.

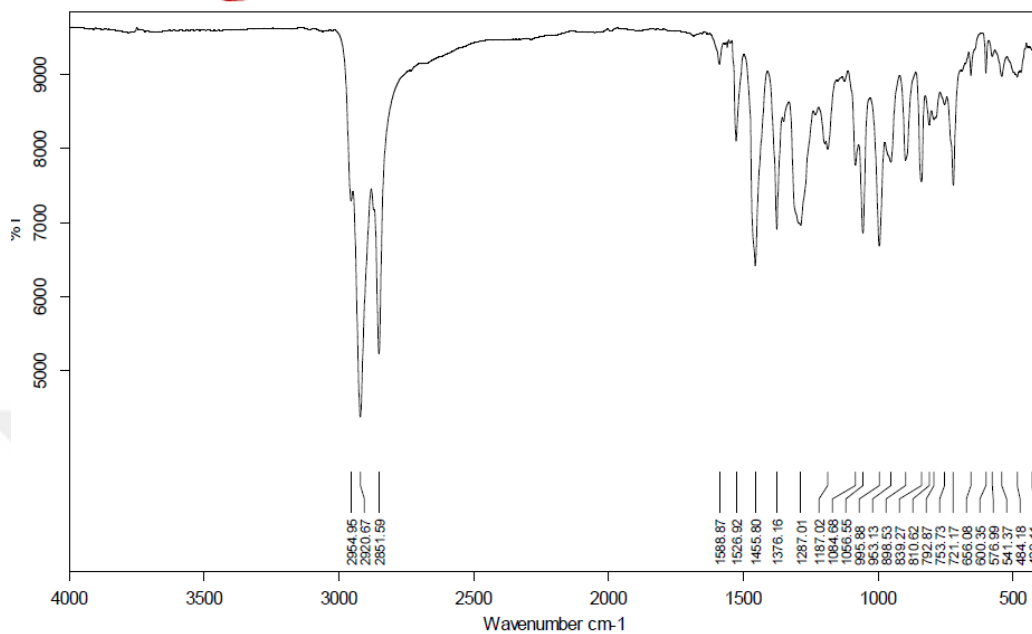
FRM-NKB-03 Rev.No/Tarih: 00/-

6/6

C. FTIR Analyses of Polymers



ODTU MERKEZ LABORATUVARI PERKIN ELMER Spectrum 400
(27702-02) SG-2-ST.dx

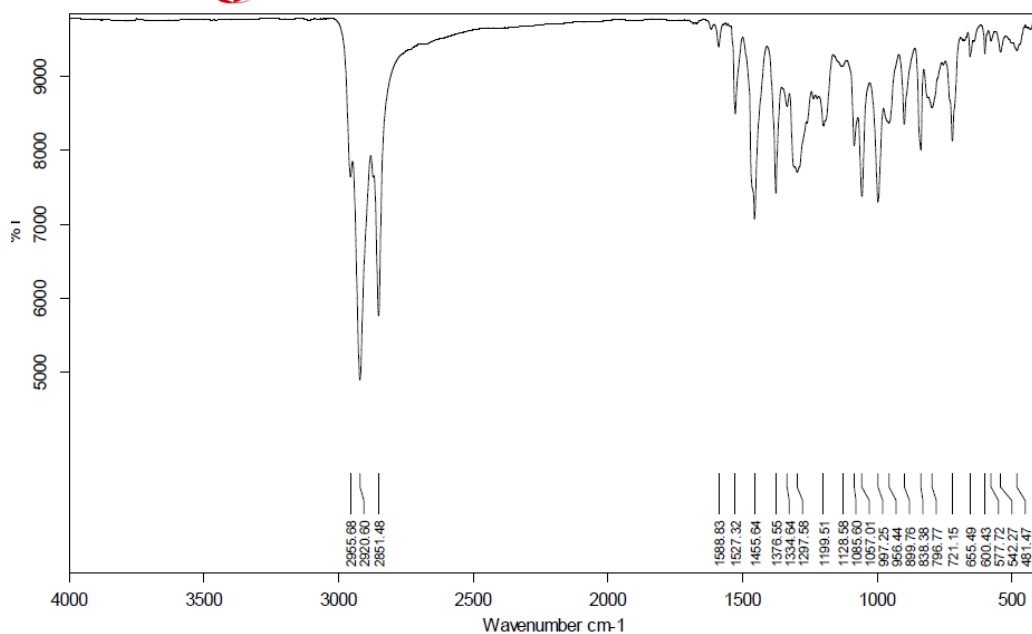


Sample Name		Date of Measurement	
Resolution	4	Sample Scans	

1



ODTU MERKEZ LABORATUVARI PERKIN ELMER Spectrum 400
(27702-01) SG-2-SX

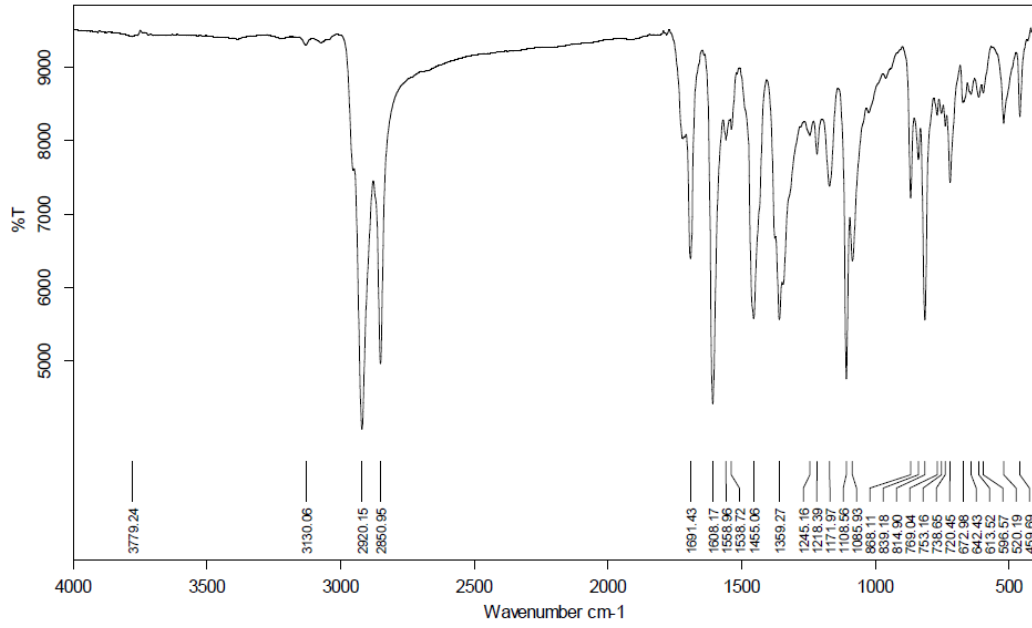


Sample Name		Date of Measurement	
Resolution	4	Sample Scans	

1



ODTU MERKEZ LABORATUVARI PERKIN ELMER Spectrum 400
(27702-03) SG-3.dx

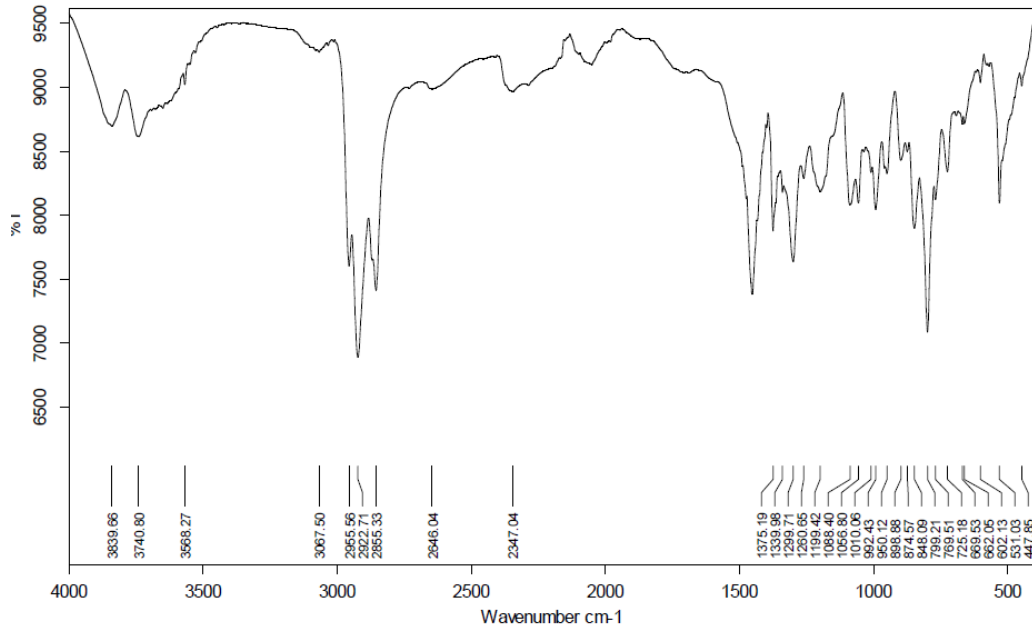


Sample Name		Date of Measurement	
Resolution	4	Sample Scans	

1



ODTU MERKEZ LABORATUVARI PERKIN ELMER Spectrum 400
(27703-01) RP1-ÖS.dx

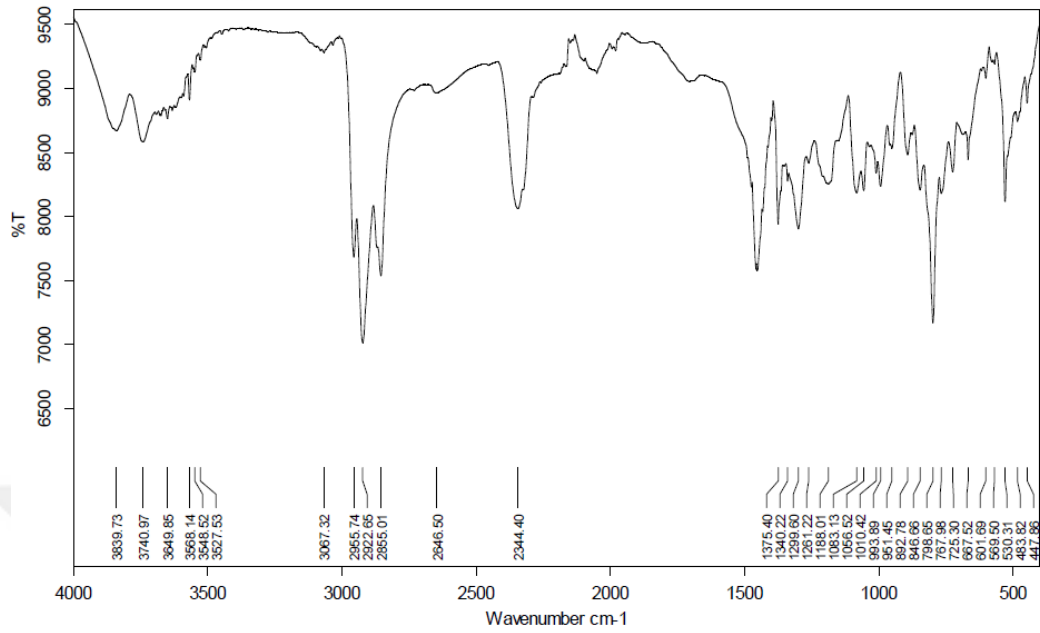


Sample Name		Date of Measurement	
Resolution	4	Sample Scans	

1



ODTU MERKEZ LABORATUVARI PERKIN ELMER Spectrum 400
(27703-02) RP1-SS.dx

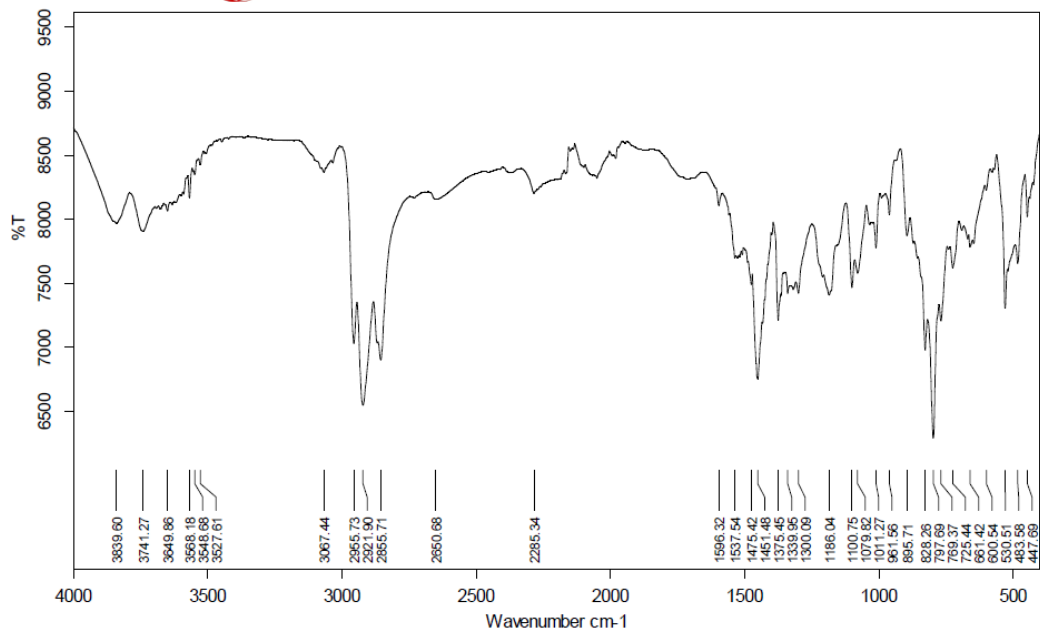


Sample Name		Date of Measurement	
Resolution	4	Sample Scans	

1



ODTU MERKEZ LABORATUVARI PERKIN ELMER Spectrum 400
(27703-03) RP2.dx

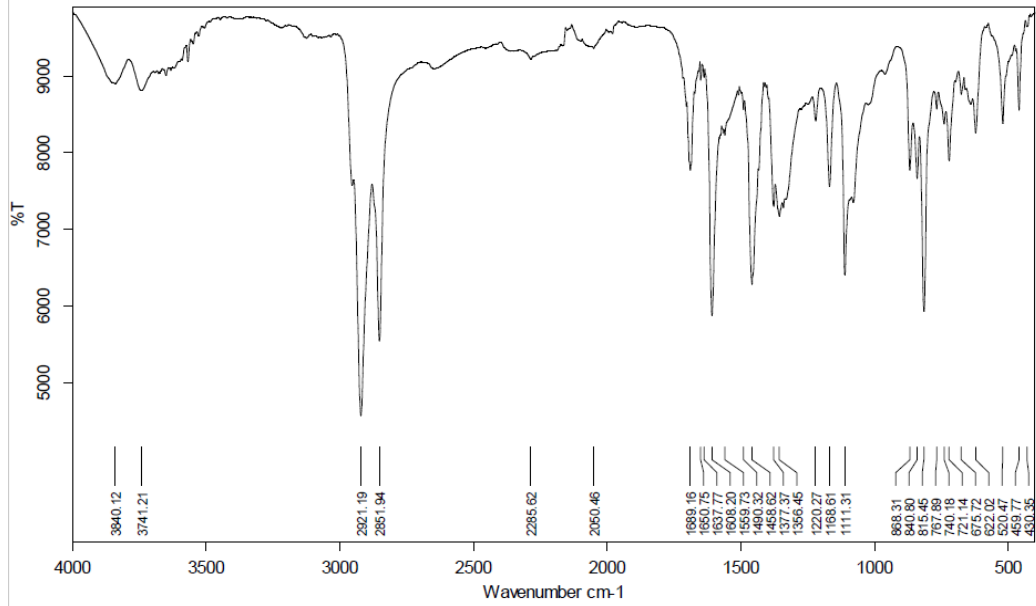


Sample Name		Date of Measurement	
Resolution	4	Sample Scans	

1



ODTU MERKEZ LABORATUVARI PERKIN ELMER Spectrum 400
(27705-01) SG6.dx

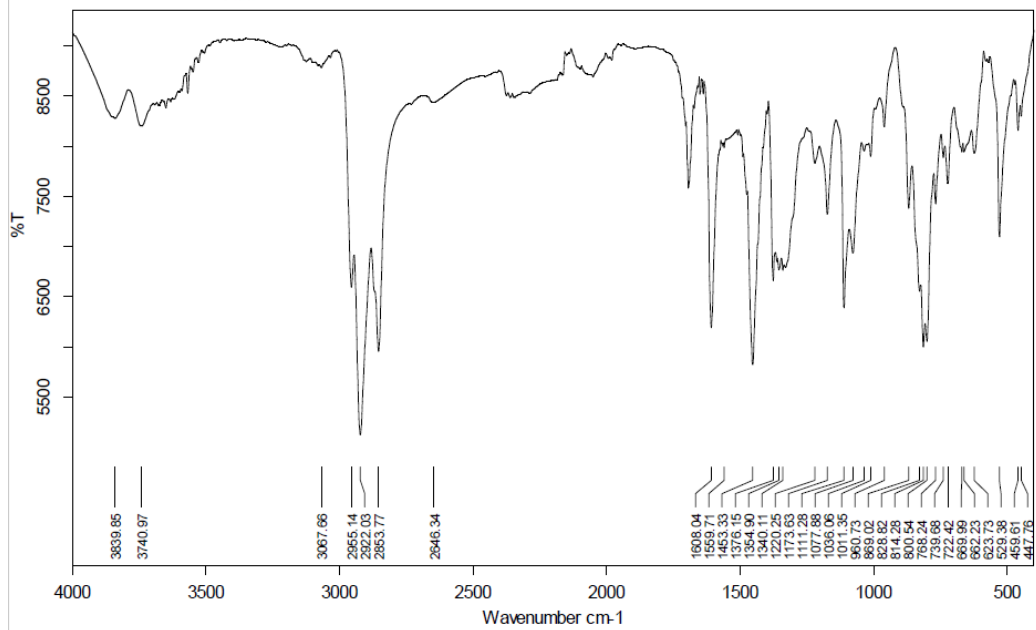


Sample Name		Date of Measurement	
Resolution	4	Sample Scans	

1



ODTU MERKEZ LABORATUVARI PERKIN ELMER Spectrum 400
(27704-01) RP3.dx

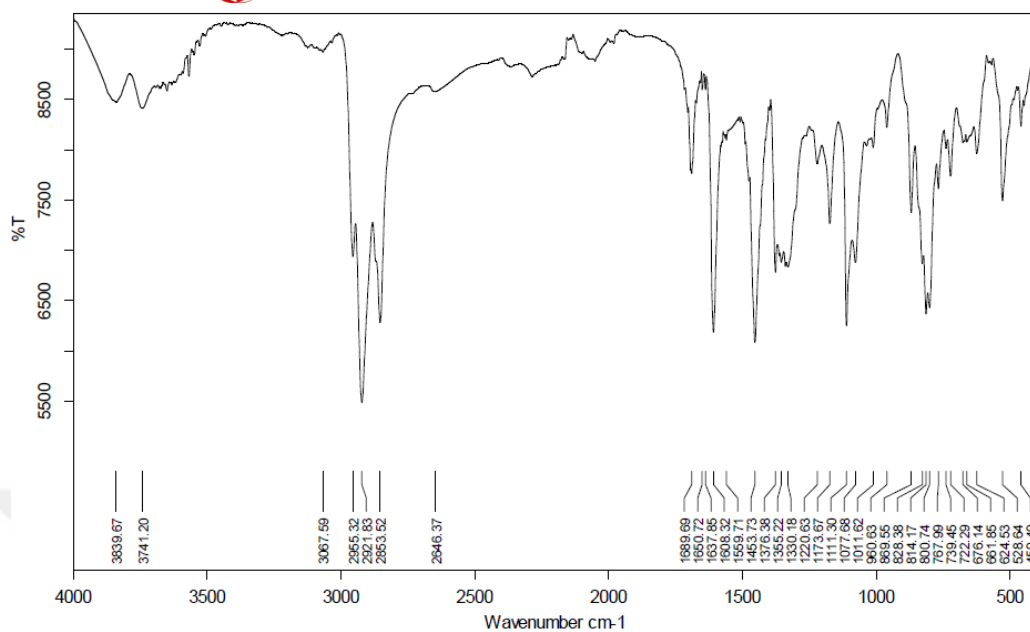


Sample Name		Date of Measurement	
Resolution	4	Sample Scans	

1



ODTU MERKEZ LABORATUVARI PERKIN ELMER Spectrum 400
(27704-02) RP3-HEX.dx

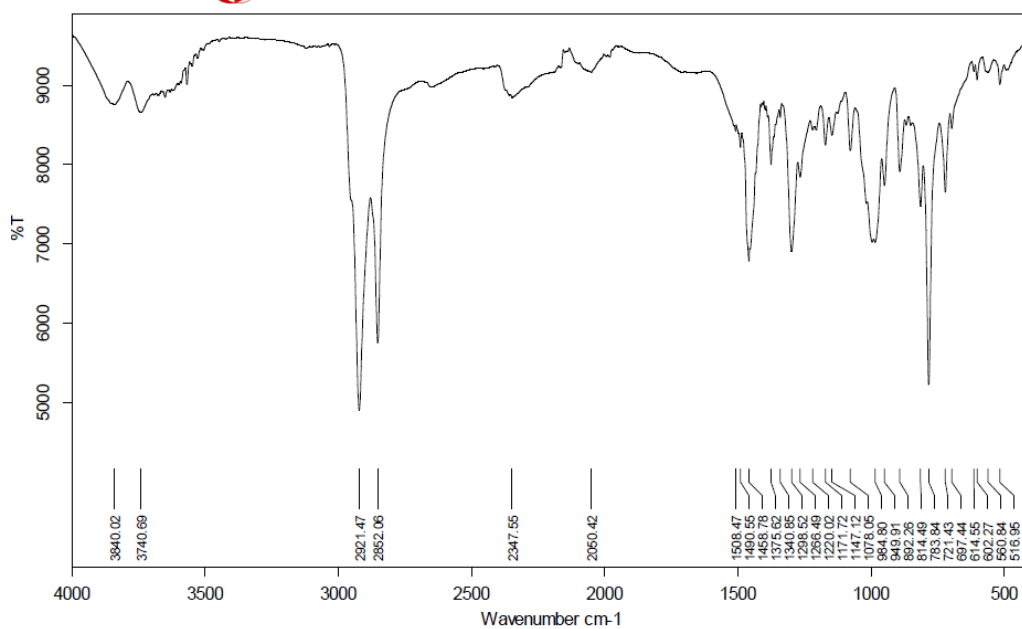


Sample Name		Date of Measurement	
Resolution	4	Sample Scans	

1

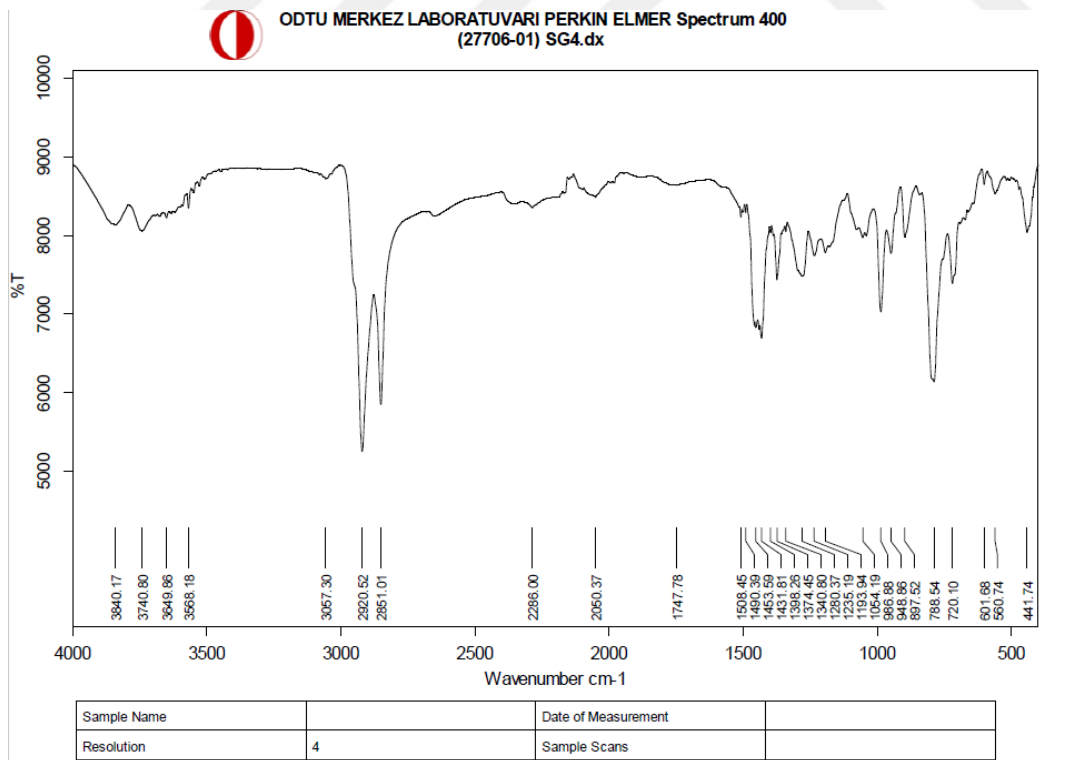
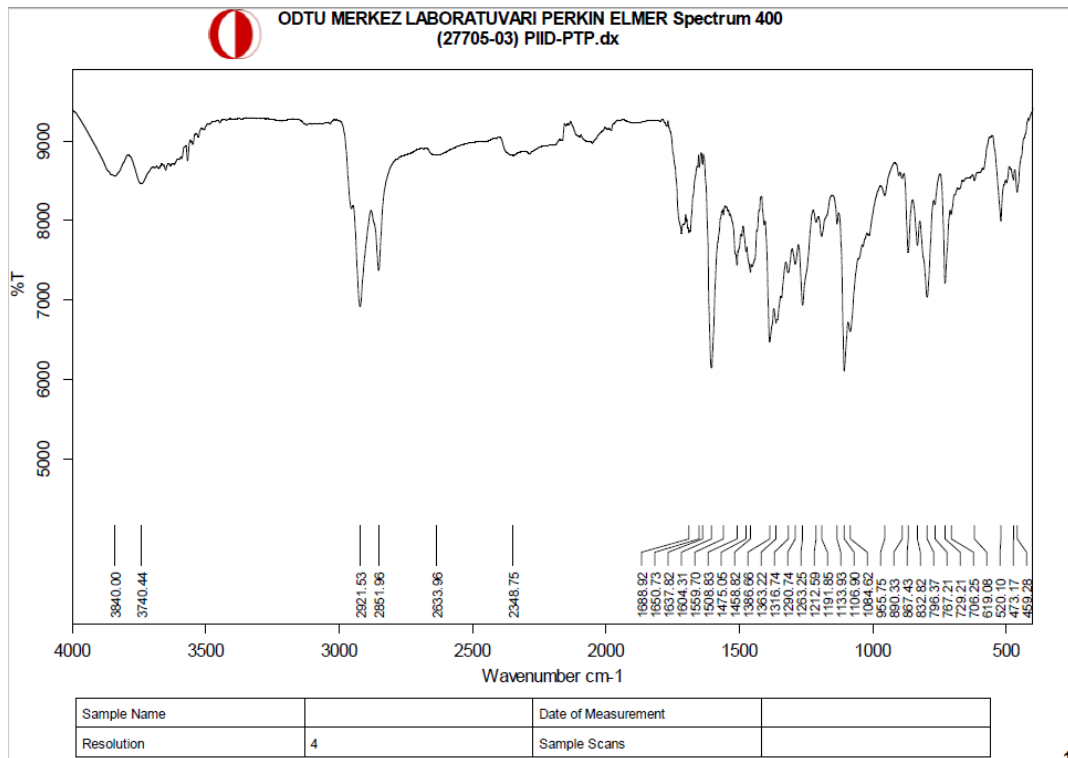


ODTU MERKEZ LABORATUVARI PERKIN ELMER Spectrum 400
(27705-02) SG9-ST.dx



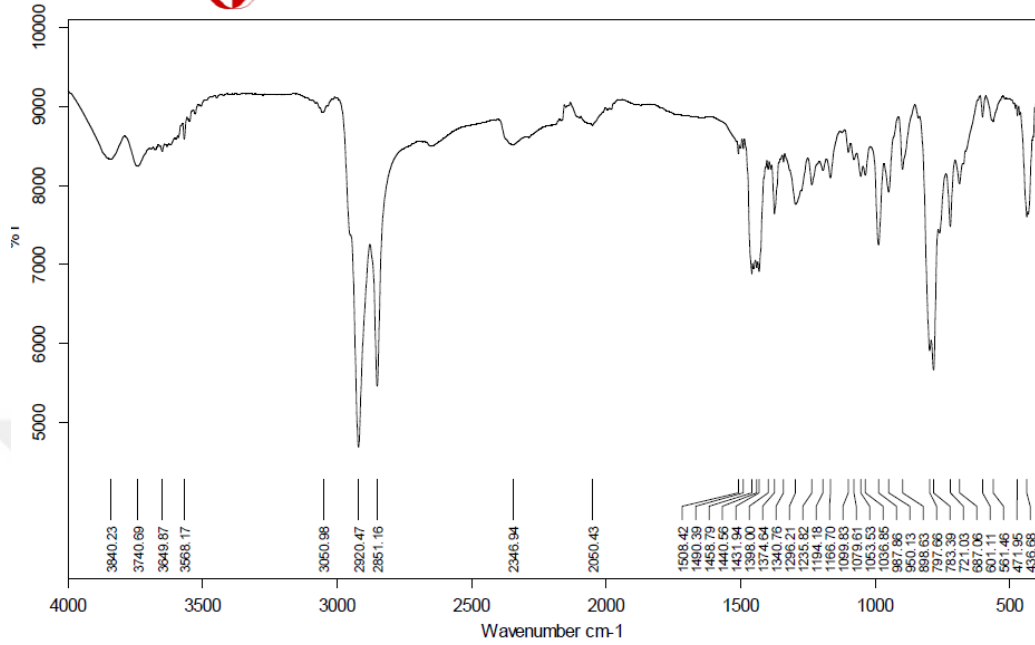
Sample Name		Date of Measurement	
Resolution	4	Sample Scans	

1





ODTU MERKEZ LABORATUVARI PERKIN ELMER Spectrum 400
(27706-02) SG4-ST.dx

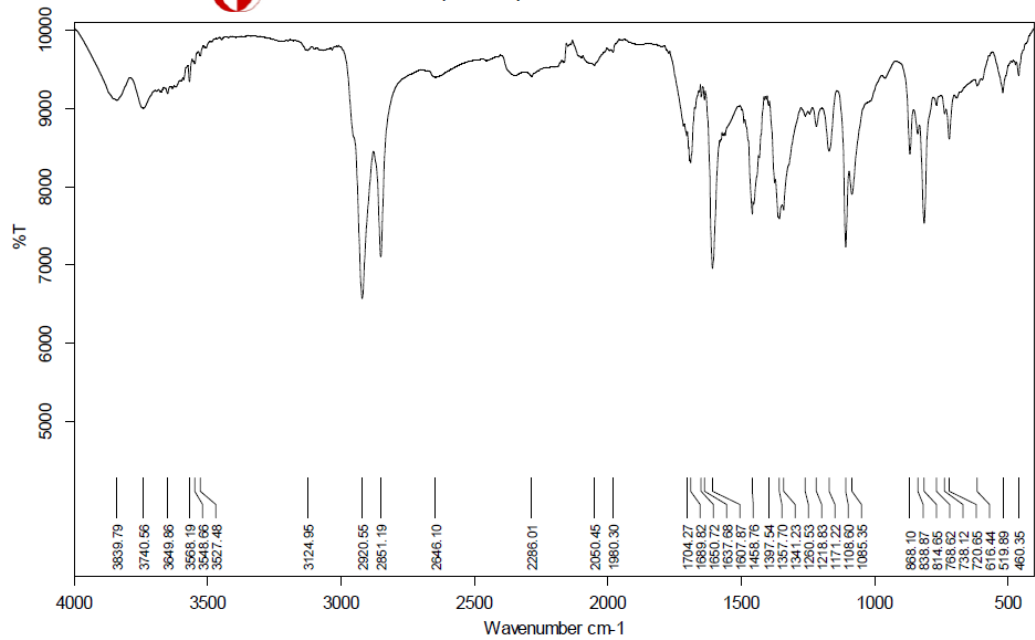


Sample Name		Date of Measurement	
Resolution	4	Sample Scans	

1



ODTU MERKEZ LABORATUVARI PERKIN ELMER Spectrum 400
(27706-03) SG-3-ST.dx



Sample Name		Date of Measurement	
Resolution	4	Sample Scans	

1

CURRICULUM VITAE

PERSONAL INFORMATION

Surname, Name : Göker, Seza
Nationality : Turkish (TC)
Date and Place of Birth : 30 March 1988, Kayseri
Phone : +90 538 557 87 91
E-mail : sezagoker@gmail.com

EDUCATION

Degree	Institution	Year of Graduation
MS	METU Department of Chemistry	2014
BS	METU Department of Chemistry (Major)	2012
BS	METU Department of Biology (Minor)	2013
High School	Cumhuriyet High School, Ankara	2005

WORK EXPERIENCES

Year	Place	Enrollment
2011-Present	Toppare Research Group	Synthesis Lab. Team Leader
2013-2014	Ministry of Science, Industry and Technology – ASELSAN- METU	Project Researcher
2014-2018	METU	Teaching Assistant
2016	Imperial College London	Visiting Researcher
June-August		
2017	Université Laval	Visiting Researcher
July-September		
2018-Present	Roketsan Missiles Inc.	R&D Engineer

FOREIGN LANGUAGES

Advanced English, German (Beginner), Italian (Beginner)

PROFESSIONAL MEMBERSHIPS

Member, American Chemical Society, 2013-present

Member, American Chemical Society, Polymeric Materials Science & Engineering Division. 2018

PUBLICATIONS

1. Yasa M., Goker S., Toppare L. 'Selenophene Bearing Low Band Gap Conjugated Polymers: Tuning Optoelectronic Properties via Fluorene and Carbazole as Donor Moieties' Polymer Bulletin, <https://doi.org/10.1007/s00289-019-02872-2> (2019)
2. Soylemez S., Goker S., Toppare L. 'A Promising Enzyme Anchoring Probe For Selective Ethanol Sensing In Beverages' Int. J. Biol. Macromol., 133, 1228-1235 (2019)
3. Soylemez S., Goker S., Toppare L. 'A newly designed anthracene and isoindigo based polymer: Synthesis, electrochemical characterization and biosensor applications' submitted, New J. Chem (2019)
4. Yasa M., Goker S., Udum Y. A., Toppare L. 'Tuning molecular energy levels and band gap of two-dimensional benzo[1,2-*b*:4,5-*b'*] dithiophene and quinoxaline bearing polymers' J. Electroanal. Chem., 847, 113260-113270 (2019)
5. Goker S., Hacioglu O. S., Hizalan G., Aktas E., Cirpan A., Toppare L. 'Triphenylamine based random copolymers: The effect of molecular weight on performance of solar cell and optoelectronic properties', Macromol. Chem. Phys. 218, 1600544 (2017)
6. Isik E., Goker S., Hizalan G., Hacioglu S. O., Toppare L. 'Random Copolymers of 1,2,3- Benzotriazole and Alkoxy-Modified Naptho[2,3-*b*:3,4-*b'*]dithiophene: Syntheses, characterization and optoelectronic properties', J. Electroanal. Chem., 786, 50-57 (2017)
7. Goker S., Hizalan G., Aktas E., Kutkan S., Cirpan A., Toppare L. '2,1,3-Benzooxadiazole, thiophene and benzodithiophene based random copolymers for organic photovoltaics: thiophene versus thieno[3,2-*b*]thiophene as π -conjugated linkers' New J. Chem., 40, 10455-10464 (2016)
8. Goker S.; Hizalan G.; Kutkan S.; Udum Y. A.; Toppare L., 'Incorporation of Different Conjugated Linkers into Low Band Gap Polymers based on 5,6-bis(octyloxy)-2,1,3 benzooxadiazole for Tuning Optoelectronic Properties' J. Polym. Sci., Part A: Polym. Chem., 54, 2459–2467 (2016)
9. Turan J., Kesik M., Soylemez S., Goker S., Coskun S., Unalan E. H., Toppare L. 'An effective surface design based on a conjugated polymer and silver nanowires for the detection of paraoxon in tap water and milk' Sens. Actuators, B, 228, 278–28 (2016)
10. Dzudzevic C. H., Soylemez S., Akpınar Y., Kesik M., Goker S., Gunbas G., Volkan M., Toppare L. 'A Novel Acetylcholinesterase Biosensor: Core-Shell Magnetic Nanoparticles Incorporating a Conjugated Polymer for the Detection of Organophosphorus Pesticides' ACS Applied Materials & Interfaces, 8, 8058–8067 (2016)

11. Rustamli E., Goker S., Tarkuc S., Udum Y. A., Toppare L. 'Synthesis and Characterization of Thiophene and Thieno[3,2-b]thiophene Containing Conjugated Polymers' J. Electrochem. Soc., 162, G75-G81 (2015)
12. Istanbuluoglu C., Goker S., Hizalan G., Hacioglu S. O., Udum Y. A., Yildiz D. E., Cirpan A., Toppare L. 'Synthesis of a Benzotriazole Bearing Alternating Copolymer For an Organic Photovoltaic Application' New J. Chem., 39, 6623-6630 (2015)
13. Goker S., Ileri M., Hizalan G., Hacioglu S. O., Toppare L. 'The effect of the different donor units on fluorescent conjugated polymers containing 2,1,3-benzooxadiazole as the acceptor unit' J. Electroanal. Chem., 751, 80-89 (2015)
14. Turan J., Kesik M., Soylemez S., Goker S., Kolb M., Bahadir M., Toppare L. 'Development of an Amperometric Biosensor Based On A Novel Conducting Copolymer for Detection of Anti-Dementia Drugs' J. Electroanal. Chem., 735, 43-50 (2014)
15. Goker S., Hizalan G., Udum Y. A., Toppare L. 'Electrochemical and optical properties of 5,6-bis(octyloxy)-2,1,3 benzooxadiazole containing low band gap polymers' Synth. Met., 191, 19-27 (2014)

CERTIFICATES

- 44th World Chemistry Congress (IUPAC 2013)
- 247th ACS National Meeting: Chemistry & Materials for Energy
- 251th ACS National Meeting: Computers in Chemistry
- 253rd ACS National Meeting: Advanced Materials, Technologies, Systems & Processes
- European Polymer Federation Congress 2015
- Third Turkish Solar Electricity Conference and Exhibition
- The Fourth Physical Chemistry Congress (National)
- Macro 2016-46th IUPAC World Polymer Congress
- E-MRS Spring Meeting 2017
- Polimer 2018
- 256th ACS National Meeting & Exposition: Nanoscience, Nanotechnology & Beyond
- 2018 MRS Spring Meeting & Exhibit

REFERENCES

- Prof. Dr. Levent Toppare
Middle East Technical University Chemistry Department 06800 Ankara – Turkey
toppare@metu.edu.tr
- Assoc. Prof. Dr. Görkem Günbaş
Middle East Technical University Chemistry Department 06800 Ankara –Turkey
ggunbas@metu.edu.tr
- Assist. Prof. Derya Baran
King Abdullah University of Science and Technology
Center of Material Science and Engineering Physical Science and Engineering
Division
derya.baran@kaust.edu.sa
- Prof. Dr. Iain McCulloch
Imperial College London RCS 1 M229 Chemistry South Kensington Campus
London-UK
i.mcculloch@imperial.ac.uk
iain.mcculloch@kaust.edu.sa
- Prof. Mario Leclerc
Université Laval
Department of Chemistry, Pavillon Alexandre-Vachon Québec-Canada
mario.leclerc@chm.ulaval.ca